eCAM Evidence-Based Complementary and Alternative Medicine

Ethnopharmacological Studies for the Development of New Drugs

Lead Guest Editor: José C. T. Carvalho
Guest Editors: Caio P. Fernandes, Jesus R. R. Amado, Andrés Navarrete, and Lucindo Q. Júnior

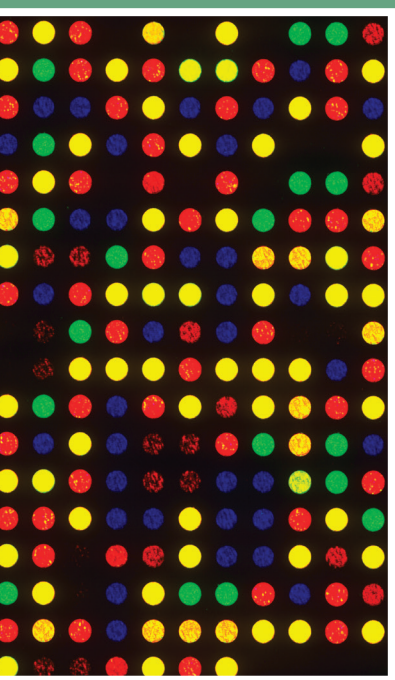

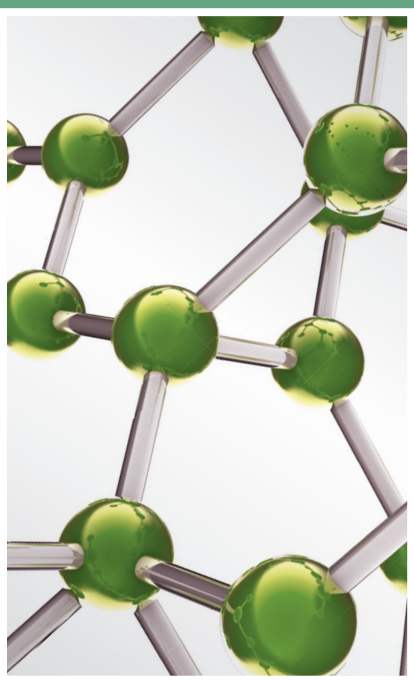


Ethnopharmacological Studies for the Development of New Drugs

Evidence-Based Complementary and Alternative Medicine

Ethnopharmacological Studies for the Development of New Drugs

Lead Guest Editor: José C. T. Carvalho
Guest Editors: Caio P. Fernandes, Jesus R. R. Amado, Andrés Navarrete, and Lucindo Q. Júnior

Editorial Board

Contents

Hindawi
Evidence-Based Complementary and Alternative Medicine
Volume 2018, Article ID 7593296, 2 pages
https://doi.org/10.1155/2018/7593296

Editorial

Ethnopharmacological Studies for the Development of New Drugs

José Carlos Tavares Carvalho,[1] **Caio Pinho Fernandes**,[2] **Jesus Rafael Rodriguez Amado**,[3] **Andrés Navarrete**,[4] **and Lucindo José Quintans-Júnior**[5]

[1]*Laboratório de Pesquisa em Fármacos, Departamento de Ciências Biológicas e da Saúde, Universidade Federal do Amapá, Macapá, AP, Brazil*
[2]*Laboratório de Nanobiotecnologia Fitofarmacêutica, Universidade Federal do Amapá, Macapá, AP, Brazil*
[3]*Facultad de Farmácia, Universidad de Oriente, Santiago de Cuba, Cuba*
[4]*Laboratório de Farmacologia de Productos Naturales, Departamento de Farmácia, Facultad de Química, Universidad Nacional Autónoma de México, Ciudad de México, Mexico*
[5]*Laboratório de Neurociências e Ensaios Farmacológicos, Departamento de Fisiologia, Centro de Ciências Biológicas e da Saúde, Universidade Federal de Sergipe, São Cristóvão, SE, Brazil*

Correspondence should be addressed to José Carlos Tavares Carvalho; farmacos@unifap.br

Received 3 January 2018; Accepted 4 January 2018; Published 31 January 2018

Ethnopharmacology is an important discipline for the development of new medicines that are of extreme importance for the conservation and enhancement of the traditional use of natural products and undoubtedly is one of the main sources faster for the rational development of new medicines. There are several examples of drugs that have been discovered from ethnopharmacologic studies. Therefore, in this context, this special issue aimed to present important studies carried out by researchers from all the areas that explore and dedicate themselves to the following themes, which were submitted for publication in this journal.

For this special publication, 43 manuscripts from various laboratories from all continents of the world were received, with the following topics: ethnopharmacy, ethnopharmacology and ethnobotanical studies, ethnomedicine and bioactive compounds from animals and plants, pharmaceutical technology with natural products, clinical application of natural products in different communities, predictions and in silico studies with natural products, and alternative biological assay for determination of natural product activity.

After careful analysis by several ad doc referees of renowned universities, 11 manuscripts were accepted for publication, standing out for the quality presented and the high possibility of impact in the field of ethnopharmacology.

In the paper "Optimized-SopungSunkiwon, a Herbal Formula, Attenuates Aβ Oligomer-Induced Neurotoxicity in Alzheimer's Disease Models," it was confirmed by in vivo data that oral administration of Optimized-SopungSunkiwon (OSS) for 14 days attenuated memory impairments and neuronal cell death by modulating gliosis, glutathione depletion, and synaptic damage in the mouse hippocampus induced by AβO.

The manuscript "EGHB010, a Standardized Extract of Paeoniae Radix and Glycyrrhizae Radix, Inhibits VEGF-Induced Tube Formation In Vitro and Retinal Vascular Leakage and Choroidal Neovascularization In Vivo" demonstrated that the EGHB010 that is a hot water extract of the rhizome mixture of *Paeonia lactiflora* Pallas and *Glycyrrhiza uralensis* Fisch and in choroidal neovascularization (CNV) area was significantly lower in EGHB010-treated rats than in vehicle-treated rats. These results suggest that EGHB010 is a potent antiangiogenic agent. Thus, the oral administration of EGHB010 may have a beneficial effect in the treatment

of vascular leakage and CNV in patients with age-related macular degeneration.

The psychotropic effects of an alcoholic extract from the leaves of *Albizia zygia* (Leguminosae-Mimosoideae) were evaluated and the hydroethanolic extract of *Albizia zygia* exhibited an antipsychotic-like activity in mice. Motor side effects are only likely to develop at higher doses of the extract. The extract does not possess any significant antidepressant effects.

The potential wound healing activities of *Oxytropis falcate* gel (OFG) was demonstrated in the manuscript "Therapeutic Effect and Mechanism of *Oxytropis falcata* Gel on Deep Second-Degree Burn in Rats," and the mechanism may be related to the increase of biosynthesis and the release of EGF and CD34 and the decreasing p38 and IL-1β levels.

In the study "A Molecular Basis for the Inhibition of Transient Receptor Potential Vanilloid Type 1 by Gomisin A," it has been demonstrated that the double mutation of Y453 and N467 significantly attenuated inhibitory effects by gomisin A. In summary, it revealed the molecular basis for the interaction between TRPV1 and gomisin A and provided a novel potent interaction ligand.

In the paper "Antcin-H Isolated from *Antrodia cinnamomea* Inhibits Renal Cancer Cell Invasion Partly through Inactivation of FAK-ERK-C/EBP-β/c-Fos-MMP-7 Pathways," luciferase reporter assay showed that antcin-H repressed the MMP-7 promoter activity, in parallel to inhibiting c-Fos/AP-1 and C/EBP-β transactivation abilities. Moreover, antcin-H suppressed the activity of ERK1/2 and decreased the binding capacity of C/EBP-β and c-Fos on the upstream/enhancer region of the MMP-7 promoter. Overall, this study demonstrated that the anti-invasive effect of antcin-H in human renal carcinoma 786-0 cells might be at least in part by abrogating focal adhesion complex and lamellipodium formation through inhibiting the Src/FAK-paxillin signaling pathways and decreasing MMP-7 expression through suppressing the ERK1/2-AP-1/c-Fos and C/EBP-β signaling axis. Thus, it was proven that the evidence that antcin-H may be an active component existed in *A. cinnamomea* with anticancer effect.

In the paper "Tang-Luo-Ning, a Traditional Chinese Medicine, Inhibits Endoplasmic Reticulum Stress-Induced Apoptosis of Schwann Cells under High Glucose Environment," the results showed that TLN attenuated apoptosis by decreasing Ca2+ level in SCs and maintaining ER morphology. TLN could decrease downstream proteins of CHOP including GADD34 and Ero1α while increasing P-eIF2α as well as decreasing the upstream proteins of CHOP including P-IRE1α/IRE1α and XBP-1, thereby reducing ER stress-induced apoptosis.

Flavonoid composition and biological activities of ethanol extracts of *Caryocar coriaceum* Wittm, a native plant from Caatinga Biome, Brazil, were a theme presented that demonstrated that the extracts present antileishmanial activity and low toxicity on murine macrophages and erythrocytes. Therefore, these results suggest a potential for the application of *C. coriaceum* fruit's ethanol extracts in the treatment of dermatophyte fungi and leishmaniasis, probably due to the presence of active flavonoids in both extracts.

In the manuscript "A New Technique Using Low Volumes: A New Technique to Assess the Molluscicidal Activity Using Low Volumes," a technique that was presented to assess the toxic effect has been proven to be a useful tool to detect the lethal and sublethal effect, which could be used as a new evaluation protocol. This data was confirmed through treatment with plant extract and exhibiting IC_{50} values similar to three methodologies.

Renal pathological changes were examined by the staining of HE, Masson, and PASM. Expressions and distributions of fibronectin (FN), laminin (LN), light chain 3 (LC3), and Beclin-1 were observed by immunohistochemistry, in the paper "Sinomenine Hydrochloride Attenuates Renal Fibrosis by Inhibiting Excessive Autophagy Induced by Adriamycin: An Experimental Study." SINHCl ameliorates proteinuria; meanwhile, it attenuates the renal pathological changes in adriamycin-induced rats and also attenuates renal fibrosis and excessive autophagy by reducing the expression of FN, LN, LC3, and Beclin-1. SIN-HCl attenuates renal fibrosis by inhibiting excessive autophagy induced by adriamycin and upregulating the basal autophagy.

In the paper "Pharmacological Effect of *Caulophyllum robustum* on Collagen-Induced Arthritis and Regulation of Nitric Oxide, NF-κB, and Proinflammatory Cytokines In Vivo and In Vitro," the authors showed that, compared with the model group, CRME significantly improved symptoms of the arthritis index, limb swelling, and histological findings by decreasing synovial membrane damage, the extent of inflammatory cell infiltration, and the expansion of capillaries in CIA mice. The results also showed that CRME could reduce the levels of IL-1, IL-6, TNF-α, and PGE2 and inhibit the expression of NF-κB p65. All these results indicated the anti-inflammatory efficacy of CRME as a novel botanical extraction for the treatment of RA.

Acknowledgments

The guest editorial team would like to thank authors of all the 43 manuscripts submitted to this special issue. Certainly, all the manuscripts that were published in this edition in the form of paper will contribute to the development of the studies in the field of ethnopharmacology. We would like to publish all of them, but the opinions issued by the referees made us finalize the edition with this number of articles that we present. We also thank the anonymous reviewers, some of whom helped with multiple review assignments. Finally, we would like to thank this journal for being very encouraging and accommodative regarding this special issue, collaborating with the expertise in the field of ethnopharmacology.

José Carlos Tavares Carvalho
Caio Pinho Fernandes
Jesus Rafael Rodriguez Amado
Andrés Navarrete
Lucindo José Quintans-Júnior

Hindawi
Evidence-Based Complementary and Alternative Medicine
Volume 2017, Article ID 8134321, 12 pages
https://doi.org/10.1155/2017/8134321

Research Article

Pharmacological Effect of *Caulophyllum robustum* on Collagen-Induced Arthritis and Regulation of Nitric Oxide, NF-κB, and Proinflammatory Cytokines In Vivo and In Vitro

Qiu-hong Wang,[1,2] Shao-wa Lv,[1] Yu-yan Guo,[1] Ji-xin Duan,[1] Shu-yu Dong,[1] Qiu-shi Wang,[1] Feng-ming Yu,[1] Hong Su,[1] and Hai-xue Kuang[1]

[1]*Heilongjiang University of Chinese Medicine, Harbin 150040, China*
[2]*Guangdong Pharmaceutical University, Guangzhou 510006, China*

Correspondence should be addressed to Yu-yan Guo; 35289740@qq.com and Hai-xue Kuang; hxkuang56@163.com

Received 9 March 2017; Revised 8 August 2017; Accepted 10 September 2017; Published 31 December 2017

Academic Editor: Andrés Navarrete

Caulophyllum robustum Maxim *(C. robustum)* has commonly been used as traditional Chinese medicine for the treatment of rheumatic pain and rheumatoid arthritis (RA) in China. This paper first investigated the anti-inflammation effect of *C. robustum* extraction (CRME) on RAW264.7 cells stimulated by lipopolysaccharide (LPS) and gene expression levels of inflammatory factors. Moreover, we first evaluated the anti-RA effects of CRME using collagen-induced arthritis (CIA) in DBA/1J mice, and the incidence, clinical score, and joint histopathology were evaluated. The levels of IL-1, IL-6, TNF-α, and PGE2 inflammatory factors in sera of mice were detected by enzyme-linked immunosorbent assay. The expression of NF-κB p65 in the joint was tested by immune histochemical technique. The results showed that, compared with the model group, CRME significantly improved symptoms of the arthritis index, limb swelling, and histological findings by decreasing synovial membrane damage, the extent of inflammatory cell infiltration, and the expansion of capillaries in CIA mice. The results also showed that CRME can reduce the levels of IL-1, IL-6, TNF-α, and PGE2 and inhibit the expression of NF-κB p65. All these results indicated the anti-inflammatory efficacy of CRME as a novel botanical extraction for the treatment of RA.

1. Introduction

As an autoimmune disease, human rheumatoid arthritis (RA) is a major cause of disability characterized by chronic inflammation and joint damage. The pathogenesis of RA is a complex process involving synovial cell proliferation and fibrosis, pannus formation, and cartilage and bone erosion [1, 2]. To date, it has been found that the joint destruction is caused by several mechanisms including the overexpression of inflammatory response cytokines and transcription factors relevant to RA inflammation during the occurrence of RA [3]. In RA, the transcription factor nuclear factor-kappa B (NF-κB) is overexpressed in the inflamed synovium [4, 5]. It participates in the transactivation of various genes and inducible nitric oxide (iNOS) [6], which mediate immune and inflammatory responses [7]. It can activate and be activated by proinflammatory cytokines, such as Tumor Necrosis Factor-alpha (TNF-α), Interleukin- (IL-) 1, Prostaglandin E (PGE), and IL-6, resulting in a positive regulatory circle that causes amplification of local inflammatory responses [8]. TNF-α stimulates synovial fibroblasts to express intercellular adhesion molecules, which increases the migration of leukocytes into the RA joints. It is a central factor in the pathogenesis of RA as it amplifies inflammation and causes joint damage. IL-6 is also known as another proinflammatory cytokine that closely contributes to vascular endothelial growth and that stimulates the growth of blood vessels, including those in hypertrophy of joints. IL-1 is another key mediator involved in bone resorption and cartilage destruction that can modulate the production of nitric oxide and PGE2. PGE2 can act to mediate hyperalgesia-induced sensitizing pain receptors and induce fever [9]. Relieving inflammation

and reducing proinflammatory cytokine overexpression are therefore regarded as one of the major approaches to help prevent the progressive damage to RA joints.

Historically, *C. robustum* is a traditional Chinese herb used in the treatment of RA [10]. It is acrid and bitter in taste and warm in nature. The Dictionary of Chinese Medicinal Plants records that *C. robustum* roots and rhizomes have the ability to expel wind, promote blood circulation, and regulate the flow of vital energy to stop pain. It is mainly used for external injuries, rheumatism, and RA treatment. Pharmacological study showed that its decoction inhibits tissue edema caused by croton oil, suppresses capillary permeability induced by acetic acid, and suppresses cotton pellet granuloma [11]. Modern studies have demonstrated that alkaloids and triterpenoid saponins seem to contribute most of the physiological anti-inflammatory activity [12]. Among them, Caulosides A~D could dramatically suppress the expression of proinflammatory factors, for instance, TNF-α, IL-1β, and IL-6 [13–15]. Magnoflorine has shown activity against FCA-induced pyrexia [16]. However, some potential toxic and side effects of *C. robustum* have been found. For its convenient clinical use, we improved the extraction technique and obtained CRME with lower toxicity (LD50 is 4.6 g).

We set out to investigate the anti-inflammation effect of CRME on RAW264.7 cells stimulated by LPS. Then, collagen-induced arthritis (CIA) by the immunization of DAB/1 mice with type II collagen in complete Freund's adjuvant was used for activity evaluation in vivo. The levels of IL-1β, IL-6, TNF-α, and PGE2 in sera of the CIA rats and of NF-κB protein were determined in synovial tissue. All the above were helpful to our investigation into the therapeutic effects of CRME on RA and its possible mechanism.

2. Materials and Methods

2.1. Sample Extraction and Isolation of C. robustum. *C. robustum* was purchased from Heilongjiang province of China and authenticated by Professor Shaowa Lv (College of Pharmacy, Heilongjiang University of Chinese Medicine). A specimen (20150301) of it was deposited in the College of Pharmacy, Heilongjiang University of Chinese Medicine. Its roots and rhizomes were extracted twice with 70% ethanol (v/v). The filter was combined and reclaimed and then loaded onto an AB-8 macropore resin column and eluted with pure water and 70% ethanol (v/v). The 70% ethanol eluate was concentrated to dryness (the powder was named CRME). We determined its main chemical components by high-performance liquid chromatography (HPLC). The result showed that there were six components in CREM, including Cauloside H, Leonticin D, Cauloside G, Cauloside D, Cauloside B, and Cauloside C and their content was 6.21%, 5.14%, 28.88%, 10.19%, 3.68%, and 2.26%, respectively (Figures 1(a) and 1(b)).

2.2. Drugs and Reagents. The RAW264.7 cell line was purchased from the Cell Resource Center, Peking Union Medical College. gDNA and cDNA Remover were purchased from TOYOBO Co., Osaka, Japan. Trizol reagent was purchased from Tiangen, Beijing, China.

LPS, vine type II collagen, Freund's incomplete adjuvant (IFA), and Freund's complete adjuvant (CFA) were purchased from Sigma (USA, St. Louis, MO). IL-1β, IL-6, TNF-α, PGE2, and NO were purchased from R&D system in the USA. NF-κBp65 was purchased from Wuhan Boster Biological Engineering Co., Ltd. The rabbit-anti-mouse second antibody and DAB were purchased from Beijing Chinese Fir Golden Bridge Biotechnology Co., Ltd.

Triptolide- (Tri-) tablets were purchased from Broad medicine Yellowstone Feiyun Pharmaceutical Co., Ltd., lot number: 20130601, standard: 10 mg. Methotrexate (MTX) tablets were purchased from Shanghai Sym. Pharma Co., Ltd., lot number: 03614040, standard: 2.5 mg. To determine the therapeutic efficiency of CRME for the treatment of RA, we chose MTX and Tri as positive medicines. MTX is the first-line therapy for this disease, and Tri is isolated from Tripterygium Wilfordii Hook f., which is a kind of Chinese medicinal plant used to ameliorate the symptoms of rheumatic diseases [17].

2.3. Cell Cultures and Their Use to Test CRME. RAW264.7 cells were maintained in DMEM containing 10% fetal bovine serum (FBS) and 1% penicillin streptomycin (PS) at 37°C in a 5% CO2 incubator. Before starting any experiment, RAW264.7 cells were seeded in culture plates and maintained for 24 h until approximately 70%–80% confluence. RAW264.7 cells were stimulated with LPS of *Escherichia coli* (serotype, 055: B5) at a concentration of 1 μg/ml for establishing the inflammatory cell model. RAW264.7 cells were incubated with CRME by the addition of different concentrations of the former (0.250 mg/mL, 0.125 mg/mL, and 0.063 mg/mL) for 1 h and then treated with 1 μg/mL LPS for an additional 24 h. After 24 h, the cell culture supernatant was collected to detect NO (nitric oxide) by Griess reagent assay. Total RNA was isolated immediately after harvesting the RAW264.7 cells for RT-PCR as described below. Unstimulated RAW264.7 cells were treated as a negative control.

2.4. RNA Extraction and RT-PCR Analysis. Total RNA was separated from RAW264.7 cells by Trizol reagent according to the protocol. For cDNA synthesis, total RNA (2 μg/sample) was reverse transcribed with ReverTra Ace qPCR RT Master Mix with the gDNA Remove. The cDNA was then amplified with THUNDERBIRD SYBR qPCR Mix. The primer sequences were as follows: for IL-1β, forward primer (FP) = (5′-CAGGATGAGGACATGAGCACC-3′) and reverse primer (RP) = (5′-CTCTGCACACTCAAACTCCAC-3′), for TNF-α, FP = (5′-GGGAGCAAAGGTTCAGTGAT-3′) and RP = (5′-CCTGGCCTCTCTACCTTGTT-3′), for IL-6, FP = (5′-CTGACAATATGAATGTTGGG-3′5′-TCCAAGAAACATCTGGCTAGG-3′); for GAPDH, FP = (5′-GTCATTGAGAGCAATGCCAG -3′) and RP = (5′- GTGTTCCTACCCCCAATGTG -3′). The PCR amplification conditions were as follows: initial denaturation at 95°C for 1 min; 40 cycles of denaturation and extension at 95°C for 15 s. Amplified products were separated by 1% agarose gel electrophoresis and visualized with ethidium bromide staining. The results are representative of three independent experiments.

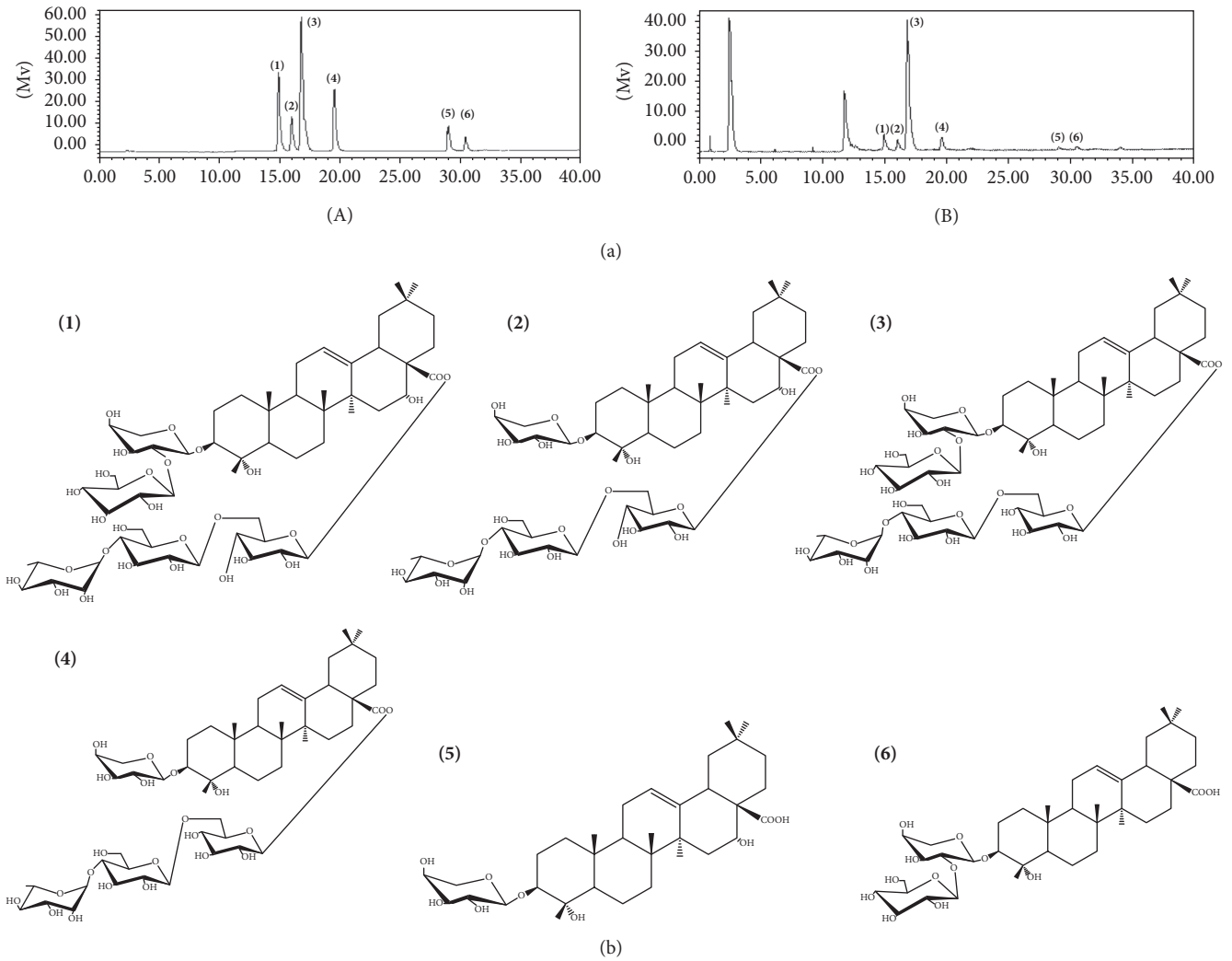

Figure 1: (a) HPLC–ELSD chromatogram of six marker compounds in CRME. HPLC–ELSD chromatogram of mixture of standard compounds (A). HPLC–ELSD chromatogram of six marker compounds in CRME (B). (b) Structure of six marker compounds. Cauloside H **(1)**. Leonticin D **(2)**. Cauloside G **(3)**. Cauloside D **(4)**. Cauloside B **(5)**. Cauloside C **(6)**.

2.5. Animals, Induction of CIA, and Compound Administration. DBA/1 mice (half male and female, 6~8 weeks old) were purchased from HFK Bioscience Co., Ltd. (Beijing, China, Certificate: 2010A050). All mice were maintained in a room with a temperature of 25 ± 2°C and humidity of 60%. Mice drank water freely and were given 12 h of light each day. Bedding was kept dry. All animal care and treatment procedures were approved by the committee of Experimental Animal Administration of Heilongjiang University of Chinese Medicine.

Forty-two DBA/1 mice were divided into seven groups with identical numbers of mice ($n = 6$). One of the groups served as "normal," whereas the other 6 groups were subjected to CIA induction. Bovine type II collagen was dissolved in 0.1 M acetic acid, mixed to 2 mg/ml mixed liquor, and incubated overnight at 4°C. The mixture and an equal volume of CFA were emulsified at low temperature. The DBA/1 mice were subcutaneously immunized at 1-2 cm from the base of the tail with 100 μL hybrid emulsion (containing 100 μg of bovine type II collagen), and this was treated as the first immunization on day 0. Mice were boosted intraperitoneally with 100 μg bovine type II collagen emulsified in an equal volume of IFA on day 21, and this was treated as the second immunization.

CRME, Tri tablets, and MTX tablets were separately dissolved in distilled water and administered orally once per day for 30 days, from day 22 to day 52. The groups are as follows: normal group (Normal), CIA model group (Vehicle), Tri group 11.3 mg/kg, MTX group 0.9 mg/kg, CRME group (L group) 24.8 mg/(kg·day), CRME group (M group) 49.7 mg/(kg·day), and CRME group (H group) 99.4 mg/(kg·day). The dosage selection for the present study was according to the LD50 (4.6 g/kg) for CRME from our previous study and reference to classical Chinese medicine books and literature. For example, Guizhou folk medicine records that 5 g *C. robustum* powder taken with wine has the most significant effect. In addition, experiments show that *C. robustum* ethanol extract (69.23, 34.61, and 17.31 mg/kg)

inhibits the swelling of the joint and decreases the spleen index and the level of inflammatory factors [18].

2.6. Morphologic and Immune Studies. Mice were observed once every 3 days after primary immunization. Arthritis severity was evaluated by arthritis index, arthritis incidence, and percentage of arthritic limbs as assessed by two independent, blinded observers. All four limbs of the mice were evaluated and scored from 0 to 4 as follows: 0, normal; 1, 1~2 toe joints swelling; 2, the whole ball with mild swelling and redness; 3, severe swelling and redness of the whole ball; 4, overall deformation and/or joint stiffness. The arthritis index of all four limbs was the total score, and the highest score for each mouse was 16 points. When the score of a paw was more than 2, the mice were considered to suffer from RA. The volume of arthritic limbs was detected with a digital plethysmometer (LE 7500, Panlab, Spain). According to the digit volume of mice and the following formula, the limb swelling of mice was calculated:

$$\text{Sweling degree (\%)} = \frac{\text{Arthritic limb volum} - \text{Normal limb volume}}{\text{Right rear normal volume}} \times 100\%. \quad (1)$$

There is a close connection between the aggressive progression of RA and the loss of body mass. After the secondary immunization, we detected the changes in body weight once every 3 days in order to evaluate CRME for the treatment of RA. The weight of individual CIA mice was calculated with the following formula:

$$\text{Change of body weight (\%)} = \frac{\text{body weight (day 31 of arthritis)}}{\text{body weight (day 1 of arthritis)}} \times 100\%. \quad (2)$$

Mice were sacrificed by cervical dislocation after a month of oral administration. The spleen and thymus were obtained, fur and blood on the surface of the viscera were rinsed clean with normal saline, and they were weighed with an analytical balance. We measured the wet weight of the immune organs to preliminarily assess CRME for treatment of RA. The computation formula is as follows:

$$\text{Viscera index (\%)} = \frac{\text{Weight of spleen (or thymus)}}{\text{Weight of mice}} \times 100\%. \quad (3)$$

2.7. Enzyme-Linked Immunosorbent (ELISA) Assay. On the 52nd day, 1 mL of blood was collected from each mouse's eye socket vein after more than 12 h fasting. Then, the blood samples stood at room temperature for 20 min. Serum was separated from the rest of the blood using a high-speed centrifuge (H2050R, China) at 10000 rpm for 10 min, and IL-1β, IL-6, TNF-α, and PGE2 levels were measured with ELISA kits. According to the manufacturer's instructions, the processed samples were measured for OD value at 450 nm. There is a certain linear relationship between cytokine concentrations in mice and the OD value, which can be determined by acknowledgement of standard curve sample concentrations of cytokines in mice, and, then, the data were analyzed to sum up the influence of CRME on the inflammatory factors.

2.8. Histological. On the 52nd day, the mice were sacrificed. The hind limbs and immune organs, such as spleen and thymus, were fixed immediately in 4% buffered formalin solution, decalcified, and embedded in paraffin, after which they were divided into 6 μm pieces. The left hind limbs and visceral organs were treated with Hematoxylin-Eosin (HE) staining for morphological examination, while the right hind limbs were used for immunohistochemistry with NF-κBp65. A Motic 3000 micrograph system served as radiography at 400 times, and Image-pro plus 6.0 pathological Image was used to analyze positive expression quantitatively. The expression of protein was represented by integral optical density (IOD), namely, integral optical density (IOD) = positive area × average optical density. Each case was analyzed randomly in two vision fields at high magnification, and, then, the relative expression was averaged, for which there were 3 cases in each group.

2.9. Statistics. The software SPSS version 19.0 for Windows was applied for statistical analysis. Measurement data were expressed as the mean ± SD, and the two-way ANOVA test followed by least-significant differences (LSD) test was used to compare between groups; count data were expressed as percentages and compared with the chi-square test between groups. Statistical significance was set at $^{*}P < 0.05$, and extreme significance was set at $^{\#}P < 0.01$.

3. Results and Discussion

3.1. Levels of Nitric Oxide (NO) in Culture Supernatant of RAW 264.7 Cells. The CRME showed dose-dependent inhibition of the generation of NO in LPS-stimulated RAW264.7 cells (Figure 2(a)). This finding suggested that the CRME may suppress the LPS-induced inflammatory response through inhibition of NO generation. Therefore, this result showed that CRME has anti-inflammatory response.

3.2. Gene Expression of IL-1 β, IL-6, and TNF-α in Cell Culture. CRME exerted an anti-inflammatory effect on LPS-induced responses accompanied by the gene expression of proinflammatory cytokines. RAW264.7 cells were treated with CRME and LPS for 24 h. The gene expression levels of TNF-α, IL-1β, and IL-6 were reduced by treatment with CRME in a dose-dependent manner (Figures 2(b), 2(c), and 2(d)). These results indicated that CRME has an anti-inflammatory effect on the gene expression of LPS-induced proinflammatory cytokines in RAW264.7 cells.

3.3. Morphologic Study of Survival State of Mice. Approximately 7 days after the secondary immunization, compared

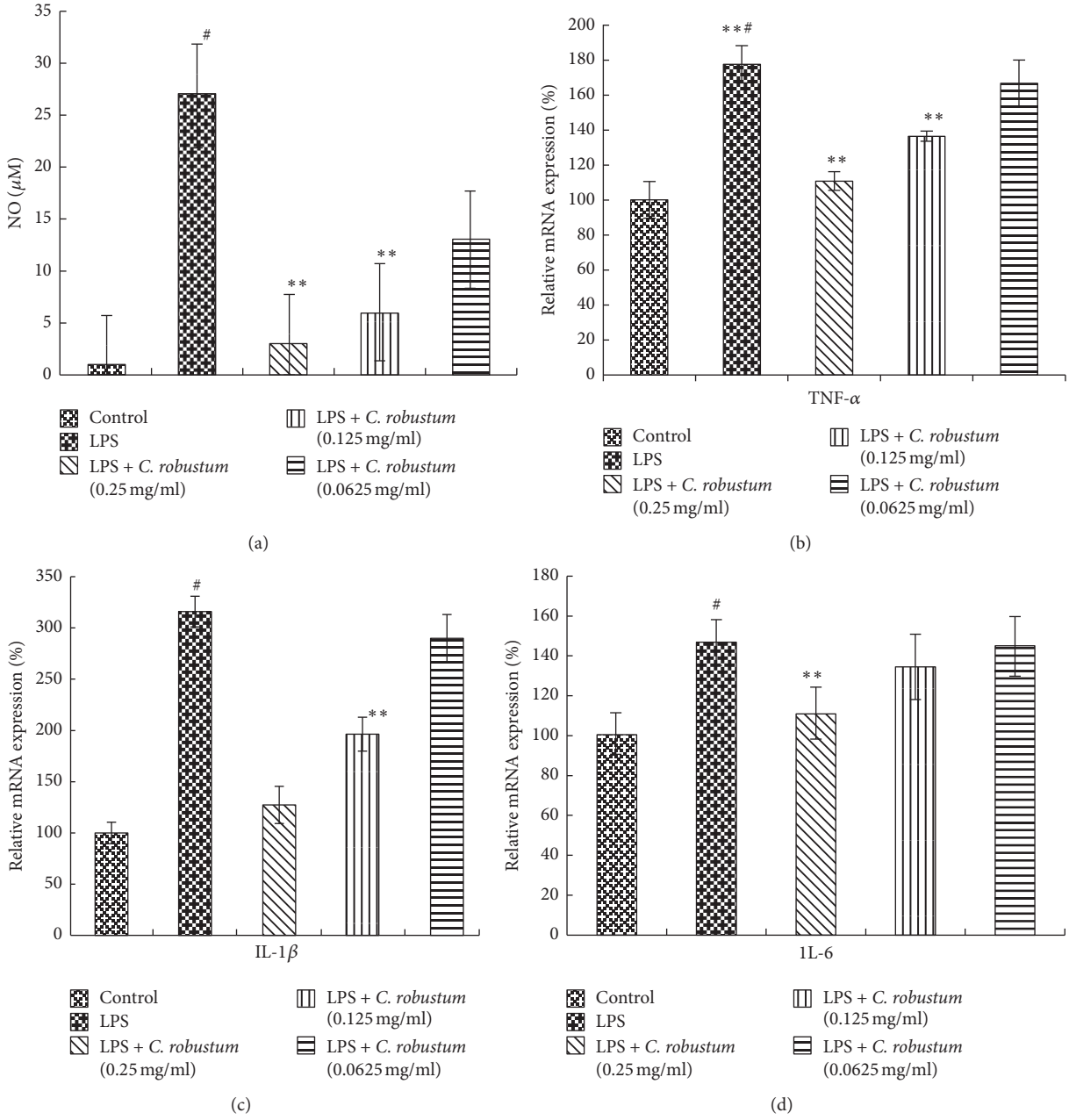

Figure 2: Effects of CRME on cytokines in RAW264.7 cells. The cells were pretreated with different concentrations (0.250, 0.125, or 0.063 mg/mL) of CRME for 1 h and then continuously incubated with 1 μg/mL LPS for 24 h. Inhibition of NO in RAW264.7 cell supernatant by Griess method. (a) Inhibition of NO in RAW264.7 cells supernatant by Griess method. (b) Real-time PCR showing the TNF-α mRNA expression in RAW264.7 cells. (c) Real-time PCR showing the IL-1β mRNA expression in RAW264.7 cells. (d) Real-time PCR showing the IL-6 mRNA expression in RAW264.7 cells. All values are expressed as the mean ± SEM from three independent experiments. Data were analyzed by two-way ANOVA, Student-Newman-Keuls test as post hoc test ($^{\#}P < 0.01$, in comparison with control; $^{**}P < 0.01$, in comparison with LPS).

with the normal group, joints of mice in the vehicle group appeared obviously swollen and red, which indicated the success of the modeling. Starting from the 10th day, arthritis indexes were significantly lower for the CIA mice in each administered group than for the model group (Figure 3(a)).

As shown in Figure 3(b), the arthritis index of the H group had a significant difference from vehicle group ($P < 0.01$) starting from the 13th day, and with the passage of time, differences between the H group and positive medicine group increased gradually with statistical significance (All $P < 0.05$). As shown in Figure 3(c), the limb swelling degree of CIA mice in the H group was significantly lower than that in the positive medicine group (All $P < 0.05$). On day 51, the CIA swelling degree of the H group had dropped to 29.8%.

Remarkably, CRME could effectively suppress the loss of body weight of CIA mice (for the L, M, and H groups versus

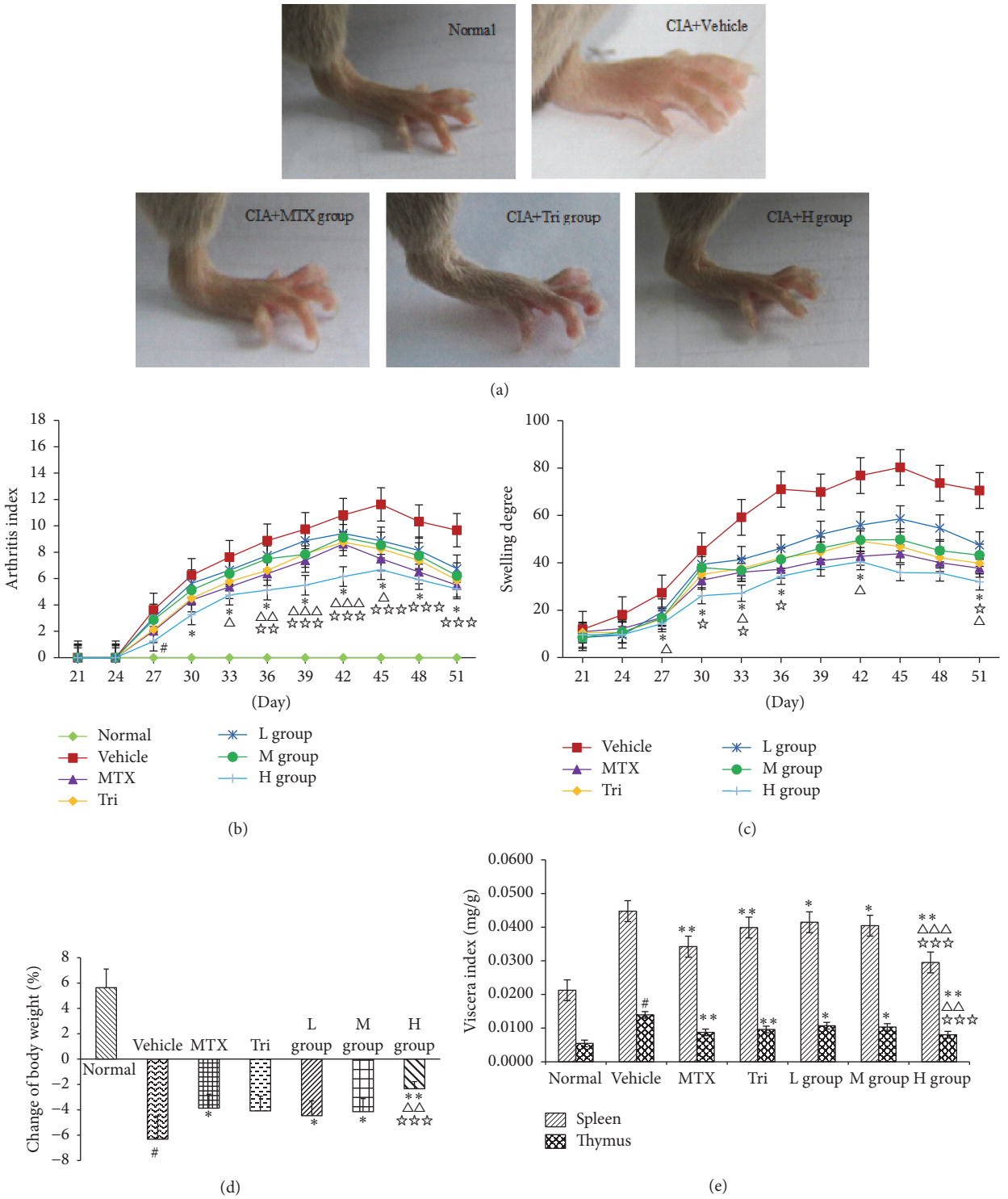

Figure 3: (a) Effect on CRME on disease progression in hind paw swelling in mice with CIA-induced arthritis. (A) Normal group, (B) CIA + vehicle, (C) CIA + MTX, (D) CIA + Tri, and (E) CIA + H group (99.4 mg/kg). Effects of CRME, MTX, and Tri treatment on the severity of disease progression as evidenced by arthritic index (b) and swelling degree (c) are presented here. There was a significant suppression of both the arthritic index and swelling degree by CRME and positive drug treatment within days 27~51. CRME on severity of arthritis of CIA mice was evaluated through body weight (d) and visceral index (e). Data are expressed as the mean ± SD of $n = 6$ animals per group. Data were analyzed by two-way ANOVA and Student-Newman-Keuls test as post hoc test ($^{\#}P < 0.01$, compared with the normal group. $^{*}P < 0.05$ and $^{**}P < 0.01$, compared with vehicle group. $^{\triangle}P < 0.05$, $^{\triangle\triangle}P < 0.01$, and $^{\triangle\triangle\triangle}P < 0.001$, compared with MTX group. $^{\star}P < 0.05$, $^{\star\star}P < 0.01$, and $^{\star\star\star}P < 0.001$, compared with Tri group).

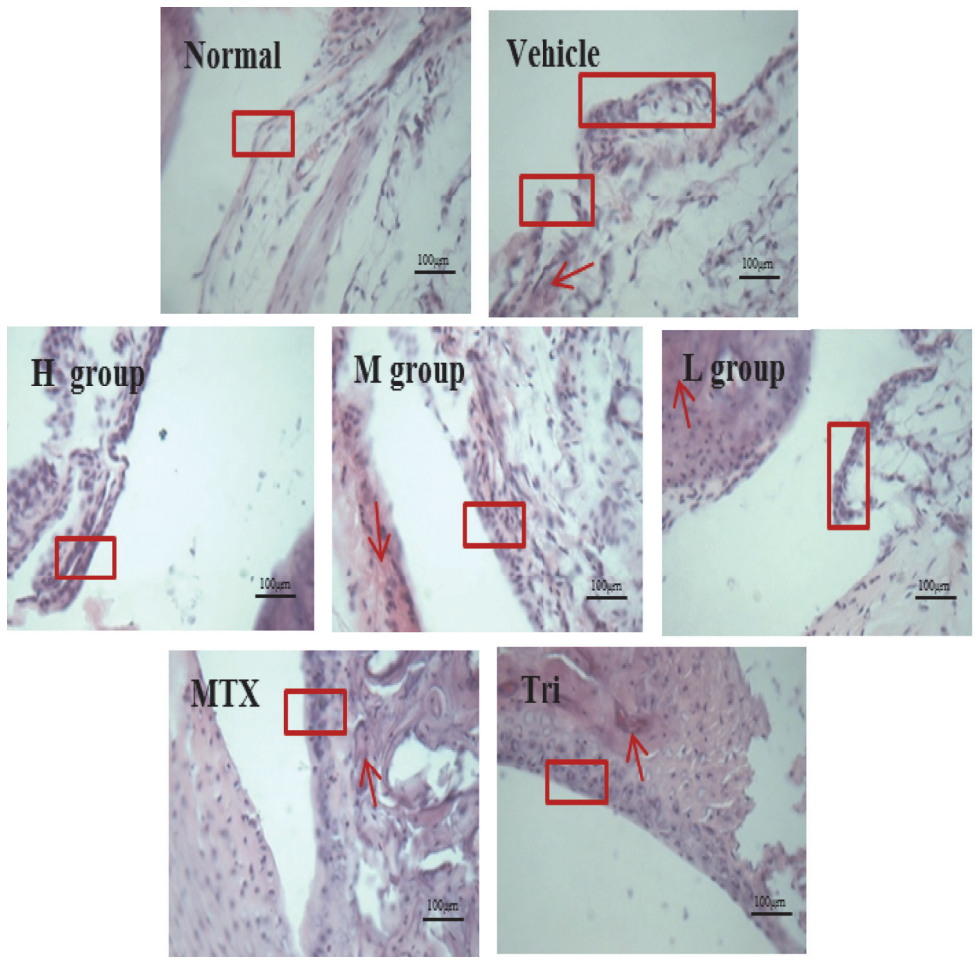

Figure 4: Influence of CRME on CIA-induced histopathological changes in the left hind limbs and immune organs of CIA-induced arthritic mice. A number of expanded vascular arteries and veins (arrows ↓) are indicated in the red boxes. HE stain, scale bars = 400 nd.

vehicle: $P < 0.05$). The weight loss of the H group was obviously lower than that of MTX and Tri, and the differences were statistically significant (All $P < 0.05$) (Figure 3(d)). In addition, the spleen index and thymus index of mice were lower in the CRME groups and positive drug groups than in the vehicle group, with significant differences (All $P < 0.01$) (Figure 3(e)).

3.4. Analysis of Histopathology. Joint pathological results (Figure 4) showed that synovial membrane hyperplasia in the normal group had not been found, its cell nuclear and cytoplasmic staining were normal, and loose underlying connective tissue was seen clearly; vascular arteries and veins showed no expansion and no blood stasis or inflammatory cell infiltration. Compared with the normal group, the synovial membrane of the vehicle group was thick, partly falling off, and uneven. It had a large number of inflammatory cells; at the same time, it was accompanied by capillary expansion. While compared with vehicle group, the synovium of CIA mice had thinned, with neat edges. The number of inflammatory cells was reduced, and capillary expansion was not obvious. Expansion of vascular arteries and veins and blood stasis were less than in the MTX (0.9 mg/kg) and Tri groups (11.3 mg/kg).

Results of histology of the left hind limbs and immune organs. At the end of the experiment, the hind limbs and immune organs of CIA mice were examined for histology. Mice in H group were orally given 99.4 mg/kg CRME. Pathological sections of joints (a part of the synovial cells in the red box, with arrows showing vascular artery and vein expansion) are shown in Figure 4.

3.5. Analysis of Proinflammatory Cytokines. TNF-α, IL-1β, IL-6, and PGE2 levels are indicated in Figure 5. As shown in the results, the levels of IL-1β, IL-6, TNF-α, and PGE2 in sera of CIA mice were apparently higher in the vehicle group than the normal group, differences that were statistically significant (All $P < 0.01$). A significant decrease in TNF-α, IL-1β, IL-6, and PGE2 levels was observed in all administered groups (H, L, and M group) when compared to the vehicle group. In addition, the levels of IL-1β, IL-6, TNF-α, and PGE2 of CIA mice were distinctly lower in the H group than in the MTX group or Tri group ($P < 0.05$), while the differences among the L group, M group, and positive drug groups were not statistically significant ($P > 0.05$) (Figure 5).

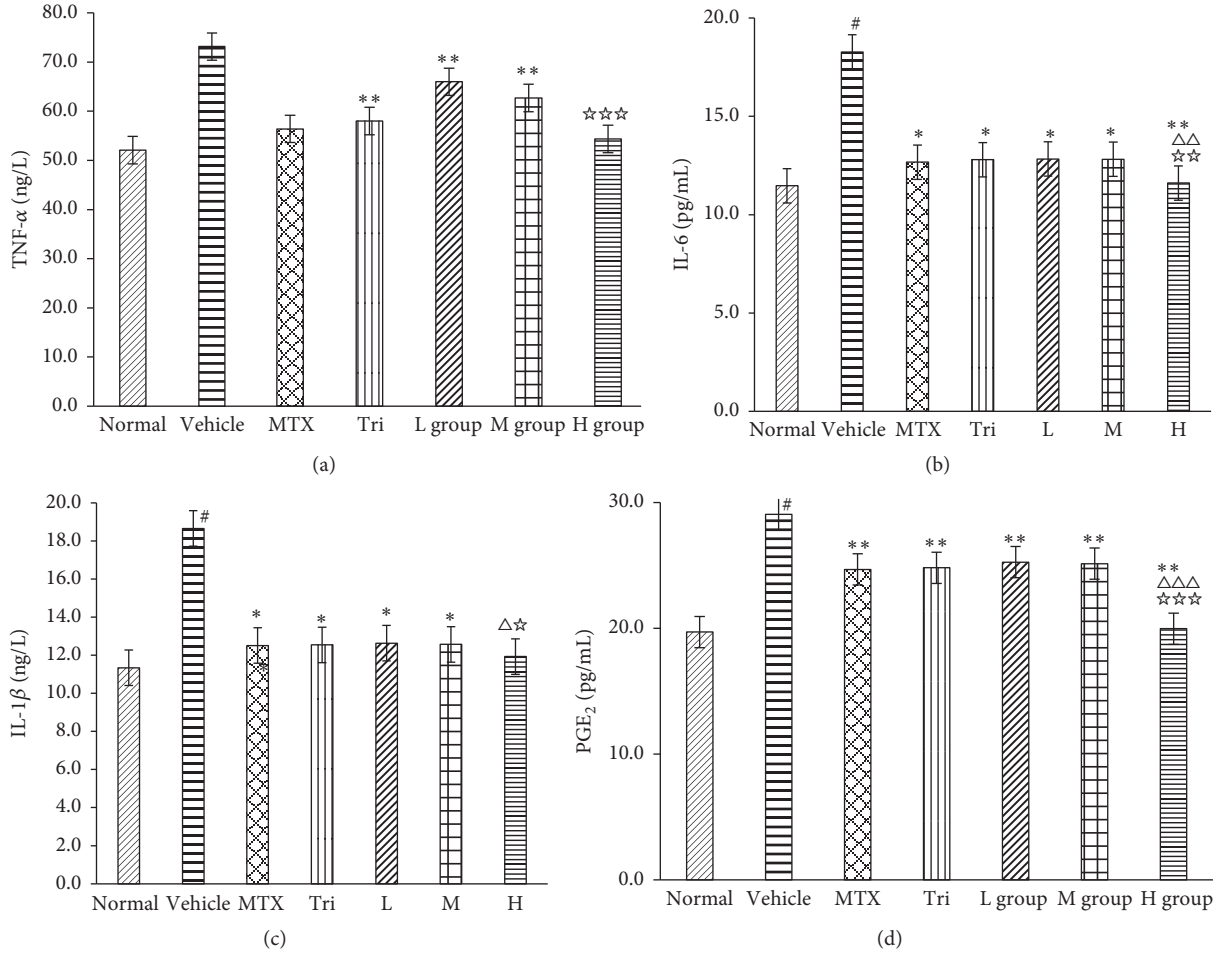

Figure 5: Effect of CRME on the secretion of proinflammatory mediators in CIA mice. The levels of TNF-α (a), IL-6 (b), IL-1β (c), and PGE2 (d) were monitored in the medium by using ELISA. Data represent the mean ± SD of three separate experiments. Data were analyzed by two-way ANOVA and Student-Newman-Keuls test as post hoc test ($^{\#}P < 0.01$, compared with the normal group. $^{*}P < 0.05$ and $^{**}P < 0.01$, compared with vehicle group. $^{\triangle}P < 0.05$, $^{\triangle\triangle}P < 0.01$, and $^{\triangle\triangle\triangle}P < 0.001$, compared with MTX group. $^{\star}P < 0.05$, $^{\star\star}P < 0.01$, and $^{\star\star\star}P < 0.001$, compared with Tri group).

3.6. Analysis of Immunohistochemistry. As shown in Figure 6(a), the NF-κB p65 positive expression parts are tan or brown particles. Data analysis indicated in Figure 6(b) shows that NF-κB p65 is expressed more positively in vehicle group than in treatment group ($P < 0.05$). What is more, the IOD volume of NF-κB p65 in CIA mice from the H group was 1325.18, which was lower than that from the positive drug group (Tri: 1765.43, MTX: 1751.42) ($P < 0.001$).

3.7. Discussion. Thus, it may be functionally important to tightly regulate the degree of phlogistic pathway activation, which could be a good therapeutic target to resist RA. For the last decade, efforts have been made to develop these agents. However, the long-term administration of anti-inflammatory drugs is limited due to the side effects. Now, there are biological inhibitors such as TNF-α inhibitors and infliximab [19, 20]. These activators can also induce specific immunity to increase the self-protection ability of the organism. An excessive inflammatory reaction can also damage target cells and tissue. Therefore, novel anti-RA agents with fewer side effects are needed. TCM can offer a promising repertoire of potentially therapeutic agents for RA [21]. *C. robustum* has often been used for treating RA patients in China. In books, such as the compendium of Chinese traditional herbal medicine, it has been recorded that *C. robustum* tincture can be made with 15 g of roots and rhizomes soaked in 300 mL of alcohol for 7 days, and this was used to treat joint pain, bruises, and RA. In this paper, we found that CRME possessed inhibitory activity against NO, IL-1β, IL-6, and TNF-α in RAW267.4 cells stimulated by LPS.

Our present data show that all the doses of CRME (24.8, 49.6, and 99.4 mg/kg) significantly inhibited edema compared to their untreated counterparts and with greater effect at 99.4 mg/kg than Tri at 11.3 mg/kg. In reducing the loss of body weight, CRME also has an advantage over MTX and Tri. Then, CRME improved histological findings by decreasing the extent of inflammatory cell infiltration and the capillary expansion of CIA mice more effectively than MTX and Tri. These results were also confirmed by the expression of inflammatory cytokines by ELISA, which showed that TNF-α, IL-6,

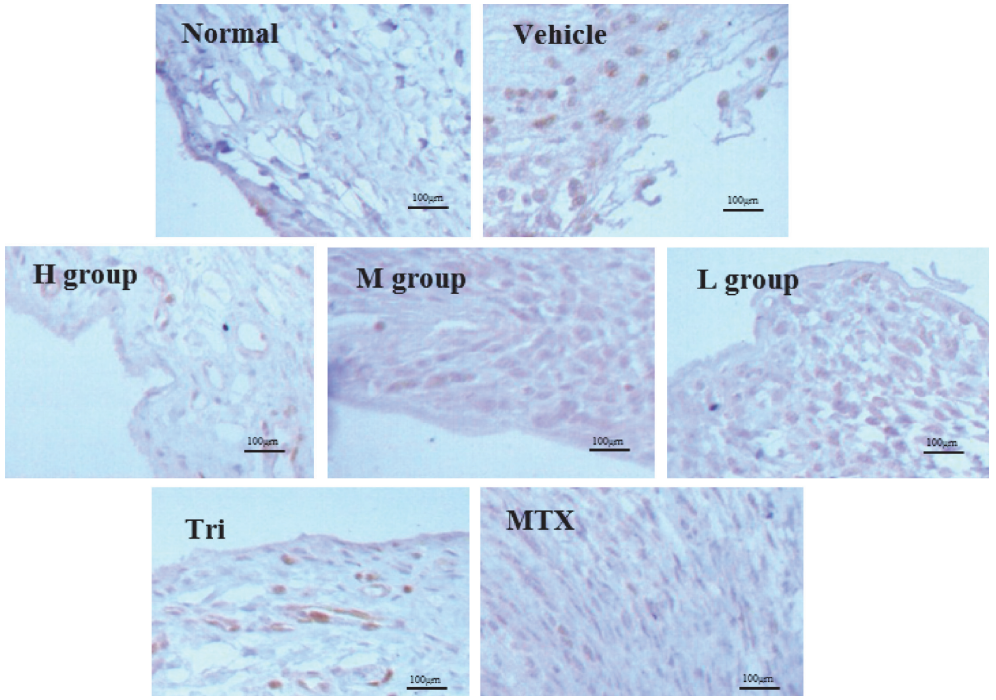

(a)

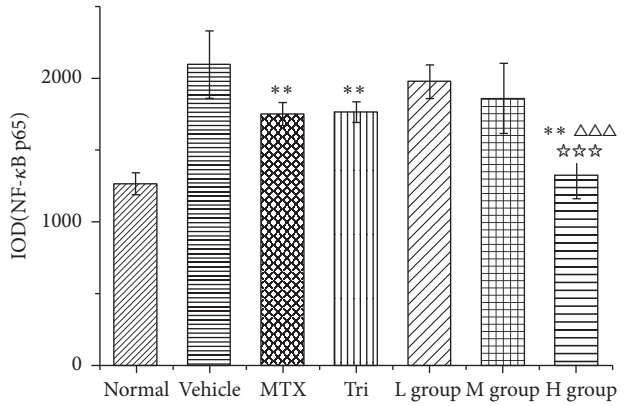

(b)

Figure 6: Analysis of immunohistochemistry of the right hind limbs. After the intervention, mice were sacrificed, and, then, the joints were subjected to immunohistochemistry for NF-κB p65. (a) NF-κB p65; (b) IOD of NF-κB p65. The data are presented as the mean ± SD with $n = 6$ mice per group. Data were analyzed by two-way ANOVA, Student-Newman-Keuls test as post hoc test ($^{*}P < 0.05$ and $^{**}P < 0.01$, compared with the vehicle group. $^{\triangle\triangle\triangle}P < 0.001$, compared with the MTX group. $^{\star}P < 0.05$ and $^{\star\star\star}P < 0.001$, compared with the Tri group). HE stain, scale bars = 400 nd.

IL-1β, and PGE2 were distinctly lower than in the MTX group and Tri group. The results showed that oral administration of CRME may effectively preserve both synovial membrane damage and inflammatory cell infiltration of inflamed joints. This clearly showed the recuperative RA function and lower toxicity of CRME at the given dosages. However, it should be noted that long-term intake of high concentration of CRME (1.59 g/kg) will show gastrointestinal irritation and vomiting from our previous study. Furthermore, Kennelly et al. showed that the alkaloid contained in the *C. robustum* had a potential teratogenic effect in mice embryonic culture experiments in vitro [12]. It has also been reported that Cauloside B and Cauloside C had cytotoxicity on the growth of sea urchin embryos by altering cell permeability [13, 14]. Kawai et al. studies have shown that Caulosides A~C have a high hemolytic effect [22]. Therefore, patients with gastrointestinal diseases and pregnant women should not use CRME.

C. robustum consists of more than 60 constituents, including sterols, triterpenes, glycosides, and alkaloids. Triterpene saponins are believed to be the major bioactive compounds contributing to the anti-inflammatory effects on RA [10]. Triterpene saponins constitute an important class of potential pharmacological agents possessing a range of different physiological activities including anticancer,

anticoagulation, anti-inflammation, antibacterial, analgesic, and comparative immune-modulation activity [23]. Recently, triterpene saponins have attracted positive research interest. Of great interest is the possibility that this class of constituents could be a source of drugs for the treatment of several diseases. We investigated the triterpene saponin content in all CRME. Our findings suggest that CRME is mainly composed of six marker compounds including Cauloside H, Leonticin D, Cauloside G, Cauloside D, Cauloside B, and Cauloside C, which constitute more than 50 percent. In particular, the abovementioned compounds seem to act as inhibitors of inflammatory factors [24].

The inhibition of NF-κB might result in a marked amelioration of chronic inflammation by suppressing the production of cytokines [25]. Measurable levels of cytokines such as TNF-α, IL-6, IL-1β, and PGE2 are found locally in synovial tissue, the major site of inflammation in CIA as well as RA, where they facilitate the local and systemic inflammatory response [26, 27]. Existing research showed that the NF-κB in synovial cells induced by TNF-α can mediate nuclear transfer leading to NF-κB signaling pathway activation [28]. To be more specific, to activate the NF-κB pathway, TNF-α has a variety of signal molecules involved, including TNFR related factor, RIP (receptor interacting protein), MAP3K (mitogen activated protein kinase 3), and IKK compounds [29]. In turn, TNF-α produces physiological reaction via NF-κB acting as an important mediator, and activated NF-κB can also induce the expression of TNF-α and enhance TNF-α gene transcription. In some cells and tissues, NF-κB p65 and TNF-α both promote each other, which creates a vicious cycle that increases RA. In RA, IL-6 mainly induces liver cell synthesis of a variety of acute phase reaction proteins and promotes the synthesis of B cells to produce immunoglobulin and rheumatoid factor [30]. It has been confirmed that NF-κB can promote gene transcription of inflammation factors such as TNF-α, IL-6, and IL-1β [31]. In addition, it might enhance the inflammatory damage of TNF-α and IL-1 by improving the generation and release of TNF-α and IL-1β [32]. IL-1β is of importance in passing information and mediating immune cell activation, proliferation, and inflammatory response. IL-1β, acting as another important extracellular cue, can activate NF-κB to amplify the inflammatory response. NF-κB is promoted to transport into the nucleus by IL-1β, where it combines with the promoters of target genes to start target protein expression [33]. As one of the most important targets for the treatment of inflammation and tumor molecules, PGE2 can promote the division and proliferation of fibroblasts and induce microvascular formation and growth [34]. Like TNF-α, IL-6, and IL-1β, PGE2 participates in synovium and joint inflammation of surrounding tissue, cartilage destruction, and hyperplasia lesions through the NF-κB signaling pathway [35].

We confirmed that the pathogenesis of CIA was accompanied by a substantial increase in the levels of TNF-α, IL-6, IL-1β, and PGE2 in the plasma of mice. Interestingly, the administration of CRME drastically reduced the levels of these four proinflammatory cytokines significantly. Our results indicated that CRME effectively improved arthritic symptoms including limb swelling by downregulating the production of proinflammatory cytokines. Further, we suspect that CRME, being an important negative regulator of these proinflammatory cytokines related to RA, might work by suppressing the expression of NF-κB.

4. Conclusions

It has been thoroughly demonstrated that CRME is an anti-inflammatory drug as observed under morphological study in CIA mice. This was evident from not only the significantly improved symptoms of the arthritis index and limb swelling but also the improved histological findings of decreased synovial membrane damage and inflammatory cell infiltration in CIA mice. We also revealed that the protective mechanisms of CRME treatment could be partially explained by a decrease in the proinflammatory cytokines TNF-α, IL-6, IL-1β, and PGE2. Specifically, it has been found to be very effective at ameliorating the damage resulting from progression of arthritis by controlling the expression of NF-κB. Additional studies are required with more physiological and pharmaceutical investigations to establish its clinical applicability.

Conflicts of Interest

The authors declare that there are no conflicts of interest.

Authors' Contributions

Qiu-hong Wang and Shao-wa Lv conceived and designed the experiments and equally contributed to this work. Hai-xue Kuang and Yu-yan Guo guided the experiment.

Acknowledgments

This work was supported by the National Major Scientific and Technological Special Project for National Natural Science Foundation of China (no. 81373929, no. 81473351, and no. 81703724); "Significant New Drugs Development" during the Twelfth Five-Year Plan Period, China (no. 2013ZX09102019); plan to the project of innovative talents of Heilongjiang University of Chinese Medicine (2012); and plan to the project of innovative talents of Education Department of Heilongjiang Province (2016).

References

[1] A. R. Mohamed and W. F. El-Hadidy, "Effect of orexin-A (hypocretin-1) on hyperalgesic and cachectic manifestations of experimentally induced rheumatoid arthritis in rats," *Canadian Journal of Physiology and Pharmacology*, vol. 92, no. 10, pp. 813–820, 2014.

[2] A. Shetty, R. Hanson, P. Korsten et al., "Tocilizumab in the treatment of rheumatoid arthritis and beyond," *Drug Design, Development and Therapy*, vol. 8, pp. 349–364, 2014.

[3] J.-D. Lee, J.-E. Huh, Y.-H. Baek, K.-C. Cho, D.-Y. Choi, and D.-S. Park, "The efficacy and mechanism action of RvCSd, a new herbal agent, on immune suppression and cartilage protection in a mouse model of rheumatoid arthritis," *Journal of Pharmacological Sciences*, vol. 109, no. 2, pp. 211–221, 2009.

[4] Z.-J. Shao, X.-W. Zheng, T. Feng et al., "Andrographolide exerted its antimicrobial effects by upregulation of human β-defensin-2 induced through p38 MAPK and NF-kB pathway in human lung epithelial cells," *Canadian Journal of Physiology and Pharmacology*, vol. 90, no. 5, pp. 647–653, 2012.

[5] Z. Han, D. L. Boyle, A. M. Manning, and G. S. Firestein, "AP-1 and NF-κB regulation in rheumatoid arthritis and murine collagen-induced arthritis," *Autoimmunity*, vol. 28, no. 4, pp. 197–208, 1998.

[6] T. Nishiya, T. Uehara, M. Kaneko, and Y. Nomura, "Involvement of nuclear factor-κB (NF-κB) signaling in the expression of inducible nitric oxide synthase (iNOS) gene in rat C6 glioma cells," *Biochemical and Biophysical Research Communications*, vol. 275, no. 2, pp. 268–273, 2000.

[7] E. B. Kopp and S. Ghosh, "NF-κB and rel proteins in innate immunity," *Advances in Immunology*, vol. 58, pp. 1–27, 1995.

[8] C. L. H. Yang, T. C. T. Or, M. H. K. Ho, and A. S. Y. Lau, "Scientific basis of botanical medicine as alternative remedies for rheumatoid arthritis," *Clinical Reviews in Allergy & Immunology*, vol. 44, no. 3, pp. 284–300, 2013.

[9] I. K. Campbell, D. S. Piccoli, and J. A. Hamilton, "Stimulation of human chondrocyte prostaglandin E_2 production by recombinant human interleukin-1 and tumour necrosis factor," *Biochimica et Biophysica Acta (BBA)—Molecular Cell Research*, vol. 1051, no. 3, pp. 310–318, 1990.

[10] Y.-G. Xia, G.-Y. Li, J. Liang, B.-Y. Yang, S.-W. Lü, and H.-X. Kuang, "Genus caulophyllum: an overview of chemistry and bioactivity," *Evidence-Based Complementary and Alternative Medicine*, vol. 2014, Article ID 684508, 18 pages, 2014.

[11] S. P. Jiao, T. L. Yu, H. Jiang et al., "Anti-inflammatory effects of water decoction of C. robustum," *Journal of Jilin medical college*, vol. 17, no. 1, pp. 8-9, 1997.

[12] E. J. Kennelly, T. J. Flynn, E. P. Mazzola et al., "Detecting potential teratogenic alkaloids from blue cohosh rhizomes using an in vitro rat embryo culture," *Journal of Natural Products*, vol. 62, no. 10, pp. 1385–1389, 1999.

[13] D. Aminin, I. Agafonova, S. Gnedoi, L. Strigina, and M. Anisimov, "The effect of pH on biological activity of plant cytotoxin cauloside C," *Comparative Biochemistry and Physiology A: Molecular Integrative Physiology*, vol. 122, no. 1, pp. 45–51, 1999.

[14] M. M. Anisimov, E. B. Shentsova, V. V. Shcheglov et al., "Mechanism of cytotoxic action of some triterpene glycosides," *Toxicon*, vol. 16, no. 3, pp. 207–218, 1978.

[15] E. Küpeli, M. Koşar, E. Yeşilada, K. H. C. Başer, and C. Başer, "A comparative study on the anti-inflammatory, antinociceptive and antipyretic effects of isoquinoline alkaloids from the roots of Turkish Berberis species," *Life Sciences*, vol. 72, no. 6, pp. 645–657, 2002.

[16] Y. C. Yang, S. Z. Chen, H. Y. Yang et al., "Experimental study on anti-inflammatory and analgesic effects of three kinds of organic extracts of Leonticerobustum," *Chinese Journal of Practical Medicine*, vol. 32, no. 2, pp. 1–3, 2007.

[17] X.-L. Wang, B.-R. Liu, C.-K. Chen, J.-R. Wang, and S.-S. Lee, "Four new fluorenone alkaloids and one new dihydroazafluoranthene alkaloid from Caulophyllum robustum Maxim," *Fitoterapia*, vol. 82, no. 6, pp. 793–797, 2011.

[18] S. Lü, H. Su, F. Yu et al., "Therapeutic effect and mechanism of caulophyllum robustum maxim extract on adjuvant arthritis rats," *Traditional Chinese Drug Research & Clinical Pharmacology*, vol. 28, no. 2, pp. 164–171, 2017.

[19] S. Lü, Q. Wang, G. Li, S. Sun, Y. Guo, and H. Kuang, "The treatment of rheumatoid arthritis using Chinese medicinal plants: from pharmacology to potential molecular mechanisms," *Journal of Ethnopharmacology*, vol. 176, pp. 177–206, 2015.

[20] C. Liu, Y. Zhang, X. Kong et al., "Triptolide prevents bone destruction in the collagen-induced arthritis model of rheumatoid arthritis by targeting RANKL/RANK/OPG signal pathway," *Evidence-Based Complementary and Alternative Medicine*, vol. 2013, Article ID 626038, 12 pages, 2013.

[21] H. Du and X. Xu, "Progress in pathogenesis of rheumatoid arthritis in recent five years," *Journal of Liaoning University of Traditional Chinese Medicine*, vol. 17, no. 10, pp. 77–80, 2015.

[22] H. Kawai, M. Kuroyanagi, K. Umehara, A. Ueno, and M. Satake, "Studies on the saponins of Lonicera japonica THUNB," *Chemical & Pharmaceutical Bulletin*, vol. 36, no. 12, pp. 4769–4775, 1988.

[23] X.-H. Cheng and Y.-Q. Xiong, "Research progress on the pharmacological action of triterpene saponins," *Chinese Traditional and Herbal Drugs*, vol. 38, no. 5, pp. 792–795, 2007.

[24] Y. Lee, J.-C. Jung, Z. Ali, I. A. Khan, and S. Oh, "Anti-inflammatory effect of triterpene saponins isolated from blue cohosh (caulophyllum thalictroides)," *Evidence-Based Complementary and Alternative Medicine*, vol. 2012, Article ID 798192, 8 pages, 2012.

[25] I. Matsumoto, A. Inoue, C. Takai et al., "Regulatory roles of tumor necrosis factor alpha-induced proteins (TNFAIPs) 3 and 9 in arthritis," *Clinical Immunology*, vol. 153, no. 1, pp. 73–78, 2014.

[26] C. Georganas, H. Liu, H. Perlman, A. Hoffmann, B. Thimmapaya, and R. M. Pope, "Regulation of IL-6 and IL-8 expression in rheumatoid arthritis synovial fibroblasts: the dominant role for NF-kappa B but not C/EBP beta or c-Jun," *The Journal of Immunology*, vol. 165, no. 12, pp. 7199–7206, 2000.

[27] D. Sahu, S. K. Raghav, H. Gautam, and H. R. Das, "A novel coumarin derivative, 8-methoxy chromen-2-one alleviates collagen induced arthritis by down regulating nitric oxide, NFκB and proinflammatory cytokines," *International Immunopharmacology*, vol. 29, no. 2, pp. 891–900, 2015.

[28] X. J. Luo, X. R. Mo, and L. L. Zhou, "Activation of NF-κB signal pathway by TNF-α in synoviocytes of Rheumatoid arthritis," *Immunological Journal*, vol. 28, no. 4, pp. 321–323, 2012.

[29] H. Shi, D. T. Wang, R. G. Wu et al., "Role of tumor necrosis factor-α mediated nuclear factor Kappa B signaling pathway in antiogenesis in rheumatoid arthritis," *Medical Recapitulate*, vol. 18, no. 15, pp. 2397–2400, 2012.

[30] T. Okamoto, S. Yamagishi, Y. Inagaki et al., "Angiogenesis induced by advanced glycation end products and its prevention by cerivastatin," *The FASEB Journal*, vol. 16, no. 14, pp. 1928–1930, 2002.

[31] Q. Li, X. Z. Huang, H. M. Ding et al., "Change of interleukin-6 level in rheumatoid arthritis patients," *Guangdong Medical Journal*, vol. 28, no. 5, pp. 712-713, 2007.

[32] M. Liu, Q. J. Ding, and T. Liang, "The potential therapeutic target of Rheumatoid arthritis-NF-κB," *Chinese Journal of Cellular and Molecular Immunology*, vol. 24, no. 6, pp. 651–653, 2008.

[33] E. Choy, "Clinical experience with inhibition of interleukin-6," *Rheumatic Disease Clinics of North America*, vol. 30, no. 2, pp. 405–415, 2004.

[34] G. D. Anderson, K. L. Keys, P. A. De Ciechi, and J. L. Masferrer, "Combination therapies that inhibit cyclooxygenase-2 and leukotriene synthesis prevent disease in murine collagen induced arthritis," *Inflammation Research*, vol. 58, no. 2, pp. 109–117, 2009.

[35] H.-S. Lee, C.-H. Lee, H.-C. Tsai, and D. M. Salter, "Inhibition of cyclooxygenase 2 expression by diallyl sulfide on joint inflammation induced by urate crystal and IL-1β," *Osteoarthritis and Cartilage*, vol. 17, no. 1, pp. 91–99, 2009.

Hindawi
Evidence-Based Complementary and Alternative Medicine
Volume 2017, Article ID 5193548, 9 pages
https://doi.org/10.1155/2017/5193548

Research Article

Tang-Luo-Ning, a Traditional Chinese Medicine, Inhibits Endoplasmic Reticulum Stress-Induced Apoptosis of Schwann Cells under High Glucose Environment

Weijie Yao, Xinwei Yang, Jiayue Zhu, Biane Gao, Renhui Liu, and Liping Xu

Beijing Key Lab of TCM Collateral Disease Theory Research, School of Traditional Chinese Medicine, Capital Medical University, Beijing, China

Correspondence should be addressed to Liping Xu; xulp@ccmu.edu.cn

Received 25 May 2017; Revised 6 September 2017; Accepted 13 September 2017; Published 21 November 2017

Academic Editor: Lucindo J. Quintans-Júnior

Tang-Luo-Ning (TLN) has a definite effect in the clinical treatment of diabetic peripheral neuropathy (DPN). Schwann cells (SCs) apoptosis induced by endoplasmic reticulum stress (ER stress) is one of the main pathogeneses of DPN. This study investigates whether TLN can inhibit SCs apoptosis by inhibiting ER stress-induced apoptosis. Our previous researches have demonstrated that TLN could increase the expression of ER stress marker protein GRP78 and inhibited the expression of apoptosis marker protein CHOP in ER stress. In this study, the results showed that TLN attenuated apoptosis by decreasing Ca^{2+} level in SCs and maintaining ER morphology. TLN could decrease downstream proteins of CHOP including GADD34 and Ero1α, while it increased P-eIF2α and decreased the upstream proteins of CHOP including P-IRE1α/IRE1α and XBP-1, thereby reducing ER stress-induced apoptosis.

1. Background

Diabetic peripheral neuropathy (DPN) is a major complication of diabetes [1] and its pathogenesis is complex. Schwann cells (SCs) apoptosis induced by hyperglycemia is involved in the pathogenesis of DPN [2]. SCs, as the peripheral myelin-forming cells, play an important role in maintaining the structure and function of peripheral nerves [3]. SCs apoptosis induced by hyperglycemia is a key factor in decreasing nerve conduction velocity and increasing thermal perception threshold, axon atrophy, and demyelination of DPN [4, 5].

Recent studies have shown that endoplasmic reticulum stress- (ER stress-) induced apoptosis is involved in the pathogenesis of DPN [6, 7]. ER stress results from the accumulation of unfolded proteins or misfolded proteins in the ER. Unfolded protein response (UPR) can be activated for restoring homeostasis of ER. But persistent ER stress can also induce apoptosis [8]. Therefore, we explore the mechanism of SCs apoptosis induced by ER stress and provide new ideas for further studying the pathogenesis of DPN.

Tang-Luo-Ning (TLN) is a traditional Chinese medicine (TCM), designed based on Huangqi Guizhi Wuwu decoction, and the treatments were replenishing Qi and nourishing Yin, nourishing liver and kidney, eliminating blood stasis, and dredging collaterals under the guidance of collateral disease theory. Previous clinical studies confirmed that TLN could improve the pain and numbness of DPN patients, decrease diabetic neuropathy score, and improve the sensory and motor nerve conduction velocity, thus improving the patient's neurological function. The total effective rate can be up to 93.8% [9, 10]. Experimental studies also showed that improving DPN is associated with antioxidant stress and decreasing SCs apoptosis [11]. Oxidative stress is closely related to ER stress. They interplay each other and both aggravate SCs apoptosis [12]. Our previous study also demonstrated that TLN could increase the expression of ER stress marker protein GRP78 and inhibited the expression of apoptosis marker protein CHOP in ER stress and then increase the expression of Bcl-2 and decrease the expression of Bax [11]. This study aims to investigate whether TLN can inhibit CHOP-related pathway to inhibit ER stress-induced apoptosis.

2. Materials and Methods

2.1. Preparation of TLN. TLN is composed of 15 g of Huangqi, 15 g of Danshen, 15 g of Gouji, 12 g of Chuanniuxi, 10 g of Yanhusuo, 15 g of Mugua, 12 g of Chishao, and 15 g of Jixueteng. The specimen of 8 crude drug materials has been stored in a publicly available herbarium in the School of Traditional Chinese Medicine. The mixture was decocted twice; then filtrate was evaporated to TLN powder. The quality control method of TLN was previously described by Yang et al. [13]. TLN powder was dissolved in distilled water. Then, TLN solution was used for intragastric administration.

2.2. Preparation of TLN Serum. 30 SPF-grade male Sprague-Dawley (SD) rats (200 ± 20 g) were obtained from Experimental Animal Center of Capital Medical University. All experimental procedures were conducted in accordance with the protocol for using animals, which were approved by the Ethics Review Committee for Animal Experimentation of Capital Medical University (Ethical Inspection Number: AEEI-2014-086). Rats were maintained at room temperature (20–25°C) under constant humidity (40–70%) under a 12-hour light-dark cycle in a pathogen-free laboratory and allowed free access to water and standard laboratory diet. Rats were randomly divided into three groups, 15 for control, 10 for trimethylamine N-oxide (TMAO, Sigma), and 10 for TLN groups, and were intragastrically given distilled water, 110 mg/kg/day TMAO suspension, and 10.9 g crude drug/kg/day TLN, respectively, for 8 days. One hour after the last administration, rats were anesthetized with 10% chloral hydrate (i.p., 0.35 g/kg body weight). Blood was sterilely collected through the ventral aorta. After settling for 2 hours at room temperature, the blood samples were centrifuged at 3000 r/min at 4°C for 15 min and inactivated at 56°C for 30 min. The samples were stored at −80°C after being filtered through a microfiltration membrane (0.22 μm).

2.3. Cell Culture. RSC96 cells (obtained from the American Type Culture Collection, ATCC) were cultured in Dulbecco's Modified Eagle's Medium (DMEM) modified to contain 4 mmol L-glutamine, 25 mmol/L glucose, 1 mmol sodium pyruvate, 1500 mg/L sodium bicarbonate, and 10% fetal bovine serum (FBS, Gibco/Invitrogen Corporation, Carlsbad, CA, USA) in a humidified atmosphere of 5% CO_2 at 37°C.

2.4. Measurement of Cell Viability. RSC96 cells were seeded at a suitable density (4×10^3 cells/well for 24 hours and 3×10^3 cells/well for 48 hours) in 96-well plate and allowed to attach overnight and then were treated with 150 mM glucose (Sigma) and various concentrations of TLN serum (10%, 1%, and 0.1%) for 24 hours and 48 hours. After treatment, 100 μL of MTT (5 mg/mL, Sigma) solution was added and incubated for 4 hours at 37°C. Then MTT solution was removed and DMSO was added (150 μL/well) for incubation for 10 min at room temperature. Cell viability was measured at 490 nm by using SpectraMax Plus 384 Microplate Reader (Molecular Devices, Sunnyvale, CA, USA). The results were indicated as a percentage of the absorbance of 25 mM glucose cells.

2.5. Measurement of Ca^{2+} Level. RSC96 cells were seeded at a suitable density (4×10^5 cells/well for 24 hours and 3×10^5 cells/well for 48 hours) in 6-well plate and allowed to attach overnight and then were treated differently as described above in Section 2.4. After that, RSC96 cells were lysed by 0.25% trypsin (without EDTA) and collected, incubated by Fluo-3 (0.5 μM, Beyotime) in 37°C for 30 min keep in dark place, and then analyzed by BD LSRFortessa™ flow cytometry (BD Biosciences, San Jose, CA, USA).

2.6. Ultrastructure Observation of ER. RSC96 cells were seeded at a suitable density (4×10^5 cells/well for 24 hours and 3×10^5 cells/well for 48 hours) in 6-well plate and allowed to attach overnight and then were treated differently as described above in Section 2.4. After that, RSC96 cells were lysed with 0.25% trypsin (without EDTA) and brought together by centrifuging (2000 rpm × 5 min) and then were fixed with 2.5% glutaraldehyde for 3 hours followed by storage in phosphate buffer (PB) and then were sent to the Electron Microscopy Center of Capital Medical University for ultrastructure observation.

2.7. High Content Analysis. RSC96 cells were seeded at a suitable density (4×10^3 cells/well for 24 hours and 3×10^3 cells/well for 48 hours) in 96-well plate and allowed to attach overnight and then were treated differently as described above in Section 2.4. After that, RSC96 cells were fixed with 4% paraformaldehyde at room temperature for 30 min and then permeabilized with 0.5% Triton-X100 in ice bath for 30 min. After being blocked by 3% BSA at room temperature for 30 min, RSC96 cells were incubated with anti-GADD34 (1 : 50, Santa Cruz, sc-8327) and anti-XBP-1 (1 : 200, Abcam, ab37152) antibodies at 4°C overnight, respectively. RSC96 cells were incubated with goat anti-rabbit IgG FITC (1 : 100) at room temperature for 2 hours (in the dark) and then were counterstained with DAPI (Roche) at room temperature for 5 min. Cell images were acquired by using Thermo Fisher Scientific Cellomics ArrayScan VTI High Content Screening Reader and images were analyzed by using the Compartmental Analysis BioApplication (Thermo Fisher Scientific). The results were indicated as a percentage of the average intensity of 25 mM glucose cells.

2.8. Western Blot Analysis. RSC96 cells were seeded at a suitable density (4×10^5 cells/well for 24 hours and 3×10^5 cells/well for 48 hours) in 6-well plate and allowed to attach overnight and then were treated differently as described above in Section 2.4. After that, cells were lysed in RIPA lysis buffer (including proteinase inhibitor cocktail and phosphatase inhibitor cocktail) in ice bath for 15 min and centrifuged (12,000 rpm/min, 4°C) for 10 min; then supernatant was collected. Then concentration of protein was measured by BCA Protein Assay Kit and DTT loading buffer was added to prepare samples. Equal amounts of protein (20 μg) were separated by electrophoresis in 10% SDS-PAGE gel and transferred to a 0.45 μm PVDF membrane (Millipore) by wet transfer system (Bio-Rad, USA) or semidry transfer system (Wealtec, USA). Blots in PVDF membrane were blocked with 5% nonfat-dried milk (phosphoproteins were

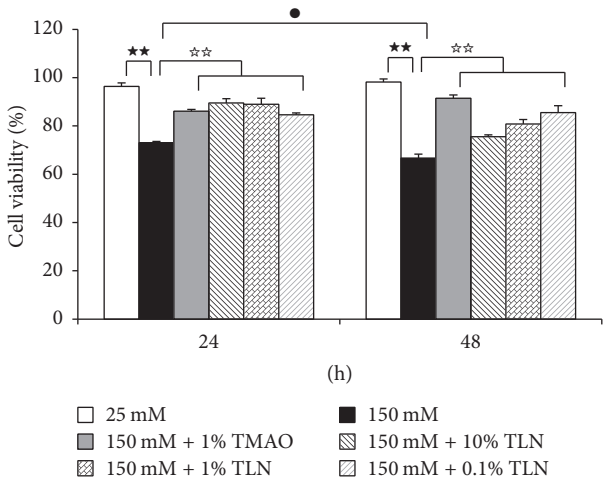

Figure 1: *TLN inhibited high glucose-induced cytotoxicity of RSC96 cells.* Data were analyzed by one-way ANOVA followed by least significant difference. Data were shown as mean ± SEM ($n = 4$). $^{\star\star}P < 0.01$ versus 25 mM glucose; $^{\star\star}P < 0.01$ versus 150 mM glucose. $^{\bullet}P < 0.05$, 150 mM glucose at 24 hours versus 150 mM glucose at 48 hours.

blocked with 2% bovine serum albumin) for 2 hours at room temperature and then incubated with primary antibodies overnight at 4°C. Then goat anti-mouse and goat anti-rabbit antibodies were added to corresponding blots and reacted for 1 hour at room temperature followed by incubation in electrochemiluminescence (ECL) reagent (Millipore). Blots were exposed to X-film to form image. β-Actin antibody (1 : 2000, Zhongshan Golden Bridge, TA-09) was to ensure normalization of results. Quantitative analysis was measured by using ImageJ software. The following primary antibodies were used: mouse monoclonal anti-Ero1α (1 : 500, Santa Cruz, sc-100805); rabbit polyclonal anti-IRE1α (1 : 2000, Santa Cruz, sc-20790), anti-P-IRE1α (1 : 2000, Abcam, ab48187), and anti-P-eIF2α (1 : 1500, Santa Cruz, sc-293100).

2.9. Statistical Analysis. SPSS17.0 was used to analysis data. Data was presented as mean ± standard error of mean (SEM). Between-group differences were assessed using one-way analysis of variance (ANOVA). $P < 0.05$ was considered to be significant.

3. Results

3.1. TLN Inhibited High Glucose-Induced Cytotoxicity of RSC96 Cells. Cell viability test was conducted by MTT assay and it aimed to evaluate the protective effect of TLN serum for SCs. The results showed that, after incubation with high glucose for 24 hours and 48 hours, cell viability in 150 mM glucose group decreased significantly ($P < 0.01$); TLN serum could increase RSC96 cell viability in high glucose environment ($P < 0.01$) (Figure 1).

3.2. TLN Decreased High Glucose-Induced Ca^{2+} Level of RSC96 Cell. Increasing Ca^{2+} level is recognized to be a factor for cell apoptosis [14, 15]. Results showed that Ca^{2+} level in 150 mM glucose group increased significantly compared with 25 mM group ($P < 0.01$), and TLN serum decreased Ca^{2+} level significantly ($P < 0.01$), thus alleviating high glucose-induced apoptosis (Figure 2).

3.3. TLN Protected the Integrity of the ER Morphology under High Glucose Environment. As shown in Figure 3, ER membrane structure in 25 mM glucose group is clear and intact (Figure 3(a) of 24 hours and 48 hours), while in 150 mM glucose group morphology of ER partially swelled and was not uniform (Figure 3(b) of 24 hours and 48 hours); particularly in 150 mM glucose group at 48 hours, fragmental morphology of ER appeared (Figure 3(b) at 48 hours). In 150 mM glucose + TLN group, morphology of ER tended to have integral structure (Figures 3(d), 3(e), and 3(f)); it demonstrates that TLN can protect the integrity of the ER morphology.

3.4. TLN Regulated Related Protein Expression of ER Stress-Induced Apoptotic Pathway of RSC96 Cells by High Glucose. CHOP can induce apoptosis directly or indirectly [16]. Our previous study also demonstrated that TLN could increase the expression of ER stress marker protein GRP78 and inhibited the expression of apoptosis marker protein CHOP in ER stress and then increased the expression of Bcl-2 and decreased the expression of Bax [11]. We further measured the expressions of GADD34, P-eIF2α, and Ero1α which are CHOP-related proteins. We first found that the expressions of GADD34 and Ero1α in 150 mM glucose group increased significantly compared with the control group ($P < 0.01$) (Figures 4(c) and 4(d)); they showed the same trend compared with the expression of CHOP, while P-eIF2α was inhibited by GADD34 and decreased ($P < 0.05$ and $P < 0.01$) (Figure 4(e)). TLN serum can decrease the expression of GADD34 and Ero1α but increase the expression of P-eIF2α ($P < 0.05$ and $P < 0.01$) (Figures 4(c), 4(d), and 4(e)). The results also show that TLN can inhibit ER stress-induced apoptosis.

Because TLN decreased ER stress-related apoptotic protein CHOP induced by high glucose, we hypothesized whether it resulted from downregulating the expression of CHOP upstream proteins. IRE1α is one of three UPR transmembrane proteins that can induce CHOP protein expression by inducing expression of XBP-1 [17]. Therefore, we continued to measure the expressions of IRE1α and XBP-1 to observe whether TLN can inhibit the ER stress-induced apoptosis by inhibiting their expression. We found that the expressions of P-IRE1α/IRE1α and XBP-1 in 150 mM glucose group increased significantly compared with the 25 mM glucose group ($P < 0.05$ and $P < 0.01$) (Figures 5(c)–5(f)); they showed the same trend compared with the expression of CHOP. The expressions of P-IRE1α/IRE1α at 48 hours and XBP-1 at both 24 hours and 48 hours decreased significantly in 150 mM glucose + TLN group compared with the 150 mM glucose group ($P < 0.05$ and $P < 0.01$) (Figures 5(c)–5(f)). This demonstrated that TLN can inhibit ER stress-induced apoptosis by inhibiting the expressions of IRE1α and XBP-1.

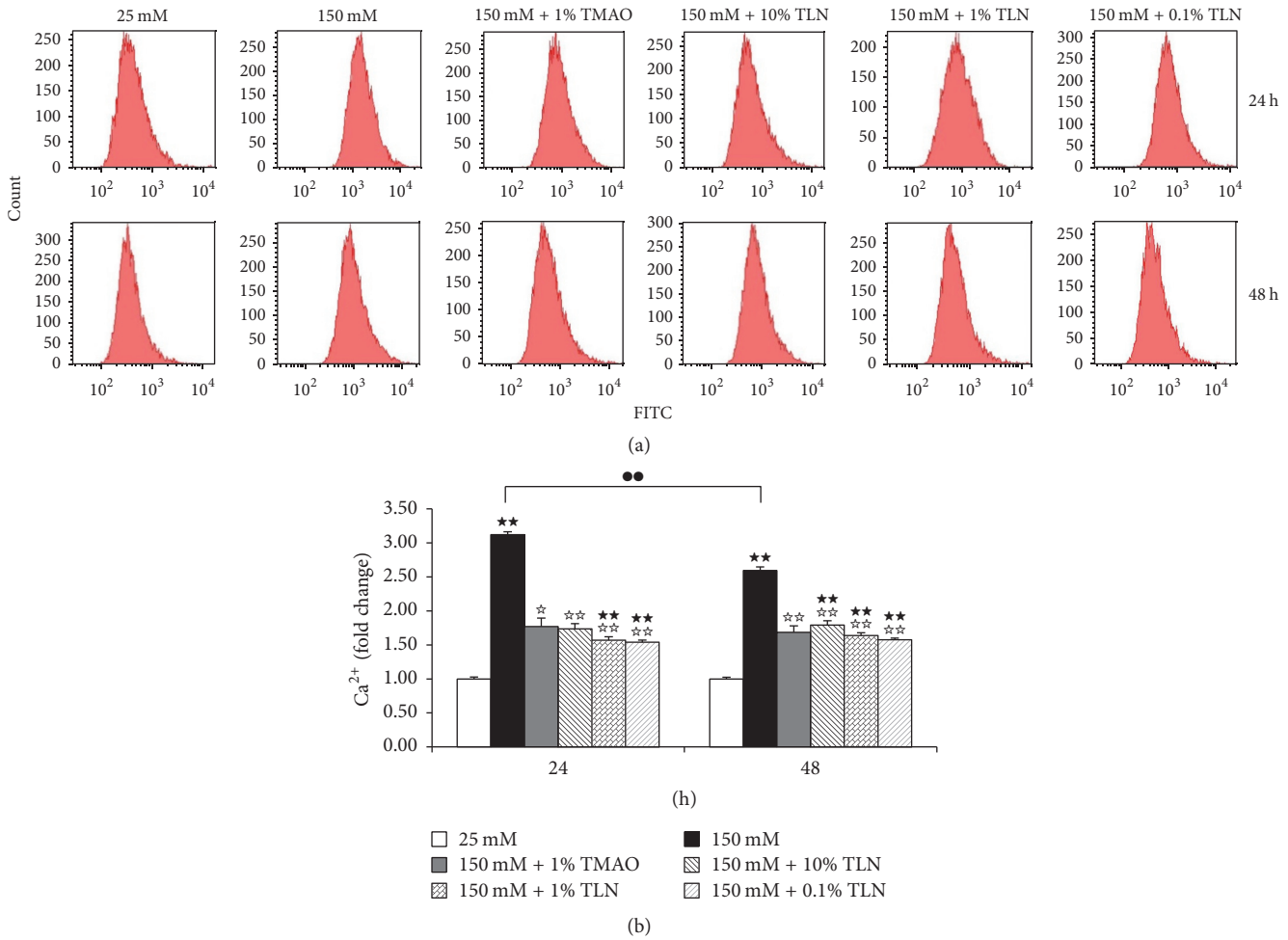

FIGURE 2: *TLN decreased high glucose-induced Ca^{2+} level of RSC96 cell.* (a) Image of Ca^{2+} level in RSC96 cells measured by flow cytometry. (b) Summarized data of Ca^{2+}, normalized as fold change of 25 mM glucose. Data were analyzed by one-way ANOVA followed by least significant difference. Data were shown as mean ± SEM ($n = 4$). $^{\star\star}P < 0.01$ versus 25 mM glucose; $^{\star\star}P < 0.01$ and $^{\star}P < 0.05$ versus 150 mM glucose; $^{\bullet\bullet}P < 0.01$ 150 mM glucose at 24 hours versus 150 mM glucose at 48 hours.

4. Discussion

TCM serum has been widely used in the mechanism study of compound of traditional Chinese medicine in vitro. It excludes interference of various factors and is close to the real process of pharmacological effects in Chinese herbal compound [18, 19]. Based on previous DPN rat models, we had verified that TLN can inhibit ER stress-induced apoptosis of sciatic nerve of DPN rats and alleviated DPN [13]. In order to further explore the mechanism of TLN on DPN, in this study, a model of SCs cultured in high glucose environment was used and treated with TLN serum. Previous studies have also found that the main chemical constituents of the TLN such as paeoniflorin and salvianolic acid B can be detected in TLN serum (see Supplementary Material available online at https://doi.org/10.1155/2017/5193548).

SCs apoptosis is one of the main pathogeneses of DPN [2]. Our previous study had demonstrated that TLN could inhibit high glucose-induced apoptosis [11]. ER is the main storage organelle of calcium and intracellular Ca^{2+} is indispensable for the development of ER. Overload calcium is identified to be a factor for cell apoptosis [14, 15] and participates in ER stress [20, 21]. In this study, Ca^{2+} level in 150 mM glucose group increased significantly compared with 25 mM group; it suggested that intracellular environmental homeostasis was destroyed and led to apoptosis. TLN serum decreased Ca^{2+} level significantly; it suggested that TLN could inhibit high glucose-induced apoptosis. We also found that the Ca^{2+} level in the 150 mM glucose group at 48 hours was significantly decreased compared to that in the 150 mM glucose group at 24 hours; we speculate that the reason may be that the cell membrane structure at 48 hours was damaged more seriously compared with that at 24 hours. PI can stain the nucleus through late apoptosis and dead cells but not the complete cell membrane. From our previous research of the Annexin V/PI staining [11], we can find that PI staining increased significantly at 48 hours compared with 24 hours; it suggested that the quantity of late apoptosis and dead cells increased; cell membrane structure was destroyed and led

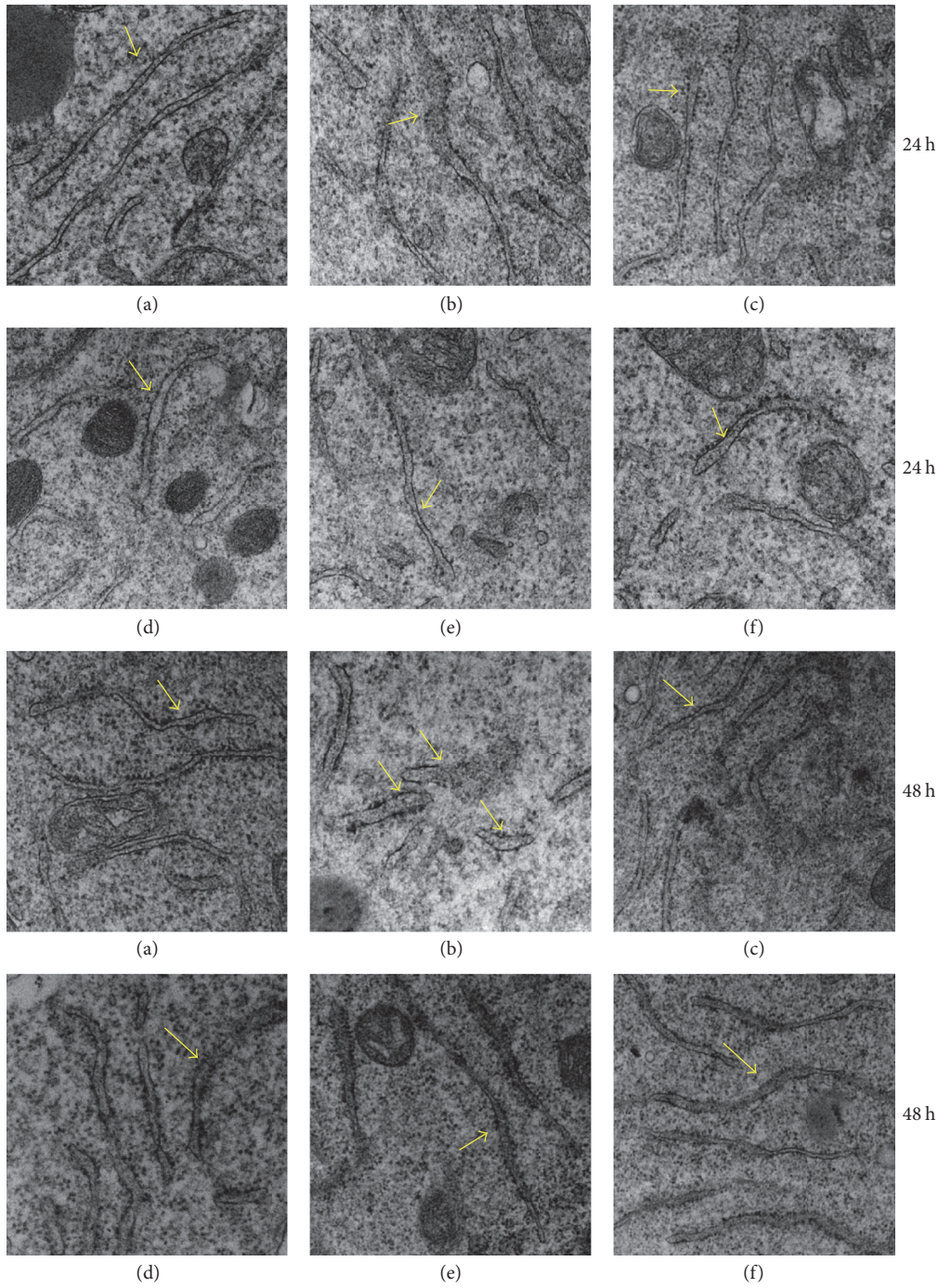

FIGURE 3: *TLN protected the integrity of the ER morphology under high glucose environment.* Ultramicrostructure of ER (magnification, 8,000x): the arrow indicates the ER morphology. (a)–(f) represent 25 mM glucose, 150 mM glucose, 150 mM glucose + 1% TMAO, 150 mM glucose + 10% TLN, 150 mM glucose + 1% TLN, and 150 mM + 0.1% TLN group, respectively.

to Ca^{2+} outflow and Ca^{2+} levels decreased; this verified our guess.

The accumulation of unfolded proteins and misfolded proteins in the ER resulted in defect in the ER homeostasis and then induced ER stress [20, 21]. In order to restore homeostasis, UPR, which is involved in three ER-transmembrane transducers, PERK, IRE1α, and ATF6, and ER chaperone GRP78 were activated [8]. We first observed the morphology of ER and found that in 150 mM group at 24 hours the morphology of ER partially swelled and in 150 mM group at 48 hours, fragmental morphology of ER appeared; it is the result of protein overaccumulation in the ER and intracellular environmental homeostasis was destroyed and then induced ER stress. In 150 mM glucose + TLN group, morphology of

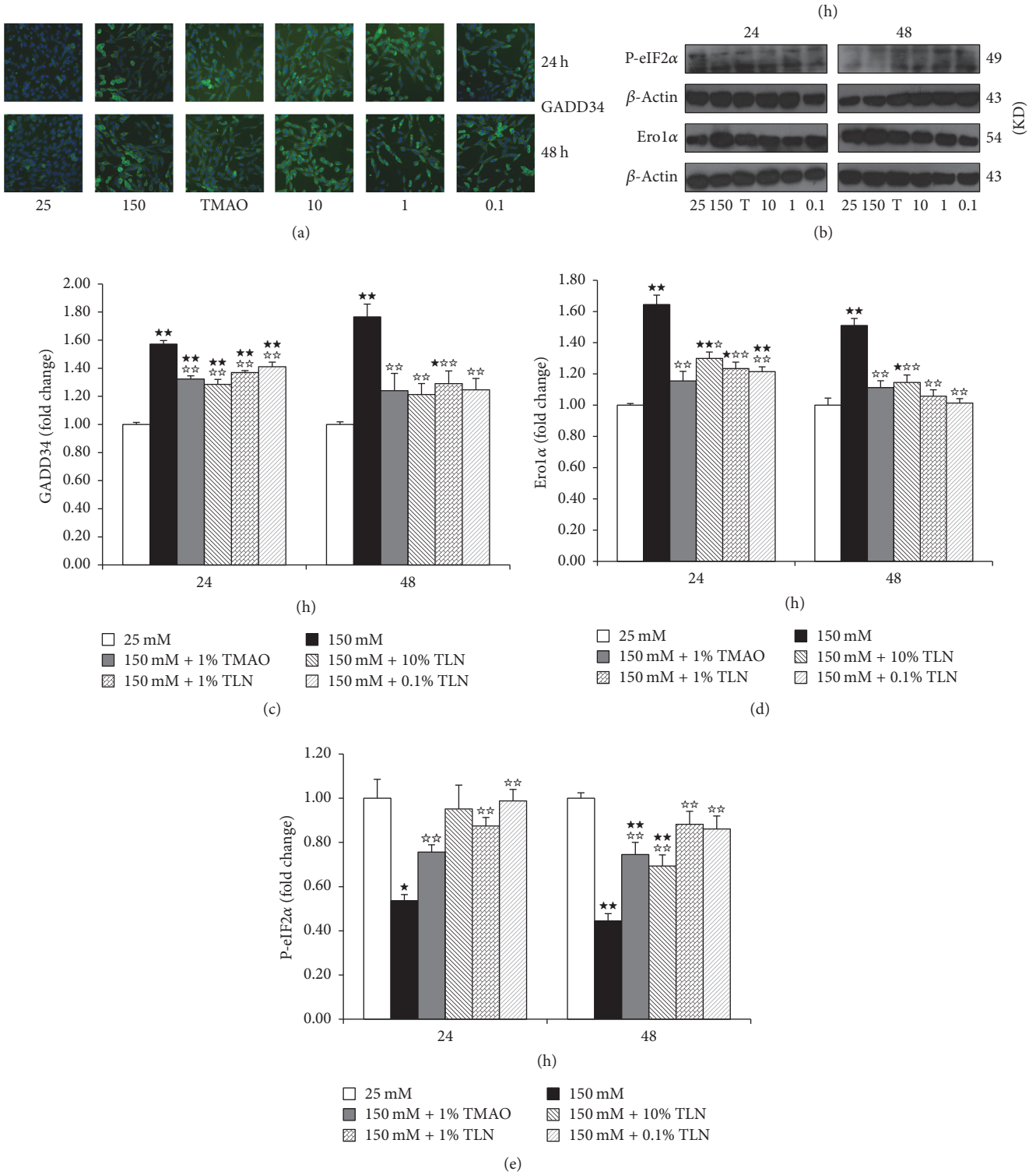

Figure 4: *TLN can decrease the expression of GADD34 and Ero1α and increase the expression of P-eIF2α in high glucose-induced RSC96 cells.* (a) Images of GADD34 relative protein level measured by high content analysis; images were viewed at a magnification of 10x. (b) Images of Ero1α and P-eIF2α relative protein level measured by Western blot, normalized to β-actin. ((c)–(e)) Summarized data of GADD34, Ero1α, and P-eIF2α, normalized as fold change of 25 mM glucose group. Data were analyzed by one-way ANOVA followed by least significant difference. Data were shown as mean ± SEM ($n = 4$). $^{\star\star}P < 0.01$ and $^{\star}P < 0.05$ versus 25 mM glucose; $^{\star\star}P < 0.01$ and $^{\star}P < 0.05$ versus 150 mM glucose.

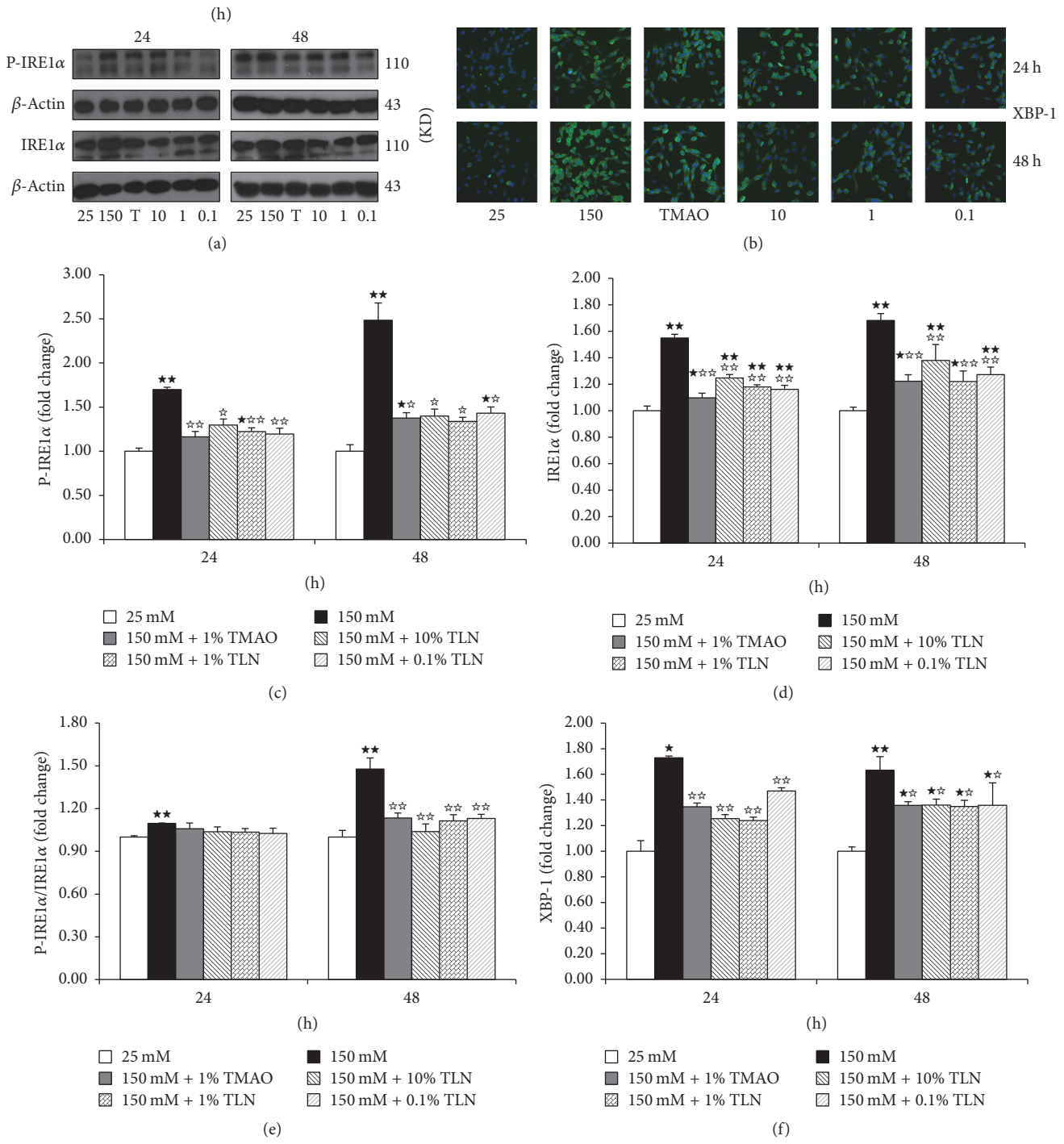

FIGURE 5: *TLN can decrease the expression of P-IRE1α/IRE1α and XBP-1 in high glucose-induced RSC96 cells.* (a) Images of P-IRE1α and IRE1α relative protein level measured by Western blot, normalized to β-actin. (b) Images of XBP-1 relative protein level measured by high content analysis; images were viewed at a magnification of 10x. ((c)–(f)) Summarized data of P-IRE1α, IRE1α, P-IRE1α/IRE1α, and XBP-1, normalized as fold change of 25 mM glucose group. Data were analyzed by one-way ANOVA followed by least significant difference. Data were shown as mean ± SEM ($n = 4$). $^{\star\star}P < 0.01$ and $^{\star}P < 0.05$ versus 25 mM glucose; $^{\star\star}P < 0.01$ and $^{\star}P < 0.05$ versus 150 mM glucose.

ER tended to have integral structure; it demonstrates that TLN can maintain the integrity of the ER morphology.

When ER stress lasts for long time, ER homeostasis cannot be restored in time; ER apoptosis mechanism will be activated [8]. Our previous study also demonstrated that TLN could increase the expression of ER stress marker protein GRP78 and inhibited the expression of apoptosis marker protein CHOP in ER stress and then increased the

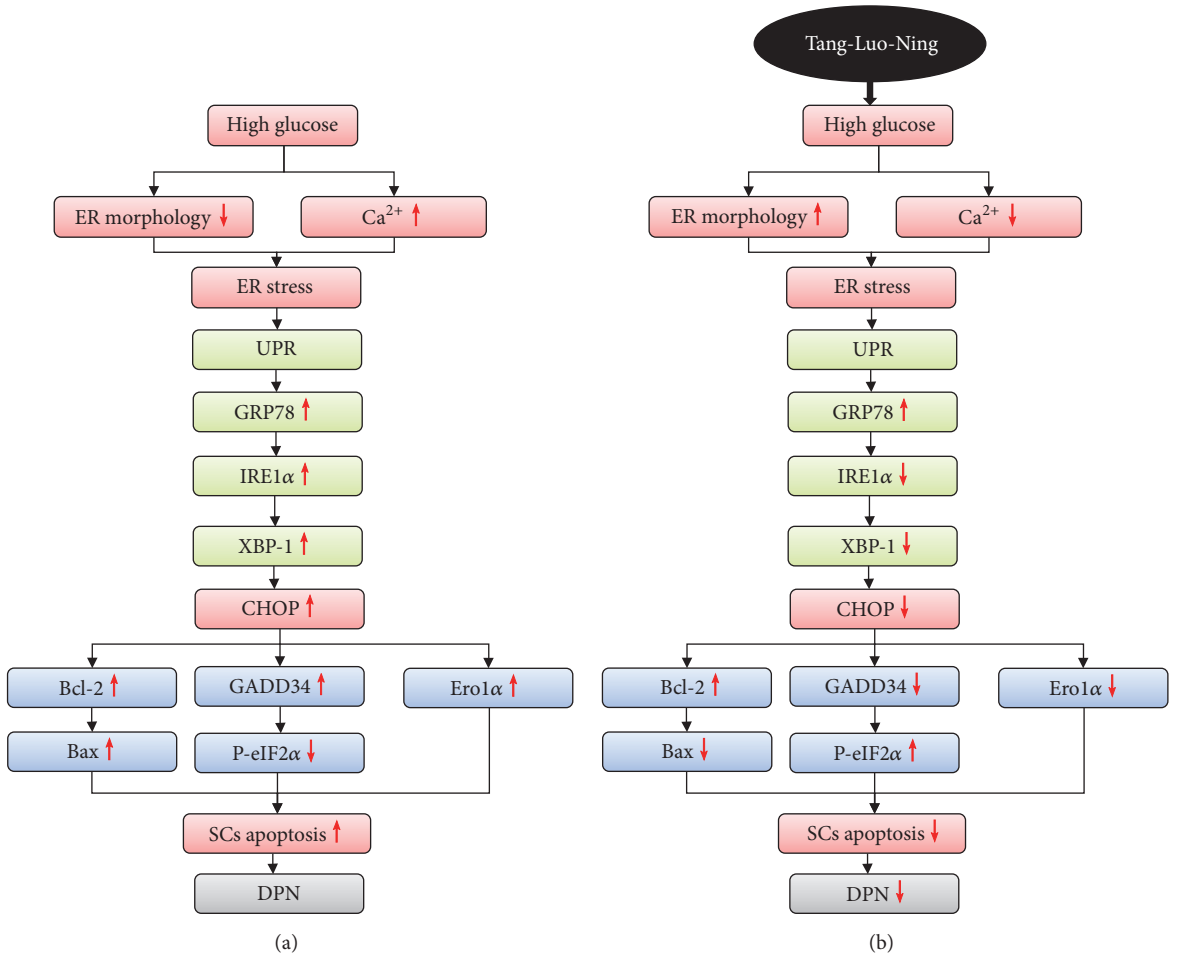

Figure 6: *(a) The mechanism of ER stress-induced apoptosis of SCs under high glucose. (b) TLN inhibits high glucose-induced ER stress-related apoptosis of SCs.*

expression of Bcl-2 and decreased the expression of Bax [11]. Upregulation of CHOP can also induce the expression of Ero1α and GADD34 [22–26], Ero1α can trigger apoptosis directly, and GADD34 can further make P-eIF2α (function is slowing down or even suspending misfolded proteins synthesis) dephosphorylated and then result in misfolded proteins synthesis conduct. This study showed that TLN serum could decrease the expression of Ero1α and GADD34 but increase the expression of P-eIF2α; it demonstrates that TLN can inhibit apoptosis and the folding of misfolded proteins.

IRE1α, as the transmembrane protein for UPR, plays a critical role in ER stress-induced apoptosis [17]. When ER stress occurs, free IRE1α is activated by dimerization and phosphorylation and induces downstream expression of XBP-1s by cleavage of transcription factor XBP-1 mRNA and ultimately activates downstream apoptotic protein CHOP [27]. In this study, we found that TLN serum could decrease the expressions of P-IRE1α/IRE1α and XBP-1; it demonstrates that TLN can inhibit CHOP-induced apoptosis by inhibiting IRE1α phosphorylation followed with inhibiting the cleavage of XBP-1.

In this study, we selected TMAO as a positive control drug. TMAO is a natural chemical chaperone that can attract chaperone proteins to treat protein-folding diseases and eliminate abnormal accumulation of misfolded proteins and thus alleviate ER stress and treat DPN effectively [28, 29]. Studies have shown that it can significantly reduce the expressions of CHOP and P-IRE1α/IRE1α and improve neurological function [30–32], so we select TMAO as positive control drug.

5. Conclusion

In summary, this study demonstrates that TLN can decrease SCs Ca^{2+} level induced by high glucose. It is related to the inhibition of CHOP-related pathway of ER stress apoptotic pathway. These results suggest a therapeutic pathway for TLN in decreasing SCs apoptosis in DPN (Figure 6).

Conflicts of Interest

The authors declare that there are no conflicts of interest.

Acknowledgments

This work is supported by the National Natural Science Foundation of China (Grant 81473642 awarded to Liping Xu).

References

[1] A. M. Vincent, B. C. Callaghan, A. L. Smith, and E. L. Feldman, "Diabetic neuropathy: cellular mechanisms as therapeutic targets," *Nature Reviews Neurology*, vol. 7, no. 10, pp. 573–583, 2011.

[2] N. P. Gonçalves, C. B. Vægter, H. Andersen et al., "Schwann cell interactions with axons and microvessels in diabetic neuropathy," *Nature Reviews Neurology*, vol. 13, no. 3, pp. 135–147, 2017.

[3] H. C. Lehmann and A. Höke, "Use of engineered Schwann cells in peripheral neuropathy: Hopes and hazards," *Brain Research*, vol. 1638, pp. 97–104, 2016.

[4] L. Cinci, F. Corti, L. Di Cesare Mannelli, L. Micheli, M. Zanardelli, and C. Ghelardini, "Oxidative, Metabolic, And Apoptotic Responses of Schwann Cells to High Glucose Levels," *Journal of Biochemical and Molecular Toxicology*, vol. 29, no. 6, pp. 274–279, 2015.

[5] L. Eckersley, "Role of the Schwann cell in diabetic neuropathy," *International Review of Neurobiology*, vol. 50, pp. 293–321, 2002.

[6] U. Özcan, Q. Cao, E. Yilmaz et al., "Endoplasmic reticulum stress links obesity, insulin action, and type 2 diabetes," *Science*, vol. 306, no. 5695, pp. 457–461, 2004.

[7] S. H. Back and R. J. Kaufman, "Endoplasmic reticulum stress and type 2 diabetes," *Annual Review of Biochemistry*, vol. 81, pp. 767–793, 2012.

[8] K. Zhang and R. J. Kaufman, "The unfolded protein response: a stress signaling pathway critical for health and disease," *Neurology*, vol. 66, supplement 1, no. 2, pp. S102–S109, 2006.

[9] B. Y. Gao, H. Zhou, J. T. Zhang et al., "Clinical research on patients of diabetic peripheral neuropathy treated with Tang luo ning," *China J Tradit Chin Med Pharm*, vol. 28, p. 5, 2013.

[10] B. Li M, Y. Gao B, J. Xia et al., "Therapeutic Effects and Antioxidative Effect of Tangluoning in Treating Diabetic Peripheral Neuropathy," *ChinJInfTCM*, vol. 18, p. 4, 2011.

[11] X. Yang, W. Yao, H. Liu, Y. Gao, R. Liu, and L. Xu, "Tangluoning, a traditional Chinese medicine, attenuates in vivo and in vitro diabetic peripheral neuropathy through modulation of PERK/Nrf2 pathway," *Scientific Reports*, vol. 7, no. 1, 2017.

[12] K. Zhang, "Integration of ER stress, oxidative stress and the inflammatory response in health and disease," *International Journal of Clinical and Experimental Medicine*, vol. 3, p. 8, 2010.

[13] X. Yang, W. Yao, Q. Li et al., "Mechanism of Tang Luo Ning effect on attenuating of oxidative stress in sciatic nerve of STZ-induced diabetic rats," *Journal of Ethnopharmacology*, vol. 174, pp. 1–10, 2015.

[14] N. Z. Shaban, A. M. Ahmed Zahran, F. H. El-Rashidy, and A. S. Abdo Kodous, "Protective role of hesperidin against γ-radiation-induced oxidative stress and apoptosis in rat testis," *Journal of Biological Research (Greece)*, vol. 24, no. 1, article no. 5, 2017.

[15] S.-Y. Hu, Y. Zhang, P.-J. Zhu, H. Zhou, and Y.-D. Chen, "Liraglutide directly protects cardiomyocytes against reperfusion injury possibly via modulation of intracellular calcium homeostasis," *Journal of Geriatric Cardiology*, vol. 14, no. 1, pp. 57–66, 2017.

[16] K. D. McCullough, J. L. Martindale, L. O. Klotz, T. Y. Aw, and N. J. Holbrook, "Gadd153 sensitizes cells to endoplasmic reticulum stress by down-regulating Bc12 and perturbing the cellular redox state," *Molecular and Cellular Biology*, vol. 21, no. 4, pp. 1249–1259, 2001.

[17] S. Oyadomari and M. Mori, "Roles of CHOP/GADD153 in endoplasmic reticulum stress," *Cell Death & Differentiation*, vol. 11, no. 4, pp. 381–389, 2004.

[18] B. Cao, Z. Zhang, Y. Zhang, J. Li, G. Liang, and J. Ling, "Effect of Smilax china L.-containing serum on the expression of POLD1 mRNA in human hepatocarcinoma SMMC-7721 cells," *Experimental and Therapeutic Medicine*, vol. 6, no. 4, pp. 1070–1076, 2013.

[19] D.-H. Wu, L. Xu, C.-P. Wen et al., "The effects of Jieduquyuzishen prescription-treated rat serum on the BAFF/BAFF-R signal pathway," *PLoS ONE*, vol. 10, no. 2, Article ID e0118462, 2015.

[20] D. R. Amici, I. Pinal-Fernandez, D. A. Mázala et al., "Calcium dysregulation, functional calpainopathy, and endoplasmic reticulum stress in sporadic inclusion body myositis," *Acta Neuropathologica Communications*, vol. 5, no. 1, 2017.

[21] G.-H. Kwak and H.-Y. Kim, "MsrB3 deficiency induces cancer cell apoptosis through p53-independent and ER stress-dependent pathways," *Archives of Biochemistry and Biophysics*, vol. 621, pp. 1–5, 2017.

[22] I. Novoa, H. Zeng, H. P. Harding, and D. Ron, "Feedback inhibition of the unfolded protein response by GADD34-mediated dephosphorylation of eIF2α," *The Journal of Cell Biology*, vol. 153, no. 5, pp. 1011–1021, 2001.

[23] S. Marciniak, C. Y. Yun, S. Oyadomari et al., "CHOP induces death by promoting protein synthesis and oxidation in the stressed endoplasmic reticulum," *Genes Development*, vol. 18, no. 24, pp. 3066–3077, 2004.

[24] G. Li, M. Mongillo, K. Chin et al., "Role of ERO1-α-mediated stimulation of inositol 1,4,5-triphosphate receptor activity in endoplasmic reticulum stress-induced apoptosis," *The Journal of Cell Biology*, vol. 186, no. 6, pp. 783–792, 2009.

[25] Y. Ma and L. M. Hendershot, "Delineation of a negative feedback regulatory loop that controls protein translation during endoplasmic reticulum stress," *The Journal of Biological Chemistry*, vol. 278, no. 37, pp. 34864–34873, 2003.

[26] R. Sano and J. C. Reed, "ER stress-induced cell death mechanisms," *Biochimica et Biophysica Acta (BBA) - Molecular Cell Research*, vol. 1833, no. 12, pp. 3460–3470, 2013.

[27] Z. Xiong, R. Jiang, X. Li, Y. Liu, and F. Guo, "Different roles of GRP78 on cell proliferation and apoptosis in cartilage development," *International Journal of Molecular Sciences*, vol. 16, no. 9, pp. 21153–21176, 2015.

[28] C. Huang, J. J. Wang, J. H. Ma, C. Jin, Q. Yu, and S. X. Zhang, "Activation of the UPR protects against cigarette smoke-induced RPE apoptosis through up-regulation of Nrf2," *The Journal of Biological Chemistry*, vol. 290, no. 9, pp. 5367–5380, 2015.

[29] B. Gong, L.-Y. Zhang, C.-P. Pang, D. S.-C. Lam, and G. H.-F. Yam, "Trimethylamine N-oxide alleviates the severe aggregation and ER stress caused by G98R αA-crystallin," *Molecular Vision*, vol. 15, pp. 2829–2840, 2009.

[30] S. Lupachyk, P. Watcho, A. A. Obrosov, R. Stavniichuk, and I. G. Obrosova, "Endoplasmic reticulum stress contributes to prediabetic peripheral neuropathy," *Experimental Neurology*, vol. 247, pp. 342–348, 2013.

[31] H. Wei, S.-J. Kim, Z. Zhang, P.-C. Tsai, K. R. Wisniewski, and A. B. Mukherjee, "ER and oxidative stresses are common mediators of apoptosis in both neurodegenerative and non-neurodegenerative lysosomal storage disorders and are alleviated by chemical chaperones," *Human Molecular Genetics*, vol. 17, no. 4, pp. 469–477, 2008.

[32] S. Lupachyk, P. Watcho, R. Stavniichuk, H. Shevalye, and I. G. Obrosova, "Endoplasmic reticulum stress plays a key role in the pathogenesis of diabetic peripheral neuropathy," *Diabetes*, vol. 62, no. 3, pp. 944–952, 2013.

Hindawi
Evidence-Based Complementary and Alternative Medicine
Volume 2017, Article ID 3729547, 7 pages
https://doi.org/10.1155/2017/3729547

Research Article

Therapeutic Effect and Mechanism of *Oxytropis falcata* Gel on Deep Second-Degree Burn in Rats

Xiao-Feng Lin,[1] Kai-Jie Chen,[1] He-Kun Shi,[1] Le Yu,[2] Jin-Shan Chen,[1] and Yan Fei[1]

[1]*Department of Pharmacy, The 175th Hospital of PLA, Affiliated Southeast Hospital of Xiamen University, Fujian, Zhangzhou 363000, China*
[2]*Department of Pathology, The 175th Hospital of PLA, Affiliated Southeast Hospital of Xiamen University, Fujian, Zhangzhou 363000, China*

Correspondence should be addressed to Jin-Shan Chen; pharzz@sina.com and Yan Fei; feiyanfy@126.com

Received 20 June 2017; Accepted 4 October 2017; Published 13 November 2017

Academic Editor: Caio P. Fernandes

Oxytropis falcata has long been used to treat inflammation, sores, and bleeding in Tibet. However, the burn remedy and underlying molecular mechanisms are not well understood. This study is aimed at assessing the effect of *Oxytropis falcate* gel (OFG) on deep second-degree burn rats and exploring its mechanism. Wistar rats with second-degree burn were treated with OFG and silver sulfadiazine. Immunohistochemical detections for EGF and VEGF were performed, and ELISA detections for EGF, VEGF, p38, and IL-1β in serum were determined. Rats treated with OFG (25, 50 g/kg) consisted of the major rhamnocitrin-3-O-β-neohesperidoside significantly accelerated incrustation ($P < 0.001$) and decrustation ($P < 0.001$). According to HE staining, edema and infiltration of inflammatory cells decrease apparently with good hyperplasia and incrustation in administration groups (7 d). The expressions of EGF and CD34 in OFG (25, 50 g/kg) treatment increased obviously from immunohistochemical assessment (7 d). Serum EGF expression reached 321.27 ± 7.20 ng/mL by OFG treatment, while p38 ($P < 0.05$) and IL-1β ($P < 0.05$) levels were significantly lower than the model and vehicle groups from day 1 to day 7. OFG possesses potential wound healing activities. The mechanism may be related to the increasing of biosynthesis and the releasing of EGF and CD34 and the decreasing p38 and IL-1β levels.

1. Introduction

Burning can cause all sorts of tissue damage depending on burn severity. Burns can be classified as first-, second-, and third-degree burns according to the involvement of skin and deeper tissues. Burns are so much different from other injuries that a separate medical superspeciality has been designated to treat them [1]. Nowadays, prescription drugs such as sulfadiazine silver and mafenide, which are effective in relieving symptoms and promoting healing, are widely used in burn. These sulfonamides show a satisfactory antibacterial effect. However, the wound contraction heals slowly because multiple biological pathways need to be activated and synchronized to respond [2]. The wound repair process can be accelerated by recombinant human fibroblast growth factor (rhFGF), basic fibroblast growth factor (bFGF), and collagenase, but the antibacterial effect is limited. Recently there was a new trend in characterizing active constituents from the Chinese ethnodrugs [3].

Oxytropis falcata Bunge (Leguminosae), known as "Er-Da-Xia" in Tibetan medicines, is a wild growing plant mainly distributed in Qinghai-Tibet Plateau at an altitude of 2700–4300 m in China. This plant has been used as folk remedies to treat inflammation, sores, and bleeding for thousands of years [4–6]. Moreover, some traditional patented prescriptions containing this herb have also been launched into the market. However, to our knowledge, the effect on burn treatment of *Oxytropis falcate* has never been reported in academic research. Therefore, in this study, we extracted the components of *Oxytropis falcata* Bunge and observed effects of OFG on rats with deep second-degree burn to explore the mechanism using pharmacological experiment and molecular biotechnology.

2. Materials and Methods

2.1. Drugs and Chemicals. *Oxytropis falcata* herb was obtained from The Huangheyuan medicinal materials company in Gansu Province. The plant was identified and authenticated by Professor Zhigang Ma at Lanzhou University (Lanzhou, China). Borneol and water-soluble chitosan (molecular weight 200 kDa, 90% deacetylation) were provided by Qingdao Shunbo Biotechnology Institute Company Limited. Take 1% silver sulfadiazine cream as positive control. Rats EGF, VEGF, p38, and IL-1β ELISA kits were obtained from American R&D Company. Rabbit anti-EGF and anti-VEGF-β were acquired from Boster Biological Company Limited (China). Rabbit anti-CD34 and immunohistochemisty strengthen kit (Envision TM plus) were obtained from Fuzhou Maixin Biotechnology Company Limited (China).

2.2. Animals. All male and female Wistar rats weighing 200–250 g were purchased from Shanghai SLAC Laboratory Animals Co., Ltd. (China). The 98 rats were randomly selected and divided into 7 groups: model group, vehicle group, administration groups (low-dose, middle-dose, and high-dose group), positive group, and normal group. They were housed in clear plastic cages with solid floors and hard wood chip bedding and placed in a temperature- and humidity-controlled environment. The experiment was conducted in the central lab of Affiliated Dongnan Hospital of Xiamen University in accordance with laboratory animal standards in China (GB14925-95) and the University Guidelines of the Ethics Committee for Animal Care and Use in Research. The experiment was performed according to the 3R principle of animals use and blinded treatment.

2.3. Prescription Preparation and Administration. The herb (200 g) was cut into small pieces and extracted with purified water (400 mL, 1.5 h reflux, 100°C, ×2). The water solution was concentrated under a reduced pressure after filtration in a Buchner funnel, enriching the total flavones by macroporous resin. The extract content of rhamnocitrin-3-O-β-neohesperidoside was 6.46% with a diode-array detector at 350 nm by RP-HPLC [7].

The extract (60 g, crude drug 15 g/g) was resuspended in distilled water with continuous stirring. Then chitosan (60 g) was added to the stirring mixture till it became swollen completely. Next, borneol (10 g, dissolved into 20 mL glycerol) was added. Subsequently, sodium benzoate (1.2 g) was cast over the gel. Finally, volume was made with distilled water and was stirred continuously till a uniform high-dose gel weighing 1000 g formed. The gel (pH 6.0–7.0) had translucent appearance, good spreadability, uniform particle size distribution, and moderate viscosity (5.73 Pa·s). And the extracts in the middle-dose and low-dose gels were 50% and 25% of high-dose, respectively. The vehicle control gel was prepared without the extract. Model group were deep second-degree burn rats without administration, and normal group were rats without modeling and without administration. Vehicle (10 g/kg), low-dose, middle-dose, high-dose (12.5, 25 and 50 g/kg), and positive (silver sulfadiazine, 10 g/kg) group were painted for administration twice a day for 28 days to monitor adverse drug reactions and other accident situations. The doses and dose interval were used according to the preliminary laboratory experiment.

2.4. Deep Second-Degree Burn Modeling. The model was built according to the scalded rat model from Fu and Wang [8]. An area (5 cm × 5 cm) was shaved on the rat back. The rats were anesthetized by the vapor of ethyl alcohol. Then cardboard with circular hole (4 cm in diameter) was prepared for burned areas. The shaved animal skin was burned for 12 s with 3 drops of ethanol. Then the fire was put off as soon as possible with a wet cloth. Moreover, the depth was confirmed by observing the pathological change with hematoxylin and eosin (HE) staining. A deep partial-thickness burn injury was observed in rats. Epidermis disappeared. Epidermis, dermis, and subcutaneous tissue were partially damaged. There were obvious subcutaneous tissue edema and infiltration of inflammatory cells. The wounds were observed daily until a complete wound healing enclosure occurred.

2.5. Immunohistochemistry. The wound tissue sections were fixed in 4% formaldehyde. Then they were penetrated with paraffin and paraffin-embedded according to conventional methods. HE staining was conducted on days 7, 14, and 21 after burn injury. For this study 4 μm thick sections were retained on poly-L-lysine coated slides and baked for 2 h at 68°C. Paraffin sections were dewaxed and rinsed with tap water. Antigen retrieval was achieved by boiling for 4 min in citrate buffer (pH 6.0). After natural cooling, endogenous peroxidase activity was blocked by using 3% hydrogen peroxide for 10 min. Next sections were washed three times with Phosphate Buffered Saline (PBS, pH 7.6). After this stage, sections were incubated with primary antibody for 1 h at 37°C and then washed three times with PBS. Then sections were incubated with secondary antibody for 15 min at room temperature and washed three times with PBS. Finally, the color was developed by 5 min incubation with diaminobenzidine solution after contrasting with hematoxylin. In order to evaluate the epithelization and angiogenesis process in rat endothelium epitope, we used anti-EGF, anti-VEGF, and anti-CD34 antibody.

2.6. ELISA. The rats were anesthetized by the vapor of ethyl alcohol after burn injury on days 1, 4, and 7, to take 2 mL blood at the inner canthus with glass capillary tube. Blood was allowed to coagulate for 15 min at room temperature. Then 200 μL supernatant was collected after the blood was centrifugated at 1000 g for 15 min. TGF-β, p38, and IL-1β were detected according to the instructions.

2.7. Statistical Analysis. Statistical analysis was performed using SPSS software version 17. All experimental parameters were expressed as the mean ± the standard error mean (SEM). Statistical comparisons were made using one-way analysis of variance (ANOVA) followed by LSD's post hoc test. P values less than 0.05 were considered to be statistically significant.

3. Results

3.1. Evaluation of Tissue Repair. The gels could serve as wound dressings to prepare an optimum wound bed without

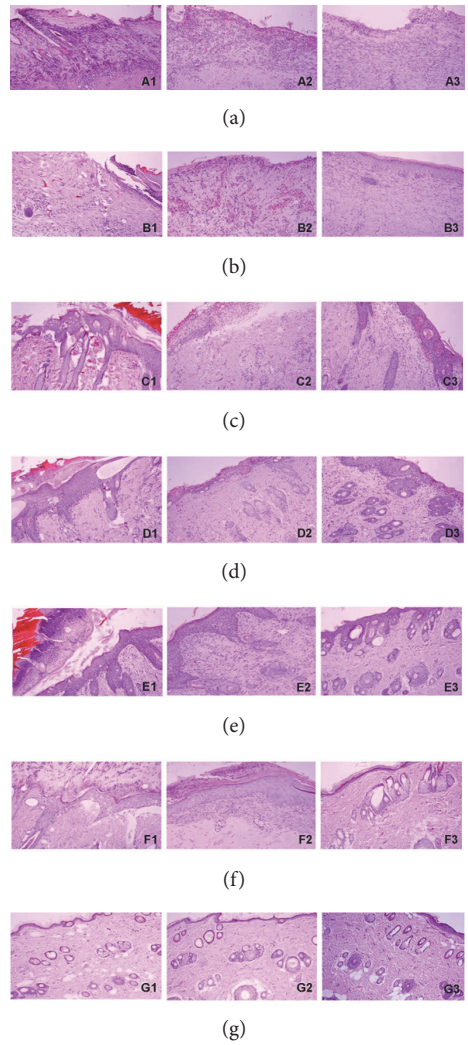

Figure 1: Therapeutic effect of OFBGC on rats with II° burn (HE staining, ×100). The measurements were carried out on day 7, day 14, and day 21. Red areas showed incrustation and purple particles were inflammatory cells. (a) model group, (b) vehicle control, (c) low-dose group, (d) middle-dose group, (e) high-dose group, (f) positive control, and (g) normal control. 1: 7 d, 2: 14 d, and 3: 21 d.

secretion. In OFG-treated groups, oedema and infiltration of inflammatory cells apparently decreased in burnt areas with good hyperplasia and incrustation (7 d). On day 14, new hair follicle and sebaceous glands were observed with almost complete epithelization and decrustation, in contrast with the incomplete epithelization in model and vehicle groups. On day 21, the administration rats showed a complete healing process contrasting the poor situation in model groups (Figure 1).

Incrustation is the solid covering or layer that is formed from necrotic tissue. Decrustation is the scab being removed from skin surface with complete wound closure [9]. The administration and vehicle rats showed significantly less time needed for incrustation ($P < 0.001$) and decrustation ($P < 0.001$) as compared with model rats. Moreover, significantly less time was needed for incrustation in vehicle, middle-dose, and high-dose groups than positive group ($P < 0.001$), and the incrustation and decrustation time in high-dose group was shorter than positive control ($P < 0.001$) (Table 1).

3.2. p38, IL-1β, EGF, and VEGF Production in Serum. The productions of p38 and IL-1β were augmented in model rats as compared with normal rats ($P < 0.05$) on days 1, 4, and 7. However, the levels of p38 in low-dose (7 d), middle-dose (1, 4, and 7 d), and high-dose groups (1, 4, and 7 d) were significantly lower than that in model group ($P < 0.05$). The level of IL-1β in low-dose (1, 4 d), middle-dose (1, 4, and 7 d), and high-dose groups (1, 4, and 7 d) were significantly lower than that in model group ($P < 0.05$). Rats with OFG expressed significantly lower levels of p38 and IL-1β compared with those without OFG (vehicle group), as shown in Table 2. There were significant increases ($P < 0.05$) in EGF in low-dose (314.39±10.18 ng/mL) and middle-dose rats (321.27 ± 7.20 ng/mL) as compared with model rats. But the

Table 1: Healing time of wound in II° burn rats.

Treatment	Incrustation time (days)	Decrustation time (days)
Model	$8.29 \pm 0.57^{\#\#\#}$	$22.25 \pm 0.56^{\#\#\#}$
Vehicle	$3.16 \pm 0.42^{***,\#\#\#}$	$16.91 \pm 0.46^{***,\#\#\#}$
Low-dose	$2.31 \pm 0.32^{***,\#\#\#}$	$13.77 \pm 0.39^{***}$
Middle-dose	$2.16 \pm 0.34^{***,\#\#\#}$	$12.18 \pm 0.58^{***,\#\#\#}$
High-dose	$1.88 \pm 0.35^{***,\#\#\#}$	$9.38 \pm 0.51^{***,\#\#\#}$
Positive	$4.14 \pm 0.45^{***}$	$13.96 \pm 0.60^{***}$

Note. $^{***}P < 0.001$ versus model group. $^{\#\#\#}P < 0.001$ versus positive control.

Table 2: Expression of p38 and IL-1β in II° burns rat serum.

Treatment	p38			IL-1		
	1 d	4 d	7 d	1 d	4 d	7 d
Model	$79.89 \pm 2.95^{\#}$	$79.98 \pm 4.37^{\#}$	$80.92 \pm 3.57^{\#}$	$26.31 \pm 1.66^{\#}$	$27.68 \pm 2.08^{\#}$	$26.84 \pm 1.66^{\#}$
Vehicle	$79.25 \pm 3.58^{\#}$	76.42 ± 4.17	77.29 ± 4.13	25.23 ± 1.99	26.34 ± 1.43	25.83 ± 1.58
Low-dose	76.21 ± 4.41	76.06 ± 4.72	$75.70 \pm 4.20^{*}$	$24.70 \pm 1.96^{*}$	$25.67 \pm 1.65^{*}$	25.40 ± 1.19
Middle-dose	$75.32 \pm 2.88^{*}$	$72.04 \pm 4.95^{*}$	$72.34 \pm 4.23^{*}$	$23.77 \pm 1.66^{*}$	$25.60 \pm 1.98^{*}$	$24.82 \pm 1.53^{*}$
High-dose	$72.40 \pm 3.86^{*}$	$72.38 \pm 4.81^{*}$	$72.29 \pm 4.22^{*}$	$23.67 \pm 1.87^{*}$	$24.70 \pm 1.25^{*}$	$24.46 \pm 1.28^{*}$
Positive	$74.32 \pm 5.12^{*}$	$73.16 \pm 3.84^{*}$	$73.26 \pm 3.26^{*}$	$23.36 \pm 1.50^{*}$	$23.35 \pm 1.11^{*}$	$23.50 \pm 1.29^{*}$
Normal	$74.40 \pm 4.91^{*}$	$74.39 \pm 4.62^{*}$	$74.31 \pm 4.31^{*}$	$24.13 \pm 1.22^{*}$	$25.12 \pm 1.49^{*}$	$24.85 \pm 1.31^{*}$

Note. $^{*}P < 0.05$ versus model group. $^{\#}P < 0.05$ versus positive control.

Table 3: Expression of EGF and VEGF in II° burns rat serum.

Treatment	EGF	VEGF
Model	305.81 ± 15.52	100.29 ± 7.42
Vehicle	310.60 ± 13.84	99.14 ± 7.07
Low-dose	$314.39 \pm 10.18^{\#}$	$110.07 \pm 1.35^{\#}$
Middle-dose	$321.27 \pm 7.20^{*,\#}$	104.40 ± 3.53
High-dose	307.98 ± 10.03	101.98 ± 4.38
Positive	$318.17 \pm 8.07^{\#}$	102.89 ± 4.19
Normal	299.49 ± 16.28	101.47 ± 3.42

Note. $^{*}P < 0.05$ versus model group. $^{\#}P < 0.05$ versus normal control.

production of VEGF in OFG-treated rats was found to be a little different from other groups. Moreover, the OFG-treated rats also showed significant increases ($P < 0.05$) in EGF and VEGF as compared with the vehicle group (Table 3).

3.3. EGF, VEGF, and CD34 Production in Tissue. On day 7, the model, vehicle, and normal control groups showed no obvious increase in EGF and VEGF in burnt tissues compared with the normal group. But there were significant expressions of EGF in low-dose and middle-dose rats. The administration rats also showed obvious increases in VEGF (Figure 2).

Normal rats were found to be of no obvious expression of CD34 because no capillary formed. There were increases in CD34 in OFG-treated rats on day 7, especially in middle-dose group, and the expression in middle-dose rats was observed in subepidermic layer on day 14 and day 21. However, the model group showed a delayed increase in CD34 from day 7 to day 21 (Figure 3).

4. Discussion

In our study, the major constituent rhamnocitrin-3-O-β-neohesperidoside, a flavonoid, in our extract was 6.46%. So rhamnocitrin-3-O-β-neohesperidoside and other flavones present in the extract are responsible for the effective epithelialization with good hyperplasia and incrustation in burn-injured rats. Some compounds in the gel would presumably have antibacterial properties because the gels could apparently decrease oedema and infiltration of inflammatory cells without secretion. These results are closely related to the reports. The total flavonoids from *Oxytropis falcate* possessed anti-inflammatory, antioxidant, and ultraviolet protective effects on the destructed skin [10] and antibacterial activities against nine Gram-positive and Gram-negative bacteria, especially *Staphylococcus aureus* [11].

Extract of *Oxytropis falcate* treatment induced moderate liver damage and mild renal damage with maximum oral gavage dose for 15 days [12]. However, our previous study suggested that OFG had good absorption and no obvious skin toxicity [13]. Externally applied agents of *Oxytropis falcate* may be a relatively safe drug and take less risk than oral and intravenous preparations. Hence, as a potential preparation, OFG needs to be further tried on small, clinical wounds and large animals wounds before being applied to humans in the future.

Although the wound healing in vehicle-treated rats was not significant when compared with OFG-treated rats, it did show improved results in comparison with no treatment rats. The probable reason was that chitosan could prevent the loss of body fluid, prevent exudate buildup, protect the wounds from external contamination, have sufficient bactericidal activity to inhibit infection, and prepare an optimum

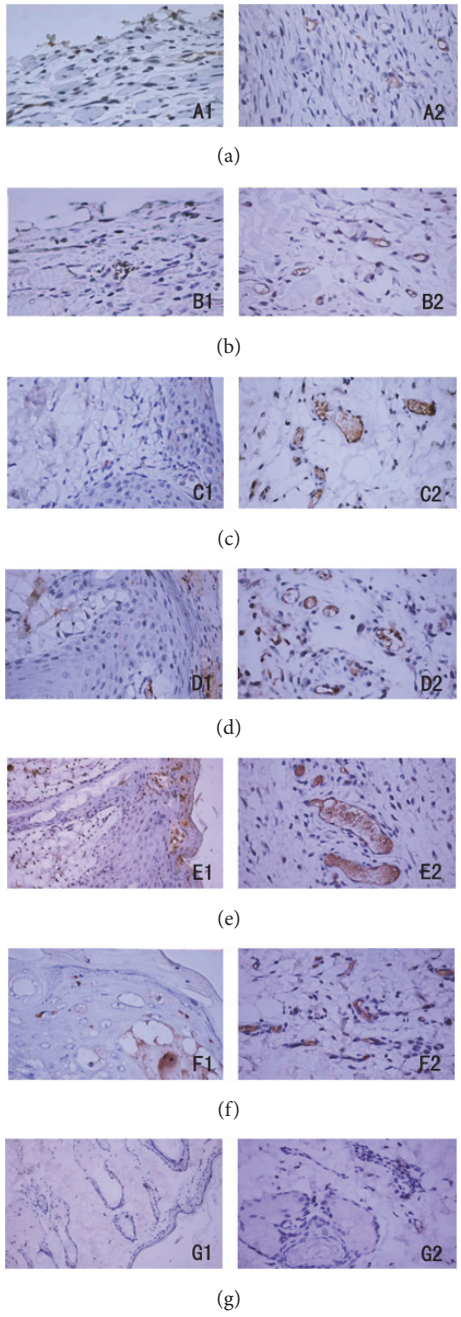

Figure 2: EGF and VEGF expression of immunohistochemical (×400) at day 7. The fuscescent ones, respectively, represented EGF and VEGF protein at different doses. 1: EGF and 2: VEGF; (a) model group, (b) vehicle control, (c) low-dose group, (d) middle-dose group, (e) high-dose group, (f) positive control, and (g) normal control.

wound bed for tissue repairing [14]. OFG accelerated wound healing, comparing with vehicle and model groups where the healing was delayed and almost spontaneous. The potential mechanisms are closely related to abnormal expressions of some cytokines in inflammatory reaction and regulation of growth factors, which are in line with findings of previous workers [15].

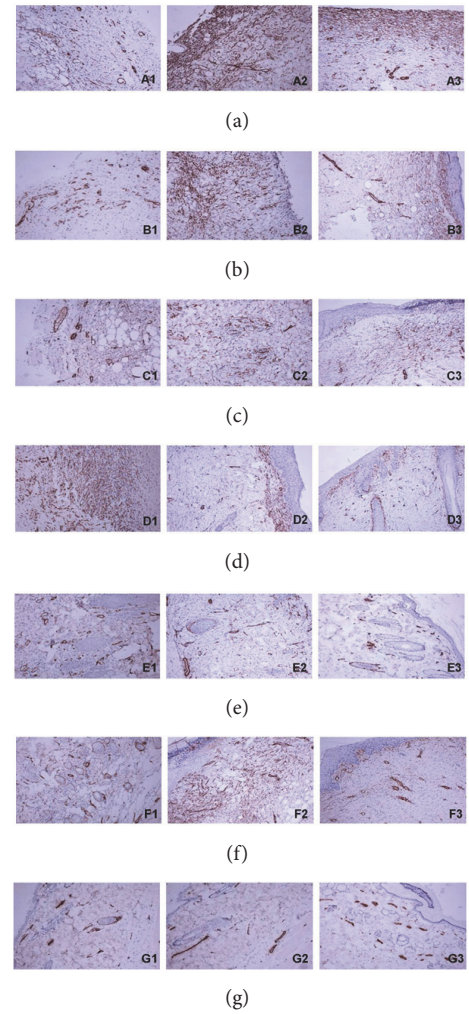

Figure 3: CD34 expression of immunohistochemical (×400). The staining CD34 protein (fuscescent ones) could represent blood vessel. The capillary was new generated in the reparative process and the coarse vessels were existing. (a) Model group, (b) vehicle control, (c) low-dose group, (d) middle-dose group, (e) high-dose group, (f) positive control, and (g) normal control. 1: 7 d, 2: 14 d, and 3: 21 d.

EGF binding to its receptor (EGFR) triggers rapid human skin fibroblast and keratinocyte locomotion. Additionally, this process plays a critical role in cell migration and human cutaneous wounds [16], not in the closure of an open wound [17]. In fact, burn wounds in OFG-treated rats were healing well by way of incrustation and decrustation, rather than gradual closure. The migrating mechanism may depend on EGFR-mediated expression of aquaporin-3 in a time- and dose-dependent manner [18]. We observed EGF expression in low-dose and middle-dose group, while no significant upregulation occurred in high-dose and normal group in serum at the same time. There are many possible reasons why the high dose was not observed to increasing EGF as we expected. Firstly, the upregulation of EGF is likely to be influenced by the presence of some active proteins, as it is also regulated in the matched unburned skin of the rats. Secondly, there were increasing EGF in burnt skin in rats, rather than in

serum. It means that maybe the releasing behavior of EGF in the serum possibly occurred earlier than in burn wound. The other reason may be that EGF is a specific marker for wound repair in tissue rather than in blood. However, it suggests that it recommended further studies.

Similar studies on VEGF were carried out. OFG treatment can accelerate VEGF expression in a dose-dependent manner in healing tissue, but weak expression in the low-dose group was observed in serum on day 7. VEGF could promote angiogenesis by promoting the formation of endothelial cells and inducing newly formed blood vessels in wound healing [19]. However, it is different from our study. Maybe VEGF is just a secondary bystander in OFG treatment. But, in our research CD34 may contribute directly to wound healing in the event of angiogenesis, which are in line with previous findings. A good angiogenesis was observed in OFG treatment following the significant increase CD34 expression. Strings of CD34 endothelial precursor cells were observed at the edges on day 3 after burn injury. The density of newly formed blood vessels on the surface unit within granulation tissue grew from 3 to 12 days [20].

Different from positive control, OFG-treated groups took less healing time for wound repair and showed more effective epithelialization by enhancing expression of EGF and in II° burn rats (Table 1, Figures 2 and 3). And they showed significant anti-inflammatory action (Table 2). Immediate or delayed topical application for p38 inhibitor remains potent in reducing full-thickness burning inflammatory signaling [21]. Similar findings were observed in our study where the expressions of p38 and IL-1β were significantly decreased in OFG-treated rats on days 1, 4, and 7 after burn injury. Hence, p38 and its downstream factor IL-1β may be the representative targets for inflammatory reaction in burn wound healing for OFG treatment.

5. Conclusions

OFG can not only remarkably intensify incrustation and decrustation processes but also relieve the inflammatory reaction with deep second-degree burn. Based on these findings, the potential mechanisms are possibly related to the increasing synthesis and releasing of EGF and CD34 in wound healing, decreasing expression of p38 and IL-1β. Therefore, OFG is recommended to be a potential compound for burn remedy. In order to provide new evidence in clinic based treatment strategies for patients with OFG, these results should be sufficiently confirmed by further experiments.

Disclosure

The funders had no role in study design, data collection and analysis, decision to publish, or preparation of the manuscript.

Conflicts of Interest

The authors declare that they have no conflicts of interest.

Acknowledgments

This work was supported by the Medical Technology Innovation Topics from Nanjing Military Area Command of PLA of China (no. 14MS085 and no. MS098).

References

[1] V. K. Tiwari, "Burn wound: How it differs from other wounds," *Indian Journal of Plastic Surgery*, vol. 45, no. 2, pp. 364–373, 2012.

[2] G. C. Gurtner, S. Werner, Y. Barrandon, and M. T. Longaker, "Wound repair and regeneration," *Nature*, vol. 453, no. 7193, pp. 314–321, 2008.

[3] Q. Song, Q. Gou, Y. Xie, Z. Zhang, and C. Fu, "Periplaneta americana Extracts Promote Skin Wound Healing via Nuclear Factor Kappa B Canonical Pathway and Extracellular Signal-Regulated Kinase Signaling," *Evidence-Based Complementary and Alternative Medicine*, vol. 2017, Article ID 5821706, 12 pages, 2017.

[4] D. Dimaer, Technology Press,, Jingzhu Materia Medica, Shanghai Science and,.

[5] W.-H. Chen, R. Wang, and Y.-P. Shi, "Flavonoids in the poisonous plant oxytropis falcata," *Journal of Natural Products*, vol. 73, no. 8, pp. 1398–1403, 2010.

[6] X.-H. Wei and L. Jin, "The research progress of Tibetan medicine Oxytropis falcata," *Chinese Pharmacological Bulletin*, vol. 26, no. 11, pp. 1535–1538, 2010.

[7] J. N. Hong, J. S. Chen, and M. X. Li, "Determination of Rhamnocitrin-3-O- β-neohesperidoside in Oxytropis falcate Bunge by HPLC," *Journal of Traditional Chinese Medicine*, vol. 26, no. 9, pp. 2068–2070, 2011.

[8] X. B. Fu and D. W. Wang, *Modern study of wound healing*, People's Military Medical Press, Beijing, Chinese, 1999.

[9] A. O. Li, *Burn Therapy*, people's medical publishing house, Beijing, China, 2nd edition, 1995.

[10] G.-M. Yang, D. Guang-Ming, W. Tang et al., "Anti-inflammatory and antioxidant activities of Oxytropis falcata fractions and its possible anti-inflammatory mechanism," *Chinese Journal of Natural Medicines*, vol. 8, no. 4, pp. 285–292, 2010.

[11] H. Jiang, J. R. Hu, X. H. Liu, and X. Cheng, "Antibacterial activity of total flavonoid aglycones from Oxytropis falcata Bunge," *Natural Product Research*, vol. 26, no. 3, pp. 407–409, 2014.

[12] X.-J. Zhang, W.-X. Liu, P. Wei et al., "Subacute toxicity and chemical analysis of Tibetan medicine Oxytropis falcata," *Zhongguo Zhongyao Zazhi*, vol. 39, no. 7, pp. 1157–1162, 2014.

[13] X. F. Lin, K. J. Chen, H. K. Shi, J. H. Zhan, and J. S. Chen, "Evaluation on skin safety for compound Oxytropis falcatagel," *Chinese Journal of Hospital Pharmacy*, vol. 35, pp. 449–453, 2015.

[14] M. D. M. Dantas, D. R. R. Cavalcante, F. E. N. Araújo et al., "Improvement of dermal burn healing by combining sodium alginate/chitosan- based films and low level laser therapy," *Journal of Photochemistry and Photobiology B: Biology*, vol. 105, no. 1, pp. 51–59, 2011.

[15] T. Muthukumar, K. Anbarasu, D. Prakash, and T. P. Sastry, "Effect of growth factors and pro-inflammatory cytokines by the collagen biocomposite dressing material containing Macrotyloma uniflorum plant extract-In vivo wound healing," *Colloids and Surfaces B: Biointerfaces*, vol. 121, pp. 178–188, 2014.

[16] F.-S. X. Yu, J. Yin, K. Xu, and J. Huang, "Growth factors and corneal epithelial wound healing," *Brain Research Bulletin*, vol. 81, no. 2-3, pp. 229–235, 2010.

[17] J. D. Chen, J. P. Kim, K. Zhang et al., "Epidermal Growth Factor (EGF) Promotes Human Keratinocyte Locomotion on Collagen by Increasing the $\alpha 2$ Integrin Subunit," *Experimental Cell Research*, vol. 209, no. 2, pp. 216–223, 1993.

[18] C. Cao, Y. Sun, S. Healey et al., "EGFR-mediated expression of aquaporin-3 is involved in human skin fibroblast migration," *Biochemical Journal*, vol. 400, no. 2, pp. 225–234, 2006.

[19] R. J. Mendonça, "Angiogenesis in Wound Healing," in *Tissue Regeneration-From Basic Biology to Clinical Application*, J. Davies, Ed., pp. 93–108, In Tech, Croatia, 2012.

[20] C. J. Busuioc, G. D. Mogosanu, F. C. Popescu, I. Lascar, H. Parvanescu, and L. Mogoanta, "Phases of the cutaneous angiogenesis process in experimental third-degree skin burns: histological and immunohistochemical study," *Romanian Journal of Morphology and Embryology*, vol. 54, pp. 163–171, 2013.

[21] D. Carter, A. Warsen, K. Mandell, J. Cuschieri, R. V. Maier, and S. Arbabi, "Delayed topical p38 MAPK inhibition attenuates full-thickness burn wound inflammatory signaling," *Journal of Burn Care & Research*, vol. 35, no. 2, pp. e83–e92, 2014.

Hindawi
Evidence-Based Complementary and Alternative Medicine
Volume 2017, Article ID 7601486, 12 pages
https://doi.org/10.1155/2017/7601486

Research Article

Optimized-SopungSunkiwon, a Herbal Formula, Attenuates Aβ Oligomer-Induced Neurotoxicity in Alzheimer's Disease Models

Jin Gyu Choi,[1] Sun Yeou Kim,[2] Jong Woo Kim,[3] and Myung Sook Oh[1,4]

[1]*Department of Life and Nanopharmaceutical Sciences, Graduate School, Kyung Hee University, 26 Kyungheedae-ro, Dongdaemun-gu, Seoul 02447, Republic of Korea*
[2]*College of Pharmacy, Gachon University, 191 Hambakmoero, Yeonsu-gu, Incheon 21999, Republic of Korea*
[3]*Department of Korean Neuropsychiatry, College of Korean Medicine and Institute of Korean Medicine, Kyung Hee University, 26 Kyungheedae-ro, Dongdaemun-gu, Seoul 02447, Republic of Korea*
[4]*Department of Oriental Pharmaceutical Science, College of Pharmacy and Kyung Hee East-West Pharmaceutical Research Institute, Kyung Hee University, 26 Kyungheedae-ro, Dongdaemun-gu, Seoul 02447, Republic of Korea*

Correspondence should be addressed to Myung Sook Oh; msohok@khu.ac.kr

Received 20 July 2017; Revised 28 September 2017; Accepted 17 October 2017; Published 7 November 2017

Academic Editor: Lucindo J. Quintans-Júnior

Alzheimer's disease (AD), the most common form of dementia, is an age-related neurodegenerative disease that is characterized by memory dysfunction, neuronal cell damage, and neuroinflammation. It is believed that AD-related pathology is mostly due to the overproduction of Aβ, especially the oligomeric form (AβO), in the brain. Evidence of the effects of multifunctional medicinal herbs in the treatment of AD has been steadily increasing. Optimized-SopungSunkiwon (OSS), a multiherbal formulation that is composed of six medicinal herbs derived from SopungSunkiwon, is a traditional medicine that is prescribed for neurodegenerative disorders in elderly patients. We previously reported that OSS showed an antiamnesic and memory enhancing effect in mice, but it is unknown whether OSS has a protective effect against AβO neurotoxicity. In this study, we investigated the effects of OSS in AD models induced by AβO *in vitro* and *in vivo*. We found that OSS protected neuronal cells and inhibited the generation of nitric oxide and reactive oxygen species against AβO toxicity *in vitro*. These results were confirmed by *in vivo* data that oral administration of OSS for 14 days attenuated memory impairments and neuronal cell death by modulating gliosis, glutathione depletion, and synaptic damage in the mouse hippocampus induced by AβO.

1. Introduction

Alzheimer's disease (AD) is characterized by progressive memory and learning disorders coupled with severe neuronal degeneration [1]. Although the exact mechanisms of AD pathogenesis remain to be established, it is widely known that amyloid-β (Aβ) deposits play a key role in the disease [2]. Among the different forms of Aβ, the oligomeric form (AβO) is thought to be primarily related to the pathogenesis of AD because of its neurotoxicity, which impairs functional synaptic plasticity and induces memory loss by inhibiting hippocampal long-term potentiation (LTP) [3–5]. AβO has also been implicated in triggering neuronal cell death by activating glial cells and generating reactive oxygen species (ROS) in AD brains [6–8]. These characteristics of AβO indicate the potential that AβO-induced experimental models to show various pathological features of AD may be useful.

The paradigm of drug discovery for neurodegenerative diseases is currently diverging from a single-target to a multitarget approach, because the effects of single-target drugs are too limited to allow for effective treatment of complex neurodegenerative diseases such as AD [9]. Recent studies have provided considerable evidence showing that the multimodal effects of several herbal extracts or herbal formulations are highly effective in the treatment of AD [10, 11]. For example, EGb761, a standardized extract of *Ginkgo biloba* leaves, inhibits Aβ-induced ROS accumulation, neuronal damage, and formation of Aβ fibrils [12–14]. B401, a herbal formulation that is famous in traditional Chinese

medicine and is widely used to treat brain diseases, attenuates glutamate-induced neuronal cell death in SH-SY5Y cells and cognitive dysfunction in triple transgenic AD mice by reducing AD-related pathological proteins including Aβ and tau [15]. Therefore, traditional herbal medicines, which have multitarget and multipotent effects, are emerging as potential treatments options for AD.

Optimized-SopungSunkiwon (OSS) is traditionally prescribed to treat senile constipation and it has been reported that it also works effectively in hyperglycemia, hyperlipidemia, and diabetic nephropathy [16, 17]. OSS consists of the following six medicinal herbs: *Bombyx mori* L., *Plantago asiatica* L., *Rheum palmatum* L., *Poria cocos* Wolf, *Gardenia jasminoides* Ellis, and *Cuscuta chinensis* Lam. A previous study showed that *Bombycis excrementum*, the herb that is present in the largest proportion in the composition of OSS, protects hippocampal neurons and ameliorates memory impairment in mice in which AD-like pathological features are induced by intrahippocampal injection of AβO$_{1-42}$ [18]. Moreover, we previously confirmed that OSS treatment results in memory enhancing activity as well as recovery from scopolamine-induced memory loss via the facilitation of acetylcholine release and regulation of synaptic proteins in mice [19]. However, the effect of OSS against Aβ neurotoxicity is yet to be investigated.

In this study, we examined whether OSS displays neuroprotective effects against cognitive deficits, neuronal cell death, neuroinflammation, and synaptic loss in AβO$_{1-42}$-induced AD models *in vitro* and *in vivo*.

2. Experimental Procedure

2.1. Materials. Roswell Park Memorial Institute (RPMI) medium, Dulbecco's modified Eagle medium (DMEM), fetal bovine serum (FBS), horse serum (HS), and penicillin–streptomycin (P/S) were purchased from Hyclone Laboratories, Inc. (Logan, UT, USA). Rabbit monoclonal antiglial fibrillary acid protein (GFAP) and rat monoclonal anti-CD11b (Mac-1) were purchased from Millipore Bioscience Research (Bedford, MA, USA). Rabbit polyclonal antipostsynaptic density protein-95 (PSD-95) was purchased from Abcam (Cambridge, MA, USA). Biotinylated goat anti-rabbit, rabbit anti-rat, goat anti-mouse antibody, normal goat serum (NGS), normal rabbit serum (NRS), and avidin–biotin complex (ABC) kit were purchased from Vector Lab (Burlingame, CA, USA). 3-(4,5-Dimethylthiazol-2-yl)2,5-diphenyltetrazolium bromide (MTT), 2,2-diphenyl-2-picrylhydrazyl (DPPH), 2,2-azinobis-(3-ethylbenzothiazoline-6-sulphonic acid) (ABTS), 2,7-dichlorodihydrofluorescein diacetate (DCFH-DA), cresyl violet, paraformaldehyde (PFA), 3,3-diaminobenzidine (DAB), sodium chloride, sodium nitrite, collagen, Griess reagent, phosphate-buffered saline (PBS), 1,1,1,3,3,3-hexafluoro-2-propanol (HFIP), dimethyl sulfoxide (DMSO), DMSO anhydrous, and mouse monoclonal antisynaptophysin (SYN) were purchased from Sigma–Aldrich (St. Louis, MO, USA). Aβ_{1-42} peptide was purchased from American Peptide (Sunnyvale, CA, USA). Bradford protein assay was purchased from Bio-Rad Laboratories (Hercules, CA, USA).

2.2. Preparation of AβO$_{1-42}$ Solution. Soluble oligomers were generated by previously described methods with slight modifications [18]. Briefly, Aβ_{1-42} peptide was dissolved in HFIP to the final concentration of 1 mg/ml at room temperature for 3 days. The peptide was aliquoted and dried under vacuum for 1 h. The aliquoted peptide was dissolved in DMSO anhydrous form to the final concentration of 1 mM. Protein determination was performed by Bradford assay to calculate molarities of solution. The Aβ_{1-42} stock in DMSO anhydrous form was diluted directly into sterilized PBS at 10 μM and incubated at 4°C for 24 h to make oligomeric form of Aβ_{1-42}.

2.3. Preparation of OSS Extract. OSS was prepared as has been previously described [19]. Briefly, OSS was made from a mixture of the following six herbs: *Bombycis excrementum, Plantaginis Semen, Rhei Rhizoma, Gardenia Fructus, Poria*, and *Cuscutae Semen* (1.5 : 1.5 : 0.5 : 1 : 1 : 1) obtained from the Kyongdong local market (Seoul, Korea). Each herb mixture (400 g) was extracted three times with sonication in distilled water for 2 h. Following filtration, the solution was evaporated in a vacuum and lyophilized (yield: 1.925%). The powder was kept at 4°C before use. This extract was previously standardized by analysis of sennoside A, crocin, and geniposide contents [19].

2.4. DPPH Radical Scavenging Activity Assay. Various concentrations of OSS were mixed with 0.20 mM DPPH ethanolic solution (1 : 1). After incubation at dark room temperature for 30 min, the mixture determined at the absorbance of 517 nm using spectrophotometer. Also, the antioxidant activity of OSS was expressed as half maximal inhibiting concentration (IC$_{50}$) which is defined as the concentration of OSS required to scavenge 50% of DPPH radicals. IC$_{50}$ values were estimated by a nonlinear regression. DPPH radical scavenging activity (%) = {control – (sample – blank)}/control × 100.

2.5. ABTS Cation Scavenging Activity Assay. 7.40 mM ABTS solution was added to 2.60 mM potassium phosphate 1 day before starting the experiment in the dark. Various concentrations of OSS were mixed with 7.40 mM ABTS solution and 2.60 mM potassium phosphate. After incubation at room temperature for 5 min, the mixture determined at the absorbance of 732 nm using spectrophotometer. Also, the antioxidant activity of OSS was expressed as IC$_{50}$, which were estimated by a nonlinear regression. ABTS cation scavenging activity (%) = (control – sample)/control × 100.

2.6. Cell Culture and Treatment. Rat pheochromocytoma PC12 cells were maintained in RPMI, supplemented with 5% heat-inactivated FBS, 10% HS, and 1% P/S in an atmosphere of 5% CO_2 at 37°C. Mouse BV-2 microglial cells were maintained in DMEM, supplemented with 10% heat-inactivated FBS and 1% P/S in the same conditions. All experiments were carried out 12 h after PC12 and BV-2 cells were seeded in 96-well plates at a density of 2.0×10^5 cells/ml. After the cells were about 70% confluent, various concentrations (0.1–100 μg/ml)

of OSS in FBS free media were added to the cells for 24 h at 37°C, with or without 1 μM AβO$_{1-42}$. An equal volume of vehicles was administered to the control and toxin groups, for each.

2.7. Measurement of Cell Viability. PC12 cells were seeded on 96-well plates and were treated with OSS at doses of 0.1–100 μg/ml for 24 h or pretreated with OSS for 1 h. They were then stimulated with 1 μM AβO$_{1-42}$ for 23 additional hours (pretreatment) or 1 μM AβO$_{1-42}$ was added for 1 h before treatment with OSS for 23 additional hours (post-treatment). After the treatment, supernatants were removed, and 1 mg/ml of tetrazolium dye (MTT) was added to the cells for 3 h. MTT medium was carefully removed from the wells, and the MTT formazan dye was eluted using dimethyl sulfoxide (DMSO). Absorbance was measured at a wavelength of 570 nm using a spectrophotometer (Versamax microplate reader, Molecular Device; Sunnyvale, CA, USA). Data were expressed as percentages of the values obtained for the controls.

2.8. Measurement of Extracellular NO. The accumulated level of NO in culture supernatants was measured using a colorimetric reaction with Griess reagent using a slightly modified variant of the methods that have previously been described [20]. The supernatants (100 μl) were transferred to a separate plate and added to 100 μl of Griess reagent in the dark for 10 min at room temperature. Absorbance at 550 nm was measured. For each experiment, freshly prepared sodium nitrite that had been serially diluted was used as a standard, in parallel with culture supernatants.

2.9. Measurement of Intracellular ROS. Intracellular ROS generation was measured with DCFH-DA fluorescence dye, using a slightly modified version of previously described methods [20]. DCFH-DA enters cells passively and is converted into nonfluorescent DCFH, which reacts with ROS to form the fluorescent product dichlorofluorescin (DCF). Cells were seeded onto coverslips in 24-well plates and treated with OSS at 0.1, 1, and 10 μg/mL for 1 h. Then, they were stimulated with 1 μM AβO$_{1-42}$ and incubated for an additional 30 min. The cells were incubated with 25 μM DCFH-DA for 30 min. The fluorescence intensity was determined at 485 nm excitation and 535 nm emission, using a fluorescence microplate reader (SpectraMax Gemini EM; Molecular Device, Sunnyvale, CA, USA). Representative images were obtained using a fluorescence microscope (Olympus Microscope System BX51; Olympus, Tokyo, Japan).

2.10. Measurement of Total Glutathione. The levels of total glutathione (GSH) were measured using the Total Glutathione Quantification kit (Dojindo Molecular Tech., Tokyo, Japan) according to the instruction manual and previously described method [21]. Briefly, hippocampal tissues were lysed and treated with 5% 5-sulfosalicylic acid. A coenzyme working solution, buffer solution, and enzyme working solution were added to each well at 37°C for 5 min. Then, a GSH standard solution, sample solution, and substrate working solution were added for 10 min each. Absorbance was measured using a spectrophotometer at a wavelength of 405 nm, and concentrations of GSH were determined in the sample solution using a GSH standard curve.

2.11. Animals and Surgery Procedure. Male ICR mice (8 weeks, 27–30 g) were purchased from Daehan Biolink Co. Ltd. (Eumseong, Korea). Animals were housed in cages of 5 or 6, had free access to water and food, and were maintained under a constant temperature (23 ± 1°C), humidity (60 ± 10%), and a 12 h light/dark cycle. Animal treatment and maintenance were carried out in accordance with the Principle of Laboratory Animal Care (NIH publication number 85-23, revised 1985) and the Animal Care and Use Guidelines of Kyung Hee University, Seoul, Korea. Stereotaxic injections of AβO$_{1-42}$ into mouse hippocampi were performed as previously described [18, 22]. In brief, mice were anesthetized and mounted in a stereotaxic apparatus (myNeuroLab, St. Louis, MO, USA). Each mouse was unilaterally injected (at a rate of 0.5 μl/min) with 3 μl of AβO$_{1-42}$ (10 μM) into the granule cell layer (GCL) of the hippocampus (coordinates with respect to bregma in mm: AP −2.0, ML 1.5, DV 2.0), according to a stereotaxic atlas of the mouse brain [23]. Sham-operated mice were injected with the same volume of saline alone. The accuracy of stereotaxic injection to the targeted region was monitored in all animals by examination of the needle tract within brain sections.

2.12. Drug Administration. Mice were randomly divided into 5 groups (n = 8 in each group), (1) sham group (sham-operated and saline-treated), (2) AβO$_{1-42}$ group (AβO$_{1-42}$-lesioned and saline-treated), (3) AβO$_{1-42}$ + OSS 50 mg/kg/day group (AβO$_{1-42}$-lesioned and OSS-treated: 50 mg/kg/day), (4) AβO$_{1-42}$ + OSS 100 mg/kg/day group (AβO$_{1-42}$-lesioned and OSS-treated: 100 mg/kg/day), and (5) AβO$_{1-42}$ + OSS 200 mg/kg/day group (AβO$_{1-42}$-lesioned and OSS-treated: 200 mg/kg/day). In all groups, saline and OSS solutions were administered intraorally. OSS dissolved in saline was administered once per day for 14 days (5 days before surgery and for 9 days after surgery).

2.13. Step-through Passive Avoidance Test. The step-through passive avoidance test (PAT) was performed according to a method described previously [18]. A learning and memory test was performed using a two-compartment step-through passive avoidance test apparatus. The box was divided into bright and dark compartments (21 × 21 × 21 cm^3 each) by a guillotine door. The bright compartment contained a 50 W electric lamp, and the floor of the dark compartment was composed of 2 mm stainless steel rods spaced 1 cm apart. Mice were treated with either OSS or vehicle 1 h before the acquisition trial and were initially placed in the bright compartment for the acquisition trial. The door between the two compartments was opened 10 s later. When the hind legs of the mice entered the dark chamber, the guillotine door was closed and an electrical foot shock (0.6 mA) was delivered through the grid floor for 3 s. The mice were again placed in the bright chamber for the retention trial, which was conducted 24 h after the acquisition trial. The time taken for a mouse to enter the dark chamber after the door was

opened was defined as the latency time. This was recorded for latencies of up to 300 s.

2.14. Novel Object Recognition Test. The novel object recognition test (NORT) was performed according to a method described previously [18]. The experiments were carried out in a grey open field box ($45 \times 45 \times 50\,cm^3$). Prior to the test, mice were habituated to the test box for 5 min without the presence of objects. After the habituation period, mice were placed into the test box containing two identical objects and were allowed to explore for 3 min. The objects used in this study were wooden blocks of the same size but different shape. The time spent by the animal exploring each object was measured (defined as the training session). Twenty-four hours after the training session, mice were allowed to explore the objects in the test box for 3 min, during which the familiar object used in the previous training session was placed with a novel object. The time that the animals spent exploring the novel and the familiar objects was recorded (defined as the test session). Animals were considered to be exploring an object when they were facing, sniffing, or biting it. The test box and objects were cleaned with 70% ethanol between sessions. Results were expressed as percentages of novel object recognition time (time percentage = exploring time for novel object/[exploring time for novel object + exploring time for familiar object] × 100).

2.15. Brain Tissue Preparation. At 24 h after the memory examination, hippocampal tissue was dissected from the brains of 3 mice from each group in order to measure total glutathione levels. The remaining mice were transcardially perfused with 0.05 M phosphate-buffered saline (PBS) and then fixed with cold 4% PFA in 0.1 M phosphate buffer for cresyl violet staining and immunohistochemistry (n = 5 per group). The perfused brains were removed (whole) and postfixed overnight at 4°C in 0.1 M phosphate buffer containing 4% PFA. The brains were then immersed in a solution containing 30% sucrose in 0.05 M PBS for cryoprotection. Coronal sections (30 μm) were serially cut using a freezing microtome (Leica, Nussloch, Germany) and stored in cryoprotectant (25% ethylene glycol, 25% glycerol, 0.05 M phosphate buffer) at 4°C until use in immunohistochemistry.

2.16. Cresyl Violet Staining and Immunohistochemistry. For histological assessment of cell loss, free floating sections of mice brains were processed for cresyl violet staining and immunohistochemistry as described in the section above, following a method that had previously been used [18]. For cresyl violet staining, the sections were stained with 0.5% cresyl violet, after which they were mounted onto gelatin-coated slides, dehydrated through graded alcohols (70%, 80%, 90%, and 100%), placed in xylene, and coverslipped using histomount medium. For immunohistochemistry, brain sections were briefly rinsed in PBS and treated with 1% hydrogen peroxide for 15 min. The sections were incubated with a rabbit anti-GFAP antibody (1 : 3000 dilution), a rat anti-Mac-1 (1 : 1000 dilution), a mouse anti-SYN (1 : 200 dilution), or a rabbit anti-PSD-95 antibody (1 : 500 dilution) overnight at 4°C in the presence of 0.3% triton x-100 and NGS or NRS. After rinsing in PBS, the sections were then incubated with biotinylated anti-rabbit IgG, anti-rat IgG, or anti-goat IgG (1 : 200 dilution) for 90 min and with ABC (1 : 100 dilution) for 1 h at room temperature. Peroxidase activity was visualized by incubating sections with DAB in 0.05 M tris-buffered saline (pH 7.6). After several rinses with PBS, sections were mounted onto gelatin-coated slides, dehydrated, and coverslipped with histomount medium. The optical densities of cresyl violet, GFAP, Mac-1, SYN, and PSD-95-positive cells in the dentate gyrus (DG) or CA3 region of the hippocampus were analyzed using ImageJ software (Bethesda, MD, USA). The images were taken at a 400x magnification using an optical light microscope (Olympus Microscope System BX51; Olympus, Tokyo, Japan) equipped with a 20x objective lens. Data are presented as percentages of the sham group values obtained.

2.17. Statistical Analysis. All statistical parameters were calculated using GraphPad Prism 5.0 software. Values are expressed as the mean ± standard error of the mean (SEM). Results were analyzed by one-way analysis of variance (ANOVA) analysis followed by the Newman-Keuls multiple comparison post hoc test. Differences with a p value lower than 0.05 were considered statistically significant.

3. Results

3.1. Effect of OSS against AβO$_{1-42}$-Induced Neurotoxicity In Vitro. It has been reported that AβO$_{1-42}$ induces PC12 cell death by inducing apoptosis [24]. In this study, we investigated whether OSS provides protection against AβO$_{1-42}$-induced cell death *in vitro*. Treatment with OSS only at 0.1–100 μg/ml for 24 h showed no significant difference in cell viability compared to the control group (Figure 1(a)). Pretreatment with OSS at 10 and 100 μg/ml significantly inhibited the reduction of cell viability (82.40 ± 3.02% and 88.40 ± 3.60%, resp.) compared with that of the 1 μM AβO$_{1-42}$ only treatment group (68.20 ± 2.16%; Figure 1(b)). Posttreatment with OSS at 10 μg/ml also significantly ameliorated cell viability (67.73 ± 2.59%) compared with that of AβO$_{1-42}$ only treatment group (55.10 ± 0.96%; Figure 1(c)).

3.2. Effect of OSS AβO$_{1-42}$-Induced NO Generation In Vitro. NO plays a key role in a variety of inflammatory statuses, being released in response to pathological stimuli [25]. Excessive concentrations of NO also lead to the formation of oxidative stress cascades, thereby contributing to a neurotoxic cascade such as Aβ-mediated neurodegeneration [26]. To examine the anti-inflammatory effects of OSS against AβO$_{1-42}$, we evaluated whether OSS inhibits NO production in activated microglia cells induced by AβO$_{1-42}$. Incubation with 1 μM AβO$_{1-42}$ increased NO production up to about 10 μM. Compared to the group treated with AβO$_{1-42}$ only, the group that underwent pretreatment with OSS at 1 and 10 μg/ml significantly inhibited NO generation (6.18 ± 0.46 μM and 5.98 ± 0.64 μM, resp.) (Figure 2(a)). Posttreatment with OSS showed that NO generation was inhibited compared to the production levels observed in the AβO$_{1-42}$ only treatment group. However, the observed difference was not significant (Figure 2(b)).

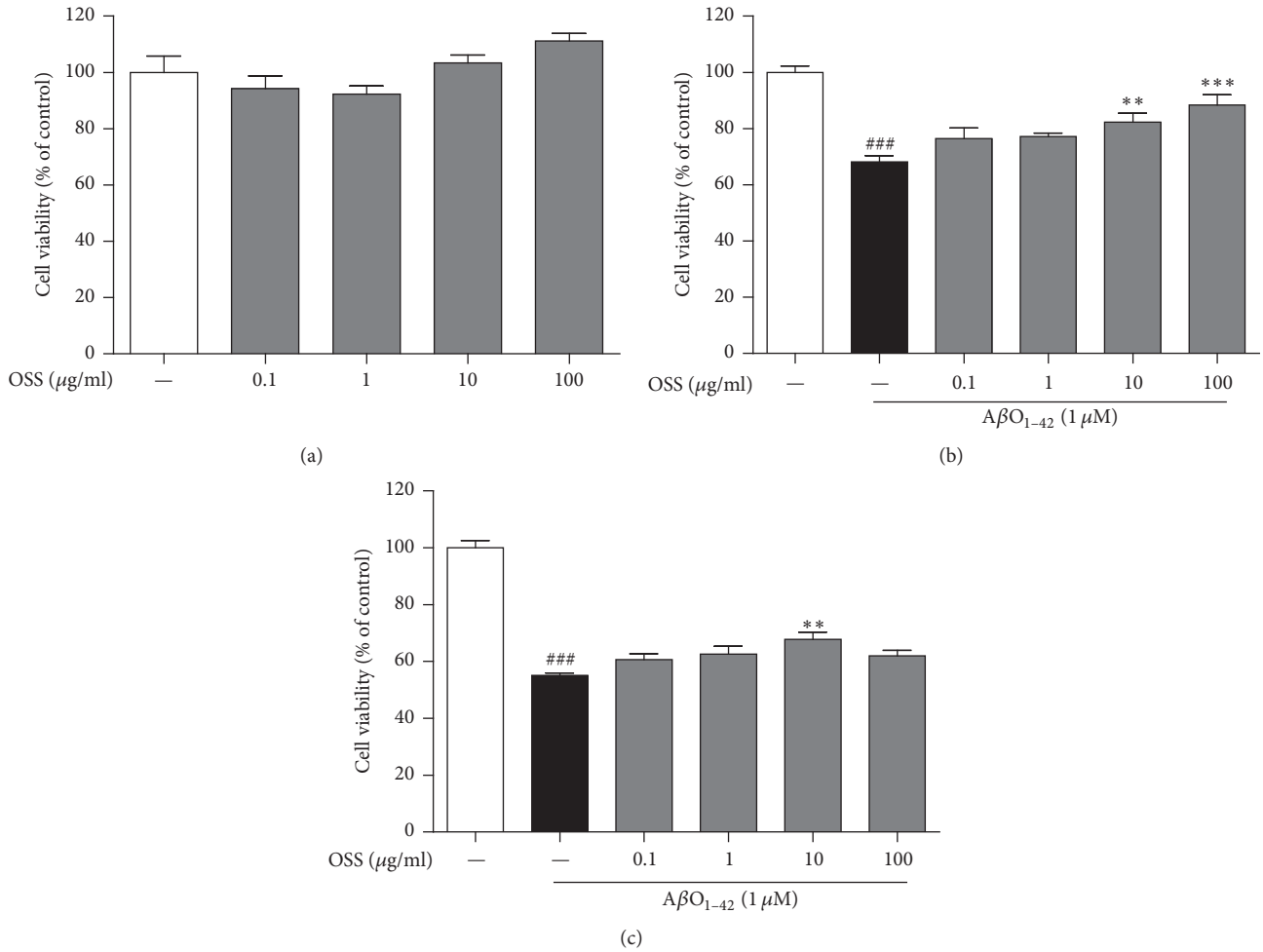

Figure 1: *Neuroprotective effect of OSS on AβO$_{1-42}$ toxicity in PC12 cells.* Cells were treated with OSS for 24 h without 1 μM AβO$_{1-42}$ (a). The cells were also treated with 1 μM AβO$_{1-42}$ 1 h after OSS treatment (b) or 1 h before OSS treatment (c). Cell viability was measured using by MTT assay. OSS treatment alone did not change their viability, while OSS pretreatment or posttreatment protected PC12 cells against AβO$_{1-42}$-induced toxicity. Data are expressed as percentages relative to untreated controls. Values are indicated as the mean ± SEM. $^{###}p < 0.001$ compared to the control group; $^{**}p < 0.01$ and $^{***}p < 0.001$ compared to the AβO$_{1-42}$-only treated group.

Table 1: *IC$_{50}$ values for DPPH and ABTS radical scavenging activity.* OSS showed higher DPPH free radical and ABTS cation scavenging activity than that of positive control. Data were expressed as IC$_{50}$ values. OSS: Optimized-SopungSunkiwon extract and SBE: *Scutellaria baicalensis* Georgi extract (used as a positive control).

	IC$_{50}$ (μg/mL)	
	DPPH assay	ABTS assay
OSS	18.33	25.34
SBE	27.75	25.40

3.3. Antioxidant Effects of OSS In Vitro and In Vivo. To evaluate the antioxidant potential of OSS, we performed the DPPH free radical and ABTS cation scavenging assay. We found that OSS showed higher scavenging activity than an extract of *Scutellaria baicalensis* Georgi (SBE), used as a positive control in both the DPPH and ABTS assays (Table 1). This trend is in accordance with the inhibitory effects of OSS against AβO$_{1-42}$-induced ROS generation. In this study, pretreatment with OSS at 10 μg/ml significantly inhibited ROS generation (144.53 ± 11.44%) when compared to the values obtained with the AβO$_{1-42}$ only treatment group (168.77 ± 14.53%; Figure 3(a)). Posttreatment with OSS at 10 μg/ml also led to significantly lower ROS generation values (109.61 ± 8.25%) after AβO$_{1-42}$ insult compared to those obtained from the AβO$_{1-42}$ only treatment group (139.74 ± 7.20%; Figure 3(b)). Moreover, we investigated the effects of OSS on the induction of GSH as an antioxidant in the mouse hippocampus. The levels of GSH, the most prevalent antioxidant in the brain, consistently decrease with increasing oxidative stress in AD [27, 28]. The hippocampal GSH concentration of 10 μM AβO$_{1-42}$-injected vehicle-treated mice was significantly reduced (58.90 ± 2.85%), while treatment with OSS at 100 and 200 mg/kg/day significantly recovered (78.78 ± 5.63% and 91.24 ± 3.23%) GSH concentration. These results indicate that OSS has antioxidant effects against oxidative stress induced by AβO$_{1-42}$.

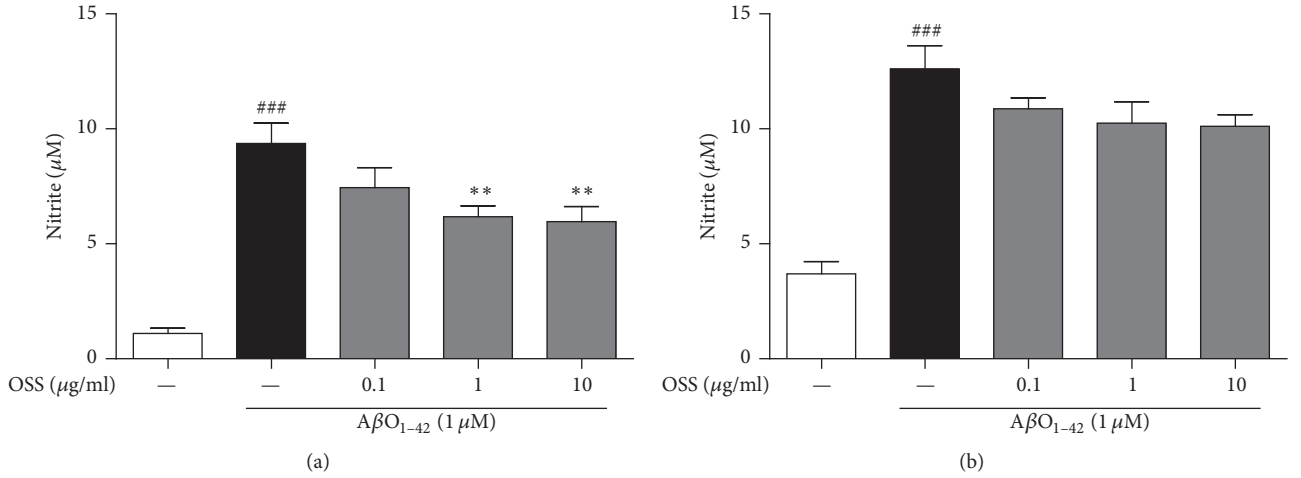

FIGURE 2: *Inhibitory effect of OSS on AβO$_{1-42}$-induced NO generation in BV-2 microglial cells.* The cells were with 1 μM AβO$_{1-42}$ 1 h after OSS treatment (a) or 1 h before OSS treatment (b). NO generation was determined by the nitrite level in the supernatant using the Griess reagent. OSS pre- or posttreatment inhibited overproduction of nitrite level by AβO$_{1-42}$ stress. Values are indicated as the mean ± SEM. $^{###}p < 0.001$ compared to the control group; $^{**}p < 0.01$ compared to the AβO$_{1-42}$-only treated group.

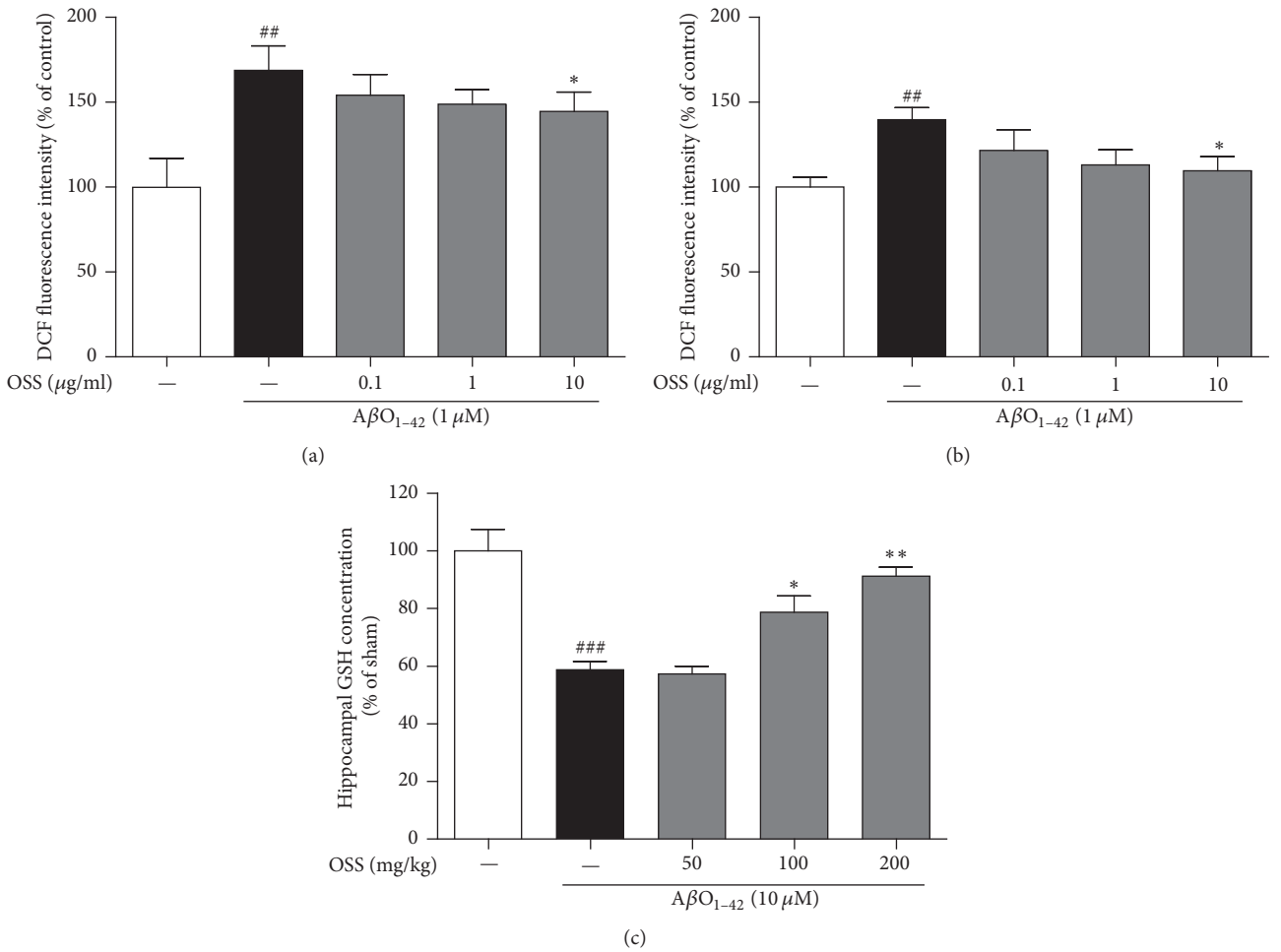

FIGURE 3: *Inhibitory effect of OSS on AβO$_{1-42}$-induced intracellular ROS generation and hippocampal GSH depletion.* The ROS and GSH levels were measured by the fluorescence dye of DCF and manufactured manual, respectively. Pre- or posttreatment with OSS inhibited ROS generation in PC12 cells (a, b) and reduction of GSH levels in hippocampal tissues (c) against AβO$_{1-42}$ toxicity. Data are expressed as percentages relative to untreated controls (intracellular ROS levels) or sham-operated group (hippocampal GSH levels). Values are indicated as the mean ± SEM of four replicates. $^{##}p < 0.01$ and $^{###}p < 0.001$ compared to the control (in PC12 cells) or sham-operated (in hippocampal tissues) group; $^{*}p < 0.05$ and $^{**}p < 0.01$ compared to the AβO$_{1-42}$-only treated group.

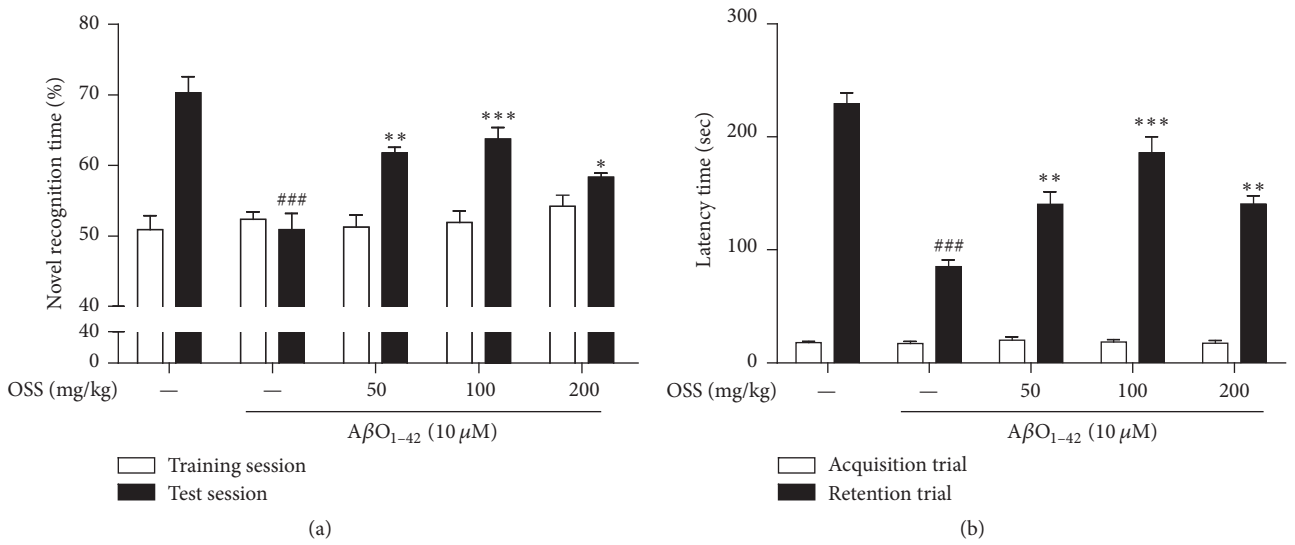

Figure 4: *Effect of OSS on $A\beta O_{1-42}$-induced memory impairment.* Mice were treated with vehicle or OSS for 14 days, starting from 5 days before stereotaxic injection of $A\beta O_{1-42}$. NORT was carried out at 7 (training session) and 8 (test session) days after $A\beta O_{1-42}$ injection (a). PAT was conducted at 9 (acquisition trial) and 10 (retention trial) days after $A\beta O_{1-42}$ injection (b). The $A\beta O_{1-42}$-injected group treated with OSS exhibited significantly ameliorating memory impairment induced by $A\beta O_{1-42}$ stress. Values are indicated as the mean ± SEM. $^{\#\#\#}p < 0.001$ compared to sham-operated group; $^{*}p < 0.05$, $^{**}p < 0.01$, and $^{***}p < 0.001$ compared to the $A\beta O_{1-42}$-only treated group.

3.4. Effect of OSS on Memory Impairment Induced by Intrahippocampal $A\beta O_{1-42}$ Injection in Mice. To investigate whether OSS ameliorated memory impairment in mice receiving an intrahippocampal injection of $A\beta O_{1-42}$, NORT and PAT were performed in this study. In the NORT, the $A\beta O_{1-42}$-injected mice spent similar amounts of time (50.90 ± 2.29%) exploring the novel object and the familiar object during the test session. In contrast, sham-operated mice spent more time exploring the novel object (70.28 ± 2.30%). Treatment with OSS at 50, 100, and 200 mg/kg/day significantly improved $A\beta O_{1-42}$-induced cognitive deficits in this test (61.76 ± 0.81%, 63.75 ± 1.62%, and 58.34 ± 0.60%, resp.; Figure 4(a)). No significant differences in novel object recognition time were found between any of the tested groups during the training session.

In PAT, the mean latency time of the $A\beta O_{1-42}$-injected vehicle-treated group (85.13 ± 6.04 s) was significantly shorter than that of the sham-operated group (229.42 ± 9.72 s). OSS administered at 50, 100, and 200 mg/kg/day significantly reversed the observed effect of the $A\beta O_{1-42}$-injected vehicle-treatment in this test (140.27 ± 11.16 s, 186.08 ± 14.08 s, and 140.51 ± 7.48 s, resp.; Figure 4(b)). No differences in latency time were observed between any of the tested groups during the acquisition trial.

3.5. Effect of OSS on $A\beta O_{1-42}$-Triggered Neuronal Atrophy in the Mouse Hippocampus. Brain atrophy caused by neuronal death is a pathological hallmark of AD in humans and hippocampal atrophy, in particular, is closely related to memory dysfunction [29, 30]. To further understand the mechanisms underlying the recovery of memory function, the inhibition of $A\beta O_{1-42}$-triggered hippocampal neuronal death by OSS was investigated using cresyl violet staining. The $A\beta O_{1-42}$-induced reductions in neuronal density in the granule cell layer (GCL) of the DG (89.23 ± 1.47%) and CA3 (60.25 ± 2.45%) hippocampal regions were significant compared to those of the sham-operated group. This loss was significantly inhibited by OSS treatment at 50, 100, and 200 mg/kg/day in the CA3 region of the mouse hippocampus (Figure 5).

3.6. Effects of OSS on $A\beta O_{1-42}$-Induced Astrocyte and Microglia Activation in the Mouse Hippocampus. It is known that the activation of astrocyte and microglia under neuroinflammatory conditions plays an important role in the destruction of neurons and leads to synaptic dysfunction, thereby resulting in memory deficits [31]. The intensity of GFAP, a specific marker for astrocytes, in the hilus region of the DG was significantly increased in the $A\beta O_{1-42}$-injected group (190.37 ± 5.10%) as compared with the sham-operated group. This intensity was significantly reduced after OSS treatment at 100 and 200 mg/kg/day (160.89 ± 4.62% and 160.27 ± 6.30%, resp.; Figure 6(a)).

The intensity of mac-1, a specific marker for microglia, in the hilus region of the DG was also nearly doubled in the $A\beta O_{1-42}$-injected group (188.56 ± 9.92%) compared with the sham-operated group. In contrast, mac-1-positive intensity of $A\beta O_{1-42}$-injected mice treated with OSS at 100 and 200 mg/kg/day was significantly decreased (159.25 ± 2.76% and 156.56 ± 4.44%, resp.; Figure 6(b)). Taken together, OSS treatment effectively inhibits hyperactivation of astrocyte and microglia triggered by $A\beta O_{1-42}$ toxicity.

3.7. Effects of OSS on Synaptic Damage Derived from $A\beta O_{1-42}$ in the Mouse Hippocampus. Growing evidence shows that $A\beta O$ induce depletion of hippocampal synaptic proteins such as SYN and PSD-95, resulting in memory dysfunction in

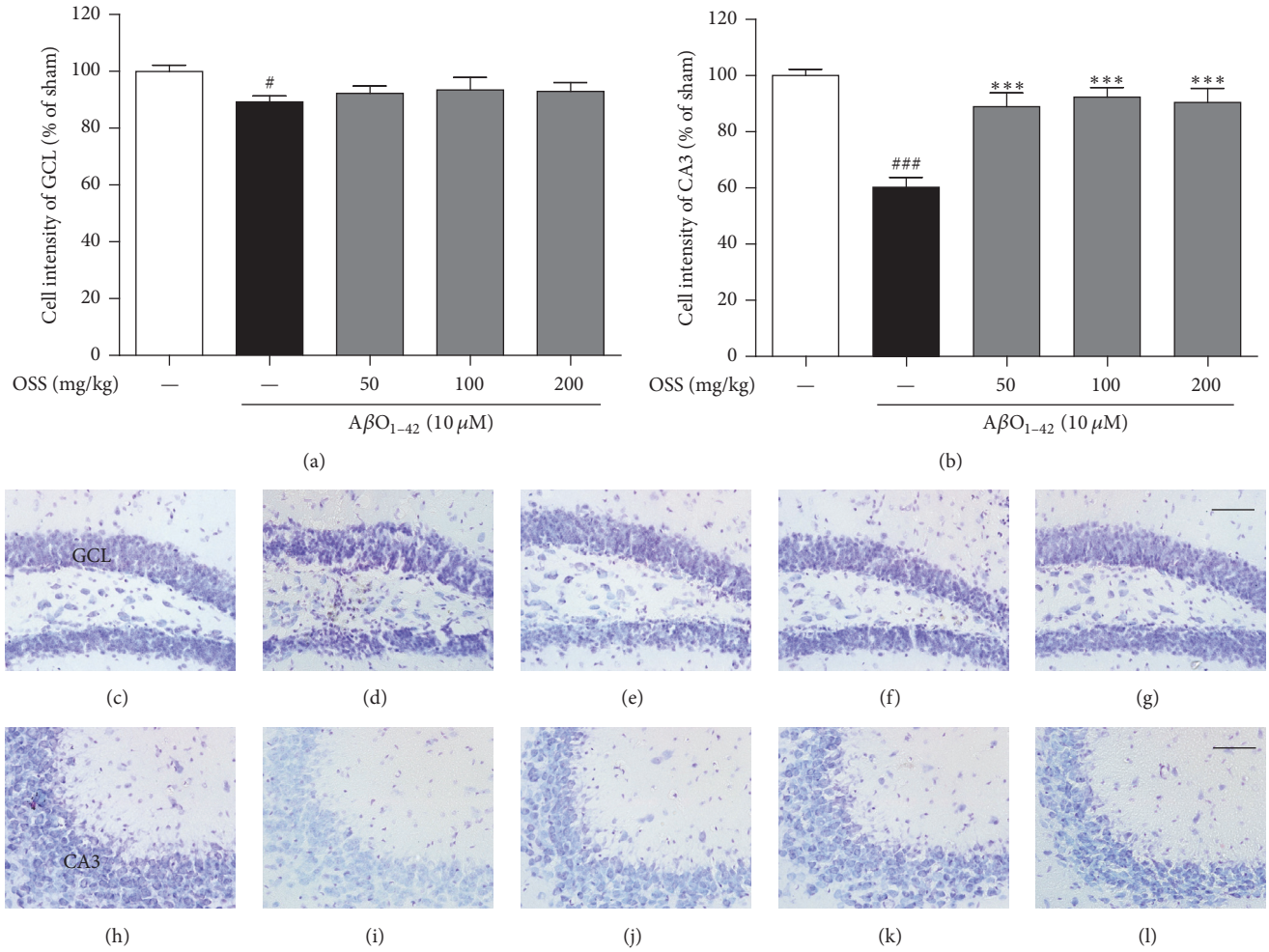

Figure 5: *Effect of OSS on hippocampal cell death induced by $A\beta O_{1-42}$ toxicity.* Mice were treated with vehicle or OSS for 14 days, starting from 5 days before stereotaxic injection of $A\beta O_{1-42}$. Hippocampal cell loss was determined using cresyl violet staining. Quantification was performed by measuring the cell intensity of stained cells in the GCL (a) and in the CA3 (b). Representative photomicrographs are shown for the GCL (c–g) and CA3 (h–l) from each group (400x magnification). Scale bar = 50 μm. (c, h) Sham-operated group; (d, i) $A\beta O_{1-42}$ only treated group; (e, j) $A\beta O_{1-42}$ + OSS 50 mg/kg/day group; (f, k) $A\beta O_{1-42}$ + OSS 100 mg/kg/day group; (g, l) $A\beta O_{1-42}$ + OSS 200 mg/kg/day group. Data are expressed as percentages relative to sham-operated group. Values are indicated as the mean ± SEM. $^{\#}p < 0.05$ and $^{\#\#\#}p < 0.001$ compared to sham-operated group; $^{***}p < 0.001$ compared to the $A\beta O_{1-42}$-only treated group.

AD [32, 33]. As shown in Figure 7, the immunoreactivity of both SYN and PSD-95 in the hippocampal CA3 region was markedly decreased in the $A\beta O_{1-42}$-injected group (75.21 ± 2.66% and 75.95 ± 1.27%, resp.) compared with sham-operated group. This trend was significantly reversed by OSS treatment at 50, 100, and 200 mg/kg/day for both SYN (85.10 ± 2.27%, 88.10 ± 1.96%, and 92.65 ± 2.70%, resp.) and PSD-95 (87.18 ± 2.12%, 92.32 ± 0.93%, and 92.74 ± 1.38%, resp.). These data suggest that OSS restores $A\beta O_{1-42}$-induced synaptic disruption, which is linked to the amelioration of memory impairment.

4. Discussion

AβO, the most toxic form of Aβ, is considered to play a central role in AD pathogenesis rather than Aβ monomers or fibrils [34, 35]. He et al. demonstrated that memory impairment and hippocampal CA1 neuronal damage were more remarkable in $A\beta O_{1-42}$-infused rats than in those where features of AD pathology were induced by $A\beta_{1-42}$ fibrils due to the observation that $A\beta O_{1-42}$ more evidently exhibited proinflammatory factor stimulation than $A\beta_{1-42}$ fibrils [36]. Our present data shows that systemic treatment with OSS ameliorates memory dysfunction by blocking $A\beta O_{1-42}$-induced hippocampal cell damage, hippocampal GSH depletion, glial hyperactivation, and synaptic disruption in a mouse model of AD. It was also confirmed that OSS directly inhibited $A\beta O_{1-42}$-induced cell degeneration as well as overproduction of NO and ROS *in vitro*.

Oxidative stress is an important pathological factor of AD [37]. Several studies indicate that $A\beta_{1-42}$ peptide is at the center of oxidative damage as it is an indicator of ROS generation in AD brains [38]. Additionally, increased Aβ-mediated ROS generation can damage the endogenous

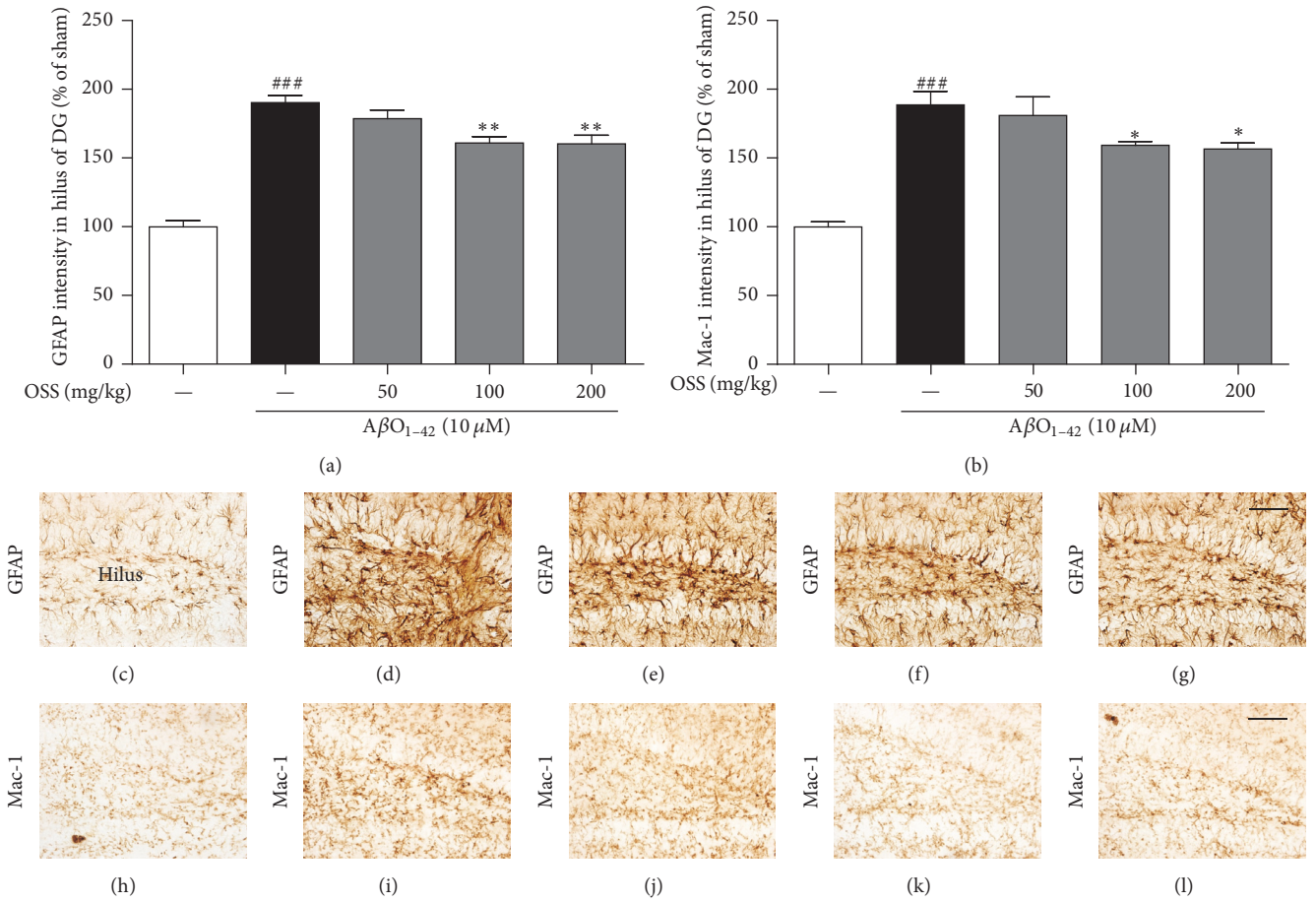

FIGURE 6: *Effect of OSS on $A\beta O_{1-42}$-induced hippocampal reactive gliosis.* Mice were treated with vehicle or OSS for 14 days, starting from 5 days before stereotaxic injection of $A\beta O_{1-42}$. Reactive gliosis was determined using GFAP and mac-1 antibody. Quantification was performed by measuring the cell intensity of GFAP-positive (a) and mac-1-positive (b) cells in the hilus region of hippocampus. Representative photomicrographs are shown for the GFAP (c–g) and mac-1 (h–l) stained cells from each group (400x magnification). Scale bar = 50 μm. (c, h) Sham-operated group; (d, i) $A\beta O_{1-42}$ only treated group; (e, j) $A\beta O_{1-42}$ + OSS 50 mg/kg/day group; (f, k) $A\beta O_{1-42}$ + OSS 100 mg/kg/day group; (g, l) $A\beta O_{1-42}$ + OSS 200 mg/kg/day group. Data are expressed as percentages relative to sham-operated group. Values are indicated as the mean ± SEM. $^{###}p < 0.001$ compared to sham-operated group; $^{*}p < 0.05$ and $^{**}p < 0.01$ compared to the $A\beta O_{1-42}$-only treated group.

antioxidant GSH and enzymes such as superoxide dismutase, GSH peroxidase, and catalase, thus inducing Aβ deposits to form in the brain [39]. Aβ deposits stimulate activation of nearby microglia and astrocytes, generating an inflammatory response through the release of proinflammatory mediators [40]. It has been suggested that activated glia are involved in neuronal degeneration because they produce potent toxic molecules including NO and cytokines [41, 42]. The present study demonstrates that OSS treatment inhibits ROS generation in PC12 cells and restores GSH contents depleted by $A\beta O_{1-42}$ in hippocampal tissue. Intracellular ROS concentration and endogenous oxidant system normalized by OSS also has an influence on the deactivation of glial cells in the hippocampus as well as on the reduction of NO production in BV-2 microglia cells.

The hippocampal synapse network originates from axons of the CA3 pyramidal region, which connect to almost all regions of the hippocampus [43, 44]. Furthermore, CA3 synapses modulate homeostatic plasticity connected to hippocampal neurons [45]. Thus, a marked decrease of synaptic density in the hippocampal CA3 region is highly relevant to synaptic disruption, which is closely linked to memory decline in the pathogenesis of AD [46]. Soluble AβO impair hippocampal LTP and can also induce memory dysfunction [3, 32]. In this study, it has been demonstrated that OSS treatment rescues synaptic damage in the hippocampal CA3 region based on the results obtained using SYN and PSD-95 markers, which are specific pre- and postsynaptic proteins, respectively [47, 48]. In this context, it can be hypothesized that the restoration of memory function after OSS treatment is mediated by facilitated hippocampal synapses.

Other approaches investigating potential therapeutics for AD indicate that the design of multitarget drugs is increasingly necessary because most single-target candidates have been unsuccessful in the treatment of AD given that it is a complex and multifaceted pathogenesis [49, 50]. This paradigm of drug discovery for AD is in accordance

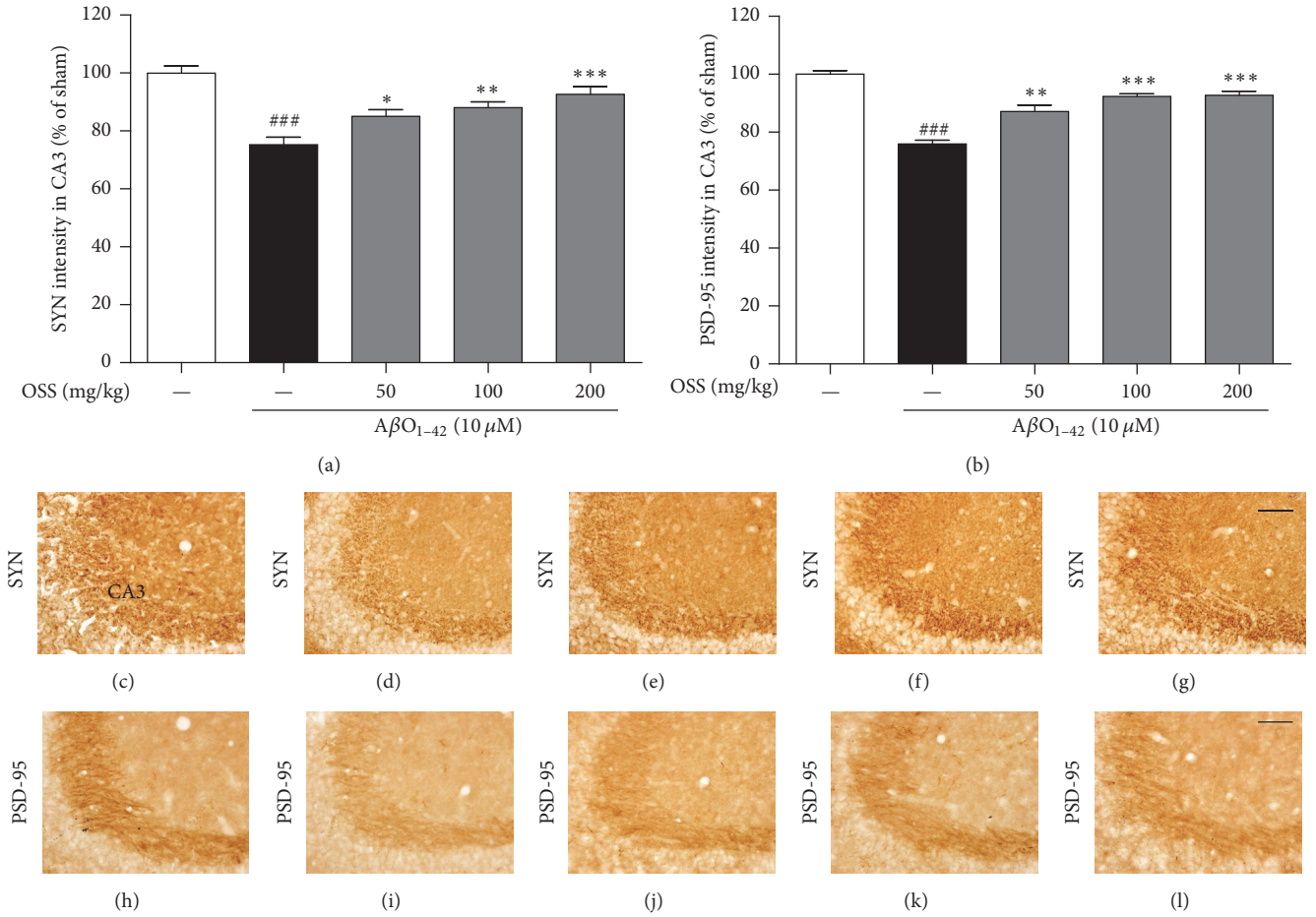

FIGURE 7: *Effect of OSS on $A\beta O_{1-42}$-induced presynaptic and postsynaptic damage in the hippocampus.* Mice were treated with vehicle or OSS for 14 days, starting from 5 days before stereotaxic injection of $A\beta O_{1-42}$. The immunoreactivity of SYN (a) and PSD-95 (b) was quantified by measuring the density of each stained area in the hippocampal CA3 region, respectively. Representative photomicrographs are shown for the SYN (c–g) and PSD-95 (h–l) stained cells from each group (400x magnification). Scale bar = 50 μm. (c, h) Sham-operated group; (d, i) $A\beta O_{1-42}$ only treated group; (e, j) $A\beta O_{1-42}$ + OSS 50 mg/kg/day group; (f, k) $A\beta O_{1-42}$ + OSS 100 mg/kg/day group; (g, l) $A\beta O_{1-42}$ + OSS 200 mg/kg/day group. Data are expressed as percentages relative to sham-operated group. Values are indicated as the mean ± SEM. $^{###}p < 0.001$ compared to sham-operated group; $^{*}p < 0.05$, $^{**}p < 0.01$, and $^{***}p < 0.001$ compared to the $A\beta O_{1-42}$-only treated group.

with the multifunctional actions of medicinal herbs. The neuroprotective effects of OSS observed in this study can be due to each individual herb of OSS. Water extract from silkworm feces (Bombycis excrementum), for example, was shown to protect hippocampal neurons and memory impairment induced by $A\beta O_{1-42}$ in our previous report [18]. Rhaponticin and rhapontigenin isolated from rhubarb roots (Rhei Rhizoma) significantly inhibit $A\beta_{1-42}$-induced apoptotic mechanisms by regulating Bax/Bcl-2 proapoptotic genes in human neuroblastoma cells [51]. Additionally, the protective effects of Poria water extract against $A\beta_{1-42}$-mediated cell death in PC12 cells were also reported [52]. Furthermore, geniposide, one of the active compounds of *Gardeniae fructus*, has been shown to exhibit multifunctional neuroprotective effects by blocking receptors for advanced end product-mediated signaling in APP/PS1 transgenic mice and BV-2 microglia cells [53, 54]. These constituents of OSS may have contributed to its neuroprotective effects against $A\beta O_{1-42}$ neurotoxicity.

5. Conclusion

In summary, OSS treatment alleviates $A\beta O_{1-42}$-induced damage of memory function and hippocampal neurons. This effect is likely to be mediated by the inhibition of oxidative stress, neuroinflammation, and decline in hippocampal synaptic density. Further detailed investigation is required to reveal the underlying mechanisms that might explain how OSS treatment regulates neuroinflammation and hippocampal neuronal and synaptic damage. Taken together, our data suggest that OSS may be a potential multitargeted candidate for AD treatment.

Conflicts of Interest

All authors declare no conflicts of interest.

Acknowledgments

This study was supported by a Grant of the Oriental Medicine R&D Project, Ministry for Health & Welfare & Family Affairs, Republic of Korea (B090039). This study was also supported by Medical Research Center Program through the National Research Foundation of Korea funded by the Ministry of Science and ICT (NRF-2017R1A5A2014768).

References

[1] R. Anand, K. D. Gill, and A. A. Mahdi, "Therapeutics of Alzheimer's disease: past, present and future," *Neuropharmacology*, vol. 76, pp. 27–50, 2014.

[2] M. P. Murphy and H. LeVine III, "Alzheimer's disease and the amyloid-β peptide," *Journal of Alzheimer's Disease*, vol. 19, no. 1, pp. 311–323, 2010.

[3] G. M. Shankar, S. Li, T. H. Mehta et al., "Amyloid-β protein dimers isolated directly from Alzheimer's brains impair synaptic plasticity and memory," *Nature Medicine*, vol. 14, no. 8, pp. 837–842, 2008.

[4] J. P. Cleary, D. M. Walsh, J. J. Hofmeister et al., "Natural oligomers of the amyloid-β protein specifically disrupt cognitive function," *Nature Neuroscience*, vol. 8, no. 1, pp. 79–84, 2005.

[5] H.-W. Wang, J. F. Pasternak, H. Kuo et al., "Soluble oligomers of β amyloid (1-42) inhibit long-term potentiation but not long-term depression in rat dentate gyrus," *Brain Research*, vol. 924, no. 2, pp. 133–140, 2002.

[6] D. Walker, L. F. Lue, G. Paul, A. Patel, and M. N. Sabbagh, "Receptor for advanced glycation endproduct modulators: A new therapeutic target in Alzheimer's disease," *Expert Opinion on Investigational Drugs*, vol. 24, no. 3, pp. 393–399, 2015.

[7] M. R. Minter, J. M. Taylor, and P. J. Crack, "The contribution of neuroinflammation to amyloid toxicity in Alzheimer's disease," *Journal of Neurochemistry*, vol. 136, no. 3, pp. 457–474, 2016.

[8] C. Giovanna, C. Cecchi, A. Pensalfini et al., "Generation of reactive oxygen species by beta amyloid fibrils and oligomers involves different intra/extracellular pathways," *Amino Acids*, vol. 38, no. 4, pp. 1101–1106, 2010.

[9] H. Zheng, M. Fridkin, and M. Youdim, "From single target to multitarget/network therapeutics in Alzheimer's therapy," *Pharmaceuticals*, vol. 7, no. 2, pp. 113–135, 2014.

[10] L. Li, L. Zhang, and C.-C. Yang, "Multi-target strategy and experimental studies of traditional Chinese medicine for Alzheimer's disease therapy," *Current Topics in Medicinal Chemistry*, vol. 16, no. 5, pp. 537–548, 2016.

[11] H. Geun Kim and M. Sook Oh, "Herbal medicines for the prevention and treatment of Alzheimer's disease," *Current Pharmaceutical Design*, vol. 18, no. 1, pp. 57–75, 2012.

[12] Y. Luo, J. V. Smith, V. Paramasivam et al., "Inhibition of amyloid-β aggregation and caspase-3 activation by the Ginkgo biloba extract EGb761," *Proceedings of the National Acadamy of Sciences of the United States of America*, vol. 99, no. 19, pp. 12197–12202, 2002.

[13] J. V. Smith and Y. Luo, "Elevation of oxidative free radicals in Alzheimer's disease models can be attenuated by Ginkgo biloba extract EGb 761," *Journal of Alzheimer's Disease*, vol. 5, no. 4, pp. 287–300, 2003.

[14] C. Shi, L. Zhao, B. Zhu et al., "Protective effects of Ginkgo biloba extract (EGb761) and its constituents quercetin and ginkgolide B against β-amyloid peptide-induced toxicity in SH-SY5Y cells," *Chemico-Biological Interactions*, vol. 181, no. 1, pp. 115–123, 2009.

[15] C.-H. Hsu, S.-E. Wang, C.-L. Lin, C.-J. Hsiao, S.-J. Sheu, and C.-H. Wu, "Neuroprotective Effects of the Herbal Formula B401 in Both Cell and Mouse Models of Alzheimer's Disease," *Evidence-Based Complementary and Alternative Medicine*, vol. 2016, Article ID 1939052, 2016.

[16] Y. Y. Kim, K. M. Kang, and S. H. Chung, "Long-term administration of Sopungsungi-won (SP) prevents diabetic nephropathy in Zucker diabetic fatty rats," *Archives of Pharmacal Research*, vol. 25, no. 6, pp. 917–922, 2002.

[17] Y. Y. Kim, H. J. Kang, S. K. Ko, and S. H. Chung, "Sopungsungi-won (SP) prevents the onset of hyperglycemia and hyperlipidemia in Zucker diabetic fatty rats," *Archives of Pharmacal Research*, vol. 25, no. 6, pp. 923–931, 2002.

[18] M. Moon, J. G. Choi, S. Y. Kim, and M. S. Oh, "Bombycis excrementum reduces amyloid-beta oligomer-induced memory impairments, neurodegeneration, and neuroinflammation in mice," *Journal of Alzheimer's Disease*, vol. 41, no. 2, pp. 599–613, 2014.

[19] J. G. Choi, W. M. Yang, T. H. Kang, and M. S. Oh, "Effects of optimized-SopungSunkiwon on memory impairment and enhancement," *Neuroscience Letters*, vol. 491, no. 2, pp. 93–98, 2011.

[20] J. G. Choi, G. Park, H. G. Kim, D.-S. Oh, H. Kim, and M. S. Oh, "In vitro and in vivo neuroprotective effects ofwalnut (juglandis semen) in models of parkinson's disease," *International Journal of Molecular Sciences*, vol. 17, no. 1, article no. 108, 2016.

[21] D.-S. Hwang, H. G. Kim, H.-J. Kwon et al., "Dangguijakyak-san, a medicinal herbal formula, protects dopaminergic neurons from 6-hydroxydopamine-induced neurotoxicity," *Journal of Ethnopharmacology*, vol. 133, no. 2, pp. 934–939, 2011.

[22] Y. Y. Jean, J. Baleriola, M. Fà, U. Hengst, and C. M. Troy, "Stereotaxic infusion of oligomeric amyloid-beta into the mouse hippocampus," *Journal of Visualized Experiments*, vol. 2015, no. 100, Article ID e52805, 2015.

[23] G. Paxinos, *The Mouse Brain in Stereotaxic Coordinates*, Academic Press, Cambridge, Massachusetts, USA, 2nd edition, 2001.

[24] C. Qiu, Y. P. Wang, X. D. Pan, X. Y. Liu, Z. Chen, and L. B. Liu, "Exendin-4 protects Abeta(1-42) oligomer-induced PC12 cell apoptosis," *American Journal of Translational Research*, vol. 8, no. 8, pp. 3540–3548, 2016.

[25] F. S. Laroux, K. P. Pavlick, I. N. Hines et al., "Role of nitric oxide in inflammation," *Acta Physiologica Scandinavica*, vol. 173, no. 1, pp. 113–118, 2001.

[26] B. Liu, H.-M. Gao, J.-Y. Wang, G.-H. Jeohn, C. L. Cooper, and J.-S. Hong, "Role of nitric oxide in inflammation-mediated neurodegeneration," *Annals of the New York Academy of Sciences*, vol. 962, pp. 318–331, 2002.

[27] V. Calabrese, R. Sultana, G. Scapagnini et al., "Nitrosative stress, cellular stress response, and thiol homeostasis in patients with Alzheimer's disease," *Antioxid Redox Signal*, vol. 8, no. 11-12, pp. 1975–1986, 2006.

[28] C. B. Pocernich and D. A. Butterfield, "Elevation of glutathione as a therapeutic strategy in alzheimer disease," *Biochimica et Biophysica Acta (BBA) - Molecular Basis of Disease*, vol. 1822, no. 5, pp. 625–630, 2012.

[29] J. Golomb, M. J. Leon, A. Kluger, C. Tarshish, S. H. Ferris, and A. E. George, "Hippocampal atrophy in normal aging: An association with recent memory impairment," *JAMA Neurology*, vol. 50, no. 9, pp. 967–973, 1993.

[30] M. R. Sabuncu, R. S. Desikan, J. Sepulcre et al., "The dynamics of cortical and hippocampal atrophy in Alzheimer disease," *JAMA Neurology*, vol. 68, no. 8, pp. 1040–1048, 2011.

[31] K. F. S. Bell and A. Claudio Cuello, "Altered synaptic function in Alzheimer's disease," *European Journal of Pharmacology*, vol. 545, no. 1, pp. 11–21, 2006.

[32] D. J. Selkoe, "Soluble oligomers of the amyloid beta-protein impair synaptic plasticity and behavior," *Behavioural Brain Research*, vol. 192, no. 1, pp. 106–113, 2008.

[33] S. A. Wilke, T. Raam, J. K. Antonios et al., "Specific disruption of hippocampal mossy fiber synapses in a mouse model of familial Alzheimer's disease," *PLoS ONE*, vol. 9, no. 1, Article ID e84349, 2014.

[34] M. Verma, A. Vats, and V. Taneja, "Toxic species in amyloid disorders: Oligomers or mature fibrils," *Annals of Indian Academy of Neurology*, vol. 18, no. 2, pp. 138–145, 2015.

[35] R. Cascella, S. Conti, F. Tatini et al., "Extracellular chaperones prevent Aβ42-induced toxicity in rat brains," *Biochimica et Biophysica Acta (BBA) - Molecular Basis of Disease*, vol. 1832, no. 8, pp. 1217–1226, 2013.

[36] Y. He, M.-M. Zheng, Y. Ma et al., "Soluble oligomers and fibrillar species of amyloid β-peptide differentially affect cognitive functions and hippocampal inflammatory response," *Biochemical and Biophysical Research Communications*, vol. 429, no. 3-4, pp. 125–130, 2012.

[37] A. S. Darvesh, R. T. Carroll, A. Bishayee, W. J. Geldenhuys, and C. J. van der Schyf, "Oxidative stress and Alzheimer's disease: dietary polyphenols as potential therapeutic agents," *Expert Review of Neurotherapeutics*, vol. 10, no. 5, pp. 729–745, 2010.

[38] D. A. Butterfield, J. Drake, C. Pocernich, and A. Castegna, "Evidence of oxidative damage in Alzheimer's disease brain: central role for amyloid β-peptide," *Trends in Molecular Medicine*, vol. 7, no. 12, pp. 548–554, 2001.

[39] S. Chakrabarti, M. Sinha, I. G. Thakurta, P. Banerjee, and M. Chattopadhyay, "Oxidative stress and amyloid beta toxicity in Alzheimer's disease: intervention in a complex relationship by antioxidants," *Current Medicinal Chemistry*, vol. 20, no. 37, pp. 4648–4664, 2013.

[40] H. Capiralla, V. Vingtdeux, H. Zhao et al., "Resveratrol mitigates lipopolysaccharide- and Aβ-mediated microglial inflammation by inhibiting the TLR4/NF-κB/STAT signaling cascade," *Journal of Neurochemistry*, vol. 120, no. 3, pp. 461–472, 2012.

[41] E. G. McGeer and P. L. McGeer, "The importance of inflammatory mechanisms in Alzheimer disease," *Experimental Gerontology*, vol. 33, no. 5, pp. 371–378, 1998.

[42] C. K. Glass, K. Saijo, B. Winner, M. C. Marchetto, and F. H. Gage, "Mechanisms underlying inflammation in neurodegeneration," *Cell*, vol. 140, no. 6, pp. 918–934, 2010.

[43] N. Ishizuka, J. Weber, and D. G. Amaral, "Organization of intrahippocampal projections originating from CA3 pyramidal cells in the rat," *Journal of Comparative Neurology*, vol. 295, no. 4, pp. 580–623, 1990.

[44] X. -. Li, P. Somogyi, A. Ylinen, and G. Buzsáki, "The hippocampal CA3 network: An in vivo intracellular labeling study," *Journal of Comparative Neurology*, vol. 339, no. 2, pp. 181–208, 1994.

[45] K. J. Lee, B. N. Queenan, A. M. Rozeboom et al., "Mossy Fiber-CA3 Synapses Mediate Homeostatic Plasticity in Mature Hippocampal Neurons," *Neuron*, vol. 77, no. 1, pp. 99–114, 2013.

[46] S. W. Scheff, D. A. Price, F. A. Schmitt, and E. J. Mufson, "Hippocampal synaptic loss in early Alzheimer's disease and mild cognitive impairment," *Neurobiology of Aging*, vol. 27, no. 10, pp. 1372–1384, 2006.

[47] B. Wiedenmann, W. W. Franke, C. Kuhn, R. Moll, and V. E. Gould, "Synaptophysin: a marker protein for neuroendocrine cells and neoplasms," *Proceedings of the National Academy of Sciences*, vol. 83, no. 10, pp. 3500–3504, 1986.

[48] D. Cheng, C. C. Hoogenraad, J. Rush et al., "Relative and absolute quantification of postsynaptic density proteome isolated from rat forebrain and cerebellum," *Molecular & Cellular Proteomics*, vol. 5, no. 6, pp. 1158–1170, 2006.

[49] K. S. T. Dias and C. Viegas Jr., "Multi-target directed drugs: a modern approach for design of new drugs for the treatment of Alzheimer's disease," *Current Neuropharmacology*, vol. 12, no. 3, pp. 239–255, 2014.

[50] R. E. Hughes, K. Nikolic, and R. R. Ramsay, "One for all? Hitting multiple Alzheimer's disease targets with one drug," *Frontiers in Neuroscience*, vol. 10, article no. 177, 2016.

[51] F. Misiti, B. Sampaolese, D. Mezzogori et al., "Protective effect of rhubarb derivatives on amyloid beta (1-42) peptide-induced apoptosis in IMR-32 cells: A case of nutrigenomic," *Brain Research Bulletin*, vol. 71, no. 1-3, pp. 29–36, 2006.

[52] Y. H. Park, I. H. Son, B. Kim, Y. S. Lyu, H. I. Moon, and H. W. Kang, "Poria cocos water extract (PCW) protects PC12 neuronal cells from beta-amyloid-induced cell death through antioxidant and antiapoptotic functions," *Pharmazie*, vol. 64, no. 11, pp. 760–764, 2009.

[53] C. Lv, L. Wang, X. Liu et al., "Geniposide attenuates oligomeric Abeta(1-42)-induced inflammatory response by targeting RAGE-dependent signaling in BV2 cells," *Current Alzheimer Research*, vol. 11, no. 5, pp. 430–440, 2014.

[54] C. Lv, L. Wang, X. Liu et al., "Multi-faced neuroprotective effects of geniposide depending on the RAGE-mediated signaling in an Alzheimer mouse model," *Neuropharmacology*, vol. 89, pp. 175–184, 2015.

Hindawi
Evidence-Based Complementary and Alternative Medicine
Volume 2017, Article ID 5052870, 15 pages
https://doi.org/10.1155/2017/5052870

Research Article

Antcin-H Isolated from *Antrodia cinnamomea* Inhibits Renal Cancer Cell Invasion Partly through Inactivation of FAK-ERK-C/EBP-β/c-Fos-MMP-7 Pathways

Kun-Yuan Chiu,[1,2,3] Tzu-Hsiu Chen,[4] Chi-Luan Wen,[5] Jin-Mei Lai,[6] Chi-Chih Cheng,[7] Hsiang-Chun Liu,[7] Shih-Lan Hsu,[3,7] and Yew-Min Tzeng[1,8]

[1]*Institute of Biochemical Sciences and Technology, Chaoyang University of Technology, Taichung, Taiwan*
[2]*Division of Urology, Department of Surgery, Taichung Veterans General Hospital, Taichung, Taiwan*
[3]*Department of Applied Chemistry, National Chi Nan University, Puli, Nantou, Taiwan*
[4]*Department of Health and Nutrition, Chia Nan University of Pharmacy & Science, Tainan, Taiwan*
[5]*Taiwan Seed Improvement and Propagation Station, Council of Agriculture, Propagation Technology Section, Taichung, Taiwan*
[6]*Department of Life Science, Fu-Jen Catholic University, New Taipei City, Taiwan*
[7]*Department of Medical Research, Taichung Veterans General Hospital, Taichung, Taiwan*
[8]*Department of Life Science, National Taitung University, Taitung, Taiwan*

Correspondence should be addressed to Shih-Lan Hsu; hsu2326@gmail.com and Yew-Min Tzeng; ymtzeng@nttu.edu.tw

Received 1 June 2017; Revised 29 September 2017; Accepted 9 October 2017; Published 2 November 2017

Academic Editor: Jesus R. R. Amado

Antcin-H, a natural triterpene, is purified from a famous anticancer medicinal mushroom, *Antrodia cinnamomea,* in Taiwan. This study showed that antcin-H inhibited the growth of human renal carcinoma 786-0 cells; the IC_{50} value (for 48 h) was 170 μM. Besides, the migration and invasion of 786-0 cells were suppressed by antcin-H under noncytotoxic concentrations (<100 μM); these events were accompanied by inhibition of FAK and Src kinase activities, decrease of paxillin phosphorylation, impairment of lamellipodium formation, and upregulation of TIMPs and downregulation of MMPs, especially MMP-7 expression. Luciferase reporter assay showed that antcin-H repressed the MMP-7 promoter activity, in parallel to inhibiting c-Fos/AP-1 and C/EBP-β transactivation abilities. Moreover, antcin-H suppressed the activity of ERK1/2 and decreased the binding ability of C/EBP-β and c-Fos on the upstream/enhancer region of MMP-7 promoter. Overall, this study demonstrated that the anti-invasive effect of antcin-H in human renal carcinoma 786-0 cells might be at least in part by abrogating focal adhesion complex and lamellipodium formation through inhibiting the Src/FAK-paxillin signaling pathways and decreasing MMP-7 expression through suppressing the ERK1/2-AP-1/c-Fos and C/EBP-β signaling axis. Our findings provide the evidence that antcin-H may be an active component existing in *A. cinnamomea* with anticancer effect.

1. Introduction

Human renal cell carcinoma (RCC), the second common but most lethal cancer of urologic origins, is relatively rare compared to the other carcinomas, but the incidence of RCC is increasing [1]. Although RCC is curable when it is diagnosed in the very early stage of the disease [2], due to its asymptomatic clinical course, by the time of diagnosis about 25% of RCC patients present with invasion of the tumor to the surrounding tissues and distant metastasis [3, 4]. New treatment modalities including immunotherapies with interferon or interleukin-2 and targeting therapies focusing on vascular endothelial growth factor and mTOR pathway have been developed recently for the patients with metastatic diseases [5, 6]. Nevertheless, relatively higher costs and unpredictable side effects limit the clinical uses of all these potential treatment options. Nowadays, no agent can be clinically used to prevent or treat the metastatic RCC and

most patients ultimately succumb to metastatic disease [7, 8]. Therefore, an effective therapeutic strategy is a critical issue in the management of these patients.

Cancer metastasis is complex and complicated process that involves several classes of proteins, including adhesion molecules and extracellular proteases. Classical and important metastatic proteins are matrix metalloproteinases (MMPs); numerous reports show that MMPs are overexpressed in metastatic human tumors [9–12]. MMPs can degrade extracellular matrix components and their overexpression correlates with metastasis and poor prognosis in most tumor types [13, 14]. Among the MMPs, MMP-7, known as matrilysin, has a broad spectrum of proteolytic activity capable of cleaving various types of extracellular matrix [15]. Strong correlations between MMP-7 overexpression and invasion are observed in cancer cell lines and mouse models across most tumor types [16, 17]. It has been demonstrated that MMP-7 is preferentially expressed at the invasive front of tumors [11, 18], and its overexpression associates with metastatic disease and unfavorable outcome in RCC [11, 12]. Overall, these findings make MMP-7 a strong and novel target for pharmacological antimetastasis therapy in RCC.

Fungi provide a huge resource and have been used for an effective way to develop new pharmaceutical products. Several studies have shown the potentials of *Antrodia cinnamomea*, a well-known medical mushroom in Taiwan, on prevention and treatment of liver diseases, food and drug intoxication, hypertension, and cancers [19]. Several compounds have been isolated and identified from fruiting bodies of *A. cinnamomea* including benzenoids, steroids, and triterpenoids [19, 20]. The precise compounds and their mode of actions responsible for the observed biological functions have been studied recently [21–24]. Antcins, steroid-like compounds, exert anti-inflammatory effect and enhance blood circulation [25]. A recent report demonstrates that antcin K triggers intrinsic apoptotic cell death through the mitochondrial and endoplasmic reticulum stress-induced signaling pathways [26]. However, there is no study exploring the effects of antcin-H, a pure compound isolated from *A. cinnamomea*, on human cancer cells. This study was aimed to examine the anticancer effect and its molecular mechanism of antcin-H in human RCC cells. Our results firstly showed that antcin-H inhibited the Src/FAK/paxillin and Src/FAK/ERK-c-Fos-C/EBP-β signaling pathways to impair lamellipodium formation and decrease MMP-7 expression, consequently suppressing RCC cell migration and invasion, suggesting that antcin-H might have the potential for treating metastatic RCC.

2. Materials and Methods

2.1. Isolation of Antcin-H. Antcin-H used in this study was provided by Professor Yew-Min Tzeng at Natural Products and Bioprocess Laboratory, the Institute of Biochemical Sciences and Technology, Chaoyang University of Technology, Taiwan. In brief, the natural product antcin-H was isolated from the cultivated fruiting bodies of *A. cinnamomea* YMT 1002 (GenBank KJ704843). The powdered fruiting bodies (30 g) were extracted through a serial solvent extraction and silica gel column chromatography operations; 65 mg yellow needle antcin-H was obtained with yield of 0.21% (W/W). All the 1H and 13C NMR spectral data derived from antcin-H were in complete accord with the assigned structure. The isolation method of the natural product antcin-H was reported by Tzeng's laboratory previously [27]. The purity (>95%) of antcin-H was confirmed by HPLC analysis [28].

2.2. Cell Culture and Viability Assay. Renal carcinoma 786-0 cell line was cultured in Roswell Park Memorial Institute 1640 medium (RPMI 1640) supplemented with 10% fetal bovine serum, 2 mM L-glutamine, 1 mM sodium pyruvate, 1% nonessential amino acid, and 1 mM HEPES. Cells were incubated in 95% air, 5% CO_2 humidified atmosphere at 37°C. Cell viability was performed with trypan blue exclusion method. Briefly, 786-0 cells plated in 12-well plate and treated with various dosages of antcin-H (0, 20, 50, 100, 200, and 300 μM) for indicated times. The viable cells were determined by trypan blue reagent.

2.3. Wound-Healing Assay in Live Cells. The *in vitro* wound-healing assay was performed by using IBIDI culture-insert (IBIDI, Martinsried, Germany) to create a defined cell gap. Briefly, without or with antcin-H treatment, 786-0 cells were trypsinized and seeded in the wells of the culture-insert containing 10% serum medium and grown until 95% confluence. For the cell culture, a linear wound was then created and treated without or with antcin-H in a low serum condition; to obtain migrating live cell imaging in wounded region, the Olympus microscope was used with a 40x objective. The image of cell migration into the wound front was microphotographed every 10 min for up to 24 h.

2.4. Migration and Invasion Assay. With or without antcin-H treatment, 786-0 cells were trypsinized and loaded in the upper chamber of the Transwell apparatus (pore size: 8 μm; Millipore, Billerica, MA, USA). After treatment, the upper chamber cells were scraped off, the filters were then washed and fixed and stained with Giemsa solution, and then the migrated cells were counted. For invasion assay, cells were loaded onto a matrigel (BD Biosciences, San Jose, CA, USA) precoated Transwell at a density of 2×10^4 cells with serum-free medium, whereas RPMI containing 10% FBS was added to lower chamber as a chemoattractant. After incubation, the cells that invaded across the matrigel to the lower surface of membrane were fixed in methanol and stained with Giemsa solution, and then the invaded cells were measured.

2.5. Western Blot Analysis. Cells were harvested by scrapping with iced cold PBS and lysed directly in RIPA buffer containing 50 mM Tris-HCl (pH 7.4), 150 mM NaCl, 1% Triton X-100, 0.25% sodium deoxycholate, 5 mM EDTA (pH 8.0), and 1 mM EGTA and supplemented with protease and phosphatase inhibitors at 4°C for 20 min and then centrifuged with 12000 rpm at 4°C for 30 min and total protein content was determined by Bradford assay. Equal amounts of total proteins were separated by SDS-polyacrylamide gel electrophoresis. Immunoblotting was performed using primary antibodies against Src, phosphorylated-Src (p-Src), paxillin,

and phosphorylated-paxillin (p-PXN) (Cell Signaling Technology, Beverly, MA) and ERK1/2, phosphorylated-ERK1/2 (p-ERK1/2), c-Fos, C/EBP-β, phosphorylated-C/EBP-β (p-C/EBP-β), FAK, and phosphorylated-FAK (p-FAK) (Santa Cruz, CA, USA). The image was investigated using an ECL-Plus detection kit (PerkinElmer Life Sciences, Inc., Boston, MA, USA).

2.6. Immunofluorescence Assay. Cells were cultured on 15 mm microscope cover glasses in 12-well plate. After antcin-H was exposed for indicated time, the cells were fixed with 4% paraformaldehyde and permeabilized by 0.1% Triton X-100 at room temperature. Samples were blocked with 1% BSA for 30 min and incubated with primary antibodies against phosphorylated-FAK and phosphorylated-paxillin overnight. After being washed with PBS, the cells were incubated with Alexa-Fluor 488-conjugated secondary antibody (Invitrogen, Carlsbad, CA, USA), and then the actin image was investigated using Phalloidin-iFluor 647 Conjugate (AAT Bioquest®, Inc., CA) and, finally, incubated with DAPI (Molecular Probes Inc., Eugene, Oregon, USA) for nucleus detection. The cells were then examined using a laser confocal microscope (FV1000, Olympus).

2.7. Quantitative-PCR and RT-PCR. 786-0 cells were exposed to antcin-H or control solvent for indicated time and total RNA was extracted by using TRIzol® isolated kit (Invitrogen, Carlsbad, CA, USA) following the manufacturer's instruction. One μg of total RNA was reverse-transcribed using the First-Strand cDNA Synthesis kit (Thermo Fisher Scientific Inc.). The cDNA products of RT-PCR were then operated with ABI PRISM 7900 Sequence Detector System to determine the mRNA levels according to the manufacturer's instructions. The quantitative RT-PCR reaction mixture contains cDNA, primers, and SYBR Green PCR master mix (Applied Biosystems, Life Technologies). β-Actin was used as an internal loading control. The used primer sequences were listed as follows: MMP-2: forward 5′-CTTCCAAGTCTGGAGCGATGT-3′, reverse 5′-TACCGTCAAAGGGGTATCCAT-3′; MMP-3: forward 5′-GAGGCATCCACACCCTAGGTT-3′, reverse 5′-TAGCTACGTCGGTAAAGACTA-3′; MMP-7: forward 5′-GGAGGAGATGCTCACTTCGAT-3′, reverse 5′-AGGAATGTCCCATACCCAAAGA; MMP-13: forward 5′-AAGGAGCATGGCGACTTCT-3′, reverse 5′-TGGTTCAGGAAAAGC; tissue inhibitors of metalloproteinases 3 (TIMP-3): forward 5′-CAGGACGCCTTCTGCAA-3′, reverse 5′-CCCCTCCTTTACCAGCTTCTTC-3′; TIMP-4: forward 5′-CACCCTCAGCAGCACATCTG-3′, reverse 5′-GGCCGGAACTACCTTCTCACT-3′.

2.8. Chromatin Immunoprecipitation (ChIP) Assay. ChIP assay was conducted as described previously [29]. Briefly, after treatment, cells were collected and fixed with 1% formaldehyde at 37°C for 10 min then treated with glycine to quench the cross-links. Cells were harvested by ice PBS containing proteinase inhibitor and lysed with SDS lysis buffer and then sonicated with the following condition: 20% amplitude for 10 seconds and rest for 10 seconds, repeated 5 times. Lysates were preincubated with the salmon sperm DNA-protein A agarose (Millipore, Billerica, MA, USA) and subjected to immunoprecipitation overnight at 4°C with normal IgG or antibody against C/EBP-β (Cell Signaling Technology, Beverly, MA) or c-Fos (Santa Cruz, CA, USA). Precipitates were washed and eluted. The chromatin extracted and protein-DNA cross-links reversed by NaCl. Then DNA was purified by DNA clean-up purification kit (Promega, Madison, WI, USA), and the relative amount of DNA sequence from the MMP-7 promoter region was estimated by PCR analysis. The used primer sequences were listed as follows: for −1.4 kb length, 5′-TGAGCTACAGTGGGAACAGG-3′ and 5′-TCATCGAAGTGAGCATCTCC-3′; for −876 to −1201 bp region, sense: 5′-CTCCAGCATATTTGGAGTGTTTCC-3′ and antisense: 5′-CTTCCAATCACTCTGACTCTGGC-3′; for −263 to −529 bp region, sense: 5′-CATCTTTCCCCTGTATGGAGAAC-3′ and antisense: 5′-GACTGCTCTCATAGGTATCATTCAGG-3′; for −138 to −288 bp region, sense: 5′-CCTGAATGATACCTATGAGAGCAG-3′ and antisense: 5′-CGAGGAAGTATTACATCGTTATTGG-3′; for +2 to −229 bp region, sense: 5′-GGAGTCAATTTATGCAGCAGACAG-3′ and antisense: 5′-GGTGTTTTCTGCTAGTGACTGCAG-3′.

2.9. Luciferase Reporter Assay. To generate luciferase reporter, the sequence of MMP-7 containing MluI and BglII restriction site was cloned into the upstream of firefly luciferase gene in PGL3 vector. The primers were +15 to −1000 bp: 5′-ACGCGTTCATTTTTGGTAAGAATGGTCATTGG-3′ (forward) and 5′-AGATCTTATGGTTGATTTGGTGTTTTCTGCTAG-3′ (reverse). After cloning, the vectors were sequenced to confirm the orientation and integrity of the inserts of each construct. For transfection, cells were cotransfected with the vector DNA and the pRL-CMV internal control which contained the Renilla luciferase gene by Lipofectamine 2000 (Invitrogen, Waltham, MA, USA) and then added with or without antrocin into each well. Cells were collected and analyzed for luciferase activity with the Dual-Luciferase Reporter Assay System kit (Promega, Madison, WI, USA).

2.10. Statistical Analysis. The results were confirmed by carrying out at least three independent experiments with similar pattern. Values were expressed as means ± SD from three separate experiments ($n = 9$). Statistical comparisons were done using one-way analysis of variance (ANOVA) with Student's t-test, the statistical significance was set at $^{*}p < 0.05$, $^{**}p < 0.01$, and $^{***}p < 0.001$.

3. Results

3.1. Growth Inhibitory Effects of Antcin-H. The chemical structure of antcin-H is shown in Figure 1(a). The effects of antcin-H on renal cancer cell proliferation and human renal carcinoma 786-0 cells were treated with antcin-H. As depicted in Figure 1(b), antcin-H inhibited 786-0 cell growth dose-dependently, and the IC_{50} value was 170 μM after 48 h exposure. Incubation of 786-0 cells with lower concentrations of antcin-H (<200 μM) caused a growth inhibitory effect but did not display any signs of cytotoxicity by morphological

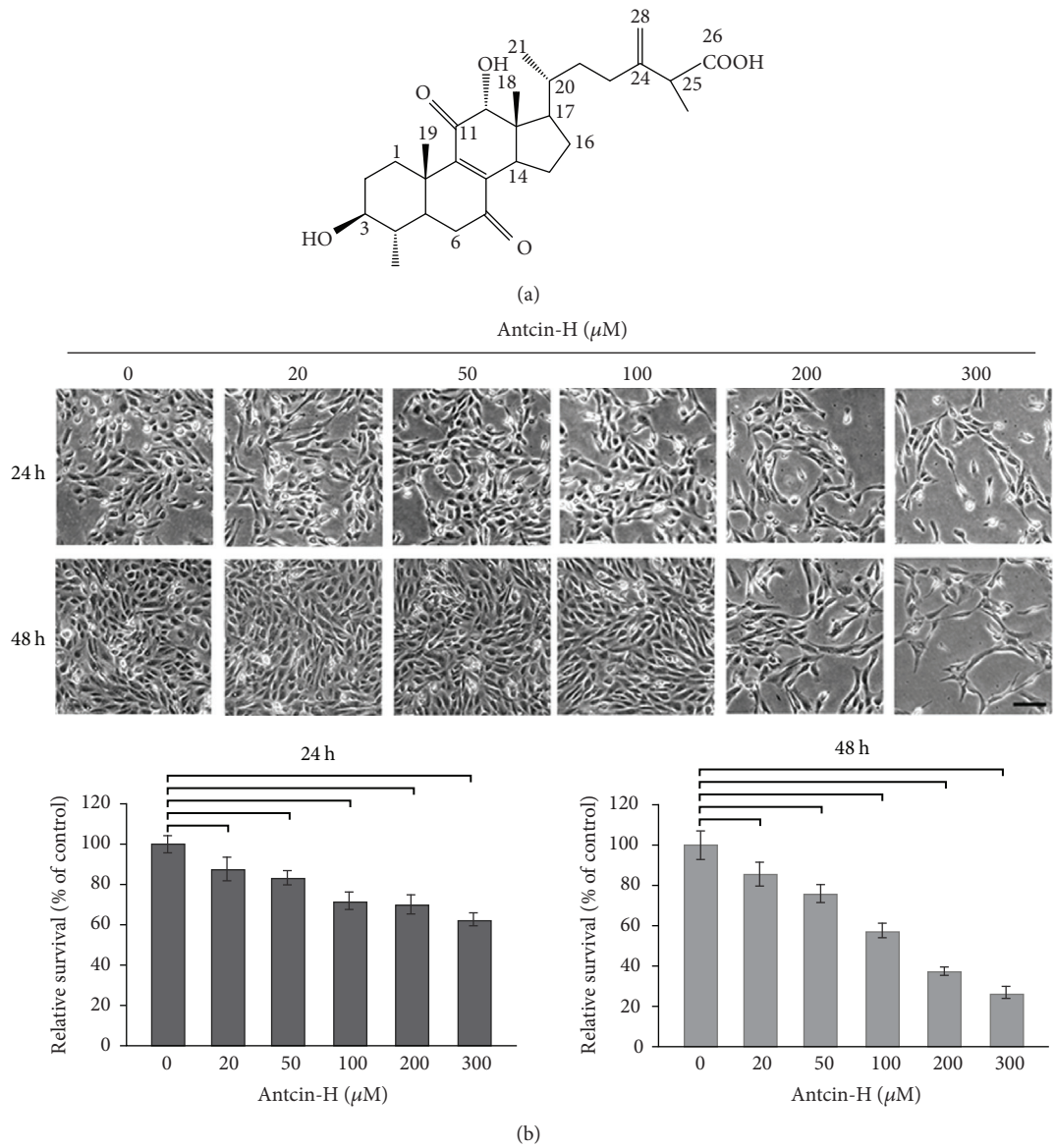

Figure 1: Growth inhibitory effect of antcin-H. (a) The chemical structure of antcin-H. (b) Human RCC 786-0 cells were treated with various concentrations (0, 20, 50, 100, 200, and 300 μM) of antcin-H for 24 and 48 h. After incubation, cell morphology was investigated using phase-contrast microscope (upper panel). Scale bar, 100 μm. The cell viability was determined by trypan blue dye exclusion method (lower panel).

investigation. However, administration of 300 μM antcin-H resulted in rounding and detaching due to cytotoxicity.

3.2. Inhibition of Migration and Regulation of Migration-Related Molecules by Antcin-H. Metastasis has been considered as a poor prognostic factor in RCC [30]; therefore, developing safe and effective therapeutic agents for the treatment of metastatic RCC is urgently required. To examine the effect of antcin-H on cell migration, Transwell migration assay was carried out. As shown in Figure 2(a), treatment of 786-0 cells with noncytotoxic concentrations of antcin-H for 24 h retarded cell migration in a concentration-dependent manner; the number of migrated cells was markedly reduced upon antcin-H treatment.

Previous study demonstrates that FAK/paxillin pathway plays a key role in formation of focal adhesion contact and concomitant cell migration and invasion [31]. Besides, epithelial mesenchymal transition (EMT) is an essential process for cancer cell to acquire migration and invasion ability [32]. Loss of E-cadherin and increase of vimentin are surrogate markers for cell migration and invasion in EMT process. To explore the molecular mechanisms involved in the inhibitory effect of antcin-H on cell migration, the expressed levels of FAK, paxillin, E-cadherin, and vimentin were examined by Western blot analysis. As depicted in Figure 2(b), antcin-H induced a dose-dependent decrease in phosphorylated FAK^{Tyr925} and $paxillin^{Tyr118}$ levels, with a significant change observed at 50 and 100 μM, which is consistent with doses

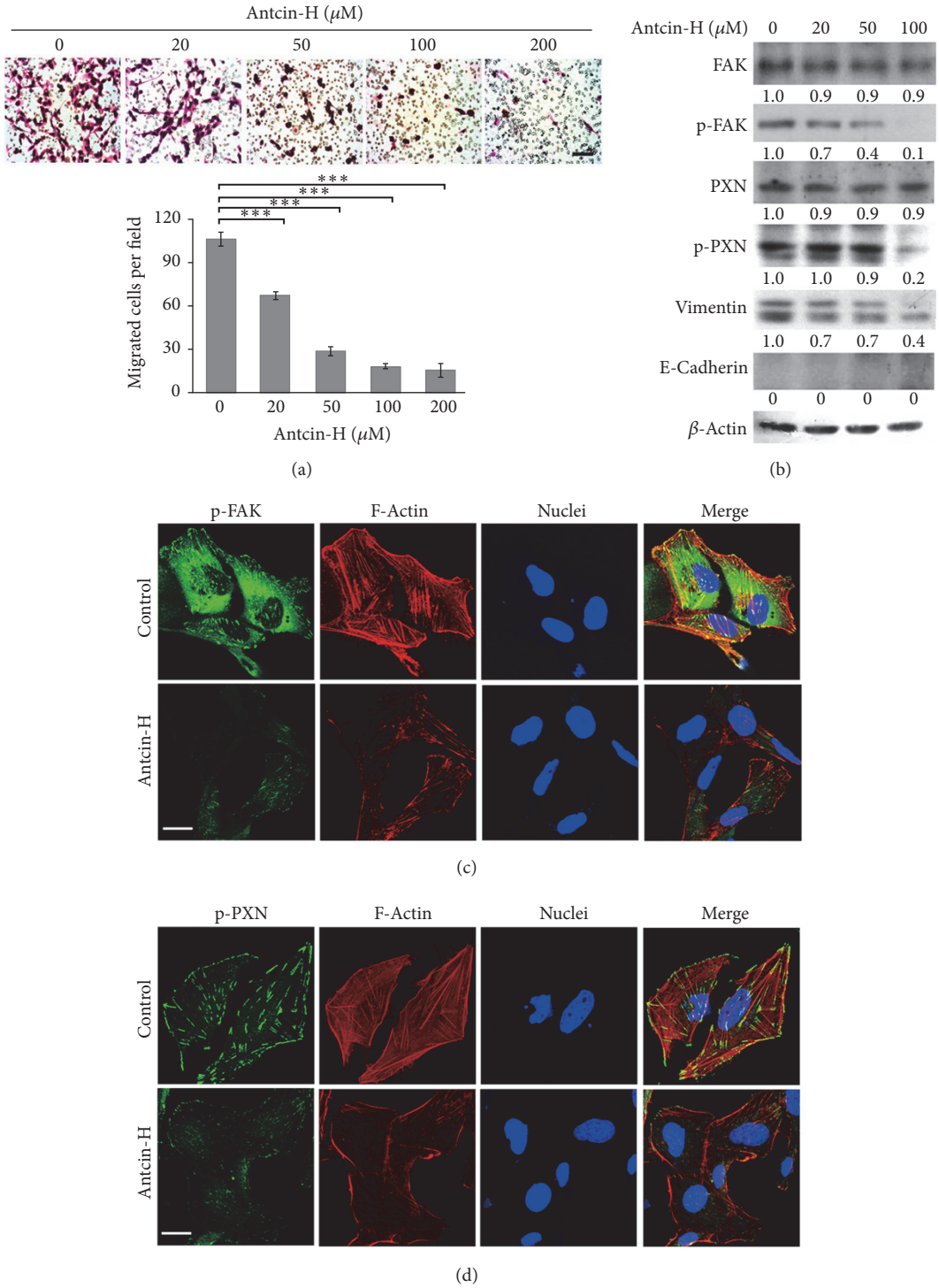

FIGURE 2: Inhibition of cell migration and modulation of migration-related proteins by antcin-H in vitro. (a) 786-0 cells were treated without or with 20, 50, 100, and 200 μM antcin-H for 24 h, and then cells were seeded in the upper part of Transwell. After 16 h, cells on the bottom side of the filter were microphotographed and counted. Data were represented as the mean ± SD of three independent experiments. Statistically significant, $^{***}p < 0.001$. Scale bar, 100 μm. (b) Regulation of FAK, paxillin, E-cadherin, and vimentin by antcin-H. 786-0 cells were treated without or with 20, 50, and 100 μM antcin-H for 24 h, and then protein lysates were isolated. The levels of phosphorylated-FAK, phosphorylated-paxillin, E-cadherin, and vimentin were examined by Western blot analysis. β-Actin was used as an internal loading control. Confocal imaging of (c) phosphorylated-FAK and (d) phosphorylated-paxillin. 786-0 cells were treated without or with 100 μM antcin-H for 24 h. The cellular distribution of phosphorylated-FAK and phosphorylated-paxillin was examined by immunofluorescence staining using phosphorylated-FAK and phosphorylated-paxillin specific antibodies. The immunoreactive images were investigated by confocal microscope. Scale bar, 20 μm.

that are antimigration (Figure 2(a)). Moreover, the expressed level of vimentin was significantly reduced by antcin-H. However, the levels of total FAK and paxillin were not affected by antcin-H. Moreover, the expression of E-cadherin could not be detected in both control and antcin-H-treated 786-0 cells (Figure 2(b)). These results reveal that FAK, paxillin, and vimentin may be targeting molecules involved in antcin-H-mediated inhibition of 786-0 cell migration.

To further examine the cellular distribution of phosphorylated-FAK and phosphorylated-paxillin, 786-0 cells were treated with 100 μM antcin-H and subjected to immunostaining analysis with anti-phosphor-FAK and anti-phosphor-paxillin antibody and then counterstained with phalloidin-rhodamine and DAPI for actin and nucleus staining, respectively. Confocal imaging revealed that the majority of control untreated cells showed small dot-like structures of phosphorylated-FAK (Figure 2(c)) and phosphorylated-paxillin (Figure 2(d)) extending into a polarized, actin-containing lamellipodia. In contrast, antcin-H treatment decreased the phosphorylated-FAK and phosphorylated-paxillin levels at the leading edge and reduced lamellipodia formation in 786-0 cells (Figures 2(c) and 2(d)).

Next, the antimigratory activity of antcin-H was evaluated by real-time, live cell imaging of wound-healing assay. 786-0 cells were incubated with 100 μM antcin-H for indicated time periods. In representative time-lapse images, antcin-H treatment significantly retarded cell migratory activity (Figure 3(a)). Because both FAK and paxillin are the important regulators of lamellipodial dynamics in motile cells [33], the formation of lamellipodium at the wound margin was investigated by immunostain with anti-phosphorylated-FAK and phosphorylated-paxillin antibody. Small dot-like structures, regarded as FAK (Figure 3(b)) and paxillin (Figure 3(c)) localized at the front edge, which associated with lamellipodium containing bundles of F-actin were detected in untreated 786-0 cells. Conversely, only a few small dot-like FAK and paxillin immunoreactivity located at front edge of wound margin, and a clear lamellipodia could not be observed in antcin-H-treated 786-0 cells. Since lamellipodia are shown to increase in highly motile cells, these results indicate that antcin-H exposure may cause a decrease of cell migratory capability in 786-0 cells.

3.3. Antcin-H Suppresses Cell Invasion and Modulates MMPs and TIMPs Expression. To examine whether antcin-H could suppress cell invasion in RCC 786-0 cells, Matrigel-coated Transwell invasion assay was conducted, and invaded cells were photographed using a microscope with a 20x objective lens. Representative images of invaded cells were shown in Figure 4(a), antcin-H effectively impaired the invasive capability of 786-0 cells, and the number of invaded cells was significantly fewer than those in untreated control. At 100 μM antcin-H treatment revealed an approximately 80% decreased invasive ability in comparison with untreated control. Because the expression of MMP and TIMP family members are critical for cancer invasion, to characterize the regulation of *MMP*s and *TIMP*s genes by antcin-H, real-time PCR analysis was carried out. Results indicated that *MMP-2*, *MMP-3*, *MMP-7*, and *MMP-13* genes were downregulated, whereas *TIMP-3* and *TIMP-4* were upregulated after exposure to antcin-H (Figure 4(b)). However, *MMP-1*, *MMP-8*, *MMP-9*, *MMP-10*, *MMP-11*, *TIMP-1,* and *TIMP-2* genes were not altered by antcin-H (data not shown).

3.4. Antcin-H Inhibits the ERK Signaling Pathway. To further characterize the possible mechanism that underlies the inhibitory effect of antcin-H on 786-0 cells, the activation of several kinases involving FAK pathway and contributing to cell migration and invasion, including Src, FAK, and ERK1/2, was examined by Western blot analysis. As shown in Figure 5(a), the phosphorylated forms of major FAK signaling pathways, including FAK, Src, and ERK1/2, were drastically decreased after exposure to 100 μM antcin-H for 4 h and continuously suppressed at 24 h. Consistently, the major ERK downstream transcription factors, such as c-Fos and phosphorylated-C/EBP-β, were also time- and dose-dependently reduced in response to antcin-H treatment (Figures 5(a) and 5(b)). However, the amount of total FAK, Src, and ERK1/2 did not change when incubated with antcin-H.

3.5. Inhibition of c-Fos and C/EBP-β DNA Binding Activity and Transactivation Ability Contributes to Antcin-H-Mediated MMP-7 Downregulation. Growing evidence indicates that MMP-7 is overexpressed in RCC [11] and was clinically associated with metastasis and poor prognosis in patients with RCC [11, 12]. The present study showed that the expression of *MMP-7* gene was unusually reduced following antcin-H administration (Figure 4(b)); to further confirm that the antcin-H-mediated MMP-7 downregulation is regulated at transcriptional level, the promoter activity of MMP-7 was evaluated by the reporter luciferase assay. As depicted in Figure 6(a), antcin-H suppressed reporter activity in 786-0 cells in a concentration-dependent manner. These data suggest that antcin-H reduced *MMP-7* gene expression through repression of *MMP-7* promoter activity.

Notably, there are two c-Fos/AP1 (c-FosRE1, −67~−59 and c-FosRE2, −981~−972) and four C/EBPβ (C/EBP-βRE1, −55~−50; C/EBP-βRE2, −250~−245; C/EBP-βRE3, −457~−451; C/EBP-βRE4, −997~−985) putative binding sites locate upstream of *MMP-7* promoter (Figure 6(b)). To determine which binding site associated with antcin-H-mediated inhibition of *MMP-7* gene expression, 786-0 cells were incubated without or with 100 μM antcin-H for 16 h, and then anti-c-Fos or anti-C/EBP-β antibody was used to carry out chromatin immunoprecipitation (ChIP) assay. As shown in Figure 6(c), in untreated 786-0 cells, c-Fos appeared to be binding on two potential c-Fos/AP1 response sites, c-FosRE1 and c-FosRE2, located upstream of *MMP-7* promoter. The interaction of c-Fos to c-FosRE1 was stronger than that to c-FosRE2. However, antcin-H treatment resulted in a great decrease in c-Fos binding on both sites. Besides, C/EBP-β appeared to bind only three putative response regions (C/EBP-βRE1, C/EBP-βRE2, and C/EBP-βRE4) in untreated cells, whereas exposure to antcin-H significantly diminished the binding of C/EBPβ on these sites. However, the interaction of C/EBP-β with C/EBP-βRE3 could not

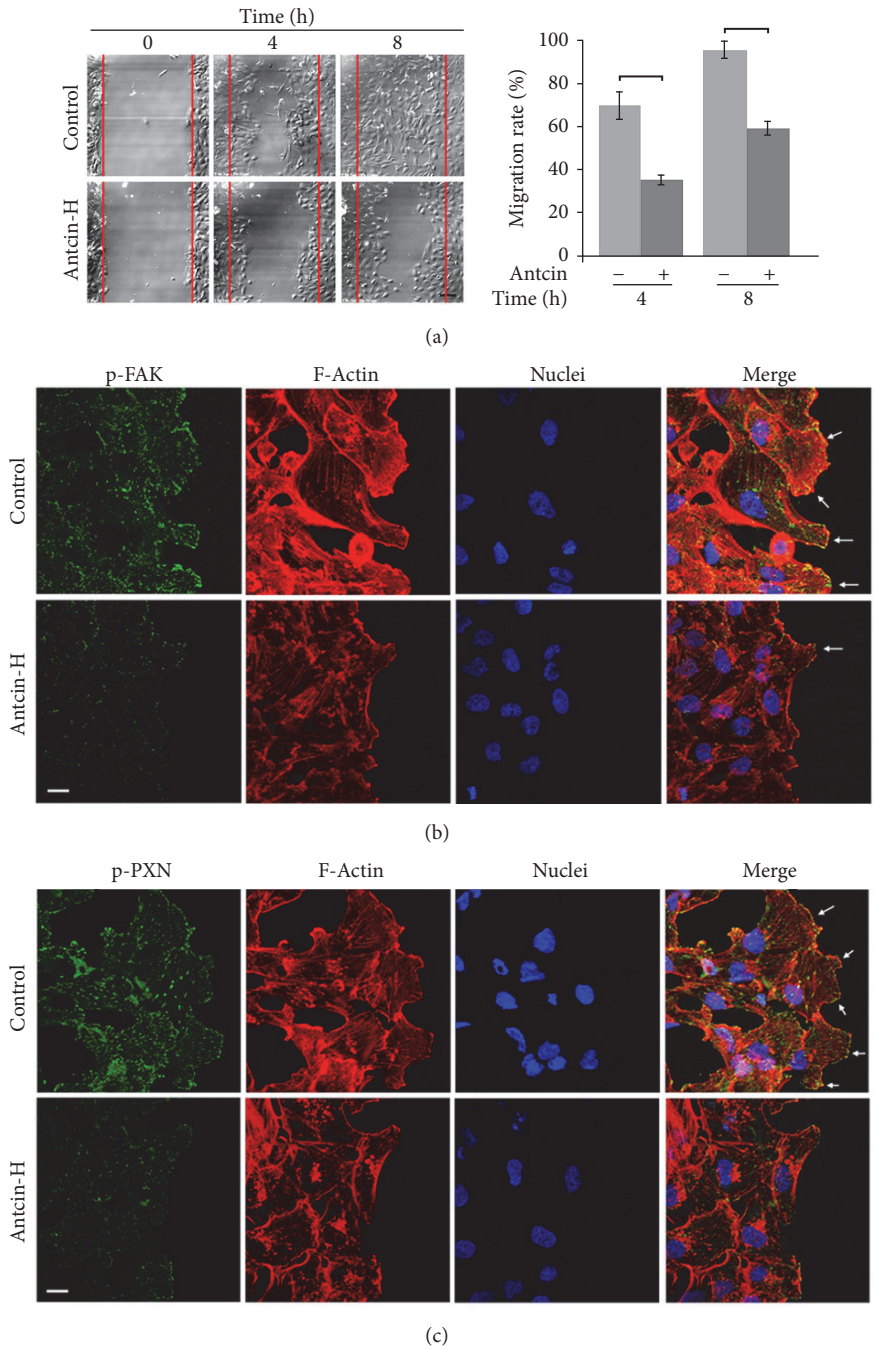

Figure 3: Suppression of wound-healing and disruption of lamellipodium formation by antcin-H. (a) Live cell time-lapse images at wound-healing front. 786-0 cells were cultured to 100% confluence on glass coverslips. After wound was made, fresh media without or with 100 μM antcin-H were added. Cells were allowed to migrate; the time-lapse of live cell imaging was observed at 4 and 8 h. Scale bar, 20 μm. (b) Immunostaining with FAK or (c) paxillin antibody. After 8 h wounding, the migrated cells were fixed, and the immunofluorescence staining was carried out using anti-phosphorylated-FAK and anti-phosphorylated-paxillin antibodies. The immunoreactive image was recorded by confocal microscope. Arrow, formation of lamellipodium. Scale bar, 20 μm.

be observed in untreated control cells. Moreover, antcin-H dose-dependently blocked c-Fos and C/EBP-β binding to their response DNA sequences located at distal and proximal *MMP-7* promoter region (c-FosRE1, c-FosRE2, C/EBP-βRE1, C/EBP-βRE2, and C/EBP-βRE4), respectively (Figure 6(d)). Additionally, no PCR amplified product was seen in sample which was processed by IgG isotype control-mediated precipitation. These results revealed that antcin-H could decrease the recruitment of both c-Fos and C/EBP-β transcriptional factors into the upstream response elements of *MMP-7* promoter, ultimately leading to inhibiting the expression of *MMP-7* gene in 786-0 RCC cells.

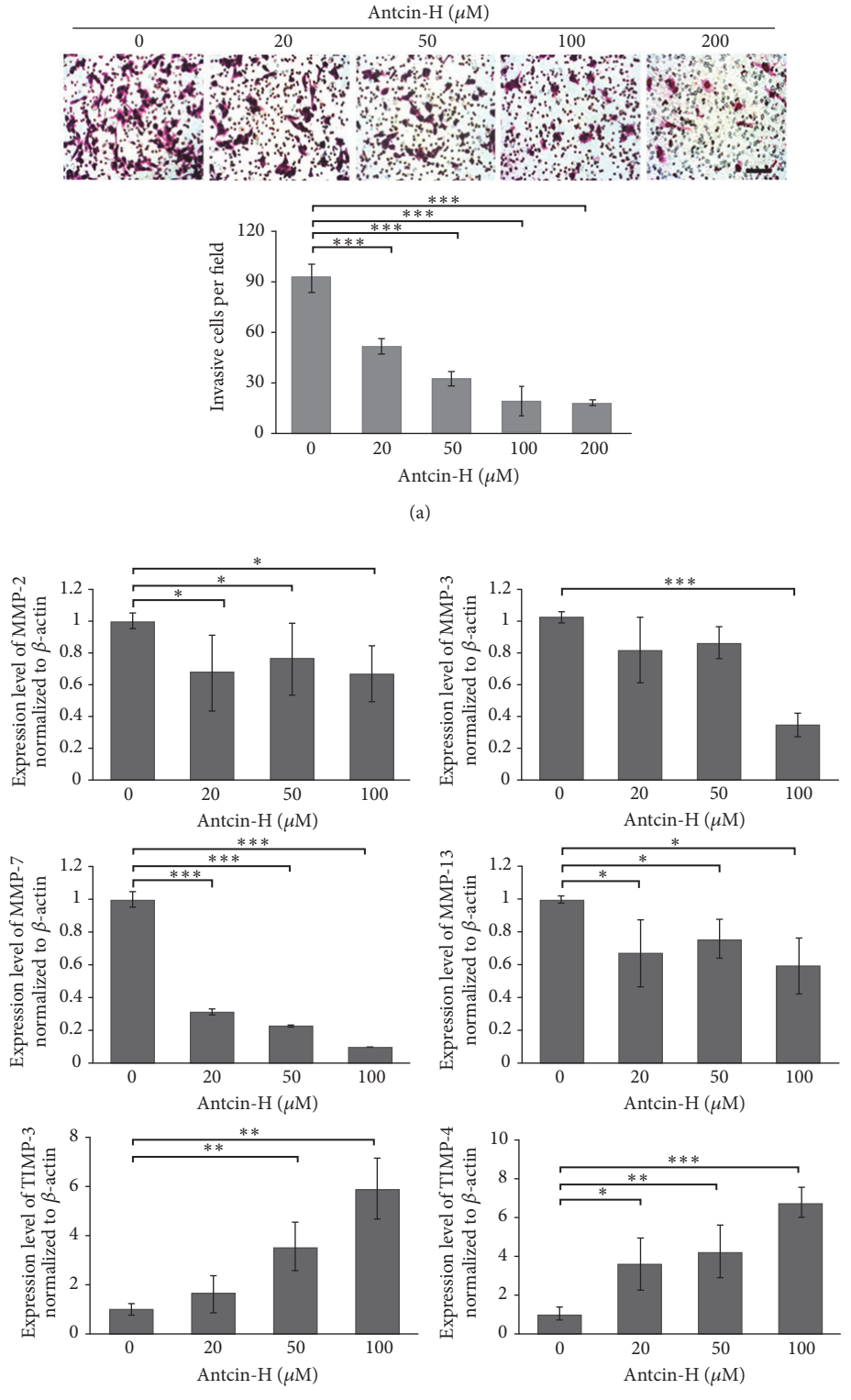

Figure 4: ANTCIN-H prevents invasion and regulates MMPs gene expression. (a) 768-0 cells were pretreated without or with 20, 50, 100, and 200 μM antcin-H for 24 h and then seeded into Matrigel-coated Transwell apparatus for another 24 h in the absence or presence of antcin-H. After incubation, the invaded cells were stained with Giemsa solution and counted using a microscope. Scale bar, 100 μm. The data were represented as the mean ± SD of nine replicates from three separated experiments. $^{***}p < 0.001$ versus control. (b) Real-time PCR analysis of MMPs and TIMPs gene expression. Cells were treated without or with 20, 50, and 100 μM antcin-H for 24 h. After treatment, the RNA extracted from 786-0 cells was subjected to a real-time PCR. β-Actin was used as an internal control. Data were represented as the mean ± SD of three independent experiments. Statistically significant, $^{*}p < 0.05$, $^{**}p < 0.01$, and $^{***}p < 0.001$.

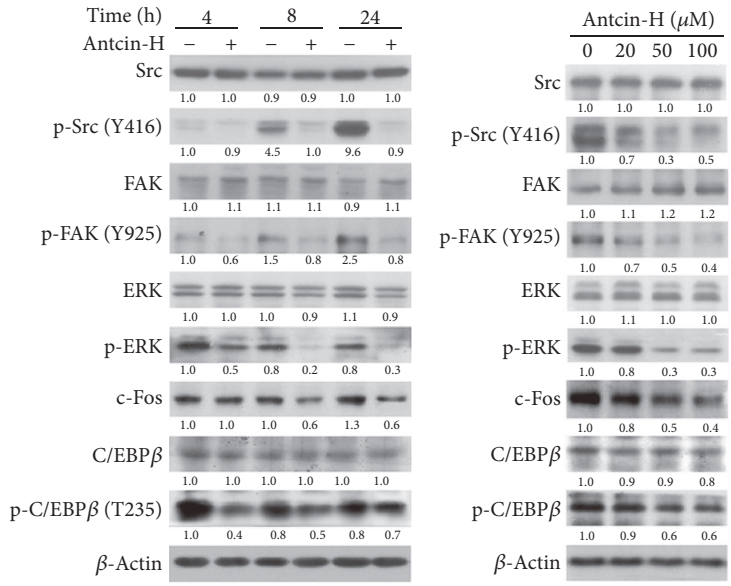

Figure 5: Suppression of Src, FAK, and ERK1/2 signaling pathways by antcin-H. (a) Time course-dependent experiment. 786-0 cells were treated without or with 100 μM antcin-H for 4, 8, and 24 h. (b) Dose-dependent experiment. Cells were treated without or with 20, 50, and 100 μM antcin-H for 24 h. After incubation, total protein lysates were isolated; the Western blotting analysis was performed to examine the levels of phosphorylated-Src, phosphorylated-FAK, phosphorylated-ERK1/2, phosphorylated-C/EBP-β, and c-Fos. β-Actin was used as an internal loading control.

4. Discussion

RCC is an epithelial malignancy of human kidney; surgery is the major strategy for treating patients with RCC. Unfortunately, approximately 30% of patients with RCC will be diagnosed with metastatic disease. Although target therapy and immunotherapy for treatment of patients with metastatic RCC have shown some positive results, continuous treatments with these drugs are associated with a high incidence of toxic effects and resistance [7], and five-year survival of patients with metastatic RCC is only 10% [34]. Therefore, developing strategies for therapeutic interventions in metastatic RCC is of utmost importance. Numerous natural substances have been found to inhibit progression and metastasis of various types of cancer cell lines and reveal that they might be useful for the treatment of metastatic cancer [35, 36]. The present study showed for the first time that antcin-H, a steroid-like compound isolated from a famous anticancer medicinal mushroom *A. cinnamomea*, inhibited Src, FAK, and ERK1/2 signaling pathways and thereby decreased phosphorylated-paxillin, phosphorylated-C/EBP-β, and total c-Fos levels and downregulated vimentin and MMPs expression, finally leading to impaired lamellipodium formation and cellular migration/invasion at nontoxic concentrations in human RCC 786-0 cells.

The FAK-Src complex is a pivotal component of focal adhesion contact, as a critical signaling module controls cell motility and potentiates tumor metastasis [31, 37]. Paxillin localizes at focal adhesion contact and acts as a scaffold molecule providing a platform for FAK and Src, which are involved in cell migration events associated with tumor metastasis [38]. Activated FAK/Src complex phosphorylates cytoskeletal adaptor paxillin which promotes cell migration [39]. FAK-Src expression and function have been associated with the majority of invasive and metastatic human cancers, with poor survival [40, 41]. Therefore, inhibition of FAK-Src function and expression is considered as a potential strategy for cancer therapy [42]. A synthetic small molecule with anticancer effect inhibits FAK, Src, and paxillin expression and activation, leading to the suppression of cell migration in colon cancer cells [43]. Src inhibitors reduce the migration of several types of human cancer cell through blocking Src, FAK, p130CAS, and paxillin activation [44, 45]. Inhibiting FAK/paxillin signaling by a sialyltransferase inhibitor effectively retards cancer cell migration [46]. In agreement with these earlier reports, this study showed that antcin-H significantly impaired cell migration by suppression of the FAK, Src, and paxillin signaling pathways. Besides, FAK, paxillin, and actin filaments play the important role in lamellipodium formation [33]. Since lamellipodium is a cell protrusion which is critical for directional migration in vary types of cell [47]. Here, we showed that antcin-H-mediated inhibition of FAK-Src-paxillin signaling axis and RCC cell migration was accompanied by decrease of lamellipodium, indicating that disruption of the lamellipodium formation as well as inhibition of migration and wound closure attributed to reducing formation of focal adhesion and actin bundles through suppressing FAK-Src-paxillin signaling pathway in antcin-H-treated cells.

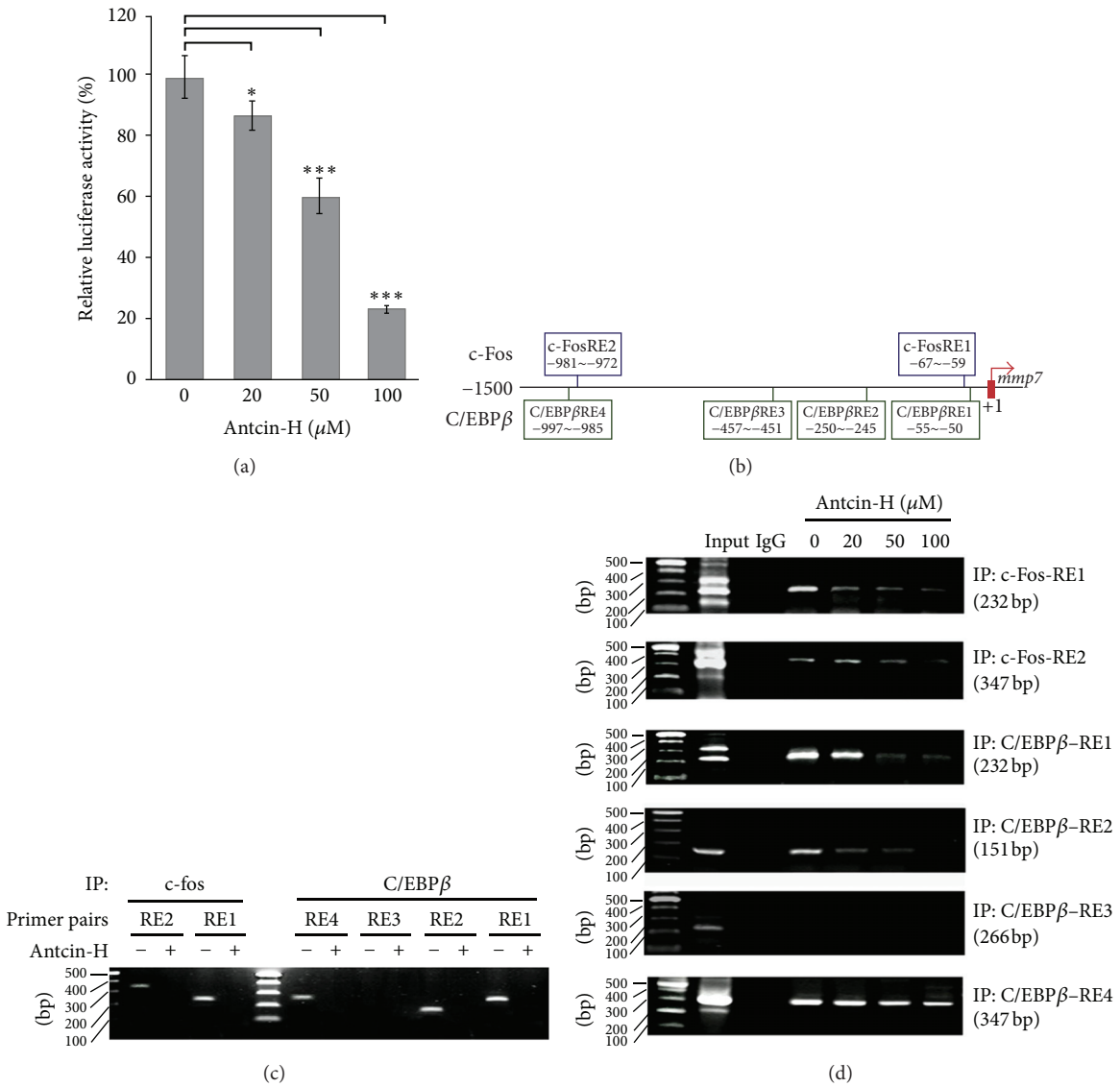

Figure 6: Inhibition of *c-Fos* and *C/EBP-β* activities involved in antcin-H-mediated *MMP-7* downregulation. (a) Reporter luciferase assay. 786-0 cells were transiently transfected with reporter vector containing *MMP-7* promoter +1~−1500 region or control vector for 24 h, and then the cells were treated without or with 20, 50, and 100 μM antcin-H for another 24 h. After incubation, the luciferase activity was measured and the relative luciferase activity was presented as means ± SD. Statistically significant, $^{*}p < 0.05$, $^{**}p < 0.01$, and $^{***}p < 0.001$. (b) Putative binding sites of c-Fos and C/EBP-β located at upstream of *MMP-7* promoter. (c) Antcin-H prevents c-Fos and C/EBP-β binding to the *MMP-7* upstream promoter/response element region. The 786-0 cells were treated without or with 100 μM antcin-H for 24 h, the cells were collected, and then ChIP assay was carried out. (d) Antcin-H dose-dependently inhibits c-Fos and C/EBP-β binding to the *MMP-7* upstream promoter/response element region. The 786-0 cells were treated without or with 20, 50, and 100 μM antcin-H for 24 h, the cells were collected, and then the activity of c-Fos and C/EBP-β binding to each response site located at *MMP-7* promoter upstream was determined by ChIP assay.

Growing evidence demonstrates that FAK/ERK-stimulated signaling activates EMT [48]. EMT is an essential step for cancer cell to acquire migration and invasion ability; loss of E-cadherin and increase of vimentin are surrogate markers for cell migration and invasion in EMT process [32]. E-cadherin is a normal epithelial cell adhesion molecule and is considered as a cancer metastasis suppressor. Nevertheless, methylation and loss of heterozygosity of E-cadherin gene are a common event in advanced renal cell carcinoma tissues and cell lines, including 786-0 cell line, which can lead to inactivation of E-cadherin transcription and loss of E-cadherin protein expression [49]. This is consistent with our observation that E-cadherin could not be detected in 786-0 cells. On the other hand, evidence supports that vimentin is a crucial cytoskeletal component of motile mesenchymal cells, including epithelium-derived metastatic tumor cells.

Downregulation of E-cadherin or overexpression of vimentin is strongly associated with metastasis, resulting in poor prognosis [50–52]. In the current study, downregulation of vimentin by antcin-H suggested that a loss of EMT and inhibition of invasion potential might occur in antcin-H-treated 786-0 cells.

Literatures show that the process of tumor growth, invasion, and metastasis is tightly regulated by MMPs in various types of malignant tumors, including RCC [11, 12]. Among MMPs, matrilysin (MMP-7) is mainly expressed in malignant tumor cells and preferentially localized at the invasive front of tumors suggesting that it may facilitate destruction of surrounding extracellular matrix and basement membrane [11, 18, 53]. Previous studies demonstrate that MMP-7 is overexpressed in RCC, and increased MMP-7 expression significantly correlates with the malignant behavior of RCC, including invasion, distant metastasis, poor prognosis, and reduced patient survival [11, 54]. These findings suggest that MMP-7 might be regarded as important targets for metastatic RCC therapy to prevent tumor progression and improve survival. In the current study, antcin-H slightly decreased MMP-2, MMP-3, and MMP-13 gene expression while it did not alter the expression of MMP-1, MMP-8, MMP-9, MMP-10, and MMP-11 mRNA levels (data not shown). Intriguingly, the expression of MMP-7 gene was drastically downregulated by antcin-H in 786-0 cells, revealing that targeted inhibition of MMP-7 gene expression might contribute to impairment of RCC cell invasion upon antcin-H administration. Previous studies have shown that MMP activities modulate at the levels of transcriptional regulation, enzymatic activation, and TIMPs inhibition [55]. TIMPs are endogenous inhibitors of MMPs, consisting of four members, TIMP-1, TIMP-2, TIMP-3, and TIMP-4, and play crucial roles in several processes, including cell proliferation, invasion and migration, angiogenesis, and apoptosis [56]. Deregulated expression of TIMPs has been implicated in tumor invasion and metastasis [56]. Overexpression of TIMPs has been reported to inhibit invasive and progressive potentials of the tumor cells [57]. Among TIMPs, TIMP-3 is a broad inhibitor against all MMPs [58], while TIMP-4 is MMP2 and MMP9 inhibitor [56, 59]. Our results indicated that upregulation of TIMP-3 and TIMP-4 expression, but not TIMP-1 and TIMP-2, might be another potential mechanism that contributes to inhibiting MMPs function in response to antcin-H treatment. Besides, TIMP family members have been shown to have proangiogenic effect. Overexpression of TIMP-1 is associated with VEGF expression and promoting neovascularization in breast carcinoma rats [60]. TIMP-2 inhibits angiogenesis by directly binding to $\alpha 3\beta 1$ integrin [61, 62] or insulin-like growth factor-1 receptor [63]. TIMP-4 is previously reported as a positive regulator of angiogenesis [64, 65]. Unlike TIMP-1 and TIMP-4, TIMP-3 inhibits angiogenesis by blocking the binding of VEGF to VEGF receptor-2 [66] and suppressing angiotensin II receptor activity [67]. These results suggest the important functions of TIMPs in cancer metastasis and angiogenesis. However, the roles of TIMP-3 and TIMP-4 induced by antcin-H in RCC progression are still poorly understood. Further *in vitro* and *in vivo* studies are needed to examine the effects and molecular mechanisms of antcin-H on TIMP-3/4 regulation and angiogenesis in metastatic RCC.

Previous reports demonstrate that FAK/ERK signaling is not only critical for cell migration and invasion, but is also involved in the regulation of MMPs activity and gene expression [68, 69]. ERK and its downstream transcriptional factor AP-1 play an important role in the regulation of MMPs gene expression [70, 71]. AP-1 is a common transcriptional activator composed of the Jun and Fos family members [72]. Besides, ERK can phosphorylate Elk-1 which subsequently upregulates c-Fos gene expression [73]. Literatures have shown that the MMP-7 expression is controlled by modulating the activation of AP-1 transcription factors, c-Fos and c-Jun, through ERK1/2 signaling pathway [17, 74–76]. In this study, we found that two putative binding sites of c-Fos were located at the promoter region of *MMP-7* (Figure 6(b)). In agreement with these previous studies, our observations provided evidence that antcin-H-inhibited MMP-7 gene expression might be through suppressing ERK/c-Fos signaling axis in RCC 786-0 cells. In addition to AP-1/c-Fos, our results indicated that antcin-H-mediated MMP-7 gene downregulation was also via C/EBP-β transcriptional repression. Previous studies demonstrate that phosphorylated-C/EBP-β by ERK can activate its transcriptional activity [77]. Our results demonstrated that antcin-H inhibited MMP-7 expression might be also via prevention of ERK-C/EBP-β activation. On the basis of these results, we suggest that the anti-invasive activity of antcin-H is in part due to the inhibition of MMP-7 expression, which plays a critical role in cancer invasion and metastasis, through the suppression of ERK-mediated AP-1/c-Fos and C/EBP-β activities in RCC cells.

In fact, our results demonstrated that, except MMP-7, antcin-H also inhibited other MMP gene expressions, such as MMP-2, MMP-3, and MMP-13, which play critical roles in cancer cell invasion. Similar to MMP-7, these MMPs were also regulated predominantly at the transcriptional level. On the basis of the composition of *cis*-regulatory elements in their promoters, MMP-2, MMP-3, and MMP-13, also contain AP-1 and C/EBP-β binding sites proximal and distal to the transcriptional start site, and their expressions have been shown to be regulated at the transcriptional levels via AP-1 and C/EBP-β [78–82]. It is possible that these MMPs are regulated similarly upon antcin-H treatment. Besides, on the basis of present results, it is still unclear how TIMP-3 and TIMP-4 expression is upregulated in response to antcin-H treatment. Several transcription factors binding sites, for example, p53, STATs, PPARs, AP-1/c-Fos, C/EBP-α, and C/EBP-β, are found in the promoter region of TIMP-3 and TIMP-4. However, which transcription factor contributes to the upregulation of TIMP-3 and TIMP-4 by antcin-H needs to be further examined.

5. Conclusion

Based on our observation, we propose a potential mechanism in antcin-H-treated RCC cells, which shows that antcin-H suppressed FAK-related signaling pathway (Src, FAK, paxillin, and ERK1/2), which impaired focal adhesion

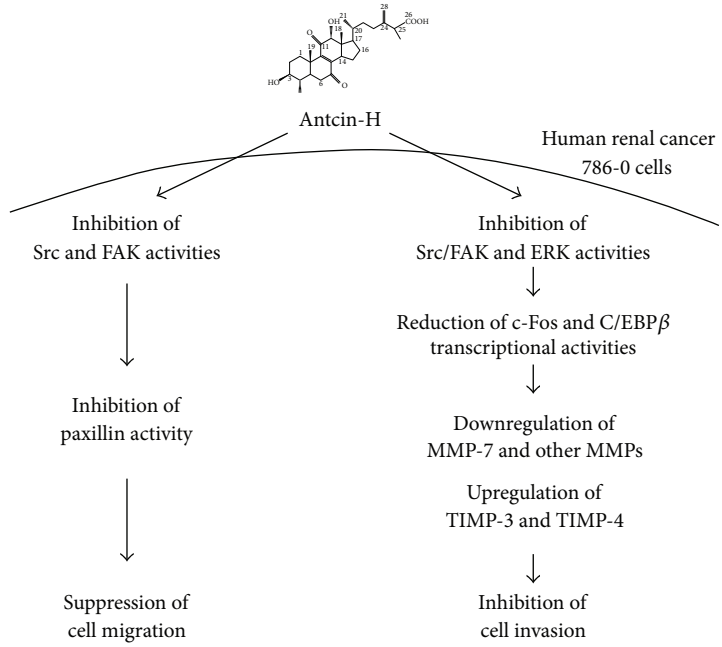

Figure 7: Schematic model of the proposed signaling pathways involved in suppressing cell migration and invasion by antcin-H in human RCC 786-0 cells. Antcin-H inhibits Src, FAK, and ERK1/2 phosphorylated activation, in turn decreasing paxillin, c-Fos, and C/EBP-β activities, reducing the binding of c-Fos and phosphorylated-C/EBP-β to AP-1 and C/EBP-β response elements, thereby decreasing MMPs gene expression, especially MMP-7. Downregulation of MMP-7 and upregulation of TIMP-3 and TIMP-4 gene expression block the degradation of the extracellular matrix proteins and impair the cell invasion. Besides, reducing paxillin phosphorylation and vimentin expression prevents 786-0 cell motility.

turnover and lamellipodium formation, inactivated c-Fos and C/EBP-β, downregulated MMPs (especially MMP-7), and upregulated TIMPs (TIMP-3 and TIMP-4) expression (Figure 7). MMP-7 has been considered as a metastatic marker and survival predictor in RCC patients; inhibition of MMP-7 expression and function in tumor cells could be one of the most powerful strategies in metastatic RCC therapy. Our findings provide new insights into the antimigratory and anti-invasive properties of antcin-H and implicate that antcin-H might be a promising phytochemical existing in *A. cinnamomea* with antimetastatic capability in treating advanced RCC.

Conflicts of Interest

The authors declare that there are no conflicts of interest regarding the publication of this paper.

Authors' Contributions

Kun-Yuan Chiu and Tzu-Hsiu Chen have equal contribution.

Acknowledgments

This study was supported by grants from the National Science Council of Taiwan (MOST 103-2320-B-075A-002-MY3 and NSC 102-2320-B-075A-003) and Taichung Veterans General Hospital (TCVGH-1037305C) for Dr. Shih-Lan Hsu.

References

[1] Taipei, Department of Health and Welfare, Vital Statistics 2014, http://ghdx.healthdata.org/organizations/ministry-health-and-welfare-taiwan-0.

[2] C. Battagli, R. G. Uzzo, E. Dulaimi et al., "Promoter hypermethylation of tumor suppressor genes in urine from kidney cancer patients," *Cancer Research*, vol. 63, no. 24, pp. 8695–8699, 2003.

[3] R. C. Flanigan, S. C. Campbell, J. I. Clark, and M. M. Picken, "Metastatic renal cell carcinoma.," *Current Treatment Options in Oncology*, vol. 4, no. 5, pp. 385–390, 2003.

[4] R. G. Uzzo, E. E. Cherullo, J. Myles, and A. C. Novick, "Renal cell carcinoma invading the urinary collecting system: Implications for staging," *The Journal of Urology*, vol. 167, no. 6, pp. 2392–2396, 2002.

[5] B. Escudier, T. Eisen, W. M. Stadler et al., "Sorafenib in advanced clear-cell renal-cell carcinoma," *The New England Journal of Medicine*, vol. 356, no. 2, pp. 125–134, 2007.

[6] B. C. Leibovich, K.-R. Han, M. H. T. Bui et al., "Scoring algorithm to predict survival after nephrectomy and immunotherapy in patients with metastatic renal cell carcinoma: a stratification tool for prospective clinical trials," *Cancer*, vol. 98, no. 12, pp. 2566–2575, 2003.

[7] M. I. Khan, A. M. Czarnecka, R. Duchnowska, W. Kukwa, and C. Szczylik, "Metastasis-initiating cells in renal cancer," *Current Signal Transduction Therapy*, vol. 8, no. 3, pp. 240–246, 2014.

[8] C. N. Sternberg, R. E. Hawkins, J. Wagstaff et al., "A randomised, double-blind phase III study of pazopanib in patients with

advanced and/or metastatic renal cell carcinoma: Final overall survival results and safety update," *European Journal of Cancer*, vol. 49, no. 6, pp. 1287–1296, 2013.

[9] R. D. Bonfil, S. Chinni, R. Fridman, H.-R. Kim, and M. L. Cher, "Proteases, growth factors, chemokines, and the microenvironment in prostate cancer bone metastasis," *Urologic Oncology: Seminars and Original Investigations*, vol. 25, no. 5, pp. 407–411, 2007.

[10] E. I. Deryugina and J. P. Quigley, "Matrix metalloproteinases and tumor metastasis," *Cancer and Metastasis Reviews*, vol. 25, no. 1, pp. 9–34, 2006.

[11] Y. Miyata, T. Iwata, K. Ohba, S. Kanda, M. Nishikido, and H. Kanetake, "Expression of matrix metalloproteinase-7 on cancer cells and tissue endothelial cells in renal cell carcinoma: prognostic implications and clinical significance for invasion and metastasis," *Clinical Cancer Research*, vol. 12, no. 23, pp. 6998–7003, 2006.

[12] A. Ramankulov, M. Lein, M. Johannsen, M. Schrader, K. Miller, and K. Jung, "Plasma matrix metalloproteinase-7 as a metastatic marker and survival predictor in patients with renal cell carcinoma," *Cancer Science*, vol. 99, no. 6, pp. 1188–1194, 2008.

[13] A. K. Chaudhary, S. Pandya, K. Ghosh, and A. Nadkarni, "Matrix metalloproteinase and its drug targets therapy in solid and hematological malignancies: an overview," *Mutation Research*, vol. 753, no. 1, pp. 7–23, 2013.

[14] R. Roy, J. Yang, and M. A. Moses, "Matrix metalloproteinases as novel biomarkers and potential therapeutic targets in human cancer," *Journal of Clinical Oncology*, vol. 27, no. 31, pp. 5287–5297, 2009.

[15] U. I. Sires, G. L. Griffin, T. J. Broekelmann et al., "Degradation of entactin by matrix metalloproteinases. susceptibility to matrilysin and identification of cleavage sites," *The Journal of Biological Chemistry*, vol. 268, no. 3, pp. 2069–2074, 1993.

[16] L. E. Jones, M. J. Humphreys, F. Campbell, J. P. Neoptolemos, and M. T. Boyd, "Comprehensive analysis of matrix metalloproteinase and tissue inhibitor expression in pancreatic cancer: increased expression of matrix metalloproteinase-7 predicts poor survival," *Clinical Cancer Research*, vol. 10, no. 8, pp. 2832–2845, 2004.

[17] W. Yue, Q. Sun, R. Landreneau et al., "Fibulin-5 suppresses lung cancer invasion by inhibiting matrix metalloproteinase-7 expression," *Cancer Research*, vol. 69, no. 15, pp. 6339–6346, 2009.

[18] Y. Adachi, H. Yamamoto, F. Itoh, Y. Hinoda, Y. Okada, and K. Imai, "Contribution of matrilysin (MMP-7) to the metastatic pathway of human colorectal cancers," *Gut*, vol. 45, no. 2, pp. 252–258, 1999.

[19] M. Geethangili and Y.-M. Tzeng, "Review of pharmacological effects of *Antrodia camphorata* and its bioactive compounds," *Evidence-Based Complementary and Alternative Medicine*, vol. 2011, Article ID 212641, 17 pages, 2011.

[20] M. Geethangili, Y. K. Rao, and Y. M. Tzeng, "Development and validation of a HPLC-DAD separation method for determination of bioactive antrocin in medicinal mushroom antrodia camphorata," *International Journal of Applied Science and Engineering Research*, vol. 2, pp. 195–201, 2013.

[21] C.-W. Chang, Y.-S. Chen, C.-C. Chen et al., "Targeting cancer initiating cells by promoting cell differentiation and restoring chemosensitivity via dual inactivation of STAT3 and src activity using an active component of antrodia cinnamomea mycelia," *Oncotarget* , vol. 7, no. 45, pp. 73016–73031, 2016.

[22] K.-Y. Chiu, C.-C. Wu, C.-H. Chia, S.-L. Hsu, and Y.-M. Tzeng, "Inhibition of growth, migration and invasion of human bladder cancer cells by antrocin, a sesquiterpene lactone isolated from Antrodia cinnamomea, and its molecular mechanisms," *Cancer Letters*, vol. 373, no. 2, pp. 174–184, 2016.

[23] C.-C. Lin, C.-C. Chen, Y.-H. Kuo, J.-T. Kuo, K. J. Senthil Kumar, and S.-Y. Wang, "2,3,5-Trimethoxy-4-cresol, an anti-metastatic constituent from the solid-state cultured mycelium of Antrodia cinnamomea and its mechanism," *Journal of Natural Medicines*, vol. 69, no. 4, pp. 513–521, 2015.

[24] M.-K. Lu, T.-Y. Lin, C.-H. Chao, C.-H. Hu, and H.-Y. Hsu, "Molecular mechanism of Antrodia cinnamomea sulfated polysaccharide on the suppression of lung cancer cell growth and migration via induction of transforming growth factor β receptor degradation," *International Journal of Biological Macromolecules*, vol. 95, pp. 1144–1152, 2017.

[25] T.-Y. Chung, F.-Y. Li, C.-I. Chang, T.-R. Jinn, and J. T. C. Tzen, "Inhibition of Na+/K+-ATPase by antcins, unique steroid-like compounds in Antrodia camphorate," *American Journal of Chinese Medicine*, vol. 40, no. 5, pp. 953–965, 2012.

[26] C.-I. Lai, Y.-L. Chu, C.-T. Ho, Y.-C. Su, Y.-H. Kuo, and L.-Y. Sheen, "Antcin K, an active triterpenoid from the fruiting bodies of basswood cultivated Antrodia cinnamomea, induces mitochondria and endoplasmic reticulum stress-mediated apoptosis in human hepatoma cells," *Journal of Traditional and Complementary Medicine*, vol. 6, no. 1, pp. 48–56, 2016.

[27] K. B. Male, Y. K. Rao, Y.-M. Tzeng, J. Montes, A. Kamen, and J. H. T. Luong, "Probing inhibitory effects of Antrodia camphorata isolates using insect cell-based impedance spectroscopy: inhibition vs chemical structure," *Chemical Research in Toxicology*, vol. 21, no. 11, pp. 2127–2133, 2008.

[28] Y. K. Rao, M. Geethangili, and Y.-M. Tzeng, "Development of a high performance liquid chromatography method for the quantitative determination of bioactive triterpenoids in the extracts of Antrodia camphorata," *Analytical Methods*, vol. 5, no. 20, pp. 5724–5730, 2013.

[29] R. Kajanne, P. Miettinen, A. Mehlem et al., "EGF-R regulates MMP function in fibroblasts through MAPK and AP-1 pathways," *Journal of Cellular Physiology*, vol. 212, no. 2, pp. 489–497, 2007.

[30] H. T. Cohen and F. J. McGovern, "Renal-cell carcinoma," *The New England Journal of Medicine*, vol. 353, no. 23, pp. 2477–2490, 2005.

[31] J. Zhao and J. Guan, "Signal transduction by focal adhesion kinase in cancer," *Cancer and Metastasis Reviews*, vol. 28, no. 1-2, pp. 35–49, 2009.

[32] L. Li and W. Li, "Epithelial-mesenchymal transition in human cancer: comprehensive reprogramming of metabolism, epigenetics, and differentiation," *Pharmacology & Therapeutics*, vol. 150, pp. 33–46, 2015.

[33] P. S. Leventhal, E. A. Shelden, B. Kim, and E. L. Feldman, "Tyrosine phosphorylation of paxillin and focal adhesion kinase during insulin-like growth factor-I-stimulated lamellipodial advance," *The Journal of Biological Chemistry*, vol. 272, no. 8, pp. 5214–5218, 1997.

[34] R. J. Motzer, T. E. Hutson, D. Cella et al., "Pazopanib versus sunitinib in metastatic renal-cell carcinoma," *The New England Journal of Medicine*, vol. 369, no. 8, pp. 722–731, 2013.

[35] A. AlQathama and J. M. Prieto, "Natural products with therapeutic potential in melanoma metastasis," *Natural Product Reports*, vol. 32, no. 8, pp. 1170–1182, 2015.

[36] T. N. Chinembiri, L. H. Du Plessis, M. Gerber, J. H. Hamman, and J. Du Plessis, "Review of natural compounds for potential skin cancer treatment," *Molecules*, vol. 19, no. 8, pp. 11679–11721, 2014.

[37] P. Kratimenos, I. Koutroulis, D. Marconi et al., "Multi-targeted molecular therapeutic approach in aggressive neuroblastoma: The effect of Focal Adhesion Kinase-Src-Paxillin system," *Expert Opinion on Therapeutic Targets*, vol. 18, no. 12, pp. 1395–1406, 2014.

[38] C. E. Turner, "Paxillin interactions," *Journal of Cell Science*, vol. 113, part 23, pp. 4139-4140, 2000.

[39] T. S. Panetti, "Tyrosine phosphorylation of paxillin, FAK, and p130CAS: effects on cell spreading and migration," *Frontiers in Bioscience*, vol. 7, pp. d143–d150, 2002.

[40] N. A. Chatzizacharias, G. P. Kouraklis, and S. E. Theocharis, "Clinical significance of FAK expression in human neoplasia," *Histology and Histopathology*, vol. 23, no. 5, pp. 629–650, 2008.

[41] M. Luo, H. Fan, T. Nagy et al., "Mammary epithelial-specific ablation of the focal adhesion kinase suppresses mammary tumorigenesis by affecting mammary cancer stem/progenitor cells," *Cancer Research*, vol. 69, no. 2, pp. 466–474, 2009.

[42] M. J. van Nimwegen and B. van de Water, "Focal adhesion kinase: a potential target in cancer therapy," *Biochemical Pharmacology*, vol. 73, no. 5, pp. 597–609, 2007.

[43] F. Dai, Y. Chen, L. Huang et al., "A novel synthetic small molecule YH-306 suppresses colorectal tumour growth and metastasis via FAK pathway," *Journal of Cellular and Molecular Medicine*, vol. 19, no. 2, pp. 383–395, 2015.

[44] L. Bai, J. C. Yang, J.-H. Ok, P. C. MacK, H.-J. Kung, and C. P. Evans, "Simultaneous targeting of Src kinase and receptor tyrosine kinase results in synergistic inhibition of renal cell carcinoma proliferation and migration," *International Journal of Cancer*, vol. 130, no. 11, pp. 2693–2702, 2012.

[45] L. Rice, S. Lepler, C. Pampo, and D. W. Siemann, "Impact of the SRC inhibitor dasatinib on the metastatic phenotype of human prostate cancer cells," *Clinical & Experimental Metastasis*, vol. 29, no. 2, pp. 133–142, 2012.

[46] J.-Y. Chen, Y.-A. Tang, S.-M. Huang et al., "A novel sialyltransferase inhibitor suppresses FAK/paxillin signaling and cancer angiogenesis and metastasis pathways," *Cancer Research*, vol. 71, no. 2, pp. 473–483, 2011.

[47] C. Ballestrem, B. Wehrle-Haller, B. Hinz, and B. A. Imhof, "Actin-dependent lamellipodia formation and microtubule-dependent tail retraction control-directed cell migration," *Molecular Biology of the Cell (MBoC)*, vol. 11, no. 9, pp. 2999–3012, 2000.

[48] D. C. Radisky and M. A. LaBarge, "Epithelial-mesenchymal transition and the stem cell phenotype," *Cell Stem Cell*, vol. 2, no. 6, pp. 511-512, 2008.

[49] D. Nojima, K. Nakajima, L. Li et al., "CpG methylation of promoter region inactivates E-cadherin gene in renal cell carcinoma," *Molecular Carcinogenesis*, vol. 32, no. 1, pp. 19–27, 2001.

[50] A. Katagiri, R. Watanabe, and Y. Tomita, "E-cadherin expression in renal cell cancer and its significance in metastasis and survival," *British Journal of Cancer*, vol. 71, no. 2, pp. 376–379, 1995.

[51] M. Schoumacher, R. D. Goldman, D. Louvard, and D. M. Vignjevic, "Actin, microtubules, and vimentin intermediate filaments cooperate for elongation of invadopodia," *The Journal of Cell Biology*, vol. 189, no. 3, pp. 541–556, 2010.

[52] M. Wu, X. Bai, G. Xu et al., "Proteome analysis of human androgen-independent prostate cancer cell lines: variable metastatic potentials correlated with vimentin expression," *Proteomics*, vol. 7, no. 12, pp. 1973–1983, 2007.

[53] M. Ii, H. Yamamoto, Y. Adachi, Y. Maruyama, and Y. Shinomura, "Role of matrix metalloproteinase-7 (matrilysin) in human cancer invasion, apoptosis, growth, and angiogenesis," *Experimental Biology and Medicine*, vol. 231, no. 1, pp. 20–27, 2006.

[54] M. Lein, K. Jung, C. Laube et al., "Matrix-metalloproteinases and their inhibitors in plasma and tumor tissue of patients with renal cell carcinoma," *International Journal of Cancer*, vol. 85, no. 6, pp. 801–804, 2000.

[55] Y. Gong, U. D. Chippada-Venkata, and W. K. Oh, "Roles of matrix metalloproteinases and their natural inhibitors in prostate cancer progression," *Cancers*, vol. 6, no. 3, pp. 1298–1327, 2014.

[56] K. Brew and H. Nagase, "The tissue inhibitors of metalloproteinases (TIMPs): an ancient family with structural and functional diversity," *Biochimica et Biophysica Acta (BBA)—Molecular Cell Research*, vol. 1803, no. 1, pp. 55–71, 2010.

[57] A. H. Baker, S. J. George, A. B. Zaltsman, G. Murphy, and A. C. Newby, "Inhibition of invasion and induction of apoptotic cell death of cancer cell lines by overexpression of TIMP-3," *British Journal of Cancer*, vol. 79, no. 9-10, pp. 1347–1355, 1999.

[58] S. S. Apte, B. R. Olsen, and G. Murphy, "The gene structure of tissue inhibitor of metalloproteinases (TIMP)-3 and its inhibitory activities define the distinct TIMP gene family," *The Journal of Biological Chemistry*, vol. 270, no. 24, pp. 14313–14318, 1995.

[59] M. Bodnar, L. Szylberg, W. Kazmierczak, and A. Marszalek, "Tumor progression driven by pathways activating matrix metalloproteinases and their inhibitors," *Journal of Oral Pathology & Medicine*, vol. 44, no. 6, pp. 437–443, 2015.

[60] H. Yoshiji, S. R. Harris, E. Raso et al., "Mammary carcinoma cells over-expressing tissue inhibitor of metalloproteinases-1 show enhanced vascular endothelial growth factor expression," *International Journal of Cancer*, vol. 75, no. 1, pp. 81–87, 1998.

[61] H.-J. Kim, Y.-R. Cho, S. H. Kim, and D.-W. Seo, "TIMP-2-derived 18-mer peptide inhibits endothelial cell proliferation and migration through cAMP/PKA-dependent mechanism," *Cancer Letters*, vol. 343, no. 2, pp. 210–216, 2014.

[62] D.-W. Seo, H. Li, L. Guedez et al., "TIMP-2 mediated inhibition of angiogenesis: an MMP-independent mechanism," *Cell*, vol. 114, no. 2, pp. 171–180, 2003.

[63] C. A. Fernandez, R. Roy, S. Lee et al., "The anti-angiogenic peptide, Loop 6, binds insulin-like growth factor-1 receptor," *The Journal of Biological Chemistry*, vol. 285, no. 53, pp. 41886–41895, 2010.

[64] M. Boufraqech, L. Zhang, N. Nilubol et al., "Lysyl Oxidase (LOX) transcriptionally regulates SNAI2 expression and TIMP4 secretion in human cancers," *Clinical Cancer Research*, vol. 22, no. 17, pp. 4491–4504, 2016.

[65] W. G. Stetler-Stevenson, "Tissue inhibitors of metalloproteinases in cell signaling: metalloproteinase-independent biological activities," *Science Signaling*, vol. 1, re6, no. 27, 2008.

[66] J. H. Qi, Q. Ebrahem, N. Moore et al., "A novel function for tissue inhibitor of metalloproteinases-3 (TIMP3): inhibition of angiogenesis by blockage of VEGF binding to VEGF receptor-2," *Nature Medicine*, vol. 9, no. 4, pp. 407–415, 2003.

[67] K.-H. Kang, S.-Y. Park, S. B. Rho, and J.-H. Lee, "Tissue inhibitor of metalloproteinases-3 interacts with angiotensin II

type 2 receptor and additively inhibits angiogenesis," *Cardiovascular Research*, vol. 79, no. 1, pp. 150–160, 2008.

[68] Y.-J. Chen, Y.-Y. Wei, H.-T. Chen et al., "Osteopontin increases migration and MMP-9 up-regulation via $\alpha v\beta 3$ integrin, FAK, ERK, and NF-κB-dependent pathway in human chondrosarcoma cells," *Journal of Cellular Physiology*, vol. 221, no. 1, pp. 98–108, 2009.

[69] H.-Y. Xu, A.-R. Qian, P. Shang et al., "siRNA targeted against HAb18G/CD147 inhibits MMP-2 secretion, actin and FAK expression in hepatocellular carcinoma cell line via ERK1/2 pathway," *Cancer Letters*, vol. 247, no. 2, pp. 336–344, 2007.

[70] H.-J. Cho, J. H. Kang, J.-Y. Kwak et al., "Ascofuranone suppresses PMA-mediated matrix metalloproteinase-9 gene activation through the Ras/Raf/MEK/ERK- and Ap1-dependent mechanisms," *Carcinogenesis*, vol. 28, no. 5, pp. 1104–1110, 2007.

[71] H. Han, B. Du, X. Pan et al., "CADPE inhibits PMA-stimulated gastric carcinoma cell invasion and matrix metalloproteinase-9 expression by FAK/MEK/ERK-mediated AP-1 activation," *Molecular Cancer Research*, vol. 8, no. 11, pp. 1477–1488, 2010.

[72] P. Verde, L. Casalino, F. Talotta, M. Yaniv, and J. B. Weitzman, "Deciphering AP-1 function in tumorigenesis: Fra-ternizing on target promoters," *Cell Cycle*, vol. 6, no. 21, pp. 2633–2639, 2007.

[73] Y.-C. Tu, D.-Y. Huang, S.-G. Shiah, J.-S. Wang, and W.-W. Lin, "Regulation of c-Fos gene expression by NF-κB: A p65 homodimer binding site in mouse embryonic fibroblasts but not human HEK293 cells," *PLoS ONE*, vol. 8, no. 12, Article ID e84062, 2013.

[74] M. C. Chang, C. A. Chen, P. J. Chen et al., "Mesothelin enhances invasion of ovarian cancer by inducing MMP-7 through MAPK/ERK and JNK pathways," *Biochemical Journal*, vol. 442, no. 2, pp. 293–302, 2012.

[75] B.-Y. Ho, Y.-M. Wu, K.-J. Chang, and T.-M. Pan, "Dimerumic acid inhibits SW620 cell invasion by attenuating H_2O_2-mediated MMP-7 expression via JNK/C-Jun and ERK/C-Fos activation in an AP-1-Dependent manner," *International Journal of Biological Sciences*, vol. 7, no. 6, pp. 869–880, 2011.

[76] Z.-C. Jia, Y.-L. Wan, J.-Q. Tang et al., "Tissue factor/activated factor VIIa induces matrix metalloproteinase-7 expression through activation of c-Fos via ERK1/2 and p38 MAPK signaling pathways in human colon cancer cell," *International Journal of Colorectal Disease*, vol. 27, no. 4, pp. 437–445, 2012.

[77] D. M. Cortez, M. D. Feldman, S. Mummidi et al., "IL-17 stimulates MMP-1 expression in primary human cardiac fibroblasts via p38 MAPK- and ERK1/2-dependent C/EBP-β, NF-κB, and AP-1 activation," *American Journal of Physiology-Heart and Circulatory Physiology*, vol. 293, no. 6, pp. H3356–H3365, 2007.

[78] D. A. Armstrong, L. N. Phelps, and M. P. Vincenti, "CCAAT enhancer binding protein-β regulates matrix metalloproteinase-1 expression in interleukin-1β-stimulated A549 lung carcinoma cells," *Molecular Cancer Research*, vol. 7, no. 9, pp. 1517–1524, 2009.

[79] G. Buttice, M. Duterque-Coquillaud, J. P. Basuyaux, S. Carrere, M. Kurkinen, and D. Stehelin, "Erg, an Ets-family member, differentially regulates human collagenase1 (MMP1) and stromelysin1 (MMP3) gene expression by physically interacting with the Fos/Jun complex," *Oncogene*, vol. 13, pp. 2297–2306, 1996.

[80] Y. Fei, E. Shimizu, M. W. McBurney, and N. C. Partridge, "Sirtuin 1 is a negative regulator of parathyroid hormone stimulation of matrix metalloproteinase 13 expression in osteoblastic cells: role of sirtuin 1 in the action of PTH on osteoblasts," *The Journal of Biological Chemistry*, vol. 290, no. 13, pp. 8373–8382, 2015.

[81] Y. Luo, F. Liang, and Z.-Y. Zhang, "PRL1 promotes cell migration and invasion by increasing MMP2 and MMP9 expression through Src and ERK1/2 pathways," *Biochemistry*, vol. 48, no. 8, pp. 1838–1846, 2009.

[82] T. Okuma, M. Hirata, F. Yano et al., "Regulation of mouse chondrocyte differentiation by CCAAT/enhancer-binding proteins," *Biomedical Research (Japan)*, vol. 36, no. 1, pp. 21–29, 2015.

Hindawi
Evidence-Based Complementary and Alternative Medicine
Volume 2017, Article ID 6451905, 8 pages
https://doi.org/10.1155/2017/6451905

Research Article

A Molecular Basis for the Inhibition of Transient Receptor Potential Vanilloid Type 1 by Gomisin A

Sung Bae Lee,[1] Shinhwa Noh,[1] Hye Duck Yeom,[1] Heejin Jo,[2] Sanung Eom,[1] Yoon Suh Kim,[1] Sangsoo Nam,[2] Hyunsu Bae,[2] and Jun-Ho Lee[1]

[1]*Department of Biotechnology, Chonnam National University, Gwangju 61886, Republic of Korea*
[2]*College of Korean Medicine, Kyung Hee University, Seoul 02447, Republic of Korea*

Correspondence should be addressed to Hyunsu Bae; hbae@khu.ac.kr and Jun-Ho Lee; leejunho@chonnam.ac.kr

Received 13 June 2017; Accepted 2 August 2017; Published 26 October 2017

Academic Editor: José C. T. Carvalho

Transient receptor potential (TRP) channel has critical actions as conditional sensors in primary afferent neurons. We studied the regulatory action of gomisin A on TRPV1 channel current in this report. *Schisandra chinensis* contains bioactive compounds such as the gomisin derivatives and their related compounds. Coapplication with gomisin A inhibited the capsaicin-mediated inward peak current. This inhibitory effect of gomisin A on capsaicin-induced inward current showed concentration-dependence and was reversible. The half maximal inhibitory concentration of gomisin A was 62.7 ± 8.4 μM. In addition, this inhibition occurred in a noncompetition regulation mode and voltage insensitive manner. Furthermore, molecular docking studies of gomisin A on TRPV1 showed that it interacted predominantly with residues at cavities in the segments 1 and 2 of each subunit. Four potential binding sites for this ligand in the extracellular region at sensor domain of TRPV1 channel were identified. Point mutagenesis studies were undertaken, and gomisin A potency decreased for both the Y453A and N467A mutants. The double mutation of Y453 and N467 significantly attenuated inhibitory effects by gomisin A. In summary, this study revealed the molecular basis for the interaction between TRPV1 and gomisin A and provides a novel potent interaction ligand.

1. Introduction

TRPV1 receptor is the transient channel receptor subfamily 5 and it is reported as the receptor of capsaicin and vanilloid; nonselective cation channels became active by a wide diversity of exogeneity and endogeneity for physicochemical stimuli [1]. The representative regulators of TRPV1 are temperature, pH, and capsaicin, and its activation produced a painful and burning sensation. This receptor is responsible for the transmission or regulation of pain as well as the recognition of a variety of pain stimuli [2]. Various chemicals have a pharmacological effect by targeting this receptor, which is due to architectural resemblance with other ligand gate ion channel. This receptor has a three-dimensional structure that resembles voltage dependent ion channel very much because the membrane protein fragments 5 and 6 form ionic channels and act as pore region [3]. These center pores are enclosed by four different continuous domains, which act as voltage detectors during channel opening [4]. The common structural rearrangement of TRPs or voltage-gated ion channels are unknown, despite these structural similarities.

Schisandra chinensis is a traditional herbal medicine and spread out all around the world and cultivated in Far Eastern countries [5]. Recent studies have shown administration of *Schisandra chinensis* to have numerous beneficial medical effects, for example, as a neuroprotectant, on the significant heath progress of immune system and cardiovascular system. The lignans, schisandrin, and gomisins were chemical constituents of *Schisandra chinensis* [6]. In traditional medicine, the fruit of *Schisandra chinensis* is believed to treat diarrhea and lack of energy, arrests excessive sweating, refreshes the heart and kidneys, creates fluids, and reduces thirst [5]. *Schisandra* elevated physical durability and provides stress protection for a wide range of injurious factors including thermal shock, scalding, frostbite, and immobilization [5, 7]. *Schisandra chinensis* affects the immune system as well as nervous and gastrointestinal system [8–12]. *Schisandra*

chinensis contains bioactive compounds such as the gomisin derivatives and their related compounds. Recent studies reported many other lignans from the *Schisandra chinensis* and they showed the various biological regulatory effects. *Schisandra chinensis* is generally treated for a folk remedy use, but its concrete mechanisms in the physicochemical and pharmacological effects are not known in cell level.

The regulatory action of gomisin A on the TRPV1 receptor channel was examined in this study. Although *Schisandra chinensis* is used in folk remedy, it is not known if the folk usage is engaged in regulatory effects of ligand gated ion channels. Accordingly, TRPV1 receptor channel cRNAs were injected into *Xenopus* oocytes, and the regulatory action of gomisin A on the capsaicin-induced currents was examined. It was found that cotreatment of gomisin A attenuates the capsaicin-elicited, inward peak currents in reversible, voltage insensitive, concentration dependent, and noncompetitive manner.

2. Materials and Methods

2.1. Materials. Gomisin A was purchased from Wuhan ChemFac Biochemical (Hubei, China). Stock solutions of gomisin A of 100 mM concentration were prepared using DMSO. The plasmid DNA encoding the human TrpV1 receptor was obtained from OriGene. Other reagents were treated from Sigma-Aldrich or used as supplied, unless otherwise stated.

2.2. Preparation of X. laevis Oocytes and Mutagenesis of TRPV1 Receptors. The treatment of oocytes and mutagenesis were described in previous study [13]. Briefly, frogs caring procedures were followed by the Jonnam National University animal caring institute guidelines (JNU IACUC-YB-2017-07, July 2017). The removed oocyte from *X. laevis* was collagenized with rocking for 2 hrs in bath solution. The matured oocytes were selected and incubated in ND96 buffer with antibiotics. The introduction of complementary RNAs into the vegetable or animal pole of single cells was carried out using a microinjector. Oocyte recording experiments were tried out after 48 hrs for each expressed oocyte. The TRPV1 mutants were made by MAX-QuikChange mutagenesis protocol with Pfu DNA polymerase and desired mutation primers.

2.3. Molecular Docking Studies. The docking studies were investigated on Intel i7, PC with 16 GB RAM running the Windows 8 operating system, using AutoDock Tools (version 1.5) by the Scripps Institute. The protein structure of TRPV1 receptors was obtained from the Protein Data Bank (ID code 3J5P), and the 3D structure of the ligand (gomisin A) was obtained from Pubchem. The protein-ligand complex was programmed using AutoDock Tools and considered with minimized binding energy, inhibition constant, and intermolecular energy. The complex was analyzed using Ligplot (ver. 4.5.3) by EMBL-EBI and Pymol (ver. 1.8.4.2) by Schrödinger. Ligplot showed interactions between the protein and the ligand. Pymol was used to measure the distance between the complex and mutagenesis of amino acids of TRPV1 receptors.

2.4. Data Recording. The single cells were put in flowing buffer bath (The Warner Instruments) and flowed by ND96 medium at 1 ml/min. Each single oocyte was then penetrated with two thin electrodes filled with electrolyte solution. The microelectrodes resistance was from 0.5 to 0.8 MΩ. The electrophysiological experiment was performed at RT with Oocyte Clamp Amplifier and data collection was performed using Digidata 1320 and pClamp 9 (Molecular Devices, CA). For this study, the holding potential was clamped on −80 mV in each cell. The ramp experiments of the currents voltages relationship were shed from −80 to +60 mV of experiments of TRPV1 receptors current. Stock solution of 250 mM of gomisin A and used chemical compounds were prepared with DMSO and then they were diluted to each low concentration for actual use with ND96 bath buffer.

2.5. Data Analysis. The data analysis was described in previous study [13]. To acquire dose dependent curves for the effects of gomisin A on capsaicin-induced current, the induced peak currents at each gomisin A concentration were plotted using the Hill equation. A significance among the mean of the application values was measured using two-way ANOVA with Tukey tests of Origin pro 7.0 statistic software.

3. Results

3.1. Effect of Gomisin A on Control Oocytes and Oocytes Expressing Human TRPV1. Initially, the two microelectrode voltage clamping methods were adapted to study the regulatory action of gomisin A on the oocytes that had been injected with 40 nl H_2O (the control). Injection of capsaicin (1 μM) or gomisin A (10 μM) into oocytes did not result in any inward peak current. Coapplication of 1 μM capsaicin and 10 μM gomisin A also did not result in an inward current (data not shown). Then, the regulatory action of gomisin A against inward current was mediated by human TRPV1 receptor channel at membrane voltage potential as −80 mV. The treatment of 1 μM capsaicin stimulated an inward current, and gomisin A (100 μM) had no effect on currents of human TRPV1 receptor. Cotreatment of capsaicin (1 μM) and capsazepine (10 μM), a TRPV1 receptor channel antagonist, blocked the capsaicin-stimulated inward current, showing that expressed TRPV1 receptors were functionally operated in this experiment (Figure 1(b)).

3.2. Effect of Gomisin A on Capsaicin-Elicited Inward Peak Currents in Oocytes Expressing Human TRPV1 Receptor Channel. Next, the regulatory action of gomisin A on capsaicin-induced inward current arbitrated by human TRPV1 receptor channel was evaluated in a reversible manner. Coapplication of the oocytes with gomisin A (100 μM) with 1 μM capsaicin blocked the capsaicin-mediated current (Figures 1(c) and 1(d); n = 9–10 from nine different frogs). The percent inhibitory effect by gomisin A was 46.5 ± 4.5%. The preapplication of gomisin A was 48.2 ± 7.2%, showing that either

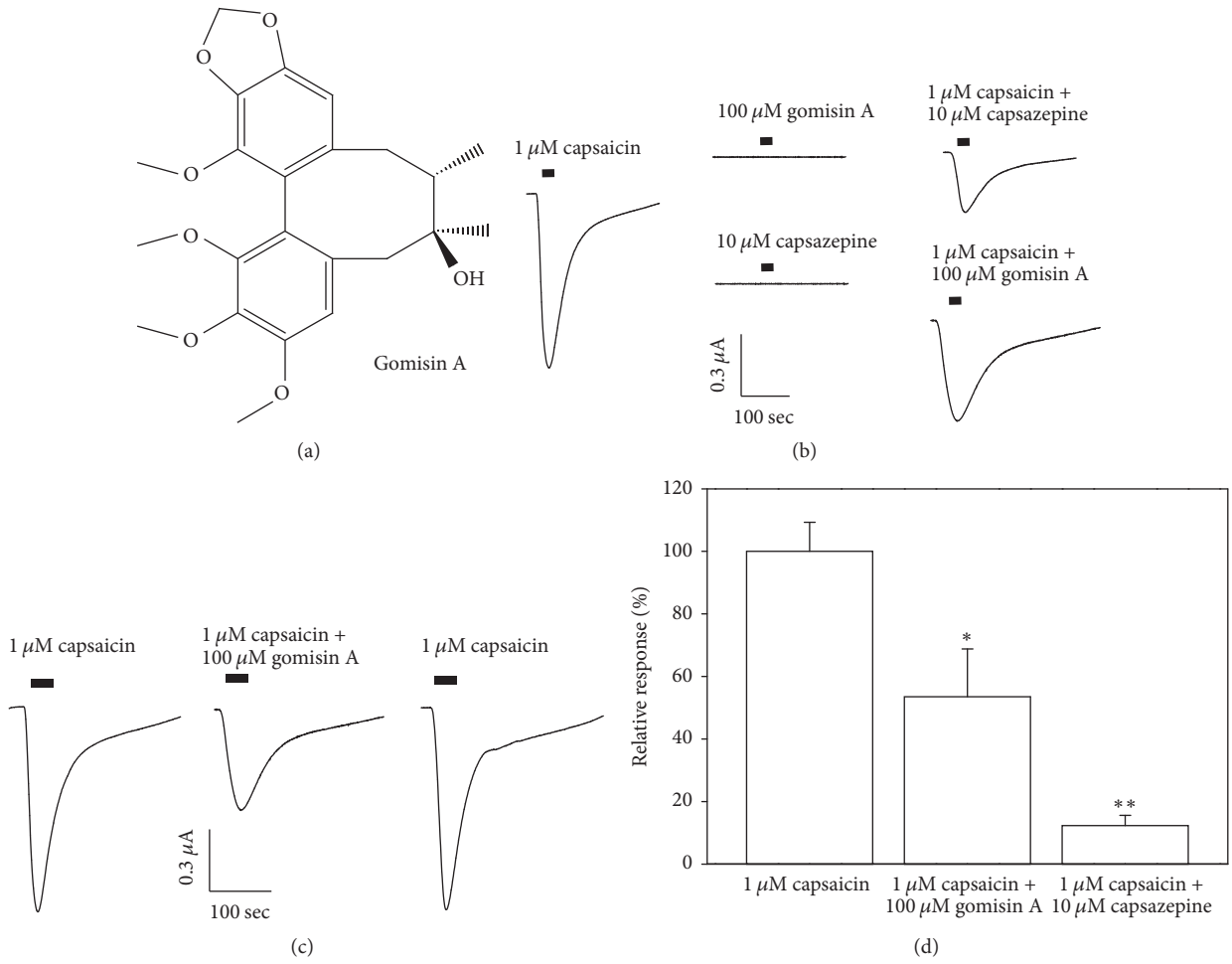

Figure 1: Effect of gomisin A on control oocytes or oocytes expressing human TRPV1 receptor channel. (a) Chemical structure of gomisin A. (b) Application of capsaicin (1 μM) stimulated an inward current, whereas gomisin A (100 μM) alone had no effect on oocytes expressing human TRPV1 receptor channel at a holding potential of −80 mV. Cotreatment of capsaicin (1 μM) and capsazepine (10 μM), which the respective TRPV1 receptor channel antagonist that blocked capsaicin-stimulated inward current, indicated that these receptors were functionally expressed in the experiment. (c) The effect of gomisin A on the capsaicin-stimulated inward current mediated by human TRPV1 receptor channel expressed in *Xenopus* oocytes. The coapplication of the oocytes with gomisin A (100 μM) with 1 μM capsaicin inhibited the capsaicin-induced inward current in a reversible manner (n = 9–12 from four different frogs). (d) The percent inhibition was 46.5 ± 4.5% and 79.5 ± 4.5% by 100 μM gomisin A and 10 μM capsazepine. The preapplication of gomisin A was 48.2 ± 7.2%, indication that either coapplication or preapplication causes the same extent of inhibition (data not shown). $^{*}p < 0.05$, $^{**}p < 0.005$ compared with response of capsaicin.

coapplication or preapplication resulted in the same degree of inhibition (data not shown).

3.3. Current–Voltage Relationship and Concentration Dependency of the Capsaicin-Stimulated Inward Current in Response on Gomisin A Induced Inhibitory Effects. In further experimental process, we evaluate the mechanism by which gomisin A inhibited capsaicin-induced current of human TRPV1 receptor channel. The current–voltage relationship elicited by only 1 μM capsaicin or by 1 μM capsaicin plus gomisin A (100 μM) was measured. These responses to treatment were then checked by holding membrane voltage potential as −80 mV and then increasing it from −100 to +80 mV on intensity of 1 sec (Figure 2(a)). The reversal membrane voltage potential of capsaicin-induced inward current was negative voltage near −10 mV. Coapplication of gomisin A with capsaicin blocked both inward (minus currents area) and outward (plus currents area) currents smaller than those induced by only capsaicin treatment. The inhibition of gomisin A on capsaicin-induced inward current was voltage insensitive. Gomisin A inhibited the capsaicin-induced inward current by 71.1 ± 16.2% at −100 mV and 42.6 ± 11.2% at + 80 mV (n = 7–9 from three different frogs). Concentration response tests elicited that coapplication with capsaicin plus different concentrations of gomisin A inhibited the capsaicin-stimulated inward peak current in human TRPV1 receptor (Figure 2(b)). The IC_{50} values were 62.1 ± 3.7 μM for capsaicin-stimulated inward current. Hill coefficients were 1.9 ± 0.1 for the capsaicin-induced inward current (n = 8–12 from five different baths). It indicates that gomisin A

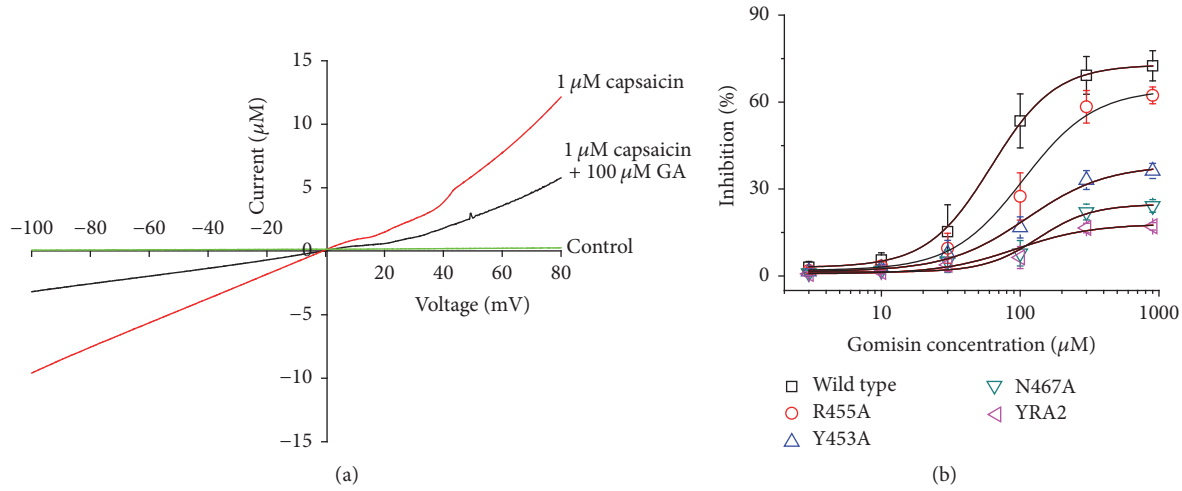

Figure 2: The voltage-dependency and concentration dependency of gomisin A on capsaicin-stimulated inward current in oocytes expressing human TRPV1 receptor channel. (a) The representative current–voltage relationship was obtained using 1 sec duration voltage ramps from −100 to +80 mV, at a holding potential of −80 mV. Voltage steps were applied before and after the application of capsaicin in the presence or absence of gomisin A (100 μM). (b) The capsaicin-induced inward current in oocytes was elicited at a holding potential of −80 mV for the indicated time, in the presence of 1 μM capsaicin, after which the indicated concentrations of gomisin A were coapplied with capsaicin. Concentration response curves for the effect of gomisin A on oocytes expressing the TRPV1 receptor. The percentage inhibition by gomisin A was calculated based on the average of the peak inward current elicited by capsaicin and that of the peak inward current elicited by capsaicin plus gomisin A. Each point represents the mean ± SEM (n = 7–12/group).

inhibits the capsaicin-stimulated inward current in a voltage insensitive and concentration dependent way.

3.4. Dock Modeling of TRPV1 and Gomisin A. To analyze the possible interaction way in gomisin A and TRPV1 channel, our team used wild type and mutant covalent docking homology modeling (Figure 3). The best-fit docking results showed gomisin A to form strong H bonds with wild type TRPV1, but not with mutants (Figure 4). The Y453, Y454, R455, and N467 residues in each subunit were assigned as the active site amino acid and it was set as 5 Å from those. Molecular docking revealed that gomisin A could fit into this pocket, interacting with previously unidentified residues, notably the positively charged amino acids from TRPV1 and hydroxyl group of gomisin A. In Figure 4(c), segment 1 or 2 of each TRPV1 subunits interacted with gomisin A, where each Y453 residue interacts with gomisin A (distance = 3.9 Å), Y454 (3.2 Å), R455 (3.5 Å), and N467 (3.4 Å).

3.5. Site-Directed Mutagenesis Study of TRPV1 and Gomisin A. To confirm the activity of each residue, the ability of gomisin A to regulate the current of a TRPV1 mutant in which each residue was replaced by an alanine residue was tested. The inhibitory effects of gomisin A on each of mutant channels is shown in Figure 2(b) and Table 1. The Y453A or N467A mutant showed significant attenuation of the inhibitory effects of gomisin A; the double mutation (YRA2) to alanine reduced the activity by 75.4%; the V_{max} value was reduced from 72.9 ± 1.0 to 17.9 ± 6.5; and the n value changed from 1.9 to 1.2. It indicates that gomisin A-mediated regulatory effects of TRPV1 channel activity were very closely associated with the Y453A or N467A residues.

Table 1: Effects of gomisin A on mutant TRPV1 receptor channel.

	Vmax	IC_{50}	n
Wild type	72.9 ± 1.0	62.1 ± 3.7	1.9 ± 0.1
A452Y	79.2 ± 3.1	94.7 ± 12.3	2.2 ± 0.8
Y453A	38.3 ± 2.4	111.6 ± 19.5	1.2 ± 0.5
Y454A	59.2 ± 3.0	94.7 ± 9.5	2.2 ± 0.8
R455A	64.4 ± 2.6	82.5 ± 8.2	1.7 ± 0.6
V456A	91.5 ± 2.6	72.2 ± 9.2	1.8 ± 0.8
L465A	68.3 ± 3.5	78.2 ± 4.6	1.8 ± 0.3
K466A	64.7 ± 2.1	81.5 ± 5.9	2.3 ± 0.5
N467A	24.7 ± 2.0	134.7 ± 12.5	1.3 ± 0.5
T468A	67.9 ± 1.5	94.3 ± 8.2	1.6 ± 0.5
V469A	72.5 ± 5.6	82.5 ± 12.5	2.1 ± 0.7
YNA2	17.9 ± 6.5	193.9 ± 33.5	1.2 ± 1.5

Values represent the means ± SEM (n = 7–12/group). Currents were elicited at a holding potential of −80 mV. IC_{50} (μM), V_{max}, and Hill coefficient values were determined as described in Materials and Methods.

4. Discussion

We demonstrated that gomisin A can regulate human TRPV1 receptor channel activity in *Xenopus* oocytes in the present report. Three pieces of hypothetical reasoning to support these conclusions were obtained. Firstly, gomisin A was found to impart a reversible, inhibitory effect (Figure 1) on TRPV1 activity. Secondly, gomisin A inhibited a capsaicin-induced inward current in TRPV1, in a concentration dependent way, and the inhibition of capsaicin-induced inward current by gomisin A occurred in a voltage insensitive way (Figure 2). Thirdly, in an in silico study, gomisin A interacted

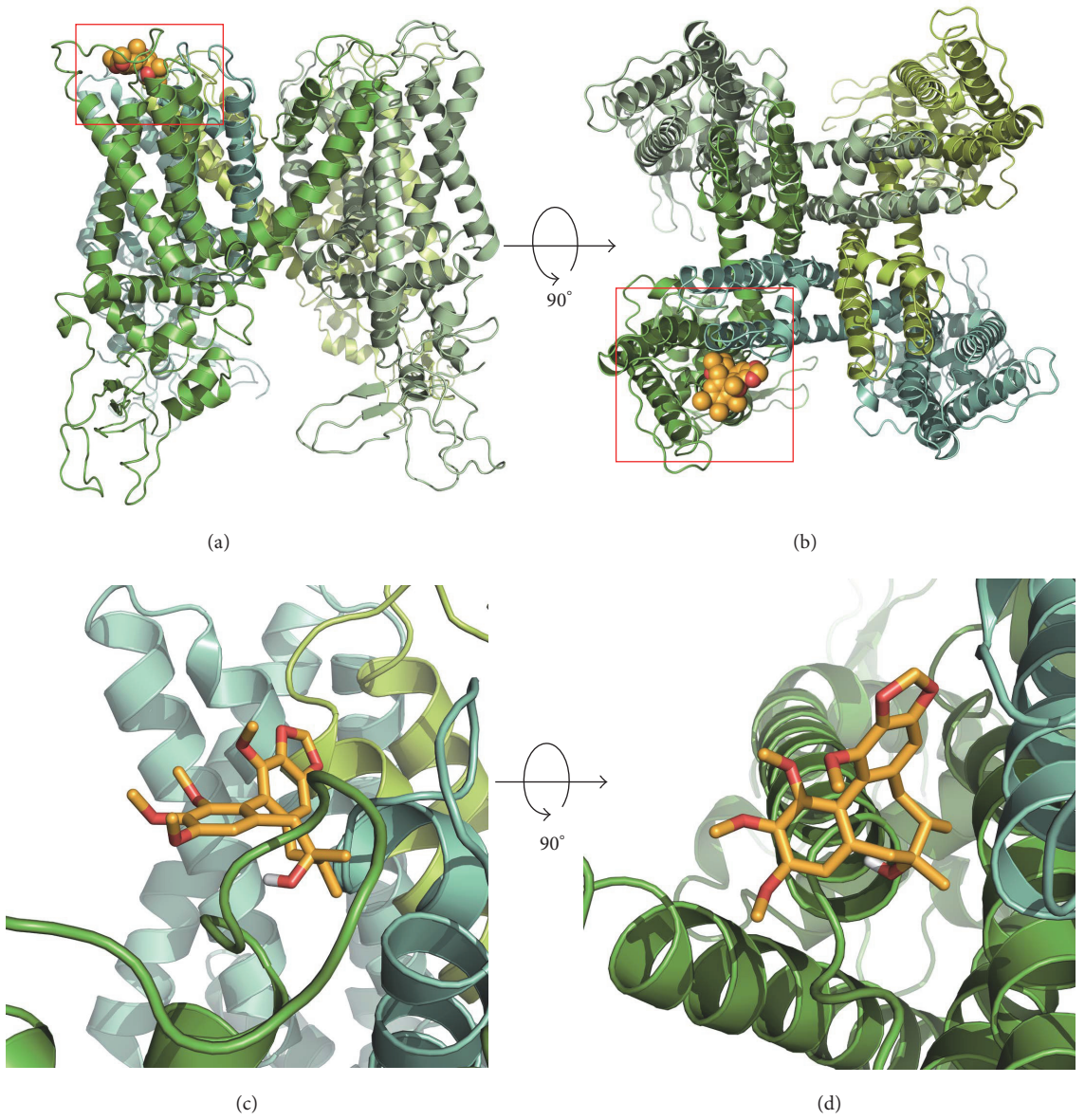

Figure 3: Computational molecular modeling of gomisin A docked to TRPV1 channel. (a and c) Side views of the docked gomisin A in complex with TRPV1 channel and (b and d) top views of docking model.

predominantly with residues at cavities in the segments 1 and 2 of each subunit of TRPV1 channel. This pocket indicated four potential binding sites, and mutants of Y453A or N467A showed significantly reduced activity of gomisin A on currents of TRPV1 channel.

Schisandra chinensis contained gomisin derivatives, and the berries were associated with the five flavors such as sweet, sour, bitter, astringent, and salty. Thus, the taste of acidic and salty were known hepatoprotective effects, while the bitter and puckery tastes have curative effects on the cardiovascular system, and the sweet flavor has a curative effect on the gastric system [5, 7]. Specifically, *Schisandra chinensis* has protective effects on cold stress-induced malondialdehyde in hepatic system [14, 15] and antioxidant activity [16], hepatic protective [5, 17–19], myocardial protective [17, 20], antitumor [21–23], antivirus [24], and anti-inflammatory [25] actions. In neuronal system, gomisin A was shown to reverse scopolamine-induced cognitive impairments in rodents [26, 27]. The beneficial facts of *Schisandra chinensis* suggest that gomisin derivatives can be treated on memory impairment and the protective effects as medications are intermediated by protective improvement of nerve system.

As mentioned previously, capsaicin evokes the sensation of burning pain and hyperalgesia when applied subcutaneously or intradermally [3, 28]. These effects are mediated predominantly by the action of capsaicin at primary nociceptive afferent neurons [29, 30]. The enhancement of capsaicin-stimulated currents in peripheral sensory-neurons

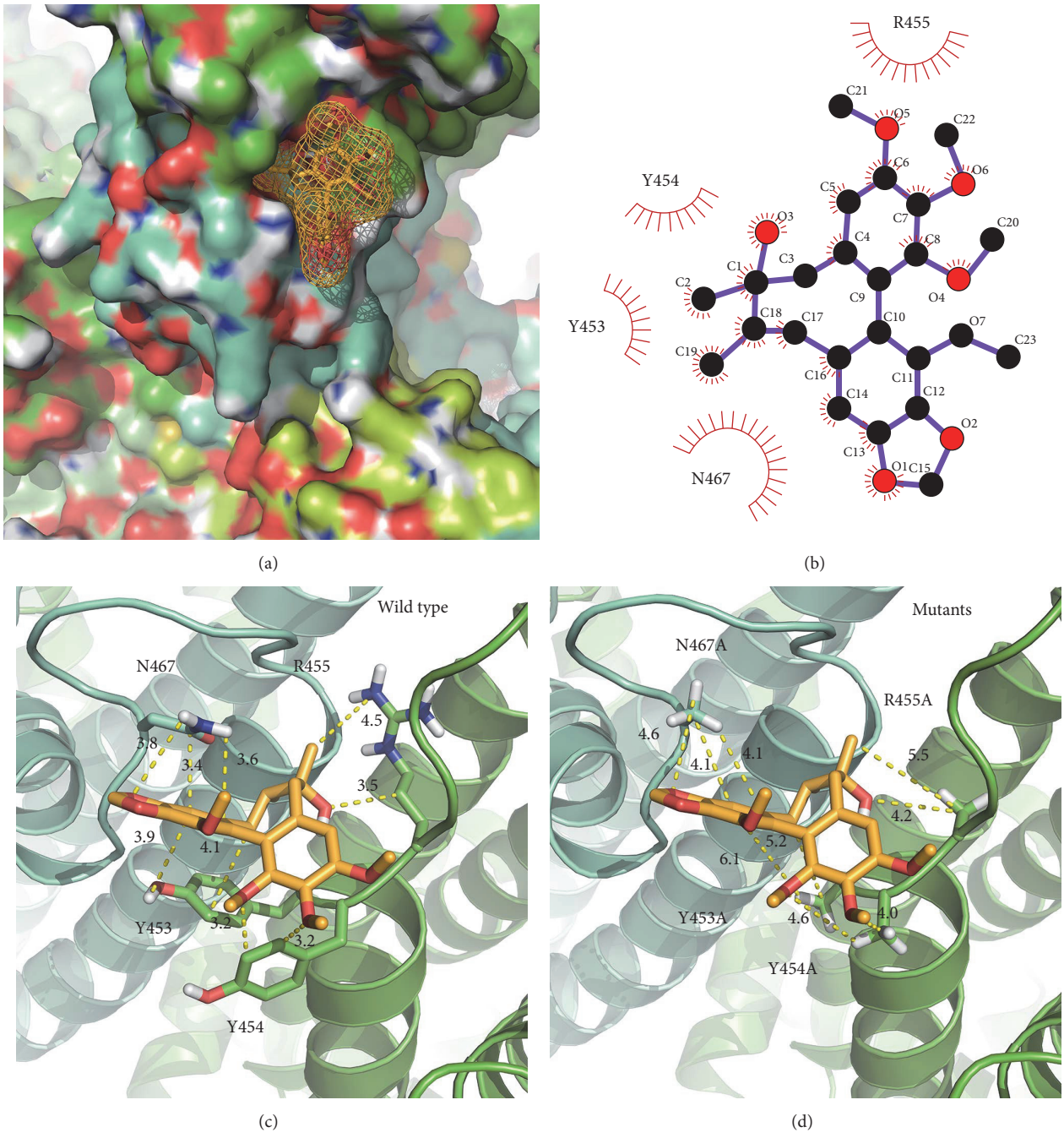

FIGURE 4: The binding pocket and docking results of gomisin A and TRPV1 channel. (a) Gomisin A located in binding pocket in extracellular area between segments 1 and 2 of TRPV1 channel. (b) 2D schematic presentation of the predicted binding mode of gomisin A in the ligand binding pocket. The ligands and important residues are shown. (c and d) Binding interface and gomisin A of the wild type (c) and the four mutant channels, whose mutations disturb the interaction with gomisin A to varying degrees.

usually results in the release of more pain-causing neurotransmitters. Previous reports showing the neuroprotective effect of gomisin A, and its capacity to attenuate neuronal related behavior induced by capsaicin treatment, are more likely to be due to their interaction at the sites of the central nervous system. Moreover, *Schisandra chinensis* can recover hypersensitive stomach ache induced by intestine 5-HT pathway in rats [31]. However, the present results do not inform how the *in vitro* improvement of capsaicin-stimulated currents by gomisin A relates to the *in vivo* inhibition of the capsaicin-stimulated, agony related behavior. One possibility is that gomisin A might interact with the TRPV1 receptor at the spinal level. Thus, *in vivo* administration of gomisin A at the central nervous system prior to administration of capsaicin might positively exert an effect on TRPV1 receptor channel activity.

Many previous reports show that various agents regulate ligand gated-ion channels expressed in *Xenopus* oocytes [32, 33]. These results indicate that gomisin A may play a role in regulation of neurotransmitter release or excitable neuron induced by TRPV1 receptor channel activation. In addition, our research results show that gomisin A can be used as a therapeutic medication for the relief TRPV1 receptor channel-related clinical symptoms.

In conclusion, we have shown that gomisin A inhibits capsaicin-induced inward current by interacting with segments 1 and 2 of the TRPV1 receptor channel. These inhibitory effects of gomisin A on the agonist gated-gated ion channel may explain some of its pharmacological effects.

Conflicts of Interest

The authors declare no conflicts of interest.

Authors' Contributions

Sung Bae Lee and Shinhwa Noh contributed equally to this work.

Acknowledgments

This work was supported by Korea Institute of Planning and Evaluation for Technology in Food, Agriculture, Forestry and Fisheries (IPET) through High Value-added Food Technology Development Program, funded by Ministry of Agriculture, Food and Rural Affairs (MAFRA) (116006–2).

References

[1] A. E. Chávez, C. Q. Chiu, and P. E. Castillo, "TRPV1 activation by endogenous anandamide triggers postsynaptic long-term depression in dentate gyrus," *Nature Neuroscience*, vol. 13, no. 12, pp. 1511–1518, 2010.

[2] C.-K. Park, N. Lü, Z.-Z. Xu, T. Liu, C. N. Serhan, and R.-R. Ji, "Resolving TRPV1- and TNF-α-mediated spinal cord synaptic plasticity and inflammatory pain with neuroprotectin D1," *The Journal of Neuroscience*, vol. 31, no. 42, pp. 15072–15085, 2011.

[3] E. Cao, M. Liao, Y. Cheng, and D. Julius, "TRPV1 structures in distinct conformations reveal activation mechanisms," *Nature*, vol. 504, no. 7478, pp. 113–118, 2013.

[4] W. A. Catterall, "Ion channel voltage sensors: Structure, function, and pathophysiology," *Neuron*, vol. 67, no. 6, pp. 915–928, 2010.

[5] A. Panossian and G. Wikman, "Pharmacology of *Schisandra chinensis* Bail.: an overview of Russian research and uses in medicine," *Journal of Ethnopharmacology*, vol. 118, no. 2, pp. 183–212, 2008.

[6] Y. Lu and D.-F. Chen, "Analysis of *Schisandra chinensis* and *Schisandra sphenanthera*," *Journal of Chromatography A*, vol. 1216, no. 11, pp. 1980–1990, 2009.

[7] J. N. Chun, M. Cho, I. So, and J.-H. Jeon, "The protective effects of Schisandra chinensis fruit extract and its lignans against cardiovascular disease: a review of the molecular mechanisms," *Fitoterapia*, vol. 97, pp. 224–233, 2014.

[8] X. Li, X. Fan, D. Li et al., "Schisandra sphenanthera extract facilitates liver regeneration after partial hepatectomy in mice," *Drug Metabolism and Disposition*, vol. 44, no. 5, pp. 647–652, 2016.

[9] H. Y. Kwan, X. Niu, W. Dai et al., "Lipidomic-based investigation into the regulatory effect of Schisandrin B on palmitic acid level in non-alcoholic steatotic livers," *Scientific Reports*, vol. 5, article 9114, 2015.

[10] V. V. Giridharan, R. A. Thandavarayan, S. Arumugam et al., "Schisandrin B ameliorates ICV-infused amyloid β induced oxidative stress and neuronal dysfunction through inhibiting RAGE/NF-κB/MAPK and Up-regulating HSP/beclin expression," *PLoS ONE*, vol. 10, no. 11, Article ID e0142483, 2015.

[11] T. Zhao, Y. Feng, J. Li et al., "*Schisandra* polysaccharide evokes immunomodulatory activity through TLR 4-mediated activation of macrophages," *International Journal of Biological Macromolecules*, vol. 65, pp. 33–40, 2014.

[12] C. Zhang, X. Mao, X. Zhao et al., "Gomisin N isolated from Schisandra chinensis augments pentobarbital-induced sleep behaviors through the modification of the serotonergic and GABAergic system," *Fitoterapia*, vol. 96, pp. 123–130, 2014.

[13] H. D. Yeom and J.-H. Lee, "Regulation of human Kv1.4 channel activity by the antidepressant metergoline," *Biological & Pharmaceutical Bulletin*, vol. 39, no. 6, pp. 1069–1072, 2016.

[14] A. V. Lupandin, "The general mechanism of body adaptation under the influence of polyphenol adaptogens," *Uspekhi Fizicheskikh Nauk*, vol. 22, no. 1, pp. 20–39, 1991.

[15] A. V. Lupandin, "The adaptation to extreme natural and technogenic factors in trained and untrained subjects under the influence of adaptogens," *Fiziologiia cheloveka*, vol. 16, no. 3, pp. 114–119, 1990.

[16] J.-H. Kim, Y.-W. Choi, C. Park et al., "Apoptosis induction of human leukemia U937 cells by gomisin N, a dibenzocyclooctadiene lignan, isolated from Schizandra chinensis Baill," *Food and Chemical Toxicology*, vol. 48, no. 3, pp. 807–813, 2010.

[17] G.-T. Liu, T.-M. Zhang, B.-E. Wang, and Y.-W. Wang, "Protective action of seven natural phenolic compounds against peroxidative damage to biomembranes," *Biochemical Pharmacology*, vol. 43, no. 2, pp. 147–152, 1992.

[18] M. Kim, S. J. Lim, H.-J. Lee, S. Y. Kim, and C. W. Nho, "Gomisin J Inhibits Oleic Acid-Induced Hepatic Lipogenesis by Activation of the AMPK-Dependent Pathway and Inhibition of the Hepatokine Fetuin-A in HepG2 Cells," *Journal of Agricultural and Food Chemistry*, vol. 63, no. 44, pp. 9729–9739, 2015.

[19] H. Teng and W. Y. Lee, "Antibacterial and antioxidant activities and chemical compositions of volatile oils extracted from Schisandra chinensis Baill. seeds using simultaneous distillation extraction method, and comparison with Soxhlet and microwave-assisted extraction," *Bioscience, Biotechnology, and Biochemistry*, vol. 78, no. 1, pp. 79–85, 2014.

[20] J. M. McCord, "Free radicals and myocardial ischemia: overview and outlook," *Free Radical Biology & Medicine*, vol. 4, no. 1, pp. 9–14, 1988.

[21] N.-H. Yim, A. Kim, Y. P. Jung, T. Kim, C. J. Ma, and J. Y. Ma, "Fermented So-Cheong-Ryong-Tang (FCY) induces apoptosis via the activation of caspases and the regulation of MAPK signaling pathways in cancer cells," *BMC Complementary and Alternative Medicine*, vol. 15, no. 1, article 336, 2015.

[22] X. Liu, C. Ni, C. Li, and T. Liu, "Drug-drug interation prediction between ketoconazole and anti-liver cancer drug gomisin G," *African Health Sciences*, vol. 15, no. 2, pp. 590–593, 2015.

[23] E. Casarin, S. Dall'Acqua, K. Šmejkal, T. Šlapetová, G. Innocenti, and M. Carrara, "Molecular mechanisms of antiproliferative

effects induced by Schisandra-derived dibenzocyclooctadiene lignans (+)-deoxyschisandrin and (-)-gomisin N in human tumour cell lines," *Fitoterapia*, vol. 98, pp. 241–247, 2014.

[24] R. Bai, X.-J. Zhang, Y.-L. Li et al., "SJP-L-5, a novel small-molecule compound, inhibits HIV-1 infection by blocking viral DNA nuclear entry Microbe-host interactions and microbial pathogenicity," *BMC Microbiology*, vol. 15, no. 1, article no. 274, 2015.

[25] X. Wang, D. Hu, L. Zhang et al., "Gomisin A inhibits lipopolysaccharide-induced inflammatory responses in N9 microglia via blocking the NF-κB/MAPKs pathway," *Food and Chemical Toxicology*, vol. 63, pp. 119–127, 2014.

[26] N. Egashira, K. Kurauchi, K. Iwasaki et al., "Schizandrin reverses memory impairment in rats," *Phytotherapy Research*, vol. 22, no. 1, pp. 49–52, 2008.

[27] D. H. Kim, T. M. Hung, K. H. Bae et al., "Gomisin A improves scopolamine-induced memory impairment in mice," *European Journal of Pharmacology*, vol. 542, no. 1-3, pp. 129–135, 2006.

[28] S. Bevan and J. Szolcsányi, "Sensory neuron-specific actions of capsaicin: mechanisms and applications," *Trends in Pharmacological Sciences*, vol. 11, no. 8, pp. 331–333, 1990.

[29] E. Cao, J. F. Cordero-Morales, B. Liu, F. Qin, and D. Julius, "TRPV1 channels are intrinsically heat sensitive and negatively regulated by phosphoinositide lipids," *Neuron*, vol. 77, no. 4, pp. 667–679, 2013.

[30] D. D. McKemy, W. M. Neuhausser, and D. Julius, "Identification of a cold receptor reveals a general role for TRP channels in thermosensation," *Nature*, vol. 416, no. 6876, pp. 52–58, 2002.

[31] J.-M. Yang, Y.-F. Xian, P. S. P. Ip et al., "Schisandra chinensis reverses visceral hypersensitivity in a neonatal-maternal separated rat model," *Phytomedicine*, vol. 19, no. 5, pp. 402–408, 2012.

[32] K. Sobczak, N. Bangel-Ruland, G. Leier, and W.-M. Weber, "Endogenous transport systems in the Xenopus laevis oocyte plasma membrane," *Methods*, vol. 51, no. 1, pp. 183–189, 2010.

[33] W.-M. Weber, "Ion currents of Xenopus laevis oocytes: State of the art," *Biochimica et Biophysica Acta (BBA) - Biomembranes*, vol. 1421, no. 2, pp. 213–233, 1999.

Hindawi
Evidence-Based Complementary and Alternative Medicine
Volume 2017, Article ID 1568702, 7 pages
https://doi.org/10.1155/2017/1568702

Research Article

EGHB010, a Standardized Extract of Paeoniae Radix and Glycyrrhizae Radix, Inhibits VEGF-Induced Tube Formation In Vitro and Retinal Vascular Leakage and Choroidal Neovascularization In Vivo

Eunsoo Jung,[1] Wookwon Jung,[2] Su-Bin Park,[2] Chan-Sik Kim,[3] Jin Sook Kim,[3] and Junghyun Kim[2,3]

[1]*Laboratory of Toxicology, Research Institute for Veterinary Science and College of Veterinary Medicine, Seoul National University, Seoul, Republic of Korea*
[2]*Department of Oral Pathology, School of Dentistry, Chonbuk National University, Jeonju 54896, Republic of Korea*
[3]*Korean Medicine Convergence Research Division, Korea Institute of Oriental Medicine, Daejeon, Republic of Korea*

Correspondence should be addressed to Junghyun Kim; dvmhyun@jbnu.ac.kr

Received 12 July 2017; Accepted 29 August 2017; Published 4 October 2017

Academic Editor: Lucindo Quintans

EGHB010 is a hot water extract of the rhizome mixture of *Paeonia lactiflora* Pallas and *Glycyrrhiza uralensis* Fisch. Choroidal neovascularization (CNV) and vascular leakage are the common pathophysiologies of age-related macular degeneration. In this study, we aimed to evaluate the effect of EGHB010 on retinal vascular leakage and laser-induced CNV in a rat model. Vascular endothelial growth factor- (VEGF-) induced tube formation was assayed in human retinal microvascular endothelial cells. Intravitreal VEGF-induced blood-retinal barrier breakdown was assayed in Sprague-Dawley rats. Experimental CNV was induced by laser photocoagulation in Brown Norway rats. EGHB010 (50 and 100 mg/kg/day) was administered orally for 10 days after laser photocoagulation. Choroidal flat mounts were prepared to measure the lesion size of CNV. Incubation of retinal vascular endothelial cells with EGHB010 (12.5 and 25 μg/mL) resulted in the inhibition of VEGF-induced tube formation in a dose-dependent manner. VEGF-mediated retinal vascular leakage was blocked by the oral administration of EGHB010. The CNV area was significantly lower in EGHB010-treated rats than in vehicle-treated rats. These results suggest that EGHB010 is a potent antiangiogenic agent. Thus, the oral administration of EGHB010 may have a beneficial effect in the treatment of vascular leakage and CNV in patients with age-related macular degeneration.

1. Introduction

Age-related macular degeneration (AMD) is the most common cause of vision loss in individuals older than 65 years [1]. Choroidal neovascularization (CNV) is a severe complication of AMD. AMD is classified into dry and wet forms. The dry form of AMD is characterized by the loss of retinal pigment epithelial cells and photoreceptors. The hallmark of wet or neovascular form of AMD is the growth of new vessels into the retina [2]. These newly formed vessels grow from the choroid through Bruch's membrane and lead to the formation of CNV in the subretinal pigment epithelium space. Diabetic retinopathy is a common complication of diabetes mellitus. Increased retinal vascular permeability caused by the breakdown of the blood-retinal barrier (BRB) results in diabetic macular edema, which is a major cause of vision loss in diabetic patients [3].

Vascular endothelial growth factor (VEGF) is a well-known proangiogenic and vascular permeability factor and a key mediator in the pathogenesis of wet AMD and diabetic retinopathy [4, 5]. Recently, the use of VEGF antagonists to inhibit VEGF signaling pathway has successfully diminished the formation of CNV in several experimental animal models [6] and human subjects [7]. In numerous clinical trials, intravitreally injected anti-VEGF agents, such as bevacizumab, ranibizumab, and aflibercept, notably suppressed

neovascularization and stabilized vision loss in patients with neovascular AMD [8–10] and improved retinal edema and vision in patients with diabetic macular edema [11]. However, the intravitreal injection of anti-VEGF agents poses the risk of drug-associated or postinjection-associated adverse events [12, 13]. Repeated intravitreal injection increased the incidence of ocular complications, including endophthalmitis, ocular inflammation, traumatic cataract, intraocular pressure elevation, retinal detachment, and vitreous hemorrhage [14]. Despite the benefits of intravitreal anti-VEGF drugs, interest in the use of oral drug candidates has been increasing [15–17].

Some natural and synthetic compounds have been proposed as antiangiogenic agents [18]. Generally, botanical products are often perceived as safe when compared to synthetic compounds. Therefore, there has been an increasing interest in the use of herbal products [19]. EGHB010 is a hot water extract of the rhizome mixture of *Paeonia lactiflora* Pallas and *Glycyrrhiza uralensis* Fisch. (ratio of 2 : 1), which is formulated based on a well-known traditional herbal formula Jakyakgamcho-tang (Shaoyao-gancao-tang in Chinese; Shakuyaku-kanzo-to in Japanese). This herbal formula has been used as an analgesic and antispasmodic agent [20]. However, the inhibitory effects of this herbal formula on neovascular AMD and diabetic retinopathy have not been reported. Therefore, in this study, we investigated the inhibitory effects of EGHB010 on subretinal neovascularization in a rat model of laser-induced CNV and VEGF-induced vascular leakage in a rat model of BRB breakdown. We also investigated the inhibitory effect of EGHB010 on the VEGF-induced tube formation of human retinal microvascular endothelial cells.

2. Materials and Methods

2.1. Preparation of EGHB010. Standardized EGHB010 was provided by EYEGENE Co. Ltd. (Seoul, Korea). Paeoniae radix and Glycyrrhizae radix were purchased from CK herb store (Boeun, Chungcheongbuk-do, Korea) and Gamcho Farming Association Corporation (Jecheon, Chungcheongbuk-do, Korea), respectively. For the preparation of EGHB010, 200 kg of Paeoniae radix and 100 kg of Glycyrrhizae radix were weighed accurately and mixed. Distilled water (3,000 L) was added to the mixed herbs and extracted at 90°C for 8 h. The extract solution was filtered and concentrated to obtain a 50 kg extract. The extract was then mixed with maltodextrin (120 kg) as a carrier and stirred to form an aqueous solution. Then, the resulting mixture was spray-dried and filtered through a 400-mesh sieve to give an extract powder of EGHB010 (140 kg). The contents of the major components in EGHB010 were determined by high-performance liquid chromatography (HPLC) analysis according to the previously reported method [21].

2.2. Cell Viability Assay. Cell viability was examined using an MTS assay kit (CellTiter 96 AQueous One Solution Cell Proliferation Assay, Promega, WI, USA). Human retinal microvascular endothelial cells (HRMECs, Cell Systems, WA, USA) were plated (1×10^4 cells/well) in quadruplicate into 96-well plates containing different doses of EGHB010 (0, 1, 5, 10, 25, 50, and 100 μg/mL). Cell viability was measured 24 h after incubation. The results of MTS assay were obtained by measuring absorbance using a microplate reader (Tecan, Männedorf, Switzerland) at 490 nm. All experiments were repeated three times.

2.3. Tube Formation Assay. Tissue culture plates (96 well) were coated with 400 μL of growth factor reduced basement membrane matrix (Matrigel, Becton Dickinson, NJ, USA). Human retinal microvascular endothelial cells (HRMECs, Cell Systems, WA, USA) were seeded at a density of 1×10^6 cells/well and treated with serum-free CSC complete medium (Cell Systems) containing recombinant human VEGF (20 ng/mL) and EGHB010 (0, 12.5, and 25 μg/mL) or ranibizumab (50 μg/mL), a positive control anti-VEGF agent, for 17 h at 37°C. Capillary-like tube structures formed by HRMECs on the Matrigel were photographed with a digital camera (DP71, Olympus, Tokyo, Japan). Tube formation was quantified by counting the branching points of capillary-like structures per visual field. The experiments were repeated three times independently.

2.4. Laser-Induced CNV in Rats. Eight-week-old male Brown Norway (BN) rats (SLC, Hamamatsu, Japan) were anesthetized with isoflurane, and the pupils were dilated with topical 0.5% tropicamide ophthalmic solution (Santen Pharmaceutical, Osaka, Japan). To induce CNV formation, four photocoagulation sites were generated using a diode laser (577 nm wavelength, 0.1 s duration, 100 μm spot size, 150 mW intensity, Oculight Slx, IRIS medical, CA, USA) between the retinal vessels equidistant from the optic nerve head in each eye. The formation of a subretinal bubble soon after laser treatment indicates the rupture of Bruch's membrane and induction of enough damage to form CNV. The rats were then divided into three groups of seven rats each as follows: (1) laser-induced CNV rats (CNV); (2) laser-induced CNV rats treated with EGHB010 (50 mg/kg body weight), and (3) laser-induced CNV rats treated with EGHB010 (100 mg/kg body weight). EGHB010 was dissolved in distilled water and orally administered for 10 days. The other group was given the same amount of vehicle gavage for 10 days. All procedures were approved by the Institutional Animal Care and Use Committee (IACUC Approval number 17-023).

2.5. Lectin Staining for CNV Size Analysis. At necropsy (10 days after laser treatment), all rats were sacrificed with CO_2, and eyecups were fixed in 4% paraformaldehyde for 2 h. The eyecups were dissected to remove the anterior segment and neural retina. The RPE-choroidal complex was then stained with Rhodamine-labeled *Bandeiraea simplicifolia* isolectin B4 (BSI-IB4, Vector Laboratories, CA, USA). The CNV areas labeled with lectin were examined using a fluorescence microscope (Olympus, Tokyo, Japan). The size of CNV was calculated using the ImageJ software (NIH, MD, USA).

2.6. VEGF-Induced Retinal Vascular Hyperpermeability in Rats. VEGF-induced breakdown of the blood-retinal barrier (BRB) was induced according to the published protocol with modifications [22]. Briefly, seven-week-old male Sprague-Dawley rats were purchased from Koatech (Pyeongtaek,

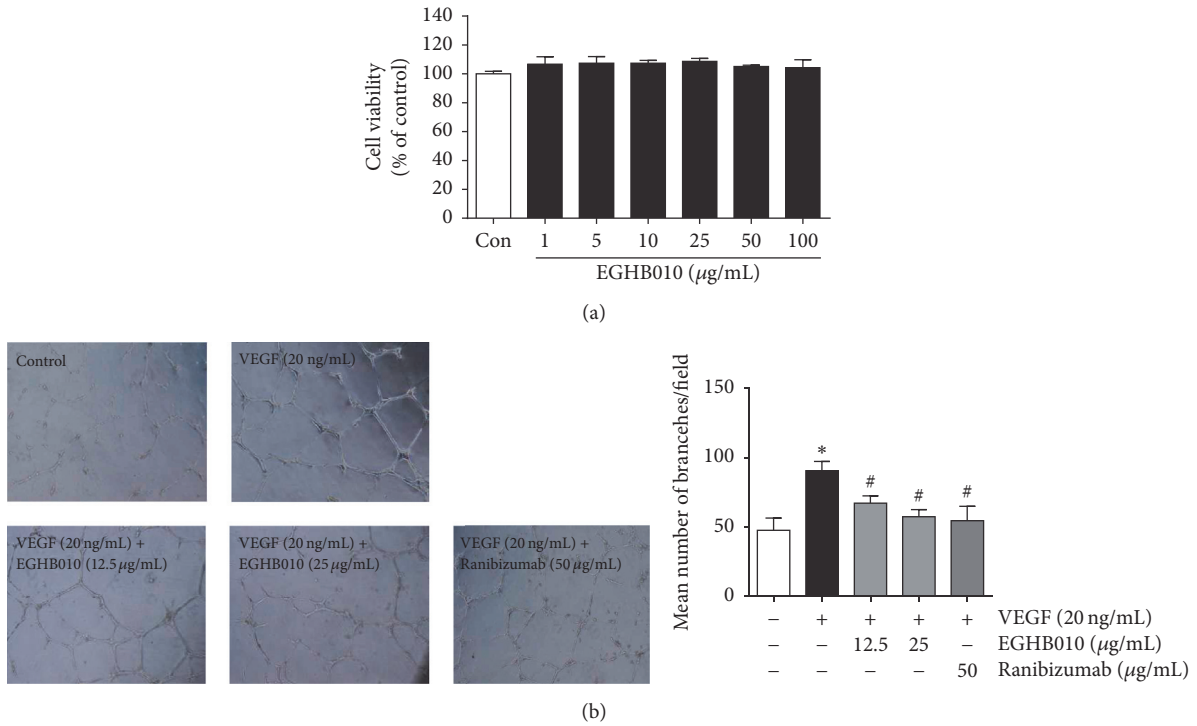

Figure 1: *EGHB010 inhibits tube formation in HRMECs*. (a) Effect of EHGB010 on the viability of HRMECs was determined by MTS assay. Data are expressed as percentage of control, $n = 4$. (b) HRMECs were treated with recombinant human VEGF (20 ng/mL) and EGHB010 (0, 12.5, and 25 μg/mL) or ranibizumab (50 μg/mL) for 17 h. Tube formation by HRMECs on Matrigel was observed with a microscope and quantified. Data are expressed as mean ± SEM, $n = 4$. $^{*}P < 0.01$ versus control; $^{\#}P < 0.01$ versus VEGF.

Korea). The rats were anesthetized with isoflurane and the pupils were dilated with 0.5% tropicamide (Santen Pharmaceutical, Osaka, Japan). Recombinant human VEGF (200 ng/1.0 μL) was injected into the vitreous cavity of one eye using a microinjector (Hamilton, Reno, NV, USA). An equal volume of vehicle (PBS with 0.1% BSA) was injected into the other eye. The rats were then divided into three groups of seven rats each as follows: (1) intravitreal VEGF-injected rats (VEGF); (2) intravitreal VEGF-injected rats treated with EGHB010 (50 mg/kg body weight); and (3) intravitreal VEGF-injected rats treated with EGHB010 (100 mg/kg body weight). The rats were given EGHB010 (50 and 100 mg/kg) or vehicle gavage once daily for 3 days after the intraocular injection of VEGF. At the end of the study, rats were anesthetized by isoflurane inhalation. The fluorescein-dextran microscopy was performed according to a method described previously [23]. Briefly, fluorescein-dextran (Sigma, St. Louis, MO, USA) in phosphate buffered saline (PBS) at a concentration of 50 mg/mL was injected into the left ventricle. The tracer dye was allowed to perfuse for 15 min and the eyeballs were then placed in 4% paraformaldehyde for 1.5 h. The fluorescein-dextran perfused retinas were dissected and flat-mounted on a microscope slide. The whole-mount retinas were observed by fluorescence microscopy (Olympus, Tokyo, Japan). Plasma was collected from rat blood before sacrifice followed by centrifugation. The concentration of fluorescein-dextran in plasma was determined with a fluorometer (Synergy™ HT, Bio-Tek, VT, USA). The fluorescence intensity was determined by ImageJ software (National Institutes of Health, Bethesda, MD, USA) and normalized to the plasma fluorescein-dextran levels for each rat.

Table 1: Paeoniflorin and glycyrrhizin content in EGHB010.

Compound	Content (mean ± SD, $n = 3$) mg/g
Paeoniflorin	15.00 ± 1.25
Glycyrrhizin	5.10 ± 0.20

2.7. Statistical Analysis. Group data were analyzed by one-way analysis of variance followed by Tukey's multiple comparison test or unpaired Student's t-test using GraphPad Prism 6.0 software (GraphPad, San Diego, CA, USA). Differences with a P value < 0.05 were considered statistically significant.

3. Results

3.1. HPLC Analysis of EGHB010. The contents of the major compounds in EGHB010 were determined by HPLC analysis. Paeoniflorin (15.0%) and glycyrrhizin (5.1%) were found to be the major components of EGHB010 (Table 1).

3.2. EGHB010 Inhibits VEGF-Induced Tube Formation in HRMECs. To investigate the cytotoxic effect of EGHB010 on HRMECs, we performed MTT assay with various concentrations of EGHB010 (1–100 μg/mL). The viability of EGHB010-treated HRMECs was not affected up to 100 μg/mL (Figure 1(a)). Next, we examined whether EGHB010 could

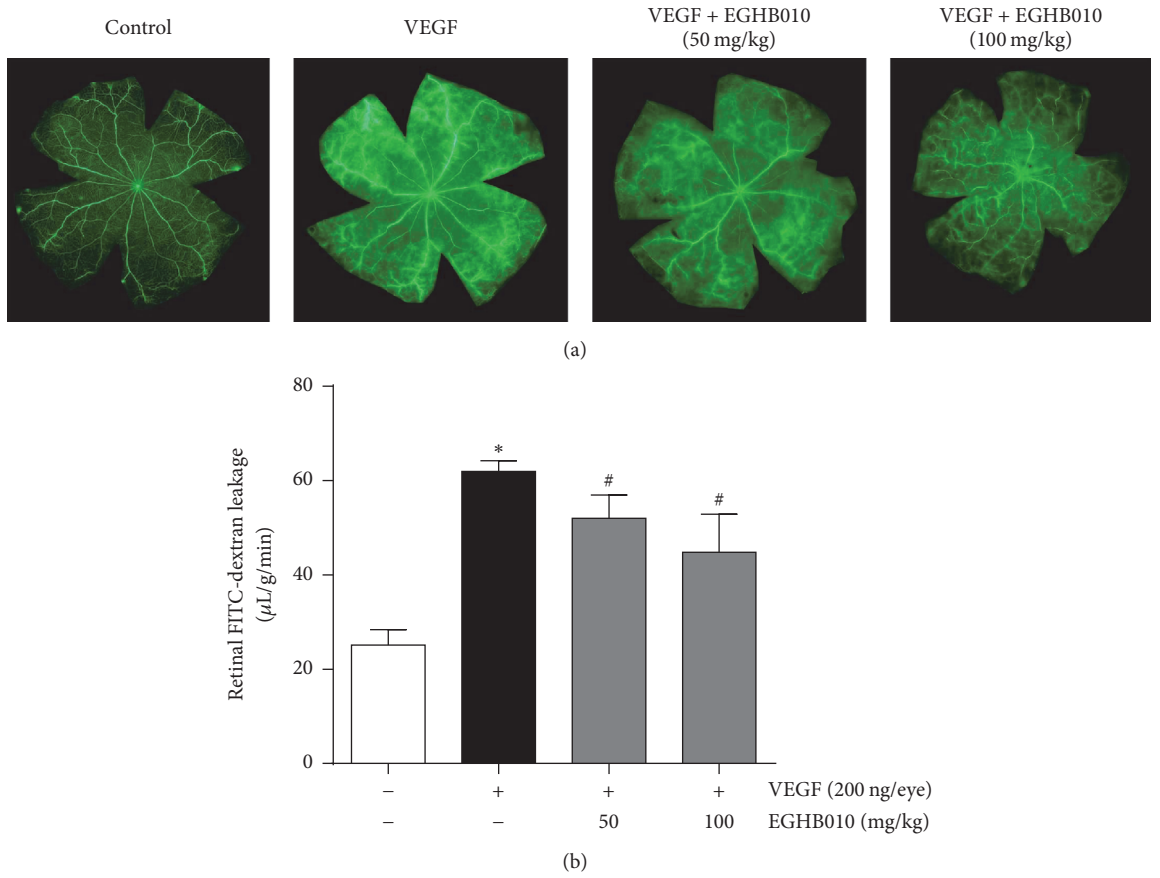

Figure 2: *EGHB010 inhibits VEGF-induced retinal vascular leakage*. (a) FITC-dextran angiography on retinal flat mounts. (b) Quantitative analysis of retinal vascular permeability. Values in the bar graphs represent the mean ± SEM, $n = 7$. $^{*}P < 0.05$ versus control rats; $^{\#}P < 0.05$ versus intravitreal VEGF-injected rats.

inhibit tube formation, an endothelial function crucial to angiogenesis, in HRMECs. VEGF was used as an angiogenic factor. HRMECs were significantly stimulated by VEGF and formed the capillary-like structures. However, EGHB010 treatment inhibited the formation of extensive capillary-like networks of HRMECs in a dose-dependent manner (Figure 1(b)). The inhibitory effect of EGHB010 on tube formation *in vitro* angiogenesis was similar to that of ranibizumab. These findings suggest that EGHB010 might inhibit VEGF-induced angiogenesis *in vitro*.

3.3. EGHB010 Inhibits VEGF-Induced Retinal Vascular Leakage. To examine VEGF-induced retinal vascular leakage *in vivo*, intravitreal injection of VEGF was administered and extravasation levels of fluorescein isothiocyanate- (FITC-) dextran were measured. The extravasation of tracer molecule was evident in rats treated with intravitreal VEGF. However, oral administration of EGHB010 ameliorated the angiographic features of VEGF-induced permeability (Figure 2).

3.4. EGHB010 Inhibits Laser-Induced CNV Formation. The rats subjected to laser photocoagulation showed CNV formation at the laser photocoagulation site. This newly formed CNV was visualized by immunofluorescence staining with isolectin B4. Oral administration of EGHB010 significantly inhibited CNV formation in the subretinal areas (Figure 3(a)). As shown in Figure 3(b), the rats in the two groups treated with EGHB010 exhibited a reduction of 21.6 ± 7.6 and 31.8 ± 5.6% in CNV formation, respectively. This result showed that EGHB010 treatment significantly reduced the size of CNV, indicating that EGHB010 has potent antiangiogenic activity.

4. Discussion

Pathogenic angiogenesis and vascular leakage are the two main causes of severe vision loss in wet AMD and diabetic retinopathy [24]. VEGF and its receptors play an important role in the development of AMD and diabetic macular edema [4]. Inhibiting angiogenesis and vascular leakage by targeting VEGF has become a major focus of drug development for AMD and diabetic macular edema [25]. In the present study, we aimed to evaluate the effect of EGHB010 on retinal vascular leakage and laser-induced CNV in the rat models. We demonstrated for the first time that EGHB010 inhibited tube formation in HRMECs *in vitro* and retinal vascular leakage *in vivo,* mediated by VEGF. In addition, EGHB010 significantly suppressed CNV formation in a rat model of experimental laser-induced CNV. Taken together, our results suggest that the inhibitory effect of EGHB010 on vascular

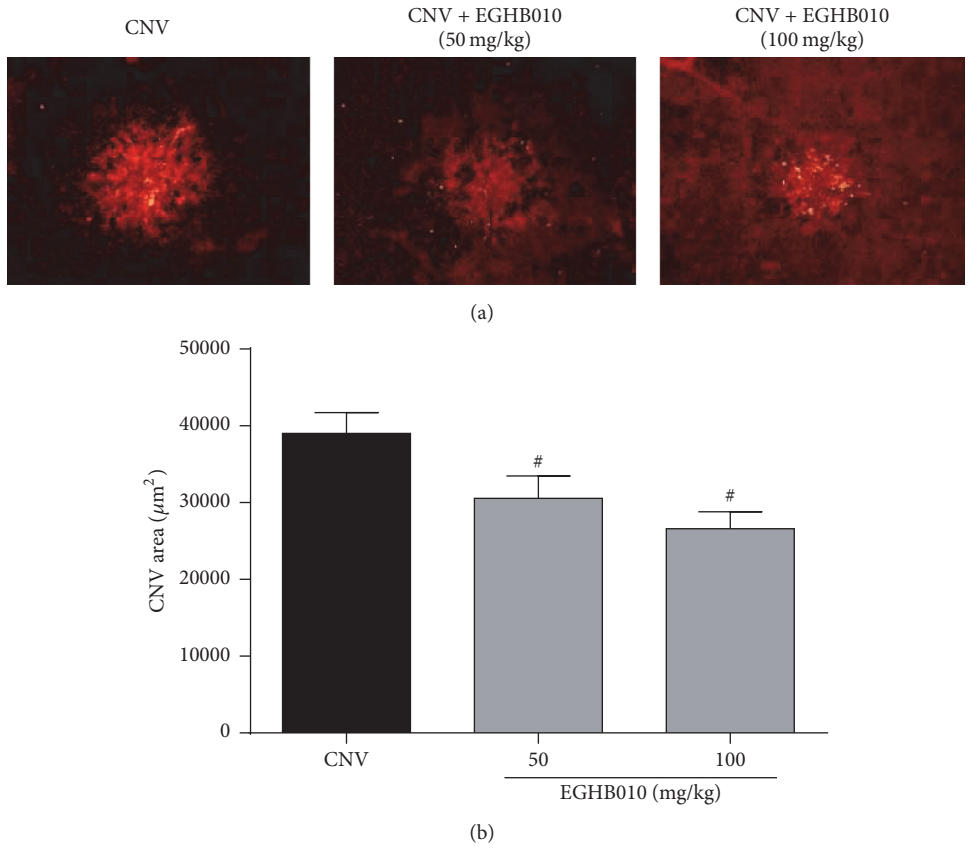

Figure 3: *EGHB010 inhibits laser-induced CNV formation*. (a) Choroidal flat mounts of laser-induced CNV. The CNV lesions were labeled with isolectin B4. (b) The areas of CNV lesions were measured in each group. The values in the bar graph represent the mean ± SEM, $n = 7$. $^{\#}P < 0.05$ versus CNV rats.

leakage and CNV formation is primarily via its potent anti-VEGF activity.

VEGF is a potent angiogenic and vascular permeability factor [26]. In the retina, elevated concentrations of VEGF correspond to BRB breakdown in animals [27] and humans [28]. Moreover, in neovascular AMD, the upregulation of proangiogenic molecules, such as VEGF, leads to the activation of angiogenic signal pathways and triggers CNV [29]. Numerous studies have suggested that VEGF plays a key role in retinal vasculopathy, and its inhibition significantly blocks the pathogenic alterations of retinal vasculature [30]. Recently, anti-VEGF agents have shown beneficial effects in patients with wet AMD [31].

Medicinal herbs are rich sources of potential preventive and therapeutic agents. EGHB010 is a standardized herbal extract, which is formulated based on a well-known traditional herbal medicine, and has an excellent safety record [32]. Our study for the first time showed the antiangiogenic effects of EGHB010 *in vitro* and *in vivo*. Several studies have reported that some crude herbal extracts and phytochemicals can inhibit pathogenic neovascularization in tumorigenesis [33, 34] and retinal neovascular diseases [35–38]. In traditional Korean medicine, Paeoniae radix has been used to nourish blood, regulate menstruation, and alleviate pain. The extract of Paeoniae radix has been confirmed as the main therapeutic component of the medicinal herb for rheumatoid arthritis [39–41]. Rheumatoid arthritis is considered to be an angiogenic disease, because synovium is rich in newly formed vessels. The overexpression of VEGF has been demonstrated in the synovium of patients with rheumatoid arthritis [42]. Furthermore, the treatment of Paeoniae radix results in a reduction of neovascularization and a reduced expression of angiogenic factors [39, 41]. Recently, Deng et al. demonstrated a direct antiangiogenic effect of Paeoniae radix on human vascular endothelial cells and chick embryo chorioallantoic membrane [43]. Glycyrrhizae radix has been used to stop cough and detoxify several toxic substances. Kobayashi et al. showed that Glycyrrhizae radix inhibited tube formation of vascular endothelial cells *in vitro* and adjuvant-induced granuloma angiogenesis *in vivo* [44]. These findings support our observation that EGHB010 inhibited tube formation of HRMEC *in vitro* and experimental vascular leakage and choroidal neovascularization *in vivo*.

In many traditional herbal medicines containing a mixture of medicinal herbs, additive and synergistic effects of phytochemicals present in the different herbs have been observed. Notably, a multiherb formula occasionally possesses additive or synergistic effects, and the pharmacological activity, toxicity, and dosage are altered by the addition of other herbs [45]. EGHB010 has been used to treat muscle

contraction and cramps. It was reported that this pharmacological effect of EGHB010 was only observed when Glycyrrhizae radix was mixed with Paeoniae radix [46]. EGHB010 contains two major compounds (paeoniflorin and glycyrrhizin). Paeoniflorin prevented oxidative stress-induced apoptosis in human RPE cells [47] and reduced VEGF levels in the synovium of rats with arthritis [48]. Glycyrrhizin inhibited neovascularization during tumor progression in mice [49]. Glycyrrhizin decreased VEGF production in rat retinal ganglion cells treated with advanced glycation end products [50]. In addition, glycyrrhizin has been known as a selective inhibitor of high-mobility group box-1, a potent proangiogenic molecule, and it attenuated ischemia-induced retinal neovascularization in a mouse model [51]. Although the detailed mechanism of action of EGHB010 as a VEGF inhibitor is still not clear, it is suggested that the antiangiogenic activity of EGHB010 may be due to the synergistic effects of paeoniflorin and glycyrrhizin.

In conclusion, this is the first study to provide evidence that EGHB010 inhibits experimental CNV formation and retinal vascular leakage. In addition, *in vitro* studies showed that EGHB010 treatment inhibited VEGF-induced tube formation in HRMECs. Further studies may be required to determine the feasibility of using EGHB010 in the treatment of human wet AMD and diabetic macular edema.

Conflicts of Interest

The authors declare that they have no conflicts of interest.

Acknowledgments

This research was supported by Korea Institute of Oriental Medicine (Grant no. K17810) and Korea Institute of Planning and Evaluation for Technology in Food, Agriculture, Forestry and Fisheries (IPET) through Agri-Bio Industry Technology Development Program, funded by Ministry of Agriculture, Food and Rural Affairs (Grant no. 116081-03-2-CG000).

References

[1] R. D. Jager, W. F. Mieler, and J. W. Miller, "Age-related macular degeneration," *The New England Journal of Medicine*, vol. 358, no. 24, pp. 2606–2617, 2008.

[2] N. Congdon, B. O'Colmain, and C. C. Klaver, "Causes and prevalence of visual impairment among adults in the United States," *Archives of Ophthalmology*, vol. 122, no. 4, pp. 477–485, 2004.

[3] S. E. Moss, R. Klein, and B. E. K. Klein, "The 14-year incidence of visual loss in a diabetic population," *Ophthalmology*, vol. 105, no. 6, pp. 998–1003, 1998.

[4] L. P. Aiello, "Vascular endothelial growth factor and the eye: Biochemical mechanisms of action and implications for novel therapies," *Ophthalmic Research*, vol. 29, no. 5, pp. 354–362, 1997.

[5] T. Qaum, Q. Xu, and A. M. Joussen, "VEGF-initiated blood-retinal barrier breakdown in early diabetes," *Investigative Ophthalmology & Visual Science*, vol. 42, no. 10, pp. 2408–2413, 2001.

[6] K. Muranaka, Y. Yanagi, Y. Tamaki et al., "Suppression of laser-induced choroidal neovascularization by oral administration of SA3443 in mice," *FEBS Letters*, vol. 579, no. 27, pp. 6084–6088, 2005.

[7] D. R. Guyer, G. Fish, J. A. Haller et al., "Anti-vascular endothelial growth factor therapy for subfoveal choroidal neovascularization secondary to age-related macular degeneration: Phase II study results," *Ophthalmology*, vol. 110, no. 5, pp. 979–986, 2003.

[8] J. E. Frampton, "Ranibizumab: a review of its use in the treatment of neovascular age-related macular degeneration," *Drugs and Aging*, vol. 30, no. 5, pp. 331–358, 2013.

[9] A. García-Layana, M. S. Figueroa, J. Araiz et al., "Treatment of Exudative Age-related Macular Degeneration: Focus on Aflibercept," *Drugs and Aging*, vol. 32, no. 10, pp. 797–807, 2015.

[10] C. Campa and S. P. Harding, "Anti-VEGF compounds in the treatment of neovascular age related macular degeneration," *Current Drug Targets*, vol. 12, no. 2, pp. 173–181, 2012.

[11] G. Virgili, M. Parravano, F. Menchini, and J. R. Evans, "Anti-vascular endothelial growth factor for diabetic macular oedema," *The Cochrane Database of Systematic Reviews*, no. 10, Article ID CD007419, 2014.

[12] T. Diago, C. A. McCannel, S. J. Bakri, J. S. Pulido, A. O. Edwards, and J. M. Pach, "Infectious endophthalmitis after intravitreal injection of antiangiogenic agents," *Retina*, vol. 29, no. 5, pp. 601–605, 2009.

[13] D. R. Fintak, G. K. Shah, K. J. Blinder et al., "Incidence of endophthalmitis related to intravitreal injection of bevacizumab and ranibizumab," *Retina*, vol. 28, no. 10, pp. 1395–1399, 2008.

[14] K. G. Falavarjani and Q. D. Nguyen, "Adverse events and complications associated with intravitreal injection of anti-VEGF agents: a review of literature," *Eye*, vol. 27, no. 7, pp. 787–794, 2013.

[15] H. Takahashi, Y. Tamaki, N. Ishii et al., "Identification of a novel vascular endothelial growth factor receptor 2 inhibitor and its effect for choroidal neovascularization in vivo," *Current Eye Research*, vol. 33, no. 11-12, pp. 1002–1010, 2008.

[16] S. Honda, T. Nagai, N. Kondo et al., "Therapeutic Effect of Oral Bisphosphonates on Choroidal Neovascularization in the Human Eye," *Journal of Ophthalmology*, vol. 2010, pp. 1–7, 2010.

[17] E. L. Meredith, N. Mainolfi, S. Poor et al., "Discovery of Oral VEGFR-2 Inhibitors with Prolonged Ocular Retention That Are Efficacious in Models of Wet Age-Related Macular Degeneration," *Journal of Medicinal Chemistry*, vol. 58, no. 23, pp. 9273–9285, 2015.

[18] T. Osawa and Y. Kato, "Protective role of antioxidative food factors in oxidative stress caused by hyperglycemia," *Annals of the New York Academy of Sciences*, vol. 1043, pp. 440–451, 2005.

[19] H.-S. Lee, S.-H. Jung, B.-S. Yun, and K.-W. Lee, "Isolation of chebulic acid from *Terminalia chebula* Retz. and its antioxidant effect in isolated rat hepatocytes," *Archives of Toxicology*, vol. 81, no. 3, pp. 211–218, 2007.

[20] J.-X. He, T. Akao, T. Nishino, and T. Tani, "The influence of commonly prescribed synthetic drugs for peptic ulcer on the pharmacokinetic fate of glycyrrhizin from Shaoyao-Gancao-tang," *Biological and Pharmaceutical Bulletin*, vol. 24, no. 12, pp. 1395–1399, 2001.

[21] J. Kim, C. S. Kim, Y. S. Kim, I. S. Lee, and J. S. Kim, "Jakyakgamcho-tang and Its Major Component, Paeonia Lactiflora, Exhibit Potent Anti-glycation Properties," *Journal of Exercise Nutrition Biochemistry*, vol. 20, no. 4, pp. 60–64, 2016.

[22] L. Scheppke, E. Aguilar, R. F. Gariano et al., "Retinal vascular permeability suppression by topical application of a novel

VEGFR2/Src kinase inhibitor in mice and rabbits," *The Journal of Clinical Investigation*, vol. 118, no. 6, pp. 2337–2346, 2008.

[23] E. Jung, J. Kim, C.-S. Kim, S.-H. Kim, and M.-H. Cho, "Gemigliptin, a dipeptidyl peptidase-4 inhibitor, inhibits retinal pericyte injury in db/db mice and retinal neovascularization in mice with ischemic retinopathy," *Biochimica et Biophysica Acta - Molecular Basis of Disease*, vol. 1852, no. 12, pp. 2618–2629, 2015.

[24] K. M. Gehrs, D. H. Anderson, L. V. Johnson, and G. S. Hageman, "Age-related macular degeneration—emerging pathogenetic and therapeutic concepts," *Annals of Medicine*, vol. 38, no. 7, pp. 450–471, 2006.

[25] P. Van Wijngaarden and S. H. Qureshi, "Inhibitors of vascular endothelial growth factor (VEGF) in the management of neovascular age-related macular degeneration: A review of current practice," *Clinical and Experimental Optometry*, vol. 91, no. 5, pp. 427–437, 2008.

[26] D. Shweiki, A. Itin, D. Soffer, and E. Keshet, "Vascular endothelial growth factor induced by hypoxia may mediate hypoxia-initiated angiogenesis," *Nature*, vol. 359, no. 6398, pp. 843–845, 1992.

[27] T. Murata, T. Ishibashi, A. Khalil, Y. Hata, H. Yoshikawa, and H. Inomata, "Vascular endothelial growth factor plays a role in hyperpermeability of diabetic retinal vessels," *Ophthalmic Research*, vol. 27, no. 1, pp. 48–52, 1995.

[28] S. A. Vinores, A. I. Youssri, J. D. Luna et al., "Upregulation of vascular endothelial growth factor in ischemic and non-ischemic human and experimental retinal disease," *Histology and Histopathology*, vol. 12, no. 1, pp. 99–109, 1997.

[29] A. Hoeben, B. Landuyt, M. S. Highley, H. Wildiers, A. T. van Oosterom, and E. A. de Bruijn, "Vascular endothelial growth factor and angiogenesis," *Pharmacological Reviews*, vol. 56, no. 4, pp. 549–580, 2004.

[30] T. N. Crawford, D. V. Alfaro III, J. B. Kerrison, and E. P. Jablon, "Diabetic retinopathy and angiogenesis," *Current Diabetes Reviews*, vol. 5, no. 1, pp. 8–13, 2009.

[31] P. A. Campochiaro, "Ocular neovascularization," *Journal of Molecular Medicine*, vol. 91, no. 3, pp. 311–321, 2013.

[32] C. Sadakane, J. Watanabe, M. Fukutake et al., "Pharmacokinetic profiles of active components after oral administration of a kampo medicine, shakuyakukanzoto, to healthy adult japanese volunteers," *Journal of Pharmaceutical Sciences*, vol. 11, pp. 3952–3959, 2015.

[33] I. M. W. Ruma, E. W. Putranto, E. Kondo et al., "Extract of *Cordyceps militaris* inhibits angiogenesis and suppresses tumor growth of human malignant melanoma cells," *International Journal of Oncology*, vol. 45, no. 1, pp. 209–218, 2014.

[34] D. R. Yance Jr. and S. M. Sagar, "Targeting angiogenesis with integrative cancer therapies," *Integrative Cancer Therapies*, vol. 5, no. 1, pp. 9–29, 2006.

[35] S. K. Gupta, B. Kumar, B. P. Srinivasan et al., "Retinoprotective effects of Moringa oleifera via antioxidant, anti-inflammatory, and anti-angiogenic mechanisms in streptozotocin-induced diabetic rats," *Journal of Ocular Pharmacology and Therapeutics*, vol. 29, no. 4, pp. 419–426, 2013.

[36] J. Tanaka, S. Nakamura, K. Tsuruma, M. Shimazawa, H. Shimoda, and H. Hara, "Purple Rice (Oryza sativa L.) extract and its constituents inhibit VEGF-induced angiogenesis," *Phytotherapy Research*, vol. 26, no. 2, pp. 214–222, 2012.

[37] J. Hua, K. I. Guerin, J. Chen et al., "Resveratrol inhibits pathologic retinal neovascularization in Vldlr(-/-) mice," *Investigative Ophthalmology & Visual Science*, vol. 52, no. 5, pp. 2809–2816, 2011.

[38] L. Cao, H. Liu, D. S.-C. Lam, G. H.-F. Yam, and C.-P. Pang, "In vitro screening for angiostatic potential of herbal chemicals," *Investigative Ophthalmology and Visual Science*, vol. 51, no. 12, pp. 6658–6664, 2010.

[39] L. Zhu, W. Wei, Y.-Q. Zheng, and X.-Y. Jia, "Effects and mechanisms of total glucosides of paeony on joint damage in rat collagen-induced arthritis," *Inflammation Research*, vol. 54, no. 5, pp. 211–220, 2005.

[40] Y.-Q. Zheng and W. Wei, "Total glucosides of paeony suppresses adjuvant arthritis in rats and intervenes cytokine-signaling between different types of synoviocytes," *International Immunopharmacology*, vol. 5, no. 10, pp. 1560–1573, 2005.

[41] Y. Chang, W. Wei, L. Zhang, and H.-M. Xu, "Effects and mechanisms of total glucosides of paeony on synoviocytes activities in rat collagen-induced arthritis," *Journal of Ethnopharmacology*, vol. 121, no. 1, pp. 43–48, 2009.

[42] Z. Szekanecz and A. E. Koch, "Mechanisms of disease: angiogenesis in inflammatory diseases," *Nature Clinical Practice Rheumatology*, vol. 3, no. 11, pp. 635–643, 2007.

[43] H. Deng, C. Yan, T. Xiao, D. Yuan, and J. Xu, "Total glucosides of Paeonia lactiflora Pall inhibit vascular endothelial growth factor-induced angiogenesis," *Journal of Ethnopharmacology*, vol. 127, no. 3, pp. 781–785, 2010.

[44] S. Kobayashi, T. Miyamoto, I. Kimura, and M. Kimura, "Inhibitory effect of isoliquiritin, a compound in licorice root, on angiogenesis in vivo and tube formation in vitro," *Biological and Pharmaceutical Bulletin*, vol. 18, no. 10, pp. 1382–1386, 1995.

[45] H.-J. Lee, E.-O. Lee, Y.-H. Rhee et al., "An oriental herbal cocktail, ka-mi-kae-kyuk-tang, exerts anti-cancer activities by targeting angiogenesis, apoptosis and metastasis," *Carcinogenesis*, vol. 27, no. 12, pp. 2455–2463, 2006.

[46] D. Bensky, S. Clavey, and E. Stoger, *Chinese Herbal Medicine: Materia Medica*, Eastland Press, Seatle, USA, 2004.

[47] X. Wankun, Y. Wenzhen, Z. Min et al., "Protective effect of paeoniflorin against oxidative stress in human retinal pigment epithelium in vitro," *Molecular Vision*, vol. 17, pp. 3512–3522, 2011.

[48] Y.-Q. Zheng, W. Wei, L. Zhu, and J.-X. Liu, "Effects and mechanisms of Paeoniflorin, a bioactive glucoside from paeony root, on adjuvant arthritis in rats," *Inflammation Research*, vol. 56, no. 5, pp. 182–188, 2007.

[49] K.-J. Kim, J.-S. Choi, K.-W. Kim, and J.-W. Jeong, "The anti-angiogenic activities of glycyrrhizic acid in tumor progression," *Phytotherapy Research*, vol. 27, no. 6, pp. 841–846, 2013.

[50] J.-J. Lee, C.-C. Hsiao, I.-H. Yang et al., "High-mobility group box 1 protein is implicated in advanced glycation end products-induced vascular endothelial growth factor a production in the rat retinal ganglion cell line RGC-5," *Molecular Vision*, vol. 18, pp. 838–850, 2012.

[51] Y. M. Lee, J. Kim, K. Jo et al., "Ethyl pyruvate inhibits retinal pathogenic neovascularization by downregulating HMGB1 expression," *Journal of Diabetes Research*, vol. 2013, Article ID 245271, 8 pages, 2013.

Hindawi
Evidence-Based Complementary and Alternative Medicine
Volume 2017, Article ID 9297808, 12 pages
https://doi.org/10.1155/2017/9297808

Research Article

Psychotropic Effects of an Alcoholic Extract from the Leaves of *Albizia zygia* (Leguminosae-Mimosoideae)

Patrick Amoateng,[1] Dorcas Osei-Safo,[2] Kennedy Kwami Edem Kukuia,[1] Samuel Adjei,[3] Obed Awintuma Akure,[1] Constance Agbemelo-Tsomafo,[3] Shirley Nyarko Adu-Poku,[3] and Kenneth Yaw Agyeman-Badu[3]

[1]*Department of Pharmacology & Toxicology, School of Pharmacy, College of Health Sciences, University of Ghana, P.O. Box LG 43, Legon, Accra, Ghana*
[2]*Department of Chemistry, School of Physical and Mathematical Sciences, College of Basic and Applied Sciences, University of Ghana, P.O. Box LG 56, Legon, Accra, Ghana*
[3]*Department of Animal Experimentation, Noguchi Memorial Institute for Medical Research (NMIMR), College of Health Sciences, University of Ghana, P.O. Box LG 581, Legon, Accra, Ghana*

Correspondence should be addressed to Patrick Amoateng; pamoateng@ug.edu.gh

Received 30 June 2017; Accepted 13 August 2017; Published 3 October 2017

Academic Editor: José C. T. Carvalho

Background. *Albizia zygia* is used in Ghanaian traditional medicine for the management of mental disorders. The present study tested the hypothesis that an extract of the leaves of *Albizia zygia* (AZE) may possess antipsychotic and antidepressant properties. *Method*. The novelty- and apomorphine-induced locomotor and rearing behaviours of AZE in mice were explored in an open-field observational test system. The effects of AZE in apomorphine-induced cage climbing test, extract-induced catalepsy, and haloperidol-induced catalepsy on mice were also investigated. Lastly, the forced swimming and tail suspension tests in mice were employed to screen the possible antidepressant effects of AZE. *Results*. AZE (100–3000 mg/kg) showed signs of central nervous system (CNS) depression under observation, with no lethality, 24 h after treatment in mice. AZE (100–1000 mg/kg) produced a significant decrease in the frequency of novelty- and apomorphine-induced locomotor activities in mice. The extract also significantly decreased the frequency and duration of apomorphine-induced climbing activities in mice. AZE, while failing to produce any cataleptic event in naïve mice, significantly enhanced haloperidol-induced catalepsy at a dose of 1000 mg/kg. However, AZE did not produce any significant antidepressant effects in the test models employed. *Conclusion*. The extract of *Albizia zygia* exhibited an antipsychotic-like activity in mice.

1. Introduction

Albizia zygia (family Leguminosae-Mimosoideae) is a medium-sized semideciduous tree that can grow up to about 30 m high and widespread in tropical Africa, known locally in Ghana as *"Okuro"* among the Akans [1]. The wood obtained from the tree is used for indoor construction, veneer and plywood, boat and ship building, implements (e.g., pestles, hoe-handles), matches, and vehicle bodies. In the Ghanaian traditional medicine, the leaves of *Albizia zygia* are used in the management of mental troubles [2]. In other indigenous African traditional health systems, the bark sap is instilled in the eyes to treat eye infections and the bark decoction is also useful for the treatment of bronchial diseases, malaria, fever, and female sterility [3]. The pounded bark is applied topically to treat yaws, sores, wounds, and toothache. Leaf decoctions are administered to treat fever and diarrhoea. Ground roots of the plant are added to food to treat cough and as an expectorant. The root bark juice is also used on wounds to promote healing [3]. In Nigeria, some communities use the plant for the treatment of waist pain [4] and in Cameroon, decoction of the leaves and stem is used in the treatment of boils, diarrhoea, male sexual impotence, oedema, and fracture [5, 6].

Three flavonoids (4′,7-dihydroxyflavanone, 3′,4′,7-trihydroxyflavone, and 3-*O*-methylfisetin (3′,4′,7-trihydroxy-3-methoxyflavone)) isolated from *Albizia zygia* were tested against *Plasmodium falciparum* K1 and only 3′,4′,7-trihydroxyflavone showed potent antimalarial activity (IC_{50} 0.078 μg/ml) [7]. Hexane and methanol extract of *Albizia zygia* has demonstrated *in vitro* free radical scavenging and antioxidant effects [8]. The aqueous methanolic stem bark extract of *Albizia zygia* has been found to possess analgesic activity and low subacute toxicity [9]. Recently, the antipyretic and analgesic properties of the plant extracts have been demonstrated [10, 11].

In African countries such as Ghana, up to 80% of the population use traditional medicine for their primary health care, and these treatment options are less expensive and easily accessible [12]. The drug discovery paradigm involving the investigation of medicinal plants has produced successful results such as the isolation of reserpine from *Rauwolfia serpentina* which is known to have antipsychotic properties [13–15], in addition to its better known antihypertensive effect.

In our quest to provide pharmacological validation of the traditional use in mental health, the antipsychotic and antidepressant effects of an ethanolic extract of the leaves of *Albizia zygia* in mice were evaluated.

2. Materials and Methods

2.1. Chemicals and Reagents. Chlorpromazine hydrochloride (Renandin, France) and haloperidol (STEROP, Belgium) were obtained from local suppliers, whereas apomorphine hydrochloride was obtained from Macfarlan Smith Ltd., Scotland, UK.

2.2. Plant Collection and Extraction. Fresh leaves of the plant were collected from the Aburi Botanical Gardens, Aburi, Ghana, in March 2015 by a curator at the Ghana Herbarium, Department of Plant and Environmental Biology, University of Ghana, Legon, Accra, who identified and authenticated them. A voucher specimen (PA03/UGSOP/GH15) was deposited at the herbarium. The leaves were air-dried for seven days and powdered. A weighed amount of the powder was cold-macerated with 70% v/v of ethanol in water. The ethanolic extract was then evaporated to dryness under reduced pressure, labelled as AZE, and stored in a desiccator.

2.3. Qualitative Phytochemical Screening of AZE. AZE was screened for the presence of alkaloids, saponins, tannins, flavonoids, and other phytochemicals using standard qualitative colorimetric methods [16].

2.4. Animals and Husbandry. Female Imprint Control Region (ICR) mice (weighing 20–30 g), 6–8 weeks old, were obtained from the Department of Animal Experimentation, Noguchi Memorial Institute for Medical Research (NMIMR), University of Ghana, Legon, Accra. The mice were accommodated in groups of five in stainless steel cages (dimensions: 34 cm × 47 cm × 18 cm) with soft wood chips as bedding and kept under laboratory conditions (temperature 22 ± 2°C, relative humidity 60–70%, and 12-hour light-dark cycle). The mice were fed with normal commercial pellet diet (AGRIMAT, Kumasi) and given water ad libitum. All the behavioural testing was conducted from 8:00 to 15:00 GMT.

2.5. Irwin's Test. Irwin's test for primary observation of AZE in mice was done as previously described [17]. Briefly, mice were treated with AZE (30, 100, 300, 1000, and 3000 mg/kg, p.o.) and vehicle (distilled water, 10 ml/kg, p.o.) as control. The mice were then observed 15, 30, 60, 120, and 180 min after administration of the extract/distilled water. The observation was repeated 24 hours later. The parameters, death, convulsions, sedation, excitation, jumping, abnormal gait (rolling, tiptoe), motor incoordination, loss of grasping, akinesia, catalepsy, loss of traction, loss of balance, forepaw treading, writhing, piloerection, stereotypies (sniffing, chewing, and head movements), head-twitches, scratching, altered respiration, aggression, altered fear, altered reactivity to touch, ptosis, exophthalmia, loss of righting reflex, loss of corneal reflex, analgesia, defecation/diarrhoea, salivation, lacrimation, and pupil diameter (myosis/mydriasis), were recorded when exhibited.

2.6. Open-Field Test: Novelty-Induced Behaviours. The extract/drug-induced locomotor and rearing behaviours were determined in an open-field observation box (dimensions: 25 cm × 25 cm × 30 cm) made of transparent Perspex. The base of the maze has 16 squares (6.5 cm × 6.5 cm) demarcated with a nontoxic permanent marker. The arena of the open field was also designated as (i) corner (one of the four corner squares); (ii) periphery (the squares along the walls); or (iii) centre (the 4 inner squares). In the investigation, groups of mice were treated with AZE (100, 300, and 1000 mg/kg, p.o.), chlorpromazine 1 mg/kg (i.p.), or vehicle (distilled water, 10 ml/kg, p.o.). The selected doses of the extract were based on the findings from Irwin's test described above. Thirty minutes later, the mice were placed individually into the open-field observational box and their behaviour was recorded for 5 min using a camcorder (Everio™ Model, GZ-MG 130 U, JVC, Tokyo, Japan) suspended above the maze with the aid of a stand. Rearing behaviour was recorded when a mouse stood on its hind limbs and placed the forelimbs against the wall of the observation cage (supported rearing) or in free air (unsupported rearing). The number of rears (both supported and unsupported) was tracked for 5 min. In addition, the number of times a mouse crosses any of the lines demarcating the base of the maze (i.e., line-crossing) was counted as a representation of locomotor activity. The total frequency and duration spent in the corner and periphery or central portions of the observation set-up by the mice were also recorded.

2.7. Open-Field Test: Apomorphine-Induced Behaviours. In the open-field paradigm, as described above, mice were pretreated with AZE (100, 300, or 1000 mg/kg, p.o.), chlorpromazine (0.1, 0.3, or 1.0 mg/kg, i.p.), or vehicle (distilled water, 10 ml/kg, p.o.) and 30 min later, they received apomorphine (2 mg/kg, i.p.). The mice were then placed in the open-field test chamber. A no-apomorphine vehicle group was also

included. The events were recorded with a camcorder for 30 min and frequency of rearing and line-crossing behaviours was tracked for each mouse. Also the total frequency and duration the mice spent in the corner, periphery, or central portions of the observation set-up were recorded.

2.8. Cage Climbing Test. The method as described previously was adopted [18]. In brief, mice were treated with AZE (100, 300, and 1000 mg/kg, p.o.), haloperidol (0.1, 0.3, and 1 mg/kg, i.p.), or vehicle (distilled water, 10 ml/kg, p.o.). After 30 min, they were injected with apomorphine (2 mg/kg, i.p.). The mice were then immediately placed individually into an all wire-meshed cage (mesh size: 1 cm × 1 cm; dimensions = 27 cm × 20 cm × 20 cm) and their climbing behaviour recorder with a camcorder which was placed above the cage for 30 min after apomorphine injection. The frequency and duration of climbing were tracked from the recorded video.

2.9. Catalepsy: Extract/Drug-Induced Motor Effect. An extract/drug-induced cataleptic test in mice was conducted as previously described [19, 20]. The set-up used in this test consists of a Perspex rod elevated with support to a height of 3.5 cm. Mice pretreated with the AZE (100, 300, and 1000 mg/kg, p.o), haloperidol (0.1, 0.3, and 1.0 mg/kg, i.p.), or vehicle were tested individually on this set-up 15, 30, and 60 min after treatment. The time a mouse spent when placed on the rod with its forepaws was recorded. The test ended when the animal removed its forepaws from the rod unto the floor or climbed the rod.

2.10. Potentiation/Inhibition of Haloperidol-Induced Catalepsy. The effect of AZE on haloperidol-induced catalepsy was performed as previously described [20, 21]. Mice were pretreated with AZE (100, 300, or 1000 mg/kg, p.o.) or vehicle (distilled water, 0.01 ml/kg, p.o.). Thirty minutes later, each mouse was treated with haloperidol 1 mg/kg (i.p.) and tested for catalepsy as described above.

2.11. Forced Swimming Test (FST). This procedure was carried out using published methods with modifications [22–24]. Briefly, mice (n = 5–10) were pretreated with AZE (100, 300, and 1000 mg/kg, p.o.), fluoxetine (3, 10, and 30 mg/kg, p.o.), or vehicle (10 ml/kg of normal saline, p.o.), one hour (p.o.) or 30 min (i.p.) before being placed individually in polypropylene cylinders (height 25 cm, diameter 10 cm) containing water to a height of 15 cm, maintained at 32°C. With a public domain software JWatcher, version 1.0 (University of California, Los Angeles, USA, and Macquarie University, Sydney, Australia), behavioural assessment was measured during the 5-minute test period. Immobility behaviours (floating passively in the water without active movement except for twitches, shivers, or corrective wall-bouncing), swimming behaviours (movement of the hind limbs or tail resulting in a propulsive force or swimming motions, more than necessary, to solely maintain their head above water), and climbing behaviours (active movements in and out of the water with forepaws, usually directed against the walls) of the mice were scored.

2.12. Tail Suspension Test. The tail suspension test (TST) was carried out according to previous descriptions with modifications [24, 25]. Animals were randomly grouped in a similar fashion as in the FST and given AZE (100, 300, and 1000 mg/kg, p.o.), fluoxetine (3, 10, and 30 mg/kg, p.o.), or vehicle (10 ml/kg of normal saline, p.o.), one hour after oral administration and 30 min after intraperitoneal injection. Mice were individually suspended by the tail by tape wrapped around the distal third of the tail such that the body hung on a horizontal ring stand bar is raised 30 cm above the floor. Test sessions lasted 5 min and were videotaped. Behaviours rated were as follows: (1) immobility: a mouse was judged to be immobile when it performs no active behaviour, (2) swinging: a mouse was judged to be swinging when it continuously moved its paws in the vertical position while keeping its body straight and/or it moved its body from side to side, and (3) curling: a mouse was judged to be curling when it engaged in active twisting movements of the entire body.

3. Results

3.1. Qualitative Phytochemical Screening of AZE. Alkaloids, flavonoids, tannins, saponins, and anthraquinone glycosides were found to be present in AZE.

3.2. Irwin's Test. AZE (100, 300, 1000, and 3000 mg/kg) showed signs of CNS depression under observation. Extract-treated mice (at all dose levels) showed dose and time dependent sedation which lasted 60 minutes. There were no signs of convulsion and no mouse died after 24 hours suggesting LD_{50} is above 3000 mg/kg.

3.3. Open-Field Test: Novelty-Induced Behaviours. AZE (100, 300, and 1000 mg/kg, p.o.) significantly decreased the frequencies of rearing ($P < 0.0001$, $F_{4,15} = 22.82$, Figure 1) and line-crossing ($P < 0.0001$, $F_{3,16} = 11.83$, Figure 1) in the mice treated, in comparison with the vehicle-treated group. The decrease in the frequency of the rearing behaviour was dose-dependent. In the 5 min test period, the AZE (100, 300, and 1000 mg/kg, p.o.) significantly increased the frequency of centre, periphery, and corner entry ($P = 0.0002$, $F_{4,20} = 9.366$; Figure 2(a), $P < 0.0001$, $F_{4,20} = 19.33$; Figure 2(b), and $P < 0.0001$, $F_{4,20} = 16.62$; Figure 2(c), resp.) compared to the vehicle-treated group. The extract significantly decreased the time spent by mice in the centre and corner ($P = 0.0013$, $F_{4,17} = 7.268$; Figure 2(a) and $P = 0.0008$, $F_{4,20} = 7.861$; Figure 2(c), resp.) of the open field. Also, AZE produced a decrease in the time spent by mice in the periphery ($P = 0.1469$, $F_{4,20} = 1.917$; Figure 2(b)) of the open field, but this was not significant.

3.4. Open-Field Test: Apomorphine-Induced Behaviours. Apomorphine (2 mg/kg, i.p.) produced a characteristic increase in rearing and locomotor activity in the vehicle-treated group when compared with the vehicle-alone-treated group of mice (i.e., no apomorphine) (Figures 3(a) and 3(b)). There was a significant and dose-dependent decrease in the frequency of line-crossing behaviour ($P = 0.0002$, $F_{3,9} = 20.90$, Figure 3(b)) in the mice treated with AZE

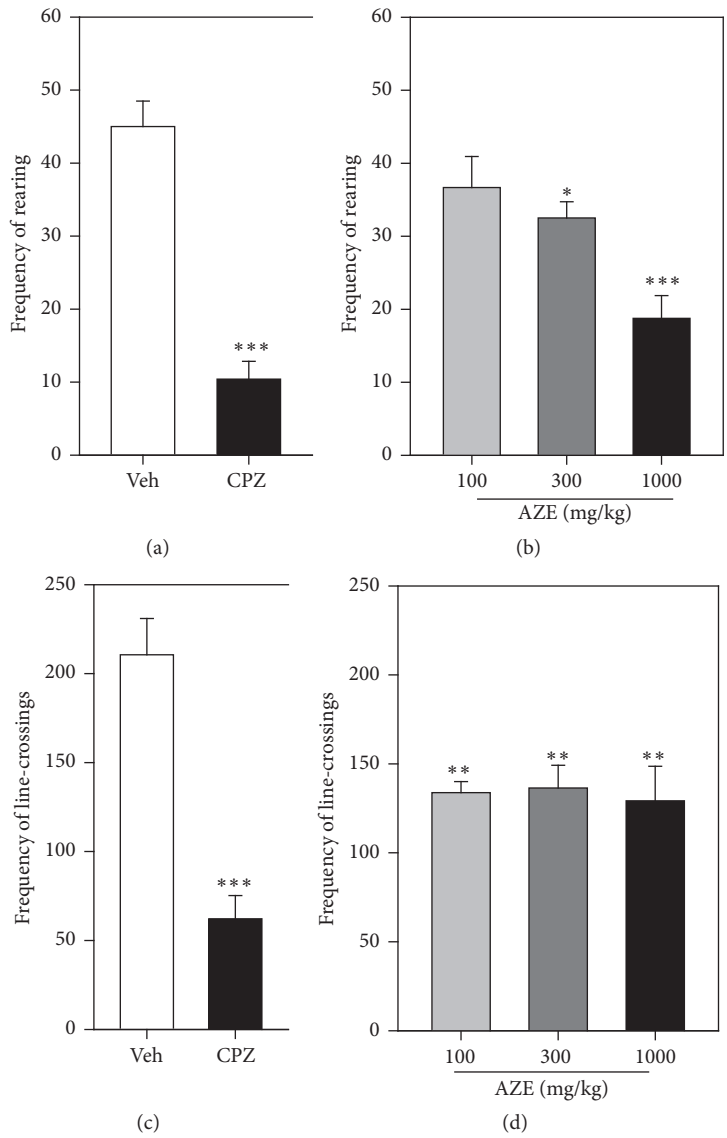

Figure 1: Frequency of rearing ((a) and (b)) and line-crossings ((c) and (d)) of mice treated with chlorpromazine (CPZ; 1 mg/kg, i.p.), AZE (100, 300, and 1000 mg/kg, p.o.), and vehicle (Veh) when observed for 5 min in an open-field paradigm. Data are mean ± SEM ($n = 5$). $^{*}P \leq 0.05$, $^{**}P \leq 0.01$, and $^{***}P \leq 0.001$ compared with vehicle group (one-way ANOVA followed by a Dunnett's multiple comparison post hoc test).

in comparison to the vehicle-treated mice. However, AZE failed to elicit any significant change in the frequency of rearing in the mice treated with it ($P = 0.2217$, $F_{3,10} = 1.741$, Figure 3(a)). Chlorpromazine significantly decreased apomorphine-induced rearing ($P = 0.0065$, $F_{3,15} = 6.067$, Figure 3(a)) and locomotor activity ($P = 0.007$, $F_{3,12} = 6.58$, Figure 3(b)) in mice that were pretreated with it. The decrease in rearing activity by CPZ was dose-dependent, whereas that of the line-crossing was not. In comparison to the vehicle-treated group, AZE (100, 300, and 1000 mg/kg, p.o.) decreased, but not significantly, the frequency of centre entry ($P = 0.5044$, $F_{4,18} = 0.8636$; Figure 4(a)) but significantly reduced the time spent by mice in the centre ($P = 0.0077$, $F_{4,15} = 5.228$; Figure 4(a)) of the open field. The extract significantly increased the frequency of periphery entry ($P = 0.0228$, $F_{4,17} = 3.761$; Figure 4(b)) and significantly decreased the time spent by animals in the periphery ($P = 0.0054$, $F_{4,17} = 5.400$; Figure 4(b)) of the open field. AZE also increased, but not significantly, the frequency of entries into the corner ($P = 0.1168$, $F_{4,18} = 2.146$; Figure 4(c)) but produced no significant change in the time spent by mice in the corner ($P = 0.1290$, $F_{4,19} = 2.043$; Figure 4(c)) of the open field.

3.5. Cage Climbing Test. Apomorphine induced a characteristic increase in the total frequency (Figure 5(a)) and duration (Figure 5(b)) of climbing of the wire-meshed cage by the animals. AZE (100, 300, and 1000 mg/kg, p.o.) significantly reduced the total frequency ($P < 0.0001$, $F_{3,16} = 247.3$; Figure 5(a)) and duration ($P < 0.0001$, $F_{3,12} = 32.79$;

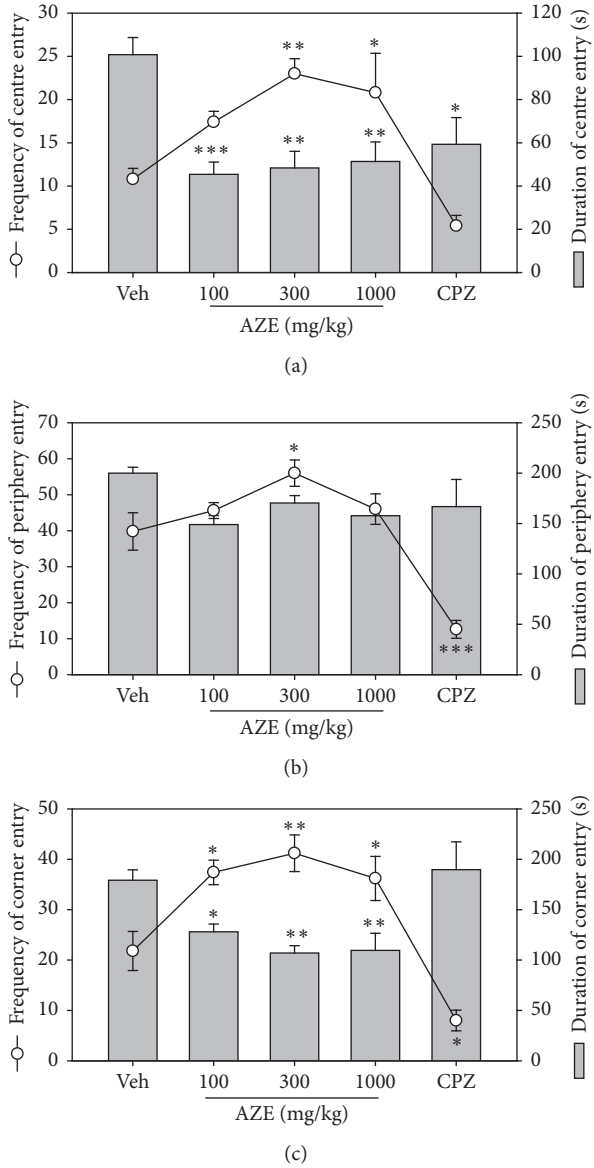

Figure 2: Effects of AZE (100–1000 mg/kg) on the frequency (line graph) and duration (column graphs) of centre entry (a), periphery entry (b), and corner entry (c). Each point represents mean ± SEM ($n = 5$). $^{*}P < 0.05$, $^{**}P < 0.01$, and $^{***}P < 0.001$, compared to vehicle-treated group (one-way ANOVA followed by Dunnett's post hoc test).

Table 1: ED_{50} values (mg/kg) ± SEM of AZE and haloperidol (HAL) on the frequency and total duration of apomorphine-induced cage climbing in mice.

	AZE	HAL
Frequency	979.4 ± 1.35	0.1391 ± 1.07
Duration	240.8 ± 0.46	0.1047 ± 1.61

Figure 5(b)) of cage climbing in the treated mice, but not in the dose-dependent manner. Haloperidol (HAL) (0.1, 0.3, and 1 mg/kg, i.p.) significantly and dose-dependently reduced the total frequency ($P < 0.0001$, $F_{3,16} = 172.1$, Figure 5(a)) and duration of cage climbing ($P < 0.0001$, $F_{3,15} = 146.7$, Figure 5(b)). Comparison of the ED_{50} values of AZE and haloperidol revealed that HAL was more potent than AZE (Table 1). However, the effect of AZE at dose of 300 mg/kg, p.o., which was the most potent ($P < 0.0001$) extract dose in reducing climbing behaviour, was comparable to haloperidol at dose 1 mg/kg, i.p.

3.6. Catalepsy: Extract/Drug-Induced Motor Effects. AZE (100, 300, and 1000 mg/kg) did not produce any cataleptic

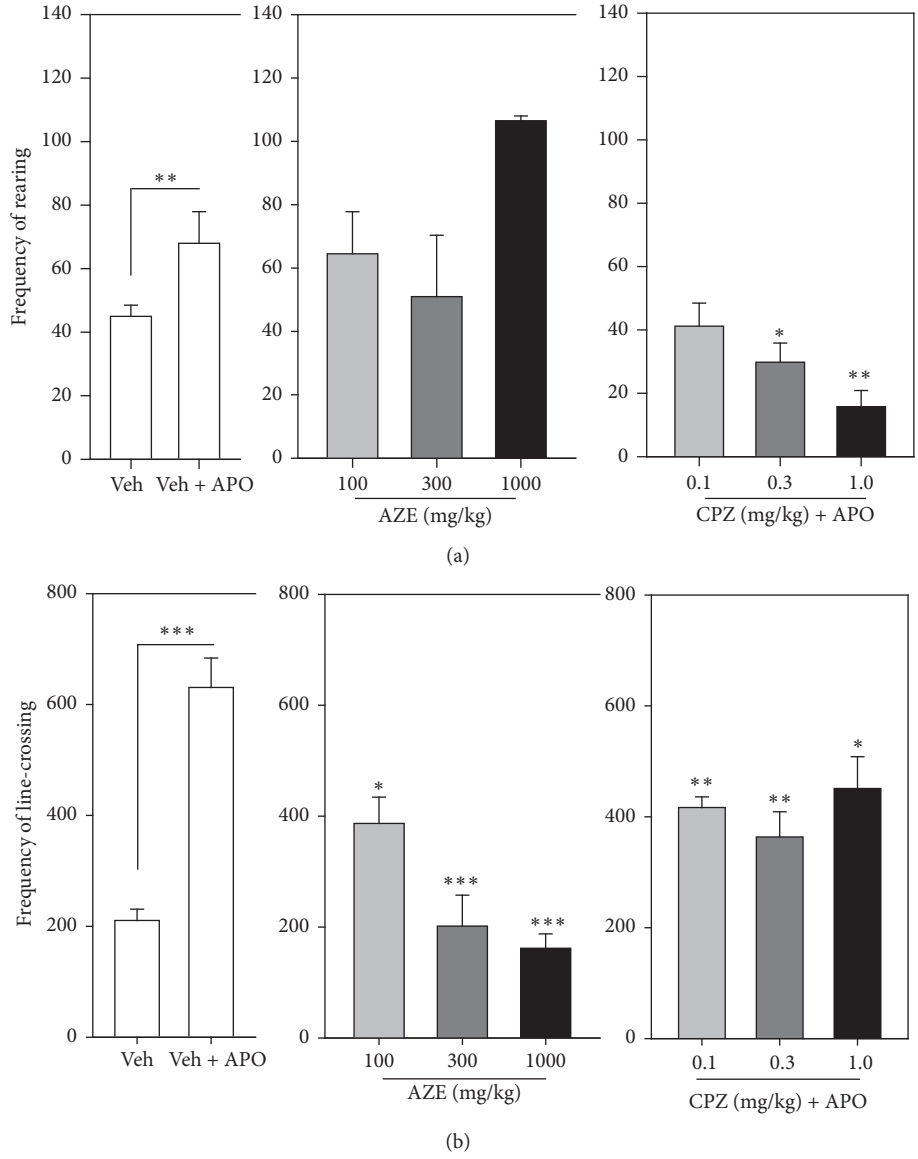

Figure 3: Effect of AZE (100, 300, and 1000 mg/kg, p.o.), CPZ (0.1, 0.3, and 1.0 mg/kg, i.p.), and vehicle (Veh) (distilled water, 0.01 ml/kg, p.o.) on the frequency of rearing (a) and line-crossings (b) of mice, 30 min after apomorphine (APO) (2 mg/kg, i.p.) treatment in an open-field paradigm. Data are mean ± SEM ($n = 5$). $^{*}P \leq 0.05$, $^{**}P \leq 0.01$, and $^{***}P \leq 0.001$ compared with Veh + APO group (one-way ANOVA followed by a Dunnett's multiple comparison post hoc test).

behaviour ($P = 0.23$, $F_{3,16} = 1.753$, Table 2) in the mice treated. Haloperidol (0.1, 0.3, and 1 mg/kg), however, exhibited a significant and dose-dependent cataleptic behaviour in the treated mice ($P = 0.01$, $F_{3,16} = 5.209$, Table 2).

3.7. Potentiation/Inhibition of Haloperidol-Induced Catalepsy. AZE 100 and 300 mg/kg inhibited the cataleptic effect of haloperidol (1 mg/kg) throughout the 60 min after haloperidol treatment. However, AZE 1000 mg/kg increased significantly the haloperidol-induced catalepsy, 30 and 60 min after haloperidol treatment (Figure 6(a)). Overall, there was a significant difference ($P = 0.0087$, $F_{3,12} = 6.200$, Figure 6(b)) between the AZE- and vehicle-treated mice in this test and only AZE 1000 mg/kg significantly increased the haloperidol-induced cataleptic behaviour ($P < 0.01$, Figure 6(b)).

3.8. Forced Swimming Test. AZE (100, 300, and 1000 mg/kg, p.o.) administered 60 min before the test period produced no significant reduction in the duration of immobility ($P = 0.6480$, $F_{3,16} = 0.5618$; Figure 7(a)) of mice in the FST. Fluoxetine (FLX) (3, 10, and 30 mg/kg, p.o.) significantly reduced the duration of immobility ($P < 0.0001$, $F_{3,18} = 151.1$; Figure 7(b)) of mice in a dose-dependent manner relative to the vehicle-treated group.

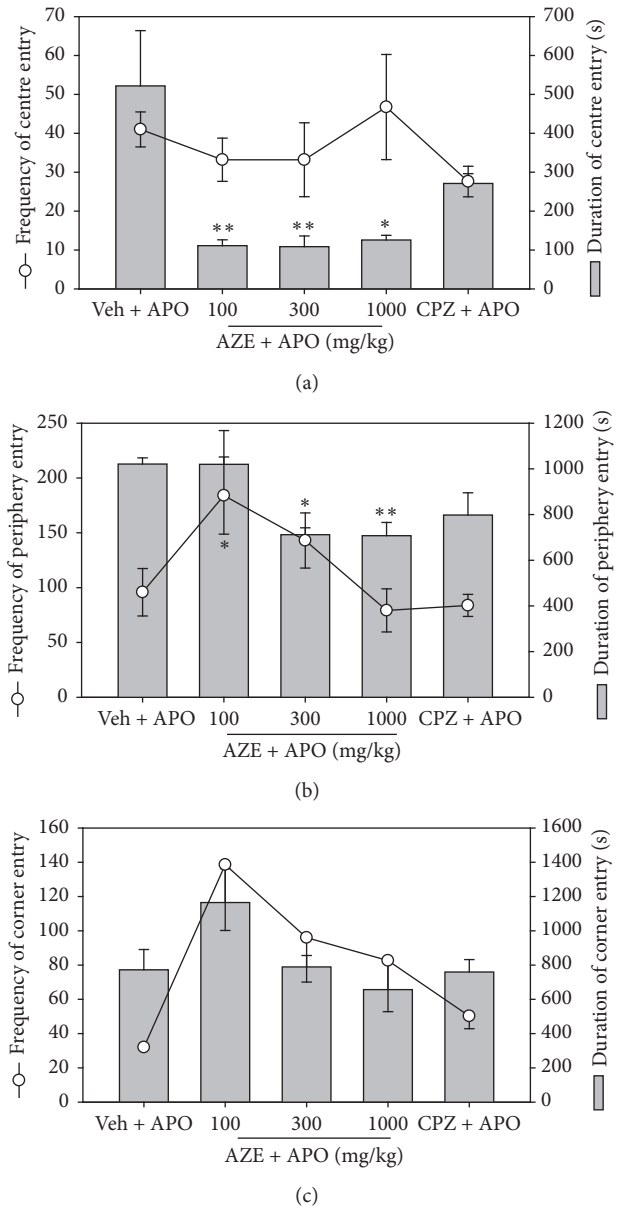

Figure 4: Effect of AZE (100, 300, and 1000 mg/kg, p.o.), CPZ (1.0 mg/kg, i.p.), and vehicle (Veh) (distilled water, 0.01 ml/kg, p.o.) on the frequency (line graph) and duration (column graphs) of centre entry (a), periphery entry (b), and corner entry (c), 30 min after apomorphine (APO) (2 mg/kg, i.p.) treatment in an open-field paradigm. Data are mean ± SEM ($n = 5$). $^{*}P \leq 0.05$ and $^{**}P \leq 0.01$ compared with Veh + APO group (one-way ANOVA followed by a Dunnett's multiple comparison post hoc test).

Table 2: Effect of extracts AZE, haloperidol (HAL), and vehicle on the duration of catalepsy. Data are mean ± SEM ($n = 5$). $^{*}P \leq 0.05$, $^{**}P \leq 0.01$, compared with vehicle group (two-way ANOVA followed by a Bonferroni's post hoc test).

Treatment (mg/kg)	Time (s)			P value
	15th min	30th min	60th min	
Vehicle	0.000 ± 0.00	0.00 ± 0.00	0.00 ± 0.00	—
AZE 100	0.000 ± 0.00	1.398 ± 0.87	1.398 ± 1.09	0.23
AZE 300	0.000 ± 0.00	0.200 ± 0.13	1.300 ± 1.07	
AZE 1000	0.400 ± 0.40	0.000 ± 0.00	0.000 ± 0.00	
HAL 0.3	34.187 ± 8.01	87.902 ± 33.81	108.892 ± 32.84	0.01
HAL 1.0	154.340 ± 42.16**	153.273 ± 52.08*	125.403 ± 55.14*	
HAL 3.0	162.660 ± 46.41**	179.510 ± 50.24**	192.122 ± 40.87**	

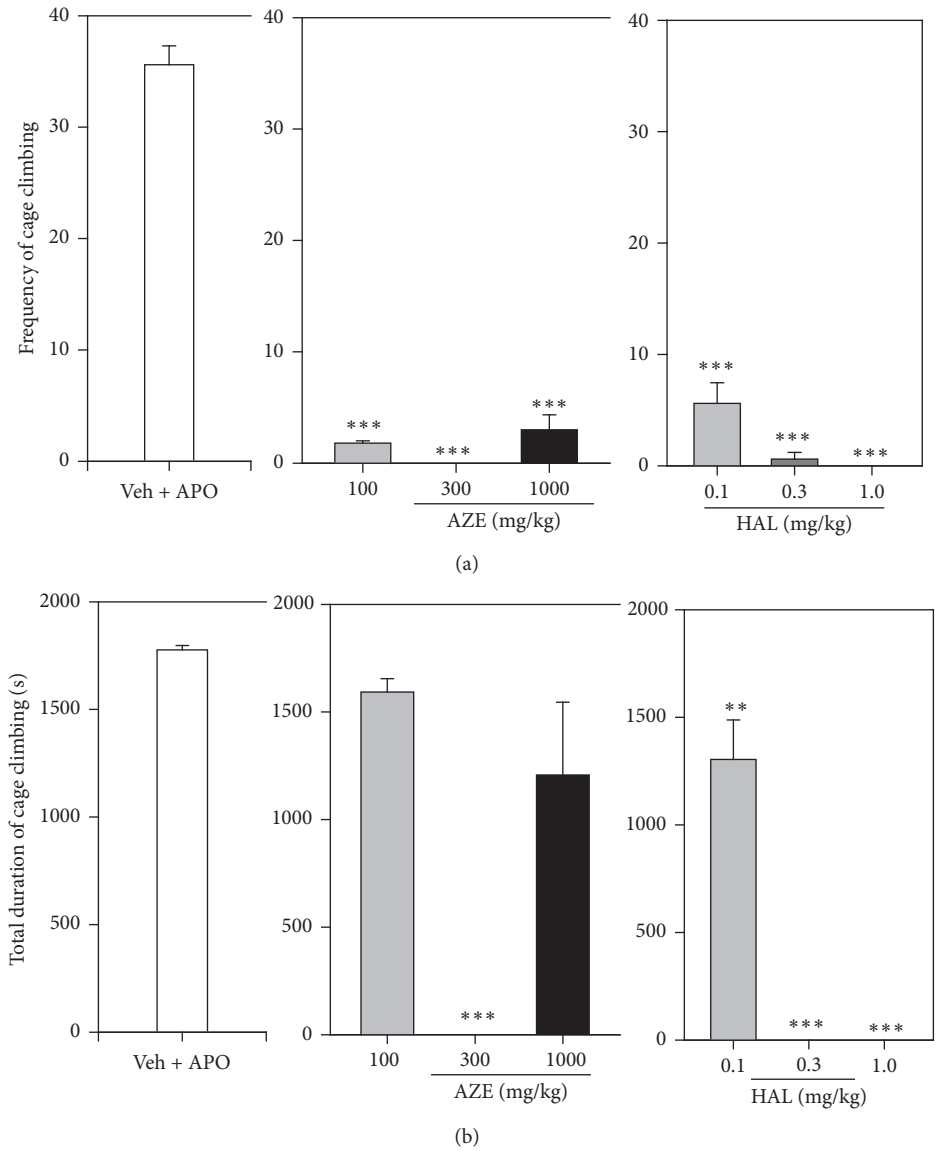

Figure 5: Effect of AZE (100, 300, and 1000 mg/kg, p.o.), HAL (0.1, 0.3, 1.0 mg/kg, i.p.), and vehicle (Veh) on the total frequency and duration of cage climbing of mice, 30 min after apomorphine (APO) (2 mg/kg, i.p.) treatment. Data are mean ± SEM ($n = 5$). $^{**}P \leq 0.01$ and $^{***}P \leq 0.001$ compared with Veh + APO group (one-way ANOVA followed by a Dunnett's multiple comparison post hoc test).

3.9. Tail Suspension Test. AZE (100, 300, and 1000 mg/kg, p.o.) administered 60 min prior to the test period failed to produce any reduction in the duration of immobility ($P = 0.8600$, $F_{3,16} = 0.2502$; Figure 8(a)) of mice in the TST. Fluoxetine (FLX) (3, 10, and 30 mg/kg, p.o.), as expected, significantly and dose-dependently reduced the duration of immobility ($P < 0.0001$, $F_{3,18} = 61.74$; Figure 8(b)) of mice with respect to the vehicle-treated group.

4. Discussion

The present study describes an antipsychotic and antidepressant potential of a hydroethanolic extract of the leaves of *Albizia zygia* (AZE) in murine models of psychosis and depression. The experimental procedures were done to rationalise the traditional uses of the plant in mental health. The behavioural effects of *Albizia zygia* in mice were examined. Mice were used as the experimental subject because they are similar to humans at the anatomical, cellular, biochemical, and molecular level and also share with humans similar brain functions such as anxiety, hunger, circadian rhythm, aggression, memory, sexual behaviour, and other emotional responses [26]. The findings of this study provide initial evidence that AZE possesses antipsychotic-like effects. However, AZE seem to be devoid of antidepressant-like activity, as seen from the findings of the effects of AZE on the murine models of depression employed.

A preliminary investigation of the effects of the AZE in Irwin's tests, novelty-induced rearing, and locomotor activity demonstrates that the extract is sedative and that it decreases

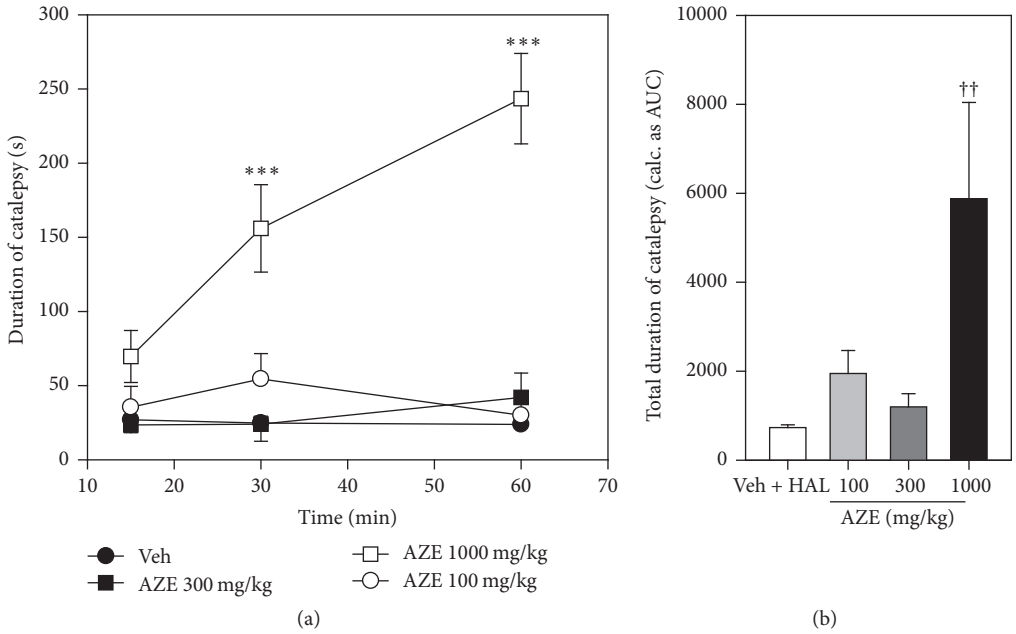

Figure 6: Effects of AZE on haloperidol- (HAL-) induced catalepsy in mice. Paneled graph (a) is the time-course effects 15, 30, and 60 min after haloperidol administration. Column graph (b) is the total duration of catalepsy (calculated as AUCs from the time-course graphs). Data are mean ± SEM ($n = 5$). $^{***}P \leq 0.001$ compared with vehicle group (two-way ANOVA followed by Bonferroni post hoc test). $^{††}P \leq 0.01$ compared with vehicle group (one-way ANOVA followed by a Dunnett's multiple comparison post hoc test).

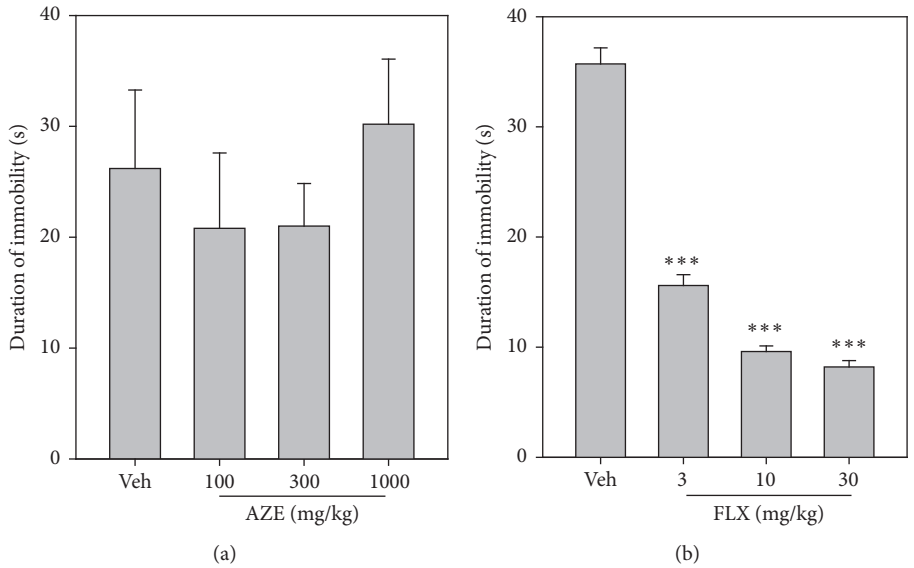

Figure 7: Effects of AZE (100–1000 mg/kg) (a) and FLX (3–30 mg/kg) (b) on the duration of immobility in the FST. Each point represents mean ± SEM ($n = 5$). $^{***}P < 0.001$, compared to vehicle-treated group (one-way ANOVA followed by Dunnett's post hoc test).

exploratory behaviour of the pretreated mice. These effects exhibited by AZE do not necessarily suggest an antipsychotic activity, though most antipsychotic agents produce similar effects in animals [27].

Stimulation of cerebral dopaminergic activity can produce psychosis de novo in some patients and psychosis has long been associated with increased cerebral dopaminergic activity. This role of dopamine in psychosis is supported by biochemical findings, clinical and imaging studies [28–31]. The clinical efficacy of most antipsychotic drugs, especially those effective against the positive psychotic symptoms such as hallucinations and delusions, may be linked to dopamine D_2 receptor antagonism [32]. Murine models of psychosis used for screening antipsychotic drugs are based on the neurochemical hypothesis of schizophrenia, involving mainly the neurotransmitters, dopamine and glutamate [33]. The

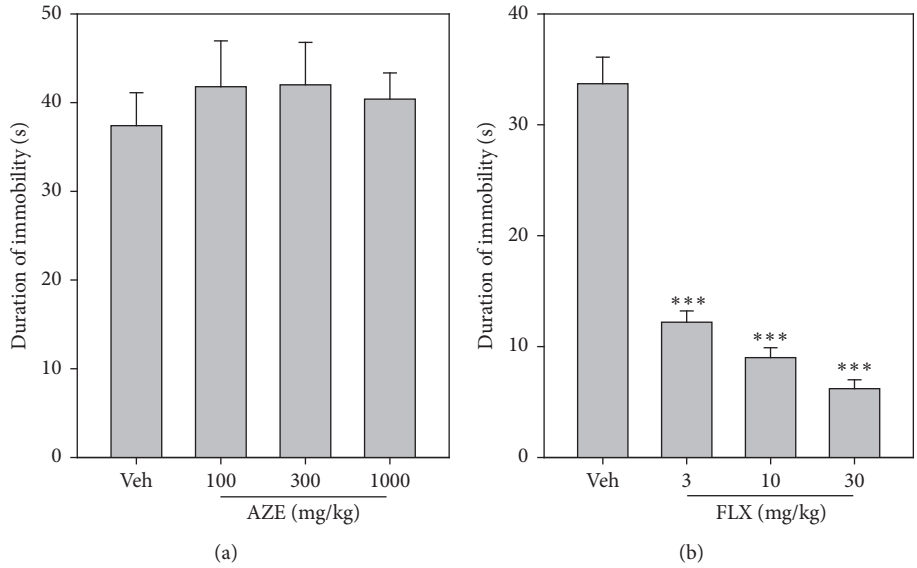

Figure 8: Effects of AZE (100–1000 mg/kg) (a) and FLX (3–30 mg/kg) (b) on the duration of immobility in the TST. Each point represents mean ± SEM ($n = 5$). $^{***}P < 0.001$, compared to vehicle-treated group (one-way ANOVA followed by Dunnett's post hoc test).

dopamine-based models usually use apomorphine, a direct dopamine agonist, or amphetamine, a drug that increases the release of dopamine and blocks its reuptake [34]. In this study, psychosis in the murine models was induced by administration of apomorphine which, being a nonselective dopamine agonist, elicits behavioural responses in animals by activating dopamine D_1 and D_2 receptors in the brain [35, 36]. Activation of these dopamine receptors is known to increase locomotor activity [37], stereotyped behaviours [38], rearing/grooming [39], and cage climbing behaviours [40, 41].

The apomorphine-induced cage climbing test is a widely used test for screening antipsychotic drugs [18, 40, 42]. It has predictive validity for antipsychotic drugs that normalize the hyperactivity and stereotypic behaviour in that almost all antipsychotics dose-dependently antagonize apomorphine-induced cage climbing behaviour of mice [42]. Mice treated with low doses of apomorphine tend to adopt a vertical position and try to climb walls. Apomorphine induces climbing behaviour in mice by activating both dopamine D_1 and D_2 receptors in the striatum [42]. Activation of either dopamine D_1 or D_2 receptors does not induce climbing behaviour; instead, activation of both receptors is required to produce climbing behaviour [43]. Therefore, it follows that antagonism of apomorphine-induced climbing behaviour is achieved by blocking either or both dopamine D_1 and D_2 receptors. Apomorphine induces a peculiar climbing behaviour in mice characterized initially by rearing and then spontaneous climbing activity. In the present study, acute pretreatment of AZE (100, 300, and 1000 mg/kg) in mice showed a significant but not dose-dependent decrease in frequency of climbing and climbing time induced by apomorphine compared to the vehicle-treated group. Haloperidol, the reference drug, significantly and dose-dependently reduced the climbing behaviour of mice as expected. AZE was less potent than HAL in reducing the apomorphine-induced climbing behaviour of mice as indicated by the ED_{50} values. However, the effects of AZE at dose of 300 mg/kg p.o. on climbing behaviour were comparable to haloperidol at dose of 1 mg/kg i.p. Based on these findings, it may be concluded that AZE produces antipsychotic activity which may be mediated through the antagonism of either or both of dopamine D_1 and D_2 receptors in the striatum of the brain.

Catalepsy test in rodents is a predictive tool for detecting the extrapyramidal side effects (EPS) of antipsychotic drugs [44]. EPS is a key side effect that is known to account for the discontinuation of antipsychotic drug use in patients [45]. Consequently, current research for new antipsychotic drug discovery is focused on agents with minimal or no EPS in addition to clinical efficacy [45, 46]. Catalepsy in laboratory animals is defined as a failure to correct an externally imposed posture and the test entails measuring the latency for the animal to remove itself from the unfamiliar and uncomfortable position [19, 47]. AZE's lack of catalepsy in the mice over the entire 60 min after administration period is an indication that it may not produce any significant EPS. However, this claim can be substantiated following the determination of the incidence of catalepsy after a chronic administration of the AZE. The extract, at the highest dose used in the study, produced a significant increase in haloperidol-induced catalepsy, suggesting it may have the ability to cause this side effect at higher doses.

The forced swimming and tail suspension tests are the two widely used animal models for antidepressant screening. They are quite sensitive and specific to all the major classes of antidepressant drugs [22]. They are sensitive to both acute and chronic treatments of antidepressants [48]. The TST has a higher pharmacological sensitivity than the FST and it is also less stressful [49]. In both tests, mice are placed in an inescapable but moderately stressful situation. Lack

of escape related behaviour is considered immobility and it reflects a state of despair which is claimed to produce in the animals a condition similar to depression in humans. This state of despair can be reduced by several agents which are therapeutically effective in human depression [48, 50]. Reduction of the immobility time has been established to depend predominantly on the enhancement of central 5-HT and catecholamine neurotransmission [51]. In the present study, AZE failed to reduce the immobility time in the FST and TST and it therefore follows that AZE possesses no potential antidepressant activity.

Alkaloids, flavonoids, tannins, saponins, and anthraquinone glycosides were found to be present in AZE. Similarly, alkaloids, tannins, saponins, flavonoids, and cardiac glycosides in the stem bark of *Albizia zygia* have been reported [9]. The observed neuropharmacological effects of the plant extract could be attributed to the presence of these phytochemical constituents. However, activity-guided characterization of these groups would be needed to comprehend their role in the observed antipsychotic effects.

5. Conclusion

The extract of *Albizia zygia* produced antipsychotic-like effects in mice. It, however, did not have any antidepressant effect. These findings support the use of the plant extract in the traditional medicinal management of psychosis in Ghana.

Conflicts of Interest

The authors declare that there are no conflicts of interest regarding the publication of this paper.

Acknowledgments

The authors acknowledge the support provided by technical staff at the Animal Experimentation Unit of the NMIMR, Accra, Ghana. The research work was financially supported by the Office of Research, Innovation and Development (ORID), University of Ghana, Accra, Ghana, grant awarded to Dr. Patrick Amoateng (Reference no. URF/6/ILG-002/2012-2013). The writing of the manuscript was supported by the University of Ghana, Building a New Generation of Academics in Africa (BANGA-Africa) Project with funding from the Carnegie Corporation of New York.

References

[1] M. M. Apetorgbor, "Albizia zygia (DC.) J.F.Macbr," in *Record from PROTA4U*, D. Louppe, A. A. OtengAmoako, and M. Brink, Eds., vol. 2015 of *Plant Resources of Tropical Africa / Ressources végétales de l'Afrique tropicale*, Wageningen, The Netherlands, 2007.

[2] D. K. Abbiw, *Useful plants of Ghana: West African uses of wild and cultivated plants*, Intermediate Technology Publications and The Royal Botanic Gardens, London, UK, 1990.

[3] U. Quattrocchi, *CRC world dictionary of medicinal and poisonous plants: common names, scientific names, eponyms, synonyms, and etymology*, vol. 5, CRC Press, Boca Raton, Fla, USA, 2012.

[4] I. O. Lawal, N. E. Uzokwe, A. B. I. Igboanugo et al., "Ethno medicinal information on collation and identification of some medicinal plants in Research Institutes of South-west Nigeria," *African Journal of Pharmacy and Pharmacology*, vol. 4, no. 1, pp. 1–7, 2010.

[5] T. Jiofack, I. Ayissi, C. Fokunang, N. Guedje, and V. Kemeuze, "Ethnobotany and phytomedicine of the upper Nyong valley forest in Cameroon," *African Journal of Pharmacy and Pharmacology*, vol. 3, no. 4, pp. 144–150, 2009.

[6] T. Jiofack, C. Fokunang, N. Guedje, V. Kemeuze, E. Fongnzossie, and B. Nkongmeneck, "Ethnobotanical uses of medicinal plants of two ethnoecological regions of Cameroon," *International Journal of Medicine and Medical Sciences*, vol. 2, no. 3, pp. 60–79, 2010.

[7] M. A. Abdalla and H. Laatsch, "Flavonoids from Sudanese Albizia zygia (Leguminosae, subfamily Mimosoideae), a plant with antimalarial potency," *African journal of traditional, complementary, and alternative medicines : AJTCAM/African Networks on Ethnomedicines*, vol. 9, no. 1, pp. 56–58, 2012.

[8] G. K. Oloyede and A. O. Ogunlade, "Phytochemical screening, antioxidant, antimicrobial and toxicity activities of polar and non-polar extracts of albizia zygia (DC) stem-bark," *Science Domain International*, vol. 3, no. 4, pp. 1–12, 2013.

[9] T. A. Abere and R. I. Jesuorobo, "Analgesic and toxicological evaluation of the stem bark of Albizia zygia Benth (Mimosoideae)," *IOSR Journal of Pharmacy and Biological Sciences*, vol. 9, no. 2, pp. 26–31, 2014.

[10] W. K. M. Abotsi, S. B. Lamptey, S. Afrane, E. Boakye-Gyasi, R. U. Umoh, and E. Woode, "An evaluation of the anti-inflammatory, antipyretic and analgesic effects of hydroethanol leaf extract of Albizia zygia in animal models," *Pharmaceutical Biology*, vol. 55, no. 1, pp. 338–348, 2017.

[11] W. K. M. Abotsi, S. B. Lamptey, E. Boakye-Gyasi, and E. Woode, "Albizia zygia (DC.) J.F. Macbr. (Leguminosae-Mimosoideae) root extract exhibits anti-nociceptive and antipyretic activities in murine models," *Journal of Ethnopharmacology*, vol. 199, pp. 183–193, 2017.

[12] World Health Organization, "Traditional Medicine," *Fact Sheet*, vol. 34, 2003.

[13] N. S. Kline, "Use of rauwolfia serpentina benth. in neuropsychiatric conditions," *Annals of the New York Academy of Sciences*, vol. 59, no. 1, pp. 107–132, 1954.

[14] J. M. Davis and D. L. Garver, "Neuroleptics: clinical use in psychiatry," in *Handbook of psychopharmacology*, vol. 10 of *Neuroleptics and Schizophrenia*, pp. 129–164, Springer, Berlin, Germany, 1978.

[15] D. Healy and M. Savage, "Reserpine exhumed," *British Journal of Psychiatry*, vol. 172, pp. 376–378, 1998.

[16] W. C. Evans, *Trease and Evans' Pharmacognosy*, Saunders Ltd, Edinburgh, Scotland, 15 edition, 2002.

[17] S. Irwin, "Comprehensive observational assessment: Ia. A systematic, quantitative procedure for assessing the behavioral and physiologic state of the mouse," *Psychopharmacologia*, vol. 13, no. 3, pp. 222–257, 1968.

[18] A. S. Davis, P. Jenner, and C. D. Marsden, "A comparison of motor behaviours in groups of rats distinguished by their climbing response to apomorphine," *British Journal of Pharmacology*, vol. 87, no. 1, pp. 129–137, 1986.

[19] P. R. Sanberg, M. D. Bunsey, M. Giordano, and A. B. Norman, "The catalepsy test: its ups and downs," *Behavioral Neuroscience*, vol. 102, no. 5, pp. 748–759, 1988.

[20] G. Sotoing Taïwe, E. Ngo Bum, E. Talla et al., "Antipsychotic and sedative effects of the leaf extract of Crassocephalum bauchiense (Hutch.) Milne-Redh (Asteraceae) in rodents," *Journal of Ethnopharmacology*, vol. 143, no. 1, pp. 213–220, 2012.

[21] S. Pemminati, V. Nair, P. Dorababu, H. N. Gopalakrishna, and M. R. S. M. Pai, "Effect of ethanolic leaf extract of Ocimum sanctum on haloperidol-induced catalepsy in albino mice," *Indian Journal of Pharmacology*, vol. 39, no. 2, pp. 87–89, 2007.

[22] R. D. Porsolt, A. Bertin, and M. Jalfre, "Behavioral despair in mice: a primary screening test for antidepressants," *Archives Internationales de Pharmacodynamie et de Thérapie*, vol. 229, no. 2, pp. 327–336, 1977.

[23] D. A. Slattery and J. F. Cryan, "Using the rat forced swim test to assess antidepressant-like activity in rodents," *Nature Protocols*, vol. 7, no. 6, pp. 1009–1014, 2012.

[24] K. K. Kukuia, P. K. Mante, E. Woode, E. O. Ameyaw, and D. W. Adongo, "Antidepressant effects of mallotus oppositifolius in acute murine models," *ISRN Pharmacology*, vol. 2014, pp. 1–12, 2014.

[25] L. Steru, R. Chermat, B. Thierry, and P. Simon, "The tail suspension test: a new method for screening antidepressants in mice," *Psychopharmacology*, vol. 85, no. 3, pp. 367–370, 1985.

[26] B. Greenwood-Van Meerveld, A. C. Johnson, S. Cochrane, J. Schulkin, and D. A. Myers, "Corticotropin-releasing factor 1 receptor-mediated mechanisms inhibit colonic hypersensitivity in rats," *Neurogastroenterology and Motility*, vol. 17, no. 3, pp. 415–422, 2005.

[27] J. L. Moreno and J. González-Maeso, "Preclinical models of antipsychotic drug action," *International Journal of Neuropsychopharmacology*, vol. 16, no. 10, pp. 2131–2144, 2013.

[28] B. G. Katzung, S. B. Masters, and A. J. Trevor, *Basic & clinical pharmacology. edn, . Lange Medical Books/McGraw-Hill [Masters, thesis]*, New York, NY, USA, 2004.

[29] V. Castagné, P. Moser, and R. D. Porsolt, "Behavioral assessment of antidepressant activity in rodents".

[30] K. M. Brophy, H. Scarlett-Ferguson, K. S. Webber, A. C. Abrams, and C. B. Lammon, *Clinical Drug Therapy for Canadian Practice*, Wolters Kluwer Health/Lippincott Williams & Wilkins, Philadelphia, Pa, USA, 2nd edition, 2010.

[31] H. P. Rang, J. M. Ritter, R. J. Flower, and G. Henderson, *Rang Dale's Pharmacology: with student consult online access*, Elsevier Health Sciences, Amsterdam, The Netherlands, 2014.

[32] D. M. Gardner, R. J. Baldessarini, and P. Waraich, "Modern antipsychotic drugs: a critical overview," *Canadian Medical Association Journal*, vol. 172, no. 13, pp. 1703–1711, 2005.

[33] B. K. Lipska and D. R. Weinberger, "To model a psychiatric disorder in animals: schizophrenia as a reality test," *Neuropsychopharmacology*, vol. 23, no. 3, pp. 223–239, 2000.

[34] V. Pandy, M. Narasingam, and Z. Mohamed, "Antipsychotic-like activity of Noni (Morinda citrifolia Linn.) in mice," *BMC Complementary and Alternative Medicine*, vol. 12, article no. 186, 2012.

[35] P. Seeman, "Brain dopamine receptors," *Pharmacological Reviews*, vol. 32, no. 3, pp. 229–313, 1980.

[36] J. C. Stoof and J. W. Kebabian, "Two dopamine receptors: biochemistry, physiology and pharmacology," *Life Sciences*, vol. 35, no. 23, pp. 2281–2296, 1984.

[37] K. Matsumoto, B. Cai, H. Ohta, L. Imamura, and H. Watanabe, "Apparent enhancement by SCH 23390 of apomorphine-induced locomotor activity in mice," *Pharmacology, Biochemistry and Behavior*, vol. 39, no. 3, pp. 699–703, 1991.

[38] J. J. Battisti, N. J. Uretsky, and L. J. Wallace, "Sensitization of apomorphine-induced stereotyped behavior in mice is context dependent," *Psychopharmacology*, vol. 146, no. 1, pp. 42–48, 1999.

[39] K. Matsumoto, C. Bing, K. Sasaki, and H. Watanabe, "Methamphetamine- and apomorphine-induced changes in spontaneous motor activity using a new system to detect and analyze motor activity in mice," *Journal of Pharmacological Methods*, vol. 24, no. 2, pp. 111–119, 1990.

[40] H. Marcais, P. Protais, J. Costentin, and J. C. Schwartz, "A gradual score to evaluate the climbing behaviour elicited by apomorphine in mice," *Psychopharmacology*, vol. 56, no. 2, pp. 233-234, 1978.

[41] R. E. Wilcox, R. V. Smith, J. A. Anderson, and W. H. Riffee, "Apomorphine-induced stereotypic cage climbing in mice as a model for studying changes in dopamine receptor sensitivity," *Pharmacology, Biochemistry and Behavior*, vol. 12, no. 1, pp. 29–33, 1980.

[42] S. H. Jeong, J. Y. Kim, E. Kim, and I. W. Chung, "Effects of newer antipsychotic drugs on apomorphine-induced climbing behavior in mice," *Korean Journal of Psychopharmacology*, vol. 16, no. 6, pp. 455–461, 2005.

[43] N. A. Moore and M. S. Axton, "Production of climbing behaviour in mice requires both D1 and D2 receptor activation," *Psychopharmacology*, vol. 94, no. 2, pp. 263–266, 1988.

[44] D. C. Hoffman and H. Donovan, "Catalepsy as a rodent model for detecting antipsychotic drugs with extrapyramidal side effect liability," *Psychopharmacology*, vol. 120, no. 2, pp. 128–133, 1995.

[45] B. Bricker, D. Sampson, and S. Y. Ablordeppey, "Evaluation of the potential of antipsychotic agents to induce catalepsy in rats: assessment of a new, commercially available, semi-automated instrument," *Pharmacology Biochemistry and Behavior*, vol. 120, pp. 109–116, 2014.

[46] K. Åberg, D. E. Adkins, J. Bukszár et al., "Genomewide association study of movement-related adverse antipsychotic effects," *Biological Psychiatry*, vol. 67, no. 3, pp. 279–282, 2010.

[47] V. Castagné, P. C. Moser, and R. D. Porsolt, "Preclinical behavioral models for predicting antipsychotic activity," *Advances in pharmacology (San Diego, Calif.)*, vol. 57, pp. 381–418, 2009.

[48] A. Can, D. T. Dao, C. E. Terrillion, S. C. Piantadosi, S. Bhat, and T. D. Gould, "The tail suspension test," *Journal of Visualized Experiments : JOVE*, no. 59, Article ID e3769, 2012.

[49] B. Thierry, L. Stéru, P. Simon, and R. D. Porsolt, "The tail suspension test: ethical considerations," *Psychopharmacology*, vol. 90, no. 2, pp. 284-285, 1986.

[50] P. Santosh, R. Venugopl, A. S. Nilakash, S. Kunjbihari, and L. Mangala, "Antidepressant activity of methanolic extract of Passiflora foetida leaves in mice," *International Journal of Pharmacy and Pharmaceutical Sciences*, vol. 3, no. 1, pp. 112–115, 2011.

[51] F. Borsini and A. Meli, "Is the forced swimming test a suitable model for revealing antidepressant activity?" *Psychopharmacology*, vol. 94, no. 2, pp. 147–160, 1988.

Hindawi
Evidence-Based Complementary and Alternative Medicine
Volume 2017, Article ID 6834218, 7 pages
https://doi.org/10.1155/2017/6834218

Research Article

Flavonoid Composition and Biological Activities of Ethanol Extracts of *Caryocar coriaceum* Wittm., a Native Plant from Caatinga Biome

Daniela Ribeiro Alves,[1] Selene Maia de Morais,[1] Fernanda Tomiotto-Pellissier,[2] Milena Menegazzo Miranda-Sapla,[2] Fábio Roger Vasconcelos,[3] Isaac Neto Goes da Silva,[1] Halisson Araujo de Sousa,[4] João Paulo Assolini,[2] Ivete Conchon-Costa,[2] Wander Rogério Pavanelli,[2] and Francisco das Chagas Oliveira Freire[3]

[1] *Veterinarian Sciences Post Graduation Program, Ceará State University, Av. Dr. Silas Munguba 1700, Campus do Itaperi, 60714-903 Fortaleza, CE, Brazil*
[2] *Pathological Sciences Center, Londrina State University, Rodovia Celso Garcia Cid, PR 445, Km 380, Campus Universitário, 86057-970 Londrina, PR, Brazil*
[3] *Embrapa Agroindústria Tropical, Rua Dra. Sara Mesquita 2270, Planalto do Pici, 60511-110 Fortaleza, CE, Brazil*
[4] *Chemical Course, Ceará State University, Av. Dr. Silas Munguba 1700, Campus do Itaperi, 60714-903 Fortaleza, CE, Brazil*

Correspondence should be addressed to Selene Maia de Morais; selene.morais@uece.br

Received 29 April 2017; Accepted 24 July 2017; Published 7 September 2017

Academic Editor: Lucindo Quintans

Caryocar coriaceum fruits, found in Brazilian Cerrado and Caatinga, are commonly used as food and in folk medicine, as anti-inflammatory, bactericide, fungicide, leishmanicide, and nematicide. Due to the biological potential of this plant, this study focuses on the evaluation of antifungal and antileishmanial activities, including anticholinesterase and antioxidant tests, correlating with total phenols and flavonoids content. Peel extracts contain higher yield of phenols and flavonoids as analyzed by spectrophotometric methods. HPLC analysis of flavonoids revealed that isoquercitrin is the main flavonoid in both parts of the fruit, and peel extract showed the best antioxidant activity. In the inhibition of the acetylcholinesterase assay, both extracts demonstrate action comparable to physostigmine. The antimicrobial activity of extracts was evaluated against strains of *Malassezia* sp. and *Microsporum canis*, using the broth microdilution technique, in which the extracts showed similar MIC and MFC. The extracts present antileishmanial activity and low toxicity on murine macrophages and erythrocytes. Therefore, these results suggest a potential for the application of *C. coriaceum* fruit's ethanol extracts in the treatment against dermatophyte fungi and leishmaniasis, probably due to the presence of active flavonoids. Further in vivo studies are recommended aiming at the development of possible new pharmaceutical compounds.

1. Introduction

In veterinary care, some diseases are common in Brazil as fungal dermatophytosis and cutaneous/mucocutaneous leishmaniasis. Regarding fungal diseases, *Malassezia, Microsporum*, and *Trichophyton* genera are the main infectious agents of human and animal cutaneous mycoses [1, 2].

Leishmaniases are zoonosis caused by protozoa of the *Leishmania* genus with a wide range of clinical symptoms: cutaneous, mucocutaneous, and visceral [3]. In these parasitic diseases, humans and wild, synanthropic, and domestic mammals act as hosts and/or reservoirs of several *Leishmania* spp. [4].

Cutaneous/mucocutaneous leishmaniasis is usually characterized by chronic skin lesions and permanent scars with deformation of the infected area [5]. This disease presented more than 1 million cases reported in the last five years, with over 431 million people living in endemic areas at risk

of infection [3]. *Leishmania* spp. are pathogens that infect mainly macrophages, but also neutrophils and dendritic cells. The parasites are able to evade the microbicidal mechanism of these cells resulting in the different forms of disease, according to the *Leishmania* species [6–8].

Although both diseases present therapeutic options such as the azoderivatives for fungal treatment, especially ketoconazole and itraconazole and pentavalent antimonial drugs for leishmaniasis chemotherapy, these drugs present low efficacy and severe side effects as cardiotoxicity and hepatotoxicity [5]. Thus, many researchers have been trying to find safer plant-derived natural products to treat these diseases [6, 7, 9, 10].

The *Caryocar* genus, known popularly as Pequi, has a wide distribution and is represented in several Brazilian biomes such as Cerrado, the Atlantic Forest, Amazon, and Caatinga [11, 12]. The fruit pulp is largely used in food preparation, mainly with rice. The fruit pulp and seed oils of *Caryocar coriaceum* have been used in wound healing, as an anti-inflammatory agent, and for the treatment of diseases of the respiratory tract, including cough, bronchial affections, and asthma The fruit crude oil is also used on small skin wounds, in the form of compresses and massage, for treatment of rheumatic and muscular pains [13].

The *Caryocar* species is considered a promising medicinal product due to its bactericidal, fungicidal, leishmanicidal, and nematicidal activities [14, 15]. In this work, ethanol extracts of pulp and peel of *C. coriaceum* fruits were evaluated in relation to phenols and flavonoids content and biological activities such as antifungal and antileishmanial activities using different microorganisms from the previous work. Thus, in this study, dermatophyte fungi and *Leishmania amazonensis* parasites were used and the antioxidant and antiacetylcholinesterase activities were investigated, which support their antileishmanial and antifungal properties.

2. Materials and Methods

2.1. Chemicals. 2,2-Diphenyl-1-picrylhydrazyl (DPPH), 5,5′-dithiobis(2-nitrobenzoic acid) (DTNB), acetylthiocholine iodide (ATCI), and other reagents were acquired from Sigma Chemical Co. (St. Louis, MO, USA). Quercetin, isoquercitrin, and rutin were obtained from the seeds of the plant *Dimorphandra gardneriana* according to a previous report [16].

2.2. Preparation of Plant Extracts. Peel and pulp of *C. coriaceum* mature fruits were obtained at the Campus of the Ceará State University (lat.: −3.792222; long.: −38.556111), Fortaleza, Brazil. These *C. coriaceum* plants were submitted and identified by Prisco Bezerra Herbarium under the code EAC57060. The extracts were obtained by cold maceration with 96% ethanol, at 12 h cycle of light, without agitation for 7 days. Filtration of the supernatant and evaporation of the solvent at reduced pressure in a rotary evaporator led to crude ethanol extracts of Pequi fruit pulp and fruit peel.

2.3. Qualitative Determination of Chemical Constituents. The presence of secondary metabolites was detected by visual observation of color changes or precipitate formation reactions [17]. The reactions were conducted by the pH variation of ethanol extracts (with sodium hydroxide and sulfuric acid) to detect the presence of flavonols, flavanones, flavanonols, anthocyanins, and catechins; Lieberman-Burchard reagent (acetic anhydride plus sulfuric acid) is used for steroids (green color) or triterpenes (red color) characterization. Ferric chloride solution was used to detect phenols and tannins, and Shinoda reagent (concentrated HCl and granulated magnesium ribbon) was used to detect flavonoids and xanthones (a pink to red color); when shaking the dry extract with distilled water, if permanent foam is formed, this characterizes the presence of saponins.

2.4. Quantitative Determination of Total Phenol Content. Total phenol content was quantitatively determined using Folin–Ciocalteu's method [18]. The absorbance was measured at 750 nm using a UV/Vis spectrophotometer. The blue color indicated the presence of phenol content. The results are expressed in mg of gallic acid equivalent per gram of extract (mg GAE/g) based on a linear equation for a standard curve prepared with gallic acid.

2.5. Quantitative Determination of Total Flavonoid Content. The flavonoid content was determined using Funari and Ferro's method [19]. The absorbance was measured at 425 nm. Yellow color indicated the presence of flavonoids. The flavonoid content is expressed in mg of quercetin equivalent per gram of extract (mg EQ/g), on a linear equation for a standard curve prepared with quercetin.

2.6. Characterization of Flavonoids by HPLC. The identification and quantification of flavonoids on EEPUCC and EEPECC were performed by high-performance liquid chromatography (HPLC) with Shimadzu liquid chromatograph coupled to an SCL-10AVP controller system, UV-Vis detector SPD-10AVP, and isocratic pump LC-10ATVP. The LC Solution software was used to record the chromatograms and measure peak areas. The column used was a Shimadzu analytical CLC-ODS M (C-18) of 25 cm. The calibration curve was constructed using the standards rutin, isoquercitrin, and quercetin, injected at different concentrations (0.25, 0.05, 0.025, and 0.005 mg/mL) into the liquid chromatograph. The flow rate was 1.8 mL per minute for quercetin and 1.25 mL per minute for rutin at a wavelength of 350 nm a mobile phase composed of acetonitrile and H_3PO_4 buffer at pH 2.8 (20% : 80%). The linear regression equation was obtained by using the Microsoft Office Excel 2010 program. The chromatographic profiles of flavonoids rutin, quercetin, and isoquercitrin, the chosen standards, were obtained by preparing ethanol solutions at a concentration of 0.5 mg/mL and then injecting them into the high-performance liquid chromatograph. As the mobile phase, the same solution was used for calibration curve at the same wavelength and flow rate of 1.80 mL per minute.

2.7. Assessment of Antioxidant Activity via 2,2-Diphenyl-1-picrylhydrazyl (DPPH) Radical Reduction. Antioxidant activity of EEPUCC and EEPECC was assessed using a previously

described method [20], with some modifications. Several dilutions of the samples and positive control (rutin) in methanol were prepared to obtain the concentrations of 100, 50, 5, and 1 μg/mL. Methanol was used as a negative control. The absorbances were measured at 515 nm using a UV-Vis spectrophotometer. The percentage inhibition (PI) was calculated according to the following equation: PI% = [(absorbance of DPPH − absorbance of the extract)/absorbance of DPPH] × 100. The IC_{50} values were determined by linear regression of the plotted data followed by Tukey's test for multiple comparisons.

2.8. Inhibition of Acetylcholinesterase (AChE) Enzyme. The AChE inhibitory activity was qualitatively assessed using Ellman's [21] methodology, adapted for thin layer chromatography by Rhee et al. [22]. Solutions of the fruit pulp and peel at the concentration of 2.0 mg/mL were applied to TLC aluminum chromatoplate silica gel 60 F254 (Merck®) forming 2 mm spots. The plate was sprayed with 5,5′-dithiobis(2-nitrobenzoic acid) (DTNB)/acetylthiocholine iodide (ATCI) reagent (1 mM DTNB and 1 mM ATCI in 50 mM Tris-HCl, pH 8) until the silica was carefully saturated with the solvent. Plates were allowed to dry and then 5 U/mL of AChE enzyme solution was sprayed. A yellow background was observed, with white zones, indicating the presence of AChE enzyme inhibiting compounds. These zones became visible after 5 min. The zones were observed, measured, and recorded. Physostigmine was used as standard.

2.9. Fungicidal Assay. The minimum concentration capable of inhibiting 100% fungi growth (MIC) was determined by the dilution technique, according to CLSI method [23]. Six strains were tested (3 *Malassezia* spp.: MA239, MA276, and MA355; 3 *Microsporum canis*: MC017/15, MC029/15, and MC115/15), isolated from infected domestic animals, identified and stocked at the Microbiology Section, and kindly donated by Vettings®. The spore suspension solution for initial inoculation was prepared from filamentous fungi cultivated on potato dextrose agar (PDA) and incubated at a temperature of 28 ± 2°C for 7 days. The spore count was performed in a Neubauer chamber to achieve the concentration of 10^5 to 10^6 cells. In laminar flow cabinet, 100.0 μL of the RPMI medium was distributed into each well of a 96-well microplate. 100.0 μL of EEPUCC and EEPECC extracts was added and serial dilution was performed from 2500.0 to 2.44 μg/mL. Finally, 50.0 μL of the fungal suspension was added to all wells except the lines intended for the control of the sterile medium. The readings were taken by checking the MIC, with the aid of stereoscopically checking the lowest concentration of the samples capable of inhibiting 100% of the growth of the microorganism, after 5 days of incubation. The plates were also inspected under an inverted microscope to ensure growth of the controls and sterile conditions. The minimal fungicide concentration (MFC), considered as the minimum concentration capable of killing 100% of fungi, was measured by transferring 50.0 μL from wells without fungal growth and inoculating on PDA. MFC was established according to the fungus growth after incubation under the same conditions for 5 days.

2.10. Leishmania Parasite. *Leishmania (Leishmania) amazonensis* (MHOM/BR/1989/166MJO) was used in promastigote forms, in the stationary growth phase (day 5 of culture). The parasites were obtained from popliteal lymph nodes of *L. amazonensis*-infected BALB/c mice and maintained in 199 culture medium (Gibco) supplemented with 10% fetal bovine serum (FBS) (Gibco), 10 mM HEPES Biological Buffer (AMRESCO), 0.1% human urine, 0.1% L-glutamine (SYNTH), penicillin (10 U/mL) and streptomycin (10 μg/mL) (Gibco), and 10% sodium bicarbonate (SYNTH). Cell cultures were incubated at 25°C in 25 cm^2 flasks. All parasites were from a culture that was serially passed for less than 5 weeks.

2.11. Viability of L. amazonensis Promastigote Forms. The direct effect of EEPUCC and EEPECC extracts against *L. amazonensis* was assessed in 24-well microtiter plates, each well containing 1000 μL of 199 supplemented culture medium with 1×10^6 promastigote forms in stationary phase with or without the extracts of interest at final concentrations of 0.1, 0.05, and 0.025 mg/mL. Viable promastigote concentration was determined by Neubauer chamber counting after 24, 48, and 72 h of treatment. In the stock solutions of extracts, 0.01% dimethyl sulfoxide (DMSO) (Gibco) was used as vehicle. Untreated parasites and vehicle only (0.01% DMSO) were included as negative controls. The plates were also inspected under an inverted microscope to ensure growth of the controls and sterile conditions. The 50% inhibitory concentration (IC_{50}) was determined by nonlinear regression analysis of the obtained data.

2.12. Animals. BALB/c mice weighing approximately 25–30 g and aged 6–8 weeks were used, according to protocols approved by the ethics committee of Londrina State University, which approved the protocol for animal use (13134.2016.62).

2.13. Peritoneal Macrophages Viability Assay. The viability of peritoneal macrophages treated with EEPUCC and EEPECC extracts was evaluated using the 3-(4,5-dimethylthiazol-2-yl)-2,5-diphenyltetrazolium bromide (MTT) assay as previously described by Mosmann [24]. BALB/c peritoneal macrophages (5×10^5 U/mL) were cultured in 24-well plates with 500 μL of 199 medium for 2 h for adherence at 37°C and 5% CO_2. The cells were washed with PBS and then adherent cells were incubated with different concentrations of extracts (2.5–0.025 mg/mL) or with vehicle (0.1% DMSO) and maintained in culture for 24 h at 37°C and 5% CO_2. After incubation with extracts, the macrophages were washed with PBS and MTT was added at a final concentration of 5 μg/mL in each well, followed by incubation for 4 h at 37°C/5% CO_2. The MTT formazan product was solubilized with 300 μL of DMSO, and plates were read at 570 nm in a spectrophotometer. The 50% cytotoxicity concentration

(CC_{50}) was determined by nonlinear regression analysis of the obtained data.

2.14. Selectivity Index (SI). The degree of selectivity of EEPUCC and EEPECC extracts was expressed as SI = IC_{50} of extracts on macrophages/IC_{50} of the same extract on promastigotes.

2.15. Hemolytic Assay. Blood from healthy subjects was collected in a heparinized vacuum tube, and the erythrocytes were washed 3 times with PBS (centrifugation at 1000 rpm for 10 minutes). A 2% red cell suspension was prepared with PBS. Sample concentrations of 0.5, 0.25, 0.1, and 0.025 μg/mL were incubated with 2% red cells in PBS in the proportion of 1 : 1 in 96-well plates for 3 hours at 37°C/5% CO_2. PBS was used as a negative control, and distilled water was used to control hemolysis. The plates were centrifuged at 1000 rpm for 10 minutes, and supernatants were collected and analyzed for absorbance reading at 550 nm. This experiment was performed in duplicate and repeated three times.

2.16. Statistical Analysis. All of the experiments were performed in triplicate, and the results were expressed as standard error of the mean (SEM) to leishmanicidal analysis and as the mean ± standard deviation (SD) to other analyses. Results were contrasted with a negative and a positive control. The differences between the values were examined using analysis of variance (ANOVA) followed by Tukey's test for multiple comparisons and a p value < 0.05 was considered to be statistically significant. Data were analyzed in GraphPad Prism 6.01 software for Windows (GraphPad Software, San Diego, California, USA).

3. Results and Discussion

In the recent decades, development of synthetic drugs caused disaffection towards natural products as an attractive resource for searching for new chemotherapy compounds. However, the emergence of some limitations in the use of synthetic drugs as high toxicity, side effects, and elevated costs caused a shift in the situation and interest in the field of ethnobotanical research [20, 25, 26].

Plant-derived natural products are valuable sources in traditional medicine because they have fewer side effects, low cost, and high availability [27]. Indeed, numerous plant-derived bioactive compounds that display a wide variety of pharmacological effects include quercetin and its glucosides rutin and isoquercitrin, common flavonoids, which display antifungal and antileishmanial activities [16, 28, 29].

The *C. coriaceum* extracts stand out due to the high antioxidant action of the pulp, which contains carotenoids and phenolic compounds [30]. In phytochemical qualitative screening, the extracts of *C. coriaceum* showed similar constituents for both extracts presenting the secondary metabolites alkaloids, steroids, saponins, tannins, phenols, and flavonoids, in part corroborating with Araruna et al. [31]. Catechins were present only in pulp extract. In phytochemical tests, both extracts showed positive results to flavonoids, which were analyzed by HPLC, and quercetin, rutin, and isoquercitrin were found as main flavonoids present in the extracts.

The fruit peel extract displays a higher amount of phenols, with 55.617 ± 7.92 mg of gallic acid equivalent (GAE)/g of extract (mg GAE/g) and flavonoids with 3.881 ± 0.10 mg quercetin equivalent (QE)/g of extract (mg QE/g) when compared with fruit pulp extract which showed 24.539 ± 3.55 GAE/g plus 1.334 ± 0.21 QE/g, as observed in Table 1.

Quantification of total phenols and flavonoids by spectrophotometry and HPLC analysis for identification of the main flavonoids from these extracts is shown in Table 1. Isoquercitrin bioavailability was shown to be higher than the other two flavonoids. Rutin is present in a lower amount in both extracts and quercetin was present only in the pulp extract.

The presence of active flavonoids in both extracts explains the biological activities found in this study, which was based on *in vitro* and *in silico* predictions with natural products [32]. Antioxidants could have a pathogen neutralizing action, directly by scavenging ROS or indirectly by activating pathways that promote ROS degradation [27].

Table 2 displays the results of the extracts and respective standard substances' biological activities, as antioxidant, AChE inhibition, and antifungal. The potential of the pulp extract and peel extracts to inhibit free radicals was evaluated. Radical inhibition was higher with increasing concentration of the extracts when compared to the standard (rutin). Comparing *C. coriaceum* fruit part extracts, the pulp presented significantly higher antioxidant potential. Regarding the capacity of scavenging free radicals of the extracts, pulp and peel of *C. coriaceum* fruit showed a better action than that obtained in other plant extracts reported by Moura et al. [33], Penido et al. [20], and Morais et al. [10].

Other studies connected antioxidant mechanisms of action with *in vitro* fungicidal activities of natural compounds [14]. By Holetz's antimicrobial activity index [25], all the extracts can be classified as good antifungals. The ethanol extracts of *C. coriaceum* fruit were effective against six animal pathogenic strains: three of the genus *Malassezia* sp. and three strains of *M. canis*. The MIC and MFC varied between 39.1 and 4.1 in tested microorganisms' strains. However, all the extracts have better results, when compared to other extracts or isolated compounds elsewhere [7, 8].

Against *M. canis*, the tested extracts obtained better results. Peel extract exhibits greater results than pulp extract that was also considered with high activity. Against *Malassezia* spp., both extracts exhibit the same MFC and peel extract demonstrates better MIC than pulp extract (Table 2).

With regard to antiacetylcholinesterase activities, the inhibition zone of pulp was greater than peel extract and similar to the control, physostigmine, which means good AChE inhibition. Other studies [16] determined that the isolated flavonoids found and quantified in this study have a remarkable antiacetylcholinesterase activity and indicate this assay as appropriate to antileishmanial studies. This result indicates that probably there is a direct relationship between inhibition of acetylcholinesterase and antileishmanial action.

Regarding leishmaniasis, the interaction between parasites and host immune cells leads to an inflammatory

Table 1: Quantification of total phenols and flavonoids by spectrophotometry and main flavonoids by high-performance liquid chromatography (HPLC) of *Caryocar coriaceum* fruit ethanol extracts.

Samples	Total phenols (mg GAE/g)	Total flavonoids (mg QE/g)	Quercetin	Rutin	Isoquercetin
Pulp extract	$24.539^{b} \pm 3.55$	1.334 ± 0.21^{b}	1.965^{a}	5.025^{a}	47.665^{b}
Peel extract	$55.617^{a} \pm 7.92$	3.881 ± 0.10^{a}	—	4.169^{b}	129.198^{a}

Similar small letters indicate significant similarities between rows ($p < 0.0001$, according to ANOVA followed by Tukey's test). —: no result.

Table 2: Biological activities of *C. coriaceum* extracts.

Extracts	Antioxidant activity (IC_{50} μg/mL)	AChE inhibition (mm)	Antifungal assay *Malassezia* spp. MFC/MIC	Antifungal assay *Microsporum canis* MFC/MIC
Pulp	49.4 ± 0.29^{c}	9.0^{a}	$39.06 \pm 1.7^{c}/19.53 \pm 1.08^{b}$	$9.77 \pm 0.12^{b}/4.88 \pm 0.09^{a}$
Peel	25.5 ± 0.26^{b}	8.5^{b}	$39.06 \pm 0.18^{c}/9.77 \pm 0.03^{a}$	$4.88 \pm 0.06^{a}/4.88 \pm 0.03^{a}$
Rutin	13.7 ± 0.25^{a}	—	—	—
Physostigmine	—	9.0^{a}	—	—

Similar letters indicate significant similarities between rows ($p < 0.05$, according to ANOVA followed by Tukey's test). For MFC/MIC assays, similar letters indicate significant similarities between rows ($p < 0.0001$, according to ANOVA followed by Tukey's test). Rutin: positive control to antioxidant activity. Physostigmine: positive control to AChE inhibition. —: not performed.

Table 3: Inhibitory concentration of *Caryocar coriaceum* fruit extracts on promastigote forms of *L. amazonensis* (IC_{50}) after 24, 48, and 72 h of treatment, toxicity to peritoneal macrophages (CC_{50}), and selectivity index (SI) after 24 h of treatment. Values are expressed in μg/mL.

	24 h IC_{50}	CC_{50}	SI	48 h IC_{50}	72 h IC_{50}
Pulp extract	30 ± 5.0^{a}	253 ± 42.0^{b}	8.43^{b}	39 ± 8.0	17 ± 7.0
Peel extract	38 ± 13.0^{a}	454 ± 11.0^{a}	11.94^{a}	31 ± 9.0	22 ± 3.0
Pentamidine [9]	23.71^{a} (18.44–30.50)	17.90^{c} (0.02–0.03)	0.75^{c}		
Glucantime [17]	13.95 (± 2.06)^{a}				

Data represent the mean ± SEM of at least three independent experiments performed in triplicate. CC_{50}: cytotoxic concentration of 50% of macrophages (μg/mL). IC_{50}: inhibitory concentration of 50% of promastigote forms (μg/mL). SI: selectivity index = CC_{50}/IC_{50}. Similar letters indicate significant similarities between rows ($p \leq 0.05$, according to ANOVA followed by Tukey's test).

response essential for parasite control. However, an exacerbated proinflammatory response may cause tissue damage, resulting in lesion formation observed in cutaneous leishmaniasis [34, 35]. On the other hand, the lack of an effective inflammatory response may promote increased parasite burden [26]. In this scenario, the antioxidant effect of *C. coriaceum* extracts can control the inflammatory response being ideal for an effective control of the disease.

Table 3 displays the inhibitory concentration of *Caryocar coriaceum* fruit extracts on promastigote forms of *L. amazonensis* (IC_{50}) after 3 days of treatment, toxicity to peritoneal macrophages (CC_{50}), and selectivity index (SI) after 24 h of treatment. IC_{50} in parasite proliferation was shown to be similar after 24 h of treatment for both extracts and the standards. At 48 h, there was yet no statistical difference between the treatments. A dose-dependent reaction was found after 72 h with IC_{50} results reduced.

To test the selectivity of pulp and peel extracts, murine macrophages were treated with different concentrations of extracts and the viability of these cells was assessed by the MTT reduction. Pulp extract induced 50 percent of cytotoxicological effect (CC_{50}) in peritoneal macrophages at lower concentration than peel at 24 h, but both extracts presented statistically the lowest toxicity compared to the standard (pentamidine). In addition, pulp extract presented a good predilection of the extract by the parasites, being better selective than pentamidine. Then, the *C. coriaceum* extracts had higher toxicity to *L. amazonensis* promastigote forms and demonstrated lower cytotoxicity on murine macrophages and erythrocytes and statistically better results than demonstrated in previous studies for pentamidine and glucantime as standards [9, 17].

Another way to evaluate the cytotoxicity of extracts is by the ability to cause hemolysis in human erythrocytes. As shown in Table 4, the pulp and peel extracts showed low toxicity. The lowest concentration determines hemolytic activities at 0.909 ± 0.746 and 0.616 ± 0.224 per cent, respectively, though with very low levels of hemolysis. The

Table 4: Hemolytic activity (%) of *Caryocar coriaceum* fruit extracts (mg/mL).

	0.025	0.05	0.1	0.25	0.5
Pulp extract	0.909 (±0.746)	1.300 (±0.341)	1.295 (±0.564)	2.406 (±1.206)	8.777 (±4.102)
Peel extract	0.616 (±0.224)	1.229 (±0.740)	0.925 (±0.315)	3.068 (±1.368)	6.872 (±3.056)

Data represent the mean ± SEM of at least three independent experiments performed in triplicate. Data were normalized to the positive control (distilled water).

C. coriaceum fruit extracts presented low hemolytic activity, and concentrations of 0.1, 0.05, and 0.025 μg/mL were not able to cause significant hemolysis.

4. Conclusions

The secondary metabolites produced by *C. coriaceum* are potentially bioactive substances acting as antifungal and antileishmanial agents, mainly by scavenging free radicals and anticholinesterase mechanisms. The flavonoids quercetin, rutin, and isoquercitrin are important indicators of these activities. The results obtained in this study corroborate the potential of these plant species and may form the basis for new antifungal and antileishmanial agents. Nevertheless, further studies are necessary for the isolation and characterization of other substances and *in vivo* studies should be performed to detect the bioavailability of these extracts, aiming at the development of possible new pharmaceutical products.

Conflicts of Interest

All the authors declare that there are no financial/commercial conflicts of interest.

Acknowledgments

The authors are grateful to the Conselho Nacional de Desenvolvimento Científico e Tecnologico (CNPq) for a fellowship to the first author, to Empresa Brasileira de Pesquisa Agropecuária (EMBRAPA), to Universidade Estadual de Londrina, to Universidade Estadual do Ceará (Núcleo de Pesquisa em Sanidade Animal, NUPESA), and to Vettings for laboratory facilities and supplying drugs and microorganisms.

References

[1] D. M. Hawkins and A. C. Smidt, "Superficial fungal infections in children," *Pediatric Clinics of North America*, vol. 61, no. 2, pp. 443–455, 2014.

[2] M. Zahur, A. Afroz, U. Rashid, and S. Khaliq, "Dermatomycoses: challenges and human immune responses," *Current Protein and Peptide Science*, vol. 15, no. 5, pp. 437–444, 2014.

[3] WHO/Department of Control of Neglected Tropical Diseases, "Leishmaniasis in high-burden countries: an epidemiological update based on data reported in 2014", *Weekly Epidemiological Record*, vol. 22, no. 91, pp. 285–296, 2016.

[4] R. M. Cardoso, N. N. S. L. de Ara, and G. A. S. Romero, "Expanding the knowledge about Leishmania species in wild mammals and dogs in the Brazilian savannah," *Parasites Vectors*, vol. 8, no. 1, p. 171, 2015.

[5] M. N. Saridomichelakis and A. F. Koutinas, "Cutaneous involvement in canine leishmaniosis due to *Leishmania infantum* (syn. L. chagasi)," *Veterinary Dermatology*, vol. 25, no. 2, pp. 61–e22, 2014.

[6] F. C. M. Rondon, C. M. L. Bevilaqua, M. P. Accioly et al., "In vitro effect of Aloe vera, Coriandrum sativum and Ricinus communis fractions on Leishmania infantum and on murine monocytic cells," *Veterinary Parasitology*, vol. 178, no. 3-4, pp. 235–240, 2011.

[7] B. V. Soares, S. M. Morais, and R. O. S. Fontenelle, "Antifungal activity of plant extracts against *Microsporum canis* and *Candida spp*," *Boletín Latinoamericano y del Caribe de Plantas Medicinales* y *Aromáticas*, vol. 14, no. 4, pp. 263–272, 2015.

[8] P. Torabzadeh and P. Panahi, "Evaluation of antifungal activity of Physalis alkekengi L. extracts on Microsporum canis, Candida albicans, Trichophyton mentagrophytes and Nocardia asteroids," *Middle East Journal of Scientific Research*, vol. 13, no. 7, pp. 926–929, 2013.

[9] A. A. S. Silva, S. M. Morais, M. J. C. Falcão et al., "Activity of cycloartane-type triterpenes and sterols isolated from Musa paradisiaca fruit peel against Leishmania infantum chagasi," *Phytomedicine*, vol. 21, no. 11, pp. 1419–1423, 2014.

[10] M. L. Morais, A. C. Silva, C. R. Araújo, E. A. Esteves, and N. A. Dessimoni-Pinto, "Determinação do potencial antioxidante in vitro de frutos do Cerrado brasileiro," *Revista Brasileira de Fruticultura*, vol. 35, no. 2, pp. 355–360, 2013.

[11] L. S. Carvalho, K. F. Pereira, and E. G. Araújo, "Características botânicas, efeitos terapêuticos e princípios ativos presentes no pequi (*Caryocar brasiliense*)," *Arquivos de Ciências da Saúde da UNIPAR*, vol. 19, no. 2, pp. 147–157, 2015.

[12] J. Ascari, J. A. Takahashi, and M. A. D. Boaventura, "The phytochemistry and biological aspects of caryocaraceae family," *Revista Brasileira de Plantas Medicinais*, vol. 15, no. 2, pp. 293–308, 2013.

[13] M. L. M. de Oliveira, D. C. S. Nunes-Pinheiro, A. R. Tomé et al., "In vivo topical anti-inflammatory and wound healing activities of the fixed oil of Caryocar coriaceum Wittm. seeds," *Journal of Ethnopharmacology*, vol. 129, no. 2, pp. 214–219, 2010.

[14] W. d. Paula-Ju, F. H. Rocha, L. Donatti, C. M. Fadel-Picheth, and A. M. Weffort-Santos, "Leishmanicidal, antibacterial, and antioxidant activities of Caryocar brasiliense Cambess leaves hydroethanolic extract," *Revista Brasileira de Farmacognosia*, vol. 16, pp. 625–630, 2006.

[15] X. S. Passos, S. Da Costa Santos, P. H. Ferri et al., "Antifungal activity of Caryocar brasiliensis (*caryocaraceae*) against Cryptococcus neoformans," *Revista da Sociedade Brasileira de Medicina Tropical*, vol. 35, no. 6, pp. 623–627, 2002.

[16] N. S. Vila-Nova, S. M. Morais, M. J. C. Falcão et al., "Leishmanicidal and cholinesterase inhibiting activities of phenolic compounds of *Dimorphandra gardneriana* and *Platymiscium floribundum*, native plants from Caatinga biome," *Pesquisa Veterinaria Brasileira*, vol. 32, no. 11, pp. 1164–1168, 2012.

[17] A. A. S. Silva, J. de, B. Alexandre, and L. G. Vieira, "Estudo fitoquímico e atividades leishmanicida , anticolinestarásica e

antioxidante de extratos de *Annona glabra*L. (araticum panã)," *Journal of Applied Pharmaceutical Science*, vol. 36, no. 2, pp. 189–194, 2015.

[18] C. M. Sousa, H. R. Silva, G. M. Jr. Vieira et al., "Fenóis totais e atividade antioxidante de cinco plantas medicinais," *Química Nova*, vol. 30, no. 2, pp. 351–355, 2007.

[19] C. S. Funari and V. O. Ferro, "Análise de própolis," *Ciencia e Tecnologia de Alimentos*, vol. 26, no. 1, pp. 171–178, 2006.

[20] A. B. Penido, S. M. De Morais, A. B. Ribeiro et al., "Medicinal plants from northeastern Brazil against alzheimer's disease," *Evidence-Based Complementary and Alternative Medicine*, vol. 2017, pp. 1–7, 2017.

[21] G. L. Ellman, K. D. Courtney, V. Andres Jr., and R. M. Featherstone, "A new and rapid colorimetric determination of acetylcholinesterase activity," *Biochemical Pharmacology*, vol. 7, no. 2, pp. 88–95, 1961.

[22] I. K. Rhee, M. van de Meent, K. Ingkaninan, and R. Verpoorte, "Screening for acetylcholinesterase inhibitors from Amaryllidaceae using silica gel thin-layer chromatography in combination with bioactivity staining," *Journal of Chromatography A*, vol. 915, no. 1-2, pp. 217–223, 2001.

[23] 3nd ed Clinical and Laboratory Standards Institute, *Clinical and Laboratory Standards Institute (CLSI) Reference Method for Broth Dilution Antifungal Sucscetibility Testing of Yeasts Approved Standard M27-A3*. Wayne, Pensilvanya, 2008.

[24] T. Mosmann, "Rapid colorimetric assay for cellular growth and survival: application to proliferation and cytotoxicity assays," *Journal of Immunological Methods*, vol. 65, no. 1-2, pp. 55–63, 1983.

[25] F. B. Holetz, G. L. Pessini, N. R. Sanches, D. A. G. Cortez, C. V. Nakamura, and B. P. Dias Filho, "Screening of some plants used in the Brazilian folk medicine for the treatment of infectious diseases," *Memorias do Instituto Oswaldo Cruz*, vol. 97, no. 7, pp. 1027–1031, 2002.

[26] I. A. Rodrigues, A. M. Mazotto, V. Cardoso et al., "Natural products: insights into leishmaniasis inflammatory response," *Mediators of Inflammation*, vol. 2015, Article ID 835910, 12 pages, 2015.

[27] L. G. Rocha, J. R. G. S. Almeida, R. O. Macêdo, and J. M. Barbosa-Filho, "A review of natural products with antileishmanial activity," *Phytomedicine*, vol. 12, no. 6-7, pp. 514–535, 2005.

[28] D. G. Valadares, M. C. Duarte, J. S. Oliveira et al., "Leishmanicidal activity of the Agaricus blazei Murill in different Leishmania species," *Parasitology International*, vol. 60, no. 4, pp. 357–363, 2011.

[29] A. M. Metwally, A. A. Omar, F. M. Harraz, and S. M. El Sohafy, "Phytochemical investigation and antimicrobial activity of Psidium guajava L. leaves," *Pharmacognosy Magazine*, vol. 6, no. 23, pp. 212–218, 2010.

[30] R. Roesler, L. C. Carrasco, and R. B. Holanda, "Antioxidant activity of cerrado fruits," *Ciência e Tecnologia de Alimentos*, vol. 27, no. 1, pp. 53–60, 2007.

[31] M. K. A. Araruna, K. K. A. Santos, J. G. M. Da Costa et al., "Phenolic composition and in vitro activity of the Brazilian fruit tree Caryocar coriaceum Wittm.," *European Journal of Integrative Medicine*, vol. 5, no. 2, pp. 178–183, 2013.

[32] A. C. F. Salgueiro, V. Folmer, H. S. da Rosa et al., "In vitro and in silico antioxidant and toxicological activities of Achyrocline satureioides," *Journal of Ethnopharmacology*, vol. 194, pp. 6–14, 2016.

[33] L. R. Moura, A. C. Martins, L. A. Vaz et al., "Extrato hidroalcoolico da casca do pequi (Caryocar brasiliense) em ratos submetidos à aplicação de doxorrubicina," *Ciência Rural*, vol. 43, no. 1, pp. 100–106, 2013.

[34] C. da Silva Santos, S. Attarha, R. K. Saini et al., "Proteome profiling of human cutaneous leishmaniasis lesion," *The Journal of Investigative Dermatology*, vol. 135, no. 2, pp. 400–410, 2014.

[35] C. D. S. Santos, V. Boaventura, C. Ribeiro Cardoso et al., "$CD8^+$ granzyme B^+-mediated tissue injury vs. $CD4^+$ $IFN\gamma^+$ -mediated parasite killing in human cutaneous leishmaniasis," *Journal of Investigative Dermatology*, vol. 133, no. 6, pp. 1533–1540, 2013.

Hindawi
Evidence-Based Complementary and Alternative Medicine
Volume 2017, Article ID 3673197, 10 pages
https://doi.org/10.1155/2017/3673197

Research Article

A New Technique Using Low Volumes: A New Technique to Assess the Molluscicidal Activity Using Low Volumes

José Augusto Albuquerque Santos,[1] Viviane Paixão Cavalcante,[1] Leonardo da Silva Rangel,[1,2] João Claudio Vitória Atico Leite,[1,2] and Robson Xavier Faria[2]

[1]*Laboratório de Avaliação e Promoção da Saúde Ambiental, Instituto Oswaldo Cruz, Fiocruz, Av. Brasil 4365, Manguinhos, 21045-900 Rio de Janeiro, RJ, Brazil*
[2]*Laboratório de Toxoplasmose e outras Protozooses, Instituto Oswaldo Cruz, Fiocruz, Av. Brasil 4365, Manguinhos, 21045-900 Rio de Janeiro, RJ, Brazil*

Correspondence should be addressed to José Augusto Albuquerque Santos; santosjaa@gmail.com

Received 31 March 2017; Accepted 8 June 2017; Published 29 August 2017

Academic Editor: José C. T. Carvalho

Schistosomiasis is a disease endemic in several states of Brazil. The population control of the transmitter mollusks is done with Bayluscide WP 70®, in the control programs. OMS preconize molluscicidal assays using Becker with 500 mL of final volume, restringing the number of natural products and synthetic drugs to be tested in function of high quantity of material necessary. A new technique to assess the toxic effects for *Biomphalaria* sp. is the purpose of this work, for developing adaptation for this aquatic organism, using a low volume of test solution in 24-well plates. We used *Biomphalaria glabrata* (10–12 mm size) in a static system, consisting of the following components: Becker containing 10 snails or 24-well plates where snails were individualized for a volume of 2 mL per well for 24 and 48 hours. For the assays, we added aqueous solutions of Bayluscide WP 70, at a concentration of 1–5 mg/L, distilled water, and 1% dimethyl sulfoxide. Data were evaluated using Kappa's coefficient, Z factor validation, and comparison study. This technique to assess the toxic effect has proven to be a useful tool to detect lethal and sublethal effects, which could be used as a new evaluation protocol.

1. Introduction

Schistosomiasis is a disease of acute and chronic character, endemic in several states of Brazil. The population control of transmitter mollusks is done with niclosamide, a molluscicide recommended by the World Health Organization for control programs [1–3].

The biological response should be combined with chemical analyses and with toxicological assessments that are commonly performed using acute toxicity tests because they are relatively simple to perform and produce fast results. However, environmental contamination in natural ecosystems often occurs at concentrations well below the lethal concentration, which may cause sublethal effects [4].

A promising field investigation was done with the latex of *Euphorbia splendens* var. *hislopii* for the control of schistosomiasis vector mollusk in restricted lentic habitats [5, 6].

Usually, the molluscicidal activity is measured using Becker with 10 snails. The habitual volume used to do the assay is Becker with 250 mL [7], but there is a description of assays using a volume of 500 mL with 10 mollusks [8]. In both situations, the quantity of substance used is extremely high for the volume used. In consequence, a large number of compounds derived from crude plant extracts, such as fractions, isolated and purified substances, and essentially synthetic substances, are neglected due to the amount required to develop biological tests with mollusks, because, in the protocol preconized for OMS, these compounds should be tested in a high final volume. Then, the plant extract or synthetic drug concentration necessary to reach the final doses will be elevated to cause a molluscicidal activity.

In this scenario, the purpose of this work was to develop a new technique to assess the toxic effects of synthetic substances, extracts, fractions, and compounds isolated from

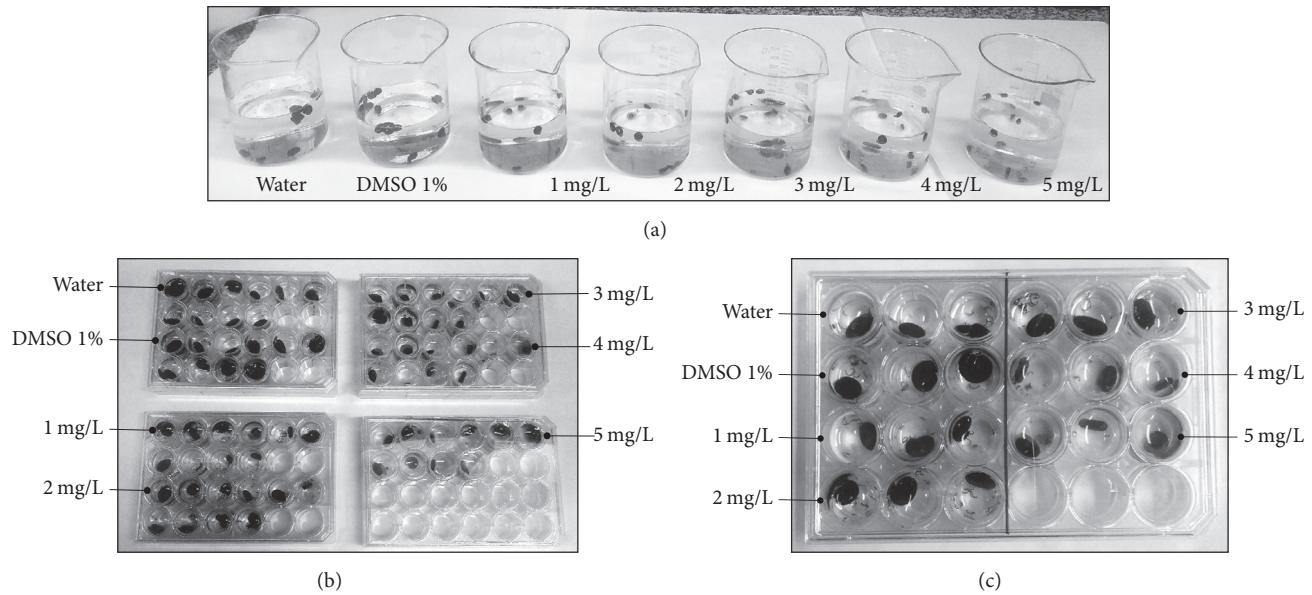

Figure 1: Molluscicidal evaluation models with niclosamide on *Biomphalaria glabrata* under laboratory conditions. (a) Becker of 1000 mL, containing the control groups, water, and 1% aqueous dimethylsulfoxide, 500 mL of aqueous solutions of niclosamide (1 mg/L, 2 mg/L, 3 mg/L, 4 mg/L, and 5 mg/L), and 10 *Biomphalaria glabrata*, with a size between 10 and 12 mm in diameter by Becker, created and kept in the laboratory. (b) Methodology with 24-well plates, containing the control groups and the doses of niclosamide and 1 snail per well with 2 mL of solution. Exposure of 10 animals per dose as described in (a). (c) Methodology with 24-well plates, containing the control groups and the doses of niclosamide and 1 mollusk per well with 2 mL of solution as described above. Exposure of 3 animals per dose.

plants of *Biomphalaria* sp. using low volumes for aquatic organisms, with the use of disposable 24-well plates.

2. Materials and Methods

2.1. Snails. For tests with adult *Biomphalaria glabrata* (i.e., 1818 Mollusca, Gastropoda, and Planorbidae) snails, the vector of *Schistosoma mansoni*, a static system was used, consisting of the following components: Becker containing 10 snails (Figure 1(a)) and 24-well plates with cover and the test substances in solution (Figure 1(b)).

We used *Biomphalaria glabrata* (10–12 mm standard size) from Sumidouro, Rio de Janeiro, RJ, maintained in aquaria with dechlorinated water and fed with lettuce in the laboratory.

2.2. Period of Exposure and Aqueous Solution Preparation. The *Biomphalaria glabrata* mollusks were exposed for 24 and 48 hours at different doses of niclosamide, in triplicate. We used the doses of 1 mg/L, 2 mg/L, 3 mg/L, 4 mg/L, and 5 mg/L of Bayluscide WP 70, initially dissolved in DMSO (dimethylsulfoxide) (experimental group), distilled water (negative control group), and 1% DMSO solution (negative control group).

2.3. Tests with the Mollusk. The final volume for each dose was 500 mL with Becker containing 10 snails. In the case of the 24-well plate, each well contained a final volume of 2 mL with one snail. In a condition, we used 10 wells with 10 mollusks for treatment (1 mollusk per well) and another 3 wells with 3 mollusks for treatment (1 mollusk per well). The observations were performed by analyzing morphological and functional criteria.

Each snail was individualized in 24-well plates, and a volume of 2 mL of the dose to be tested was added per well for the experimental group or controls and covered with a lid.

For the assays, *B. glabrata* were added to aqueous solutions of niclosamide, prepared in the laboratory at doses of 1 mg/L, 2 mg/L, 3 mg/L, 4 mg/L, and 5 mg/L (experimental group), distilled water (negative control group), and 1% DMSO solution (negative control group). To assess the toxic effect with a small volume of solution, the total number of animals used in triplicate tests was 21 snails and that used in decaplicate tests was 30 snails. During this period, the 24-well plates containing the doses were kept at room temperature and the animals were not fed. Each test was conducted for periods of 24 h, 48 h, and 72 h exposure. The tests were realized at least on three distinct days. The percentage of dead snails using a total number of 9 or 30 snails was calculated estimating the niclosamide molluscicidal activity as 100%. Triplicate or decaplicate assays were repeated on three distinct days. All other values were normalized in function niclosamide result.

2.4. Characterization of the Snails' Death. The deaths of the animals during the tests were confirmed by the change in shell color, absence of muscle contractions, whether the cephalopodal mass was distended in a distinguished fashion, and the presence of the middle *Miliammina*.

2.5. Extracts. The staff of the Natural Products Technology Laboratory FFU (LTPN) at the Jurubatiba Sandbank

National Park, in the municipality of Carapebus, RJ, collected aerial parts of the plants of concern: *Manilkara subsericea*. The herborization of the material was made by a botanist, Prof. Dr. Marcelo Guerra Santos, and exsiccated specimens were deposited at the Herbarium of the Teacher Training College (UERJ). The lab obtained authorization from SISBIO/ICMBio, code 51842449, to collect plants from Restinga Jurubatiba National Park.

In the LTPN, parts of stems and collected plants were dried in an oven at 40°C with forced ventilation for two days. Once dry, this material was triturated in a hammer mill and subjected to extraction by maceration or percolation using ethanol as a solvent. This was followed by filtration and concentration in a rotary evaporator, thereby obtaining the crude extract. Aliquots of the extracts thus obtained were further diluted in DMSO and then serial dilutions were made in distilled water for the experiments.

2.6. Ethics Approval and Consent to Participate (Ethics Statement). On July 2, 2015, representatives of the Oswaldo Cruz Institute's Ethics Committee on Animal Use (CEUA-IOC) met and decided on the basis of the documents presented; the committee decided on the need to issue a CEUA license. The project presented to this committee does not meet the requirements of Law 11794 of 2008 regulating animal research in Brazil. Article 2 of this law applies to animals of the species classified as Filo Chordata, sub-Vertebrata, subject to environmental legislation. Specifically, the project refers to the use of *Biomphalaria* sp. (Filo Mollusca) in tests of potent molluscicidal agents.

2.7. Data Analysis. The mortality rate was normalized to the maximum value using Microsoft Excel, and the results were plotted using the GraphPad Prism version 3.0 (San Diego, CA, USA). Data were expressed as mean ± SD (standard deviation), as indicated in the text. One-way Analysis of Variance (ANOVA), followed by Tukey's test, tested the statistical significance of the differences between means. A bicaudal $p < 0.05$ was considered significant.

The LC_{50} values were calculated by graphics from drug concentration versus lethality percentage using a dispersion analysis, which provides an equation for calculating the LCs.

We compare the efficacy of the methodologies using the coefficient "Kappa" (K) of Cohen that measures the nonrandom proportional agreement [9] of results independently of the laboratorial methodology used. A K value of 0.5 indicates a moderate level of agreement between the techniques. A value of $K > 0.80$ represents an excellent proportional agreement and not random. For this calculation, we used the program Win Episcope 2.0®.

3. Results

In Figure 2, we plotted niclosamide dose-response graphs against the number of dead mollusks treated for 24 and 48 hours. The linear regression analysis performed on the 24-well plate test with 10 animals, during a period of 24 and 48 hours, presented values of $R^2 = 0.5057$ and 0.5081 and standard deviations of 3.155 and 3.089, respectively. The regression analysis in the tests was considered significant, with p value < 0.0009 in both periods.

In the methodology using 24-well plates with 3 snails (1 mollusk per well), the linear regression presented values of $R^2 = 0.7014$ and 0.6665, with standard deviation of 0.7091 and 0.6711 for 24 and 48 hours, respectively. The regression analysis in the tests was considered significant, with p value < 0.0009 in both periods.

Additionally, in the Becker with 10 mollusks, the regression results were $R^2 = 0.4502$ and 0.5032, with deviation of 2.917 and 3.034 for 24 and 48 hours, respectively. The regression analysis in the tests was considered significant, with p value < 0.0009 and p value < 0.001 in the periods.

When we compared the results in the dose of 2% niclosamide among three methodologies for 24-hour of treatment, there was no statistical difference (Figure 3).

Regarding the results, we evaluated whether the optimized protocol reducing the volume and number of mollusks was comparable to the protocol with Becker or not. We compared the two protocols using Kappa's coefficient. Table 1 represents the number of dead mollusks collected in a standard assay after 24 or 48 hours of treatment, on 3 distinct days, using Becker with niclosamide concentrations in a final volume of 500 mL and 10 snails. In another assay, we treated individually 10 mollusks in wells with a final volume of 2 mL, also on three different days. Both assays were recorded until 48 hours, because after this time all mollusks were dead at all concentrations and in all protocols used. The values in the columns were used to do the contingence table to calculate Kappa's coefficient.

The strength of concordance, according to Landis and Koch [10], shows that the results of 24 and 48 hours for 1 mg/L niclosamide exhibited a moderate correlation. The dose of 2 mg/L showed a considerable association and all other doses presented perfect concordance (Table 1).

In Table 2, we compared Becker's protocol with the 24-well protocol containing 3 mollusks in a final volume of 2 mL. Exceptionally, the concordance between these protocols was more satisfactory for all doses. The results of 1 mg/L in 24 and 48 hours showed that a K value greater than 0.5 indicates a moderate to excellent level of agreement between the techniques. In the dose of 2 mg/L after 24 hours also, it was shown that a K value greater than 0.5 indicates a moderate to excellent level of agreement between the techniques and after 48 hours it was almost perfect. All other doses in the times of 24 and 48 hours exhibited an almost perfect correlation (Table 2).

When we compared the 24-well plate assays containing 10 or 3 snails, the low dose tested showed acceptable correlation after 24 hours and moderate correlation after 48 hours. In the dose of 2 mg/L, there was considerable correlation after 24 hours, but moderate correlation after 48 hours. In accordance with all correlations tests, in the doses ranging from 3 to 5 mg/L, there was almost perfect correlation (Table 3).

We evaluated the validation of the optimization using 3 mollusks in the 24-well plate, when we measured the Z factor. This coefficient also can be used to estimate the quality of assays in high throughput screening (HTS), which made it possible to use this factor with volume and number

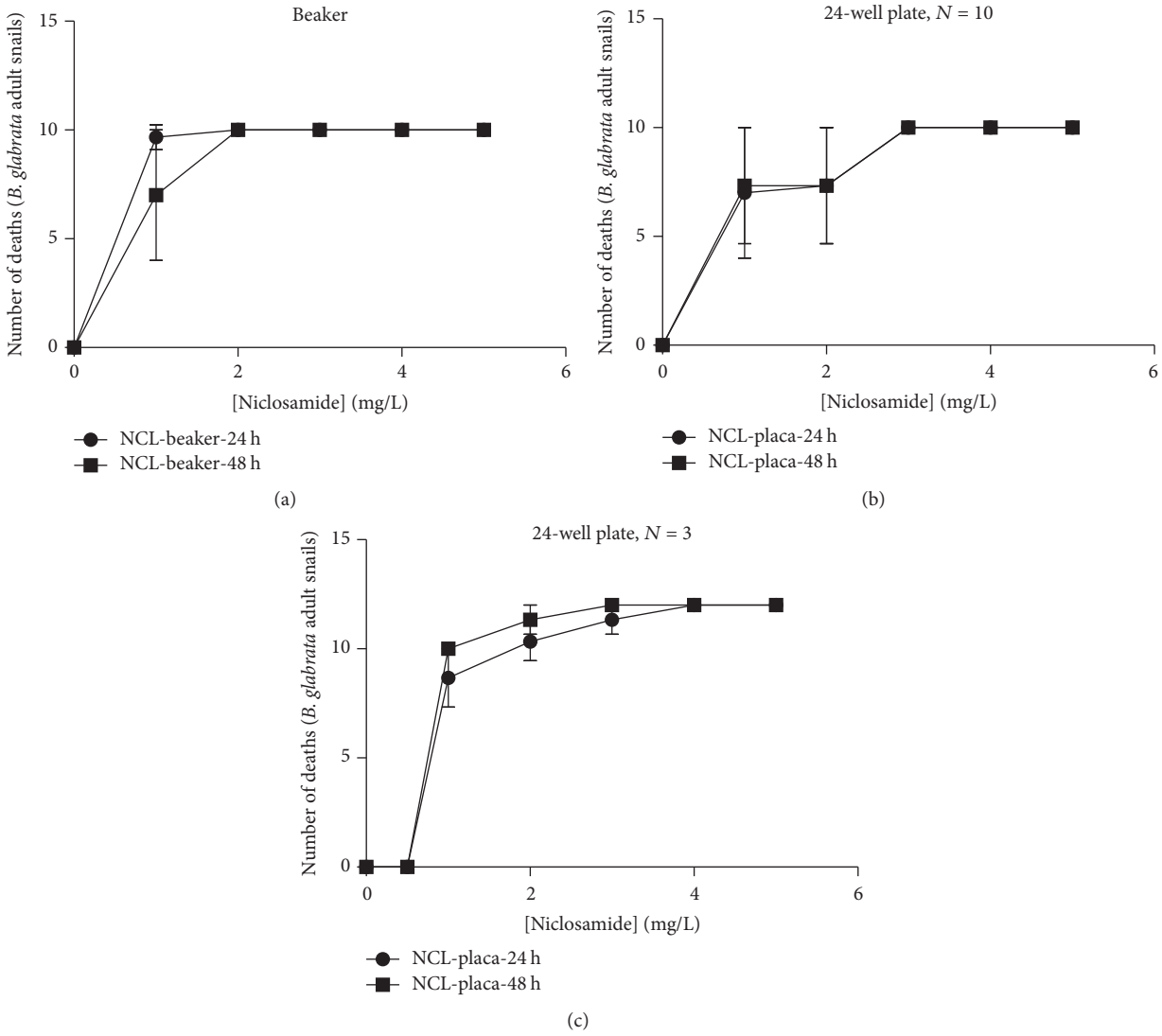

Figure 2: Niclosamide induced death of adult *B. glabrata* snails. (a) Dose-response graph representing niclosamide concentrations (24- or 48-hour stimulus) in the function of death of mollusks measured in the Becker methodology with 10 snails. (b) Dose-response graph representing niclosamide concentrations (24- or 48-hour stimulus) in the function of death of mollusks measured in the 24-well plate methodology with 10 snails. (c) Dose-response graph representing niclosamide concentrations (24- or 48-hour stimulus) in the function of death of mollusks measured in the 24-well plate methodology with 3 snails. The concentrations of the added blockers are given in the text. Experiments were performed for at least three independent days.

Table 1: Comparison between two protocols (Becker and 24-well plate) using Kappa's coefficient. $N = 10$.

Niclosamide concentrations (mg/L)	Becker $N = 10$ 24 h (number of dead snails)	24-well plate $N = 10$ 24 h (number of dead snails)	Becker $N = 10$ 48 h (number of dead snails)	24-well plate $N = 10$ 48 h (number of dead snails)	Kappa coefficient 24 h	Kappa coefficient 48 h
1	29	21	21	22	0.589	0.501
2	30	22	30	22	0.604	0.707
3	30	30	30	30	1	1
4	30	30	30	30	1	1
5	30	30	30	30	1	1

Table 2: Comparison between two protocols (Becker and 24-well plate) using Kappa's coefficient. $N = 3$.

Niclosamide concentrations (mg/L)	Becker $N = 10$ 24 h (number of dead snails)	24-well plate $N = 3$ 24 h (number of dead snails)	Becker $N = 10$ 48 h (number of dead snails)	24-well plate $N = 3$ 48 h (number of dead snails)	Kappa coefficient 24 h	Kappa coefficient 48 h
1	29	5	21	6	0.661	0.795
2	30	7	30	8	0.792	0.965
3	30	8	30	9	0.943	1
4	30	9	30	9	1	1
5	30	9	30	9	1	1

Table 3: Comparison between two protocols (24-well plate, $n = 10$ with $n = 3$) using Kappa's coefficient. $N = 3$.

Niclosamide concentrations (mg/L)	24-well plate $N = 10$ 24 h (number of dead snails)	24-well plate $N = 3$ 24 h (number of dead snails)	24-well plate $N = 10$ 48 h (number of dead snails)	24-well plate $N = 3$ 48 h (number of dead snails)	Kappa coefficient 24 h	Kappa coefficient 48 h
1	21	5	22	6	0.389	0.45
2	22	7	22	8	0.738	0.556
3	30	8	30	9	0.971	1
4	30	9	30	9	1	1
5	30	9	30	9	1	1

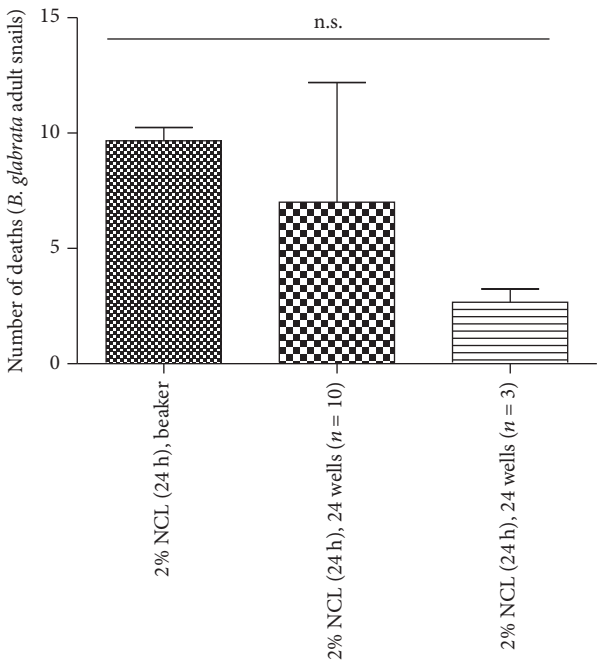

Figure 3: Comparison of the methodologies in relation to dose of 2% niclosamide against adult *B. glabrata* snails. Treatment for 24 hours with 2% niclosamide. These results are representative of three distinct days.

of mollusks reduced (Table 4). Then, we used each dose of niclosamide as a positive control to observe the quality of the assay in all doses. The Z factor for 1 mg/L was 0.92, 0.67, and 0.73 for the Becker, 24 wells with 10 mollusks, and 24 wells with 3 snails assays, respectively. According to Zhang et al. [11], all assays exhibited excellent performance. All other doses after 24 or 48 hours presented a Z factor with a value considered excellent and comparable to Becker's assay (Table 5).

We compared also the assays in relation to other reliability parameters calculated. In this case, we evaluated the sensitivity, specificity, positive predictive value (PPV), negative predictive value (NPV), and prevalence according to Watson and Petrie (2010). In Table 6, we added the values referent to comparison between Becker and 24 wells with 10 mollusks treated for 24 hours. The sensitivity for all doses was almost 100%, and the specificity was about 50% for the doses of 1 and 2 mg/L, but the other doses reached maximal specificity. PPV, NPV, and prevalence exhibited values superior to 70% for all doses tested (Table 6).

In the results after 48 hours, there was sensitivity of 82.69% in the dose of 1 mg/L; all other doses were 100%. Specificity for 1 and 2 mg/L was 68 and 50%, respectively. However, this parameter increased at the doses of 3, 4, and 5 mg/L to 100%. PPV exhibited values above 80% for all doses as observed after 24 hours. NPV was 65.83% for the dose of 1 mg/L but reached 100% in all doses. Prevalence was augmenting in accordance with the dose concentration, 67.53% for 1 mg/L and 76.47% for 2 mg/L to 100% in the other doses (Table 7).

When we compared Becker's assay with 24-well plate with 3 snails, in general, the results were extremely similar to the plate with 10 snails. The sensitivity was almost 100% for all doses tested after 24 hours of treatment. The specificity was

Table 4: A simple interpretation of screening assay quality by the value or the Z factor.

Z factor	Interpretation
1.0	Ideal Z factors can never exceed 1
Between 0.5 and 1.0	An excellent assay. Note that if $\sigma_p = \sigma_n$, 0.5 is equivalent to separation of *12* standard deviations between μ_p and μ_n
Between 0 and 0.5	A marginal assay
Less than 0	There is too much overlap between the positive and negative controls for the assay to be useful

Table 5: Validation of the optimization using 3 mollusks in a 24-well plate, with Z factor.

Niclosamide concentrations (mg/L)	Becker ($N = 10$) Z factor 24 h	Becker ($N = 10$) Z factor 48 h	24-well plate ($N = 10$) Z factor 24 h	24-well plate ($N = 10$) Z factor 48 h	24-well plate ($N = 3$) Z factor 24 h	24-well plate ($N = 10$) Z factor 48 h
1	0.92	0.67	0.67	0.92	0.73	1
2	1	1	0.70	1	0.85	0.89
3	1	1	1	1	0.89	1
4	1	1	1	1	1	1
5	1	1	1	1	1	1

Table 6: Assessment of sensitivity, specificity, positive predictive value (PPV), negative predictive value (NPV), and prevalence (24 hours).

Niclosamide concentrations (mg/L)	Becker ($n = 10$) × 24-well plate ($n = 10$) 24 h (% sensitivity)	Becker ($n = 10$) × 24-well plate ($n = 10$) 24 h (% specificity)	Becker ($n = 10$) × 24-well plate ($n = 10$) 24 h (% PPV)	Becker ($n = 10$) × 24-well plate ($n = 10$) 24 h (% NPV)	Becker ($n = 10$) × 24-well plate ($n = 10$) 24 h (% prevalence)
1	98.03	52.63	84.74	90.90	72.85
2	100	50	86.66	100	76.47
3	100	100	100	100	100
4	100	100	100	100	100
5	100	100	100	100	100

Table 7: Assessment of sensitivity, specificity, positive predictive value (PPV), negative predictive value (NPV), and prevalence (48 hours).

Niclosamide concentrations (mg/L)	Becker ($n = 10$) × 24-well plate ($n = 10$) 48 h (% sensitivity)	Becker ($n = 10$) × 24-well plate ($n = 10$) 48 h (% specificity)	Becker ($n = 10$) × 24-well plate ($n = 10$) 48 h (% PPV)	Becker ($n = 10$) × 24-well plate ($n = 10$) 48 h (% NPV)	Becker ($n = 10$) × 24-well plate ($n = 10$) 48 h (% prevalence)
1	82.69	68	84.31	65.38	67.53
2	100	50	86.66	100	76.47
3	100	100	100	100	100
4	100	100	100	100	100
5	100	100	100	100	100

about 50% in the doses until 3 mg/L, but it augmented for 100% in the doses of 4 and 5 mg/L. PPV and NPV were higher than 80% for all doses and the prevalence only was below 90% at the dose of 1 mg/L (Table 8).

The results of 48 hours demonstrated sensitivity of 75% at the dose of 1 mg/L and 100% for all doses. The specificity was maximal for higher doses, 71.42 and 50% for doses of 1 mg/L and 2 mg/L, respectively. PPV values were above 80% for all doses and NPV was maximal for all doses except dose of 1 mg/L with 62.50%. Only the dose of 1 mg/L had prevalence of 66.66%; others were higher than 95% (Table 9).

We also compared the assays using 24-well plate with 10 mollusks and 3 snails. The results for 24 hours indicate sensitivity of 70% for 1 mg/L and values superior to 90% for all doses. The specificity was 76.47% at the dose of 1 mg/L, 83.33% for 2 mg/L, 50% for 3 mg/L, and 100% for all doses. PPV

Table 8: Comparative study on the Becker test with 24-well plates with 3 snails.

Niclosamide concentrations (mg/L)	Becker ($n = 10$) × 24-well plate ($n = 3$) 24 h (% sensitivity)	Becker ($n = 10$) × 24-well plate ($n = 3$) 24 h (% specificity)	Becker ($n = 10$) × 24-well plate ($n = 3$) 24 h (% PPV)	Becker ($n = 10$) × 24-well plate ($n = 3$) 24 h (% NPV)	Becker ($n = 10$) × 24-well plate ($n = 3$) 24 h (% prevalence)
1	96.66	55.55	87.87	83.33	75
2	100	50	94.87	100	90.24
3	100	50	97.43	100	95
4	100	100	100	100	100
5	100	100	100	100	100

Table 9: Comparative study on the Becker test with 24-well plates with 3 snails.

Niclosamide concentrations (mg/L)	Becker ($n = 10$) × 24-well plate ($n = 3$) 48 h (% sensitivity)	Becker ($n = 10$) × 24-well plate ($n = 3$) 48 h (% specificity)	Becker ($n = 10$) × 24-well plate ($n = 3$) 48 h (% PPV)	Becker ($n = 10$) × 24-well plate ($n = 3$) 48 h (% NPV)	Becker ($n = 10$) × 24-well plate ($n = 3$) 48 h (% prevalence)
1	75	71.42	81.81	62.50	66.66
2	100	50	94.87	100	95
3	100	100	100	100	100
4	100	100	100	100	100
5	100	100	100	100	100

Table 10: Comparative study on the 24-well plates test with 10 snails and 3 snails.

Niclosamide concentrations (mg/L)	24-well plate ($n = 10$) × 24-well plate ($n = 3$) 24 h (% sensitivity)	24-well plate ($n = 10$) × 24-well plate ($n = 3$) 24 h (% specificity)	24-well plate ($n = 10$) × 24-well plate ($n = 3$) 24 h (% PPV)	24-well plate ($n = 10$) × 24-well plate ($n = 3$) 24 h (% NPV)	24-well plate ($n = 10$) × 24-well plate ($n = 3$) 24 h (% prevalence)
1	70	76.47	84	59.09	63.82
2	93.54	83.33	93.54	55.55	75.51
3	97.43	50	97.43	100	95
4	100	100	100	100	100
5	100	100	100	100	100

values were superior to 80% and NPV values were 59.09% and 55.55% for doses of 1 and 2 mg/L, respectively. In the higher doses, the NPV values were 100%. Prevalence in the dose of 1 mg/L and 2 mg/L was 63.82% and 75.51%; the other doses were above 95% (Table 10).

In the assays after 48 hours, sensitivity, specificity, and PPV were 90% higher for all doses except for 1 mg/L that presented sensitivity and specificity values of 77.77% and 78.57%, respectively. NPV values were maximal for doses of 3–5% and 55.89% and 52.94% for 1 and 2 mg/L. Prevalence values were higher than 70% for all doses tested (Table 11).

In relation to reliability, the doses of 3, 4, and 5 mg/L, in general, showed results almost maximal for 24 or 48 hours in all assays tested. The doses of 1 and 2 mg/L exhibited a higher fluctuation. The minor value observed for sensitivity was 70%; the specificity, in general, was about 50%. PPV and NPV values were always above 80%; however, NPV values for comparison between 24-well plate assays were reduced to values in turn of 50%. Prevalence values also were well satisfactory ranging from 63% to 95%. These results indicate a high correlation, reliability, and quality of the 24-well plate assays when compared to Becker's assays to measure the death of the snails.

Based on these results, we compared the molluscicidal effect of crude ethanol extract of stems of *Manilkara subsericea* in the three methodologies (Figure 4). The IC_{50} values calculated for Becker's assay were 11.36 ± 3.87 μg/mL and 18.2 ± 4.8 μg/mL for 24 wells with 10 snails and 15 ± 2.6 μg/mL for 24 wells with 3 snails. According to these values, the IC_{50} values calculated were similar between these mythologies, reinforcing the results with 24 wells and three snails.

4. Discussion

Our aim was to optimize a protocol to measure the molluscicidal action of plant extracts and essentially purified

Table 11: Comparative study in the 24-hour test in 24-well plates, with 10 snails and 3 snails.

Niclosamide concentrations (mg/L)	24-well plate ($n = 10$) × 24-wells plate ($n = 3$) 48 h (% sensitivity)	24-well plate ($n = 10$) × 24-well plate ($n = 3$) 48 h (% specificity)	24-well plate ($n = 10$) × 24-well plate ($n = 3$) 48 h (% PPV)	24-well plate ($n = 10$) × 24-well plate ($n = 3$) 48 h (% NPV)	24-well plate ($n = 10$) × 24-well plate ($n = 3$) 48 h (% prevalence)
1	77.77	78.57	90.32	57.89	72
2	96.77	90	96.77	52.94	77.55
3	100	100	100	100	100
4	100	100	100	100	100
5	100	100	100	100	100

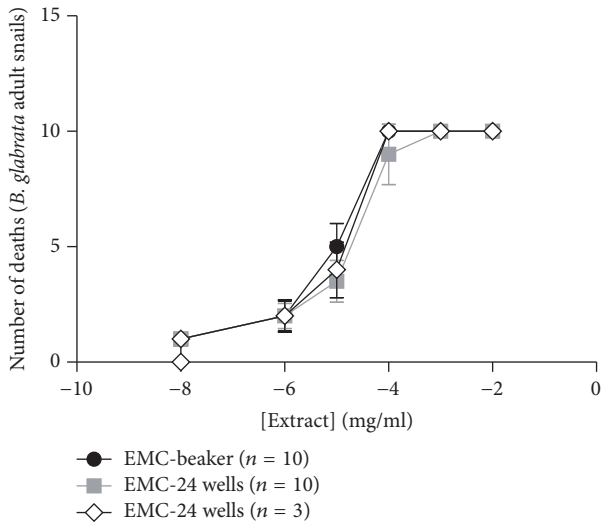

Figure 4: Dose-response effect of crude ethanol extract of stems of *Manilkara subsericea* against *Biomphalaria glabrata*. We treated the snails with crescent doses of the extract for 48 hours. These experiments were realized in three distinct days.

substances. This objective was based on the difficulty to discover new potential drugs against adult mollusks of *B. glabrata* in function of large volumes necessary to evaluate the molluscicidal action and consequently to reduce the quantity of material needed to perform the assay. This point also reflects the cost to develop a new drug and generally abolish the opportunity to test synthetic molecules.

The proposal of this paper was to diminish the volume used to dissolve the tested substances and decrease the number of mollusks used, and then we could test a large number of plant extracts, purified substances, or synthetic molecules against death of the snail.

According to WHO recommendations, the molluscicidal activity is evaluated using 10 mollusks exposed for 48 hours in a final volume of 500 mL [7]. Meanwhile, there are a large number of papers describing variations in these conditions and observing satisfactory results. There are descriptions using plastic terrariums with 9 cm diameter and 6 cm depth. The final volume was 5 mL with mollusks exposed through dermal contact directly with the extract [12]. Silva and collaborators [13] used plastic terrariums with capacity of 250 mL containing 5 adult mollusks exposed to a final volume of 8 mL sprayed with manual sprayer.

de Souza and colleagues also used terrariums; however, they pulverized 10 mollusks for terrariums with 20 mL of extract solutions [14].

In another paper, the authors used a Petri dish of 14 cm with 10 mollusks and a final volume of 100 mL to evaluate plant extract and Becker of 30 mL containing 10 mollusks and a final volume of 10 mL with purified substances [15].

There are papers using Becker with a maximal volume of 250 mL containing 10 mollusks for treatment [13, 16, 17], 500 mL with 10 mollusks [8, 18, 19], 1000 mL with 10 mollusks [20, 21], and in rare cases 2000 mL [22]. However, these papers, changing the final volume and number of mollusks, did not validate mathematically the efficiency of these protocols to measure molluscicidal activity in comparison to standard protocol.

We applied multiple doses ranging from 1 mg/L to 5 mg/L niclosamide for 24 or 48 hours. All results recorded by the three distinct methodologies were compared in relation to concordance. For this, we analyzed two-by-two methodologies using a contingence table to calculate Kappa's coefficient. We calculated a Kappa value to each dose tested, and then we observed possible discrepancies in accordance with the final dose used. The values obtained for doses ranging from 3 to 5 mg/L, in general, reached maximal correlation. In the doses of 1-2 mg/L, there was higher oscillation, and the strength of agreement to Becker's assay and 24-well plate with 10 mollusks was moderate at both doses after 24 hours of exposition. The agreement with the dose of 2 mg/L was good and that with 1 mg/L was moderate after 48 hours.

In the comparison between Becker and 24 wells with three snails, the concentration in both doses exhibited good strength of agreement after 24 hours. In 48 hours, the dose of 2 mg/L reached an almost perfect agreement and the dose of 1 mg/mL showed good correlation. All superior doses were practically perfect between these methodologies.

When we compared 24-well plates containing 10 snails for each treatment or 3 snails for each treatment, the results observed with respect to doses ranging from 3 to 5 mg/L were unchanged, when was compared with other correlations analyzed. However, there was a considerable reduction in the strength of agreement to doses of 1 and 2 mg/L. The dose of

2 mg/L exhibited a good strength after 24 hours, in contrast to the dose of 1 mg/L with a result close to K value of 0.5 indicating a moderate level. A K value of 0.5 indicated that a moderate level at 48 hours of exposition was moderated to both doses.

Based on these results, the assays in the concentrations ranging from 3 to 5 mg/L were comparable among all methodologies tested. In the doses of 1 and 2 mg/L, there was a higher variation. In relation to 24-well plate with 10 mollusks compared to Becker's assay, it is indicated to do assays with dose of 2 mg/L niclosamide. In the assays using 24-well plate with 3 mollusks compared with Becker's assay, all doses tested may be used as satisfactory, essentially after 48 hours of exposition. Then, we considered the methodology in 24-well plate with 3 mollusks as more efficient to evaluate molluscicidal activity.

Taking into consideration the better performance of methodology in 24-well plate containing 3 mollusks and its large potential to screen plant extracts and principally purified or synthetic molecules, we evaluated quality, reliability, and robustness properties.

Initially, we calculated the Z' factor for all methodologies focusing on the methodology of 24-well plate with 3 snails. As represented in Table 5, all assays displayed ideal or excellent results, when these doses were considered as maximal value after 24 or 48 hours of treatment. Then, we measured reliability factors for these methodologies. Becker's assays for 24 hours reached 100% for sensitivity, specificity, PPV, NPV, and prevalence in the doses varying from 3 to 5 mg/L (Table 6). In the doses of 1 and 2 mg/L, the specificity was in turn 50% and the prevalence inferior to 80%; all other parameters were superior to 85%. After 48 hours, the dose of 1 mg/L showed the worst reliability results (Table 7). Other doses exhibited results similar to 24 hours. The 24-well plate containing 10 mollusks treated for 24 hours was similar to Becker's assays; however, the specificity was 50% also in the dose of 3 mg/L and the dose of 1 mg/L did not reach the maximal values; however, it reached a satisfactory value (Table 8). After the exposition of 48 hours, all doses were above 90% with the exception of 1 mg/L, where the sensitivity and specificity were above 70%, but the NPV and prevalence were 62, 50% and 66, 66%, respectively (Table 9). The assay using 24-well plate with 3 mollusks in 24 hours was over 90% for all parameters in the doses of 3–5 mg/L; only the specificity in the dose of 3 mg/L was 50%. The dose displayed reduced parameters of NPV and prevalence, but the specificity and sensitivity were reasonable (Table 10). For 48 hours, all other values considerably rose for almost maximal values; the unique exception was NPV values.

5. Conclusion

These results demonstrated 24-well plate as a good tool to optimize Becker's assays reducing the final volume and number of snails, and thus a large number of plant extracts and essentially synthetic and purified molecules may be tested against mollusk survival. Consequently, this result opens a new perspective to discover and develop a novel drug capable of controlling the population number of *B. glabrata* mollusks diminishing the risk of schistosomiasis transmission.

Conflicts of Interest

The authors state that they have no conflicts of interest.

Authors' Contributions

Robson Faria performed the experiments, analyzed and interpreted data, prepared figures, and wrote the paper. José Augusto prepared mollusks in culture and wrote the paper. Leonardo Rangel, João Vitória, and Viviane Paixão performed the experiments.

Acknowledgments

This work was supported by the National Council for Scientific and Technological Development (CNPq), Foundation for Research Support of the State of Rio de Janeiro (FAPERJ), Oswaldo Cruz Institute, and PAPES (PAPES VI-CNPq). The authors would like to thank Laboratório de Tecnologia de Produtos Naturais, Departamento de Farmácia da UFF, for obtaining the extracts. In the same way, they thank the botanist Marcelo Guerra, who accompanied them in the collection of the sandbank.

References

[1] K. C. G. M. Araújo, A. P. D. C. Resendes, R. Souza-Santos, J. C. Silveira Jr., and C. S. Barbosa, "Spatial analysis of Biomphalaria glabrata foci and human cases of mansoni schistosomiasis in Porto de Galinhas, Pernambuco State, Brazil, in the year 2000," *Cadernos de Saude Publica*, vol. 23, no. 2, pp. 409–417, 2007.

[2] J. R. Coura and R. S. Amaral, "Epidemiological and control aspects of schistosomiasis in Brazilian endemic areas," *Memórias do Instituto Oswaldo Cruz*, vol. 99, supplement 1, pp. 13–19, 2004.

[3] World Health Organization, *Pesticides and Their Application for the Control of Vectors and Pests of Public Health Importance*, 2006.

[4] C. Cabrera, E. Ortega, M. Lorenzo, and M. López, "Cadmium contamination of vegetable crops, farmlands, and irrigation waters," in *Reviews of Environmental Contamination and Toxicology*, vol. 154, pp. 55–81, 1998.

[5] N. M. Mendes, D. F. Baptista, M. C. Vasconcellos, and V. T. Schall, "Evaluation of the molluscicidal properties of Euphorbia splendens var. hislopii (N.E.B.) (Euphorbiaceae) - 1: experimental test in a lentic habitat," *Memórias do Instituto Oswaldo Cruz*, vol. 87, no. 1, pp. 21–23, 1992.

[6] D. F. Baptista, M. C. Vasconcellos, F. E. Lopes, I. P. Silva, and V. T. Schall, "Evaluation of the molluscicidal property of Euphorbia splendens var. hispolii (N.E.B.) (Euphorbiaceae) - 2: investigation in lotic habitat," *Memórias do Instituto Oswaldo Cruz*, vol. 87, no. 4, pp. 549–553, 1992.

[7] World Health Organization, "Molluscicide screening and evaluation," *Bulletin of the World Health Organization*, vol. 33, pp. 567–581, 1965.

[8] M. O. Victor, D. S. Yole, M. A. Suleiman et al., "Assessment of molluscicidal, cercaricidal and miracidal activities of crude extracts of ocimum americanum, bridelia micrantha and

chenopodium ambrosoides," *Journal of Biology, Agriculture and Healthcare*, vol. 5, no. 22, 2015.

[9] D. G. Altman, *Practical Statistics for Medical Research*, Chapman and Hall, London, UK, 1991.

[10] J. R. Landis and G. G. Koch, "The measurement of observer agreement for categorical data," *Biometrics*, vol. 33, no. 1, pp. 159–174, 1977.

[11] J.-H. Zhang, T. D. Y. Chung, and K. R. Oldenburg, "A simple statistical parameter for use in evaluation and validation of high throughput screening assays," *Journal of Biomolecular Screening*, vol. 4, no. 2, pp. 67–73, 1999.

[12] B. A. de Souza, L. C. da Silva, E. D. Chicarino, and E. C. A. Bessa, "Preliminary phytochemical screening and molluscicidal activity of the aqueous extract of Bidens pilosa Linné (Asteraceae) in Subulina octona (Mollusca, Subulinidade)," *Anais da Academia Brasileira de Ciencias*, vol. 85, no. 4, pp. 1557–1566, 2013.

[13] T. M. S. Silva, T. G. D. A. Silva, R. M. Martins et al., "Molluscicidal activities of six species of Bignoniaceae from north-eastern Brazil, as measured against Biomphalaria glabrata under laboratory conditions," *Annals of Tropical Medicine and Parasitology*, vol. 101, no. 4, pp. 359–365, 2007.

[14] B. A. de Souza, L. C. da Silva, E. D. Chicarino, and E. C. D. A. Bessa, "Phytochemical and molluscicidal activity of Mikania glomerata Sprengel (Asteraceae) in different lifestages of Subulina octona (Mollusca, Subulinidade)," *Brazilian Archives of Biology and Technology*, vol. 57, no. 2, pp. 261–268, 2014.

[15] Z. Liu, Y. Li, S. Jiang, and L. Chen, "The combinations of separation modes in multidimensional high performance liquid chromatography (MDHPLC)," *Chinese Journal of Chromatography*, vol. 15, no. 6, pp. 490–493, 1997.

[16] C. A. Camara, T. M. Silva, T. G. da-Silva et al., "Molluscicidal activity of 2-hydroxy-[1,4]naphthoquinone and derivatives," *Anais da Academia Brasileira de Ciências*, vol. 80, no. 2, pp. 329–334, 2008.

[17] T. M. S. Silva, M. M. Batista, C. A. Camara, and M. F. Agra, "Molluscicidal activity of some Brazilian Solanum spp. (Solanaceae) against Biomphalaria glabrata," *Annals of Tropical Medicine and Parasitology*, vol. 99, no. 4, pp. 419–425, 2005.

[18] M. C. B. Martins, M. C. Silva, L. R. S. Silva et al., "Usnic acid potassium salt: an alternative for the control of Biomphalaria glabrata (Say, 1818)," *PLoS ONE*, vol. 9, no. 11, Article ID e111102, 2014.

[19] N. Hamed, F. Njeh, M. Damak, A. Ayadi, R. Mezghani-Jarraya, and H. Hammami, "Molluscicidal and larvicidal activities of atriplex inflata aerial parts against the mollusk galba truncatula, intermediate host of fasciola hepatica," *Revista do Instituto de Medicina Tropical de Sao Paulo*, vol. 57, no. 6, pp. 473–479, 2015.

[20] J. A. Santos, T. C. Tomassini, D. C. Xavier, I. M. Ribeiro, M. T. Silva, and Z. B. Morais Filho, "Molluscicidal activity of *Physalis angulata* L. extracts and fractions on *Biomphalaria tenagophila* (d'Orbigny, 1835) under laboratory conditions," *Memórias do Instituto Oswaldo Cruz*, vol. 98, no. 3, pp. 425–428, 2003.

[21] D. Guo, J. Chen, Y. Liu, H. Yao, F.-A. Han, and J. Pan, "A high-performance molluscicidal ingredient against Oncomelania hupensis produced by a rhizospheric strain from Phytolacca acinosa Roxb," *Pharmacognosy Magazine*, vol. 7, no. 28, pp. 277–283, 2011.

[22] D. Sukumaran, B. D. Parashar, A. K. Gupta, K. Jeevaratnam, and S. Prakash, "Molluscicidal effect of nicotinanilide and its intermediate compounds against a freshwater snail *Lymnaea luteola*, the vector of animal schistosomiasis," *Memorias do Instituto Oswaldo Cruz*, vol. 99, no. 2, pp. 205–210, 2004.

Hindawi
Evidence-Based Complementary and Alternative Medicine
Volume 2017, Article ID 6878795, 6 pages
https://doi.org/10.1155/2017/6878795

Research Article

Sinomenine Hydrochloride Attenuates Renal Fibrosis by Inhibiting Excessive Autophagy Induced by Adriamycin: An Experimental Study

Ming-ming Zhao, Bin Yang, Qiu Zhang, Jin-hu Wang, Jin-ning Zhao, and Yu Zhang

Xiyuan Hospital, China Academy of Chinese Medical Sciences, Beijing 100091, China

Correspondence should be addressed to Yu Zhang; zhangyu8225@126.com

Received 31 March 2017; Accepted 1 June 2017; Published 17 July 2017

Academic Editor: José C. T. Carvalho

The objective of this study is to investigate if sinomenine hydrochloride (SIN-HCl) could be effective against adriamycin-induced renal fibrosis by regulating autophagy in a rat model. Forty male Sprague-Dawley (SD) rats were randomly divided into control group, model group, telmisartan group, and SIN-HCl group; rat model was induced by adriamycin; all rats were given intragastric administration for 6 weeks. Urine was collected from rats in metabolic cages to determine 24 h protein level. This was done after intragastric administration for the first two weeks and then once for every two weeks. Renal pathological changes were examined by the staining of HE, Masson, and PASM. Expressions and distributions of fibronectin (FN), laminin (LN), light chain 3 (LC3), and Beclin-1 were observed by immunohistochemistry. SIN-HCl ameliorates proteinuria, meanwhile attenuating the renal pathological changes in adriamycin-induced rats and also attenuating renal fibrosis and excessive autophagy by reducing the expression of FN, LN, LC3, and Beclin-1. SIN-HCl attenuates renal fibrosis by inhibiting excessive autophagy induced by adriamycin and upregulates the basal autophagy.

1. Introduction

Chronic kidney disease (CKD) is characterized by reduced glomerular filtration rate, increased urinary albumin excretion, or both [1]. With the increase in the incidence of hypertension, diabetes, and obesity, the number of patients with CKD and end-stage renal disease (ESRD) is expected to rise in the future. Renal fibrosis is regarded as the common pathological alteration in virtually every progressive CKD [2]. With kidney injury, physiological wound healing response appears to restore normal function and tissue homeostasis. However, dysregulation of this response leads to excessive, pathological deposition of extracellular matrix (ECM) proteins such as fibrillar collagens, FN, and LN. The research of renal autophagy is still in the initial stage compared with disciplines such as oncology and neurology [3]. Autophagy in renal diseases can be either protective or detrimental depending on experimental conditions. During early disease stages, maintaining podocyte autophagic activity is a potential therapeutic strategy in the treatment of delaying the progression of podocytopathies [4]. On the contrary, excessive autophagy has been proposed to mediate autophagic cell death [5]. There is a relevance between renal fibrosis and autophagy proven by recent evidences [6]. Sinomenine (Figure 1) is an active alkaloid extracted from the roots of the Chinese medicinal plant *Sinomenium acutum*, which has been employed to treat rheumatoid arthritis and other inflammatory disorders. Pharmacological profiles of sinomenine include immunemodulating properties [7, 8], anti-inflammation [9, 10], and anti-oxidative [11, 12] stress; SIN also contains renoprotective feature.

Based on these discoveries, we hypothesized that SIN-HCl could have similar mechanism to sinomenine; meanwhile, SIN-HCl could be effective against adriamycin-induced renal fibrosis by regulating autophagy in a rat model.

2. Materials and Methods

2.1. Animals Grouping and Treatment. Forty male SPF Sprague-Dawley (SD) rats (220 ± 18 g) were purchased from

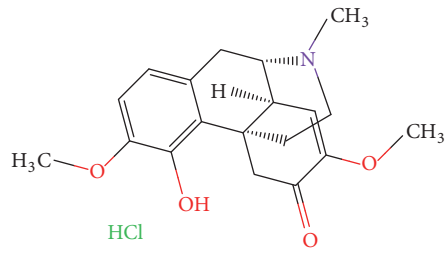

Figure 1: The structure of sinomenine hydrochloride (SIN-HCl).

Beijing HFK Bioscience Co., Ltd., Beijing, China. Rats were housed in humidity controlled (60 ± 10)% rooms at (24 ± 1)°C with a 12 h on/12 h off light cycle. The animals were maintained with free access to standard diet and tap water.

All rats were habituated to laboratory conditions for 7 days. Forty SD rats were randomly divided into either control group (n = 10) or adriamycin-induced group (n = 30). Adriamycin-induced group was treated with adriamycin at a dose of 6.2 mg/kg [13] by tail vein injection once, whereas the control group was treated with normal saline at the same dose as adriamycin-induced group by tail vein injection once. The adriamycin-induced group was further assigned to model group (n = 10), telmisartan group (n = 10), and SIN-HCl group (n = 10). Two weeks after being treated with adriamycin, 4 groups were given intragastric administration for 6 weeks: rats in control group and model group were given normal saline, rats in telmisartan group were given telmisartan (8.33 mg/kg), and rats in SIN-HCl group received SIN-HCl (18.75 mg/kg). All drugs were diluted with distilled water, and the dosages were evaluated with body surface coefficient conversion between human and rat. Urine was collected from rats in metabolic cages to determine 24 h protein level. It was done after intragastric administration for the first two weeks and then once for every two weeks. Rats were then sacrificed for the harvesting of kidney tissues. The Animal Care and Use Committee of Xiyuan Hospital of China Academy of Chinese Medical Sciences approved the experimental protocol.

2.2. Drugs. SIN-HCl (Zhengqing Fengtongning Tablet, 20 mg/pil, SFDA Approval number Z10980043) was purchased from Zhengqing Pharmaceutical Group (Hunan, China). Telmisartan (Micardis, 80 mg/pill) was purchased from Boehringer Ingelheim International GmbH Z10980043 (Import Drug License: H20090416, H20090417). Doxorubicin Hydrochloride for Injection (instant) was purchased from Pfizer Italia s.r.l. (Import Drug License: H20080278; imported drug registration standards: Jx20000016). Immunohistochemistry antibody was purchased from Abcam Companies (Item number ab52167 and ab32351); secondary antibody (PV-6000) is a general-purpose two-step immunohistochemical kit; DAB kit was purchased from ZSGB Biological Technology Co., Ltd.

2.3. Histopathological Analysis. Renal cortex tissues of right kidney were fixed in 10% buffered formalin, then embedded in paraffin, and sliced. Slices were stained with haematoxylin-eosin (HE), Masson, and methenamine silver stain (PASM), respectively, and visualized using light microscopy. The cortex tissues of left kidney were stored at −70°C for further study.

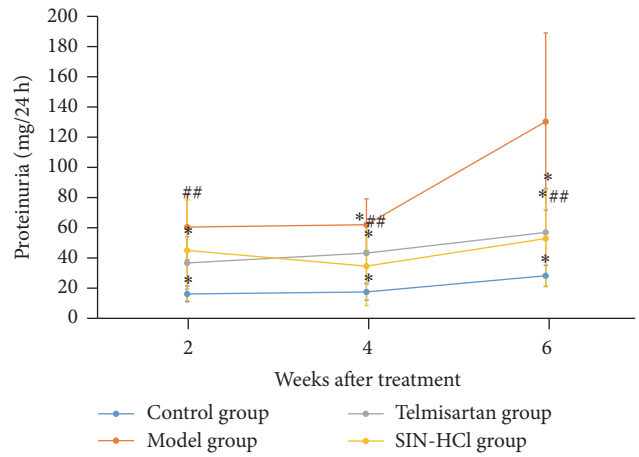

Figure 2: SIN-HCl ameliorated proteinuria. Data are shown as mean ± SD; $^{*}P < 0.05$ versus model group; $^{\#\#}P > 0.05$ versus telmisartan group. At the second week, 24 h proteinuria significantly decreased after being treated with telmisartan. At the fourth and sixth week, 24 h proteinuria significantly decreased in the telmisartan group and SIN-HCl group; meanwhile, there was no difference between telmisartan group and SIN-HCl group.

2.4. Immunohistochemistry. Expressions and distributions of FN, LN, LC3, and Beclin-1 were observed by immunohistochemistry. Renal cortical slices were dewaxed and rehydrated. Slices were incubated with 3% H_2O_2 and washed with PBS. Then slices were incubated with primary antibodies at 4°C for overnight and washed with PBS. The slices were incubated with secondary antibodies and washed with PBS. The slices were stained with DAB, washed, dehydrated, permeabilized, mounted, and viewed by light microscopy. The expression of protein was demonstrated by the ratio of integral optical density (IOD): IOD = average optical density × positive area.

3. Statistical Analysis

Statistical analysis was performed by one-way ANOVA analysis of variance using SPSS software 20.0 (SPSS, Chicago, USA). The data are expressed as mean ± standard deviation (SD). $P < 0.05$ was considered a statistically significant difference, and all P values were two-sided.

4. Results

4.1. SIN-HCl Ameliorates Proteinuria. As shown in Figure 2, rats injected with adriamycin developed proteinuria compared with control group; proteinuria continually increased. At the second week of being treated with SIN-HCl, there was no difference in 24 h proteinuria between model group and SIN-HCl group. However, 24 h proteinuria significantly decreased after four-week SIN-HCl treatment. At the fourth and sixth week, 24 h proteinuria significantly decreased in the

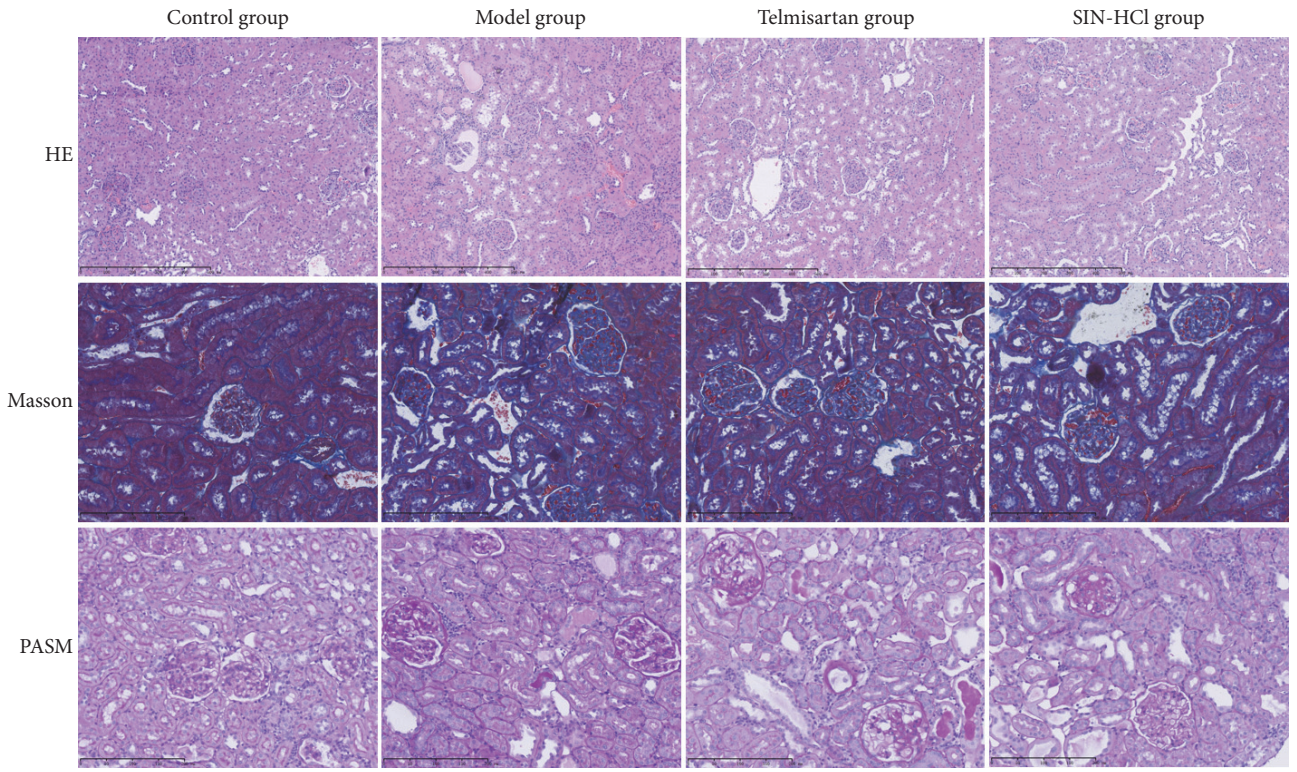

Figure 3: Telmisartan and SIN-HCl ameliorated the renal pathological changes in adriamycin-induced rats. Proliferative mesangial cells, increased ECM, thickened glomerular basement membrane, and disorderly arranged renal tubular cells were showed in the model group. Compared with model group, telmisartan and SIN-HCl ameliorated the renal pathological changes in adriamycin-induced rats.

telmisartan group and SIN-HCl group; meanwhile, there was no difference between telmisartan group and SIN-HCl group.

4.2. SIN-HCl Attenuates Renal Pathological Changes. As shown in Figure 3, renal pathological changes were examined by the staining of HE, Masson, and PASM. Proliferative mesangial cells, increased ECM, thickened glomerular basement membrane, and disorderly arranged renal tubular cells were shown in the model group. Compared with model group, telmisartan and SIN-HCl ameliorated the renal pathological changes in adriamycin-induced rats. The result proved the protective effect of SIN-HCl on kidney in adriamycin-induced rats.

4.3. SIN-HCl Attenuates Renal Fibrosis. To test the effect of SIN-HCl on renal fibrosis, we examined the expression of FN and LN protein levels, as shown in Figure 4. As a result of immunohistochemistry, the expression levels of FN (Figure 4(b)) and LN (Figure 4(c)) in glomeruli were significantly decreased in adriamycin-induced rats treated with SIN-HCl or telmisartan. There was no statistically significant difference in the expression levels of FN between SIN-HCl group and telmisartan group, but telmisartan inhibited the expression of LN superior to SIN-HCl. These results showed that SIN-HCl ameliorated the renal fibrosis in adriamycin-induced rats.

4.4. SIN-HCl Attenuates Excessive Autophagy. To test the effect of SIN-HCl on excessive autophagy, we examined the expression of LC3 and Beclin-1 by immunohistochemistry (Figure 5). The results demonstrated that adriamycin induced increased LC3 (Figure 5(b)) and Beclin-1 (Figure 5(c)), whereas the increment was inhibited after being treated with SIN-HCl or telmisartan. The difference between control group and SIN-HCl group on the expression of Beclin-1 was not statistically significant. These results showed that SIN-HCl ameliorated the excessive autophagy in adriamycin induced rats and upregulated the basal autophagy.

5. Discussion

Adriamycin-induced nephropathy is one of rat models of CKD which is considered to induce a nephrotic syndrome, leading to chronic proteinuric renal diseases and renal fibrosis [14, 15]. Clinical and laboratory-based studies have suggested that telmisartan reduces proteinuria in CKD patients [15] and attenuates oxidative stress and renal fibrosis [16, 17]. In this study, the result demonstrated the protective effective of SIN-HCl on adriamycin-induced renal injury. After being treated with adriamycin, rats developed proteinuria and the renal pathological changes were aggravated, such as proliferative mesangial cells, increased ECM, thickened glomerular basement membrane, and disorderly arranged renal tubular cells. SIN-HCl ameliorates proteinuria and renal pathological changes induced by adriamycin.

Renal fibrosis [18] is a pathological process and the common end point of virtually all kidney diseases which

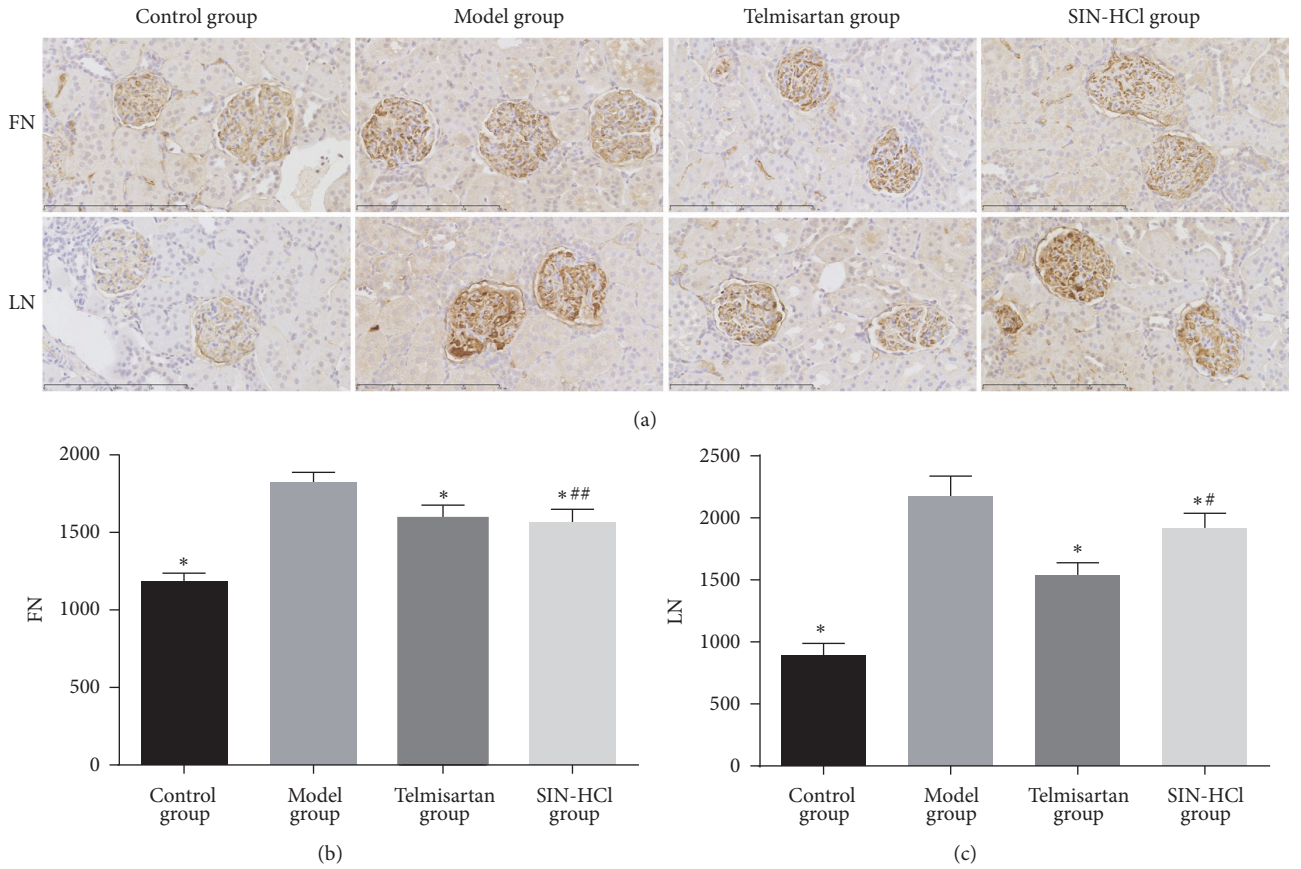

Figure 4: Telmisartan and SIN-HCl attenuated renal fibrosis (FN, LN ×400). FN: fibronectin; LN: laminin. (a) The expression of FN and LN in adriamycin-induced rat glomeruli by immunohistochemistry. (b, c) Quantitation of FN and LN. Data are shown as mean ± SD, $^{*}P < 0.05$ versus model group; $^{\#}P < 0.05$ versus telmisartan group; $^{\#\#}P > 0.05$ versus telmisartan group.

should be viewed as a dynamic system that involves mesangial cell, ECM, and many other cells. Glomerular sclerosis and interstitial fibrosis are characteristic lesions in different forms of progressive renal diseases; these pathological lesions are caused by the accumulation of ECM mainly. The ECM is composed of FN and LN mainly, and FN provides support for deposition of ECM components and formation of collagen. Meanwhile, interstitial fibroblast activation and subsequent differentiation into ECM-producing myofibroblasts also are an approach to aggravation of renal fibrosis [19–21]. For illustrating the effect of SIN-HCl on renal fibrosis, we examined the expression of FN and LN in the renal cortical of adriamycin-induced rats. The result demonstrated that SIN-HCl attenuates renal fibrosis by reducing the expression of FN and LN.

Autophagy is the degradation system and dynamic recycling system in cells, cytoplasmic materials are transported and delivered to lysosomes for degradation [22] and, subsequently, new building components and energy produced for cellular renovation and homeostasis. Autophagy includes microautophagy, macroautophagy, and molecular chaperone-mediated autophagy; macroautophagy is considered as the major type of autophagy. LC3 and Beclin-1 are markers of autophagy; LC3 is the essential macroautophagy protein [23]. Aberrant autophagy could cause renal injury and aggravation of various renal diseases. In this study, SIN-HCl attenuates excessive autophagy in kidney by down-regulating the excessive expression of LC3 and Beclin-1, meanwhile upregulating the basal autophagy.

Accumulating evidence showed a link between renal fibrosis and autophagy, but the role of autophagy in CKD is complex; induction of autophagy may be a cytoprotective mechanism, thereby negatively regulating ECM, but autophagy also can promote renal fibrosis depending on experimental conditions and cellular context [6]. The persistent and active autophagy of renal tubules aggravated renal interstitial fibrosis. The profibrotic function of autophagy is based on the regulation on tubular cells death, interstitial inflammation, and the production of profibrotic factors [24], whereas the lack of autophagy-related factors could cause the accumulation of FN and the development of renal fibrosis [25]. We found that SIN-HCl not only attenuates renal fibrosis but also attenuates excessive autophagy in renal injury caused by adriamycin; basal autophagy was also upregulated by SIN-HCl. We postulated that SIN-HCl attenuates renal fibrosis by inhibiting excessive autophagy induced by adriamycin and upregulates the basal autophagy.

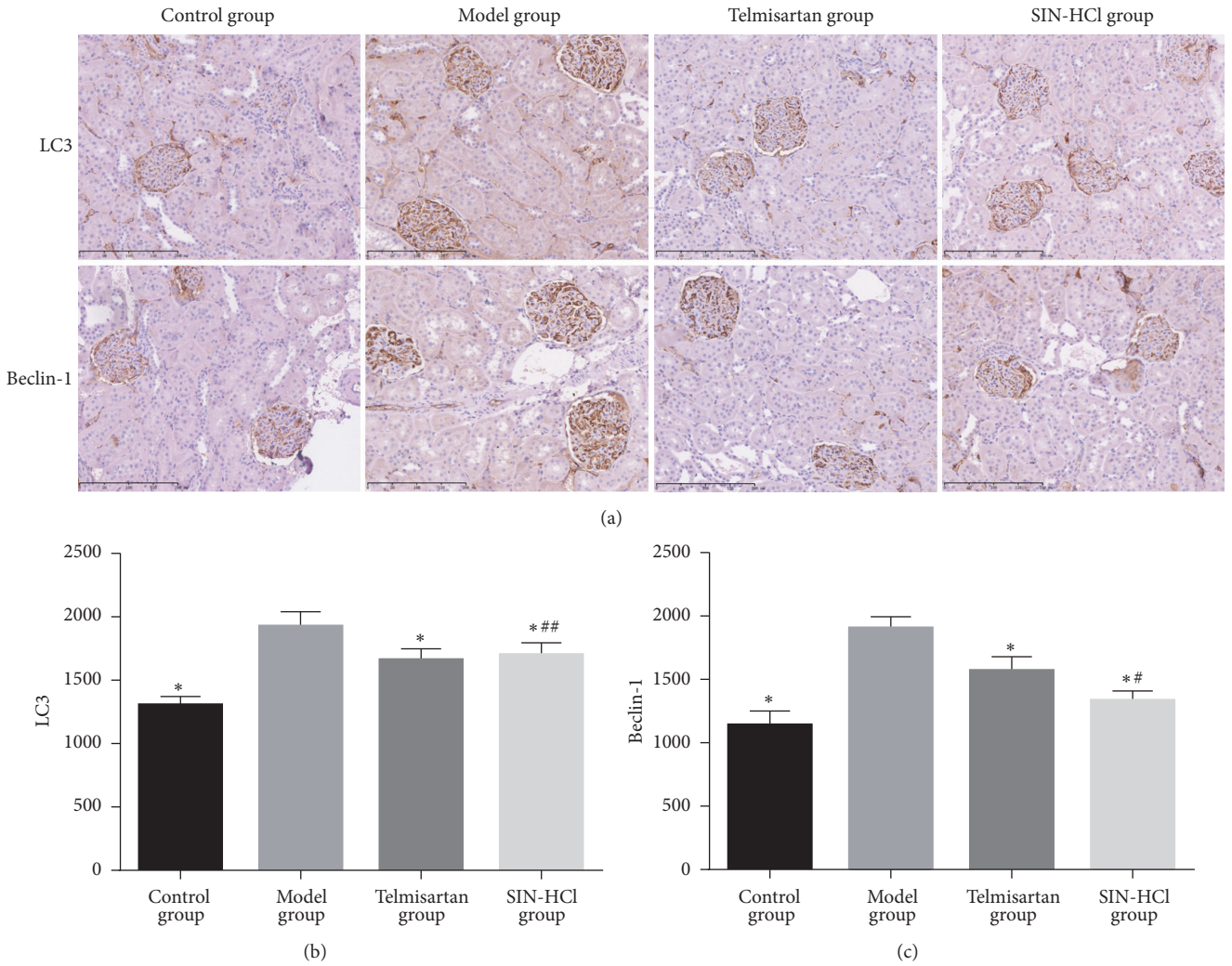

Figure 5: Telmisartan and SIN-HCl attenuated excessive autophagy (LC3, Beclin-1 ×400). (a) The expression of LC3 and Beclin-1 in adriamycin-induced rat glomeruli by immunohistochemistry. (b, c) Quantitation of LC3 and Beclin-1. Data are shown as mean ± SD, $^{*}P < 0.05$ versus model group; $^{\#}P < 0.05$ versus telmisartan group; $^{\#\#}P > 0.05$ versus telmisartan group.

Pharmacological profiles of sinomenine in treatment of CKD are of multitarget.Sinomenine could activate Nrf2 signaling to prevent hyperactive inflammation and kidney injury [26], meanwhile attenuating renal fibrosis through Nrf2-mediated inhibition of oxidative stress and TGF-β signaling [11] and alleviating high glucose-induced renal glomerular endothelial hyperpermeability [27]. However, there were some limitations in the study. Firstly, we could not identify the definite relationship between renal fibrosis and autophagy, due to the lack of autophagy inhibitor group in rats. Secondly, basal autophagy is different in different renal cells, such that the basal autophagy of podocyte is high; however, tubular cells display lower basal autophagy; SIN-HCl regulates autophagy should be verified in vitro.

6. Conclusion

In conclusion, SIN-HCl ameliorates proteinuria and, meanwhile, attenuates renal fibrosis by inhibiting excessive autophagy in adriamycin-induced nephropathy and upregulating the basal autophagy. For a future study, based on improvement of grouping, we plan to explore the relation between renal fibrosis and autophagy with SIN-HCl in vivo and in vitro.

Abbreviations

SIN-HCl: Sinomenine hydrochloride
SD: Sprague-Dawley
FN: Fibronectin
LN: Laminin
LC3: Light chain 3
CKD: Chronic kidney disease
ESRD: End-stage renal disease
ECM: Extracellular matrix
HE: Haematoxylin-eosin
PASM: Methenamine silver stain
IOD: Integral optical density
SD: Standard deviation.

Disclosure

Ming-ming Zhao and Bin Yang are the co-first authors.

Conflicts of Interest

The authors declare that there are no conflicts of interest.

Authors' Contributions

Yu Zhang conceived and designed the animal experiment and helped to draft the paper. Ming-ming Zhao, Bin Yang, Qiu Zhang, Jin-hu Wang, and Jin-ning Zhao performed the experiment. Ming-ming Zhao and Bin Yang analyzed the data and prepared the paper.

Acknowledgments

This work was supported by the Subjective Selected Subjects Program of China Academy of Chinese Medical Sciences (no. ZZ0708105).

References

[1] V. Jha, G. Garcia-Garcia, K. Iseki, and etal., "Chronic kidney disease: global dimension and perspectives," *The Lancet*, vol. 382, no. 9888, pp. 260–272, 2013.

[2] P. Boor and J. Floege, "Chronic kidney disease growth factors in renal fibrosis," *Clinical and Experimental Pharmacology and Physiology*, vol. 38, no. 7, pp. 441–450, 2011.

[3] S. De Rechter, J.-P. Decuypere, E. Ivanova, and etal., "Autophagy in renal diseases," *Pediatric Nephrology*, vol. 31, no. 5, pp. 737–752, 2016.

[4] C. Zeng, Y. Fan, J. Wu, and etal., "Podocyte autophagic activity plays a protective role in renal injury and delays the progression of podocytopathies," *Journal of Pathology*, vol. 234, no. 2, pp. 203–213, 2014.

[5] P.-L. Tharaux and T. B. Huber, "How many ways can a podocyte die?" *Seminars in Nephrology*, vol. 32, no. 4, pp. 394–404, 2012.

[6] Y. Ding and M. E. Choi, "Regulation of autophagy by TGF-β: emerging role in kidney fibrosis," *Seminars in Nephrology*, vol. 34, no. 1, pp. 62–71, 2014.

[7] S. Song, X. Shen, Y. Tang, and etal., "Sinomenine pretreatment attenuates cold ischemia/reperfusion injury in rats: the role of heme oxygenase-1," *International Immunopharmacology*, vol. 10, no. 6, pp. 679–684, 2010.

[8] H. Zhou, Y. F. Wong, J. Wang, X. Cai, and L. Liu, "Sinomenine ameliorates arthritis via MMPs, TIMPs, and cytokines in rats," *Biochemical and Biophysical Research Communications*, vol. 376, no. 2, pp. 352–357, 2008.

[9] H. Shi, K. Zheng, Z. Su, and etal., "Sinomenine enhances microglia M2 polarization and attenuates inflammatory injury in intracerebral hemorrhage," *Journal of Neuroimmunology*, vol. 299, pp. 28–34, 2016.

[10] S. Yang, F. Ning, J. Li, and etal., "Therapeutic effect analysis of sinomenine on rat cerebral ischemia-reperfusion injury," *Journal of Stroke and Cerebrovascular Diseases*, vol. 25, no. 5, pp. 1263–1269, 2016.

[11] T. Qin, S. Yin, J. Yang, and etal., "Sinomenine attenuates renal fibrosis through Nrf2-mediated inhibition of oxidative stress and TGFβ signaling," *Toxicology and Applied Pharmacology*, vol. 304, pp. 1–8, 2016.

[12] W. Wang, J. Cai, S. Tang, and etal., "Sinomenine attenuates angiotensin II-induced autophagy via inhibition of P47-phox translocation to the membrane and influences reactive oxygen species generation in podocytes," *Kidney and Blood Pressure Research*, vol. 41, no. 2, pp. 158–167, 2016.

[13] Y. Zhang, B. Zhang, and H. Ning, "Establishment of a rat model of nephrosis induced by single tail vein injection of doxorubicin," *Zhong Guo Shi Yan Dong Wu Xue Bao*, vol. 21, no. 1, pp. 1–4, 2013.

[14] T. Bertani, A. Poggi, R. Pozzoni, and etal., "Adriamycin-induced nephrotic syndrome in rats. Sequence of pathologic events," *Laboratory Investigation*, vol. 46, no. 1, pp. 16–23, 1982.

[15] V. W. Lee and D. C. Harris, "Adriamycin nephropathy: a model of focal segmental glomerulosclerosis," *Nephrology*, vol. 16, no. 1, pp. 30–38, 2011.

[16] A. P. Lakshmanan, K. Watanabe, and R. A. Thandavarayan, "Telmisartan attenuates oxidative stress and renal fibrosis in streptozotocin induced diabetic mice with the alteration of angiotensin-(1–7) mas receptor expression associated with its PPAR-γ agonist action," *Free Radical Research*, vol. 45, no. 5, pp. 575–584, 2011.

[17] H. Sugiyama, M. Kobayashi, D.-H. Wang, and etal., "Telmisartan inhibits both oxidative stress and renal fibrosis after unilateral ureteral obstruction in acatalasemic mice," *Nephrology Dialysis Transplantation*, vol. 20, no. 12, pp. 2670–2680, 2005.

[18] P. Boor, T. Ostendorf, and J. Floege, "Renal fibrosis: novel insights into mechanisms and therapeutic targets," *Nature Reviews Nephrology*, vol. 6, no. 11, pp. 643–656, 2010.

[19] J. S. Duffield, "Cellular and molecular mechanisms in kidney fibrosis," *Journal of Clinical Investigation*, vol. 124, no. 6, pp. 2299–2306, 2014.

[20] V. S. Lebleu, G. Taduri, J. O'Connell, and etal., "Origin and function of myofibroblasts in kidney fibrosis," *Nature Medicine*, vol. 19, no. 8, pp. 1047–1053, 2013.

[21] S. Meran and R. Steadman, "Fibroblasts and myofibroblasts in renal fibrosis," *International Journal of Experimental Pathology*, vol. 92, no. 3, pp. 158–167, 2011.

[22] N. Mizushima and M. Komatsu, "Autophagy: renovation of cells and tissues," *Cell*, vol. 147, no. 4, pp. 728–741, 2011.

[23] S. Romao and C. Münz, "LC3-associated phagocytosis," *Autophagy*, vol. 10, no. 3, pp. 526–528, 2014.

[24] M. J. Livingston, H.-F. Ding, S. Huang, J. A. Hill, X.-M. Yin, and Z. Dong, "Persistent activation of autophagy in kidney tubular cells promotes renal interstitial fibrosis during unilateral ureteral obstruction," *Autophagy*, vol. 12, no. 6, pp. 976–998, 2016.

[25] G. Xu, F. Yue, H. Huang, etal., Q. Chen, and L. Liu, "Defects in MAP1S-mediated autophagy turnover of fibronectin cause renal fibrosis," *Aging*, vol. 8, no. 5, pp. 977–985, 2016.

[26] T. Qin, R. Du, F. Huang, and etal., "Sinomenine activation of Nrf2 signaling prevents hyperactive inflammation and kidney injury in a mouse model of obstructive nephropathy," *Free Radical Biology and Medicine*, vol. 92, pp. 90–99, 2016.

[27] Q. Yin, Y. Xia, and G. Wang, "Sinomenine alleviates high glucose-induced renal glomerular endothelial hyperpermeability by inhibiting the activation of RhoA/ROCK signaling pathway," *Biochemical and Biophysical Research Communications*, vol. 477, no. 4, pp. 881–886, 2016.